申报	系列：教师系列
	专业：农业机械化工程
	职称：副教授

业绩成果材料

（申报人的业绩成果材料包括论文、科研项目、获奖以及其他成果等）

单　位（二级单位）_____工程学院_____

姓　名　__李成杰_____

材料核对人：　　单位盖章：

核对时间：

华南农业大学制

目　录

三、论文、著作等

四、科研成果

五、其他业绩

华南农业大学文件

华南农教〔2024〕52 号

关于公布华南农业大学 2024 年度校级本科教学质量与教学改革工程项目立项名单的通知

各学院、部处、各单位:

根据《关于开展 2024 年度校级本科教学质量与教学改革工程项目申报工作的通知》精神,经项目负责人申报、所在单位推荐和学校组织专家评审、公示等程序，决定立项“基于大湾区新能源汽车人才需求的智能网联技术课程改革”等 121 个项目为 2024 年度校级本科教学改革项目；立项“涉外法治人才培养实验班”等 36 个项目为 2024 年度校级本科质量工程项目；根据学校年度人才培养工作重点及本年度申报项目质量，立项“‘长基计划’下新文科历史学课程体系的改革与实践”等 11 个项目为 2024 年度“长基计划”教学质量和教学改革工程专项项目（经

费由“长基计划”专业专项资金资助）。具体名单见附件。

请各项目负责人按照项目建设任务及要求，及时开展各项工作，加快推进学校人才培养改革，并力争取得高水平的教学成果。各单位要切实履行项目建设主体责任，加强对项目建设的督促、指导，以确保项目能如期高质量完成建设任务。

特此通知。

附件：1. 华南农业大学2024年度校级本科教学改革立项名单

2. 华南农业大学2024年度校级本科质量工程立项名单

3. 华南农业大学2024年度校级“长基计划”教学质量和教学改革工程专项立项名单

华南农业大学

2024年8月15日

（联系人：孙齐胜；电话：85288020）

公开方式：主动公开

华南农业大学党政办公室　　2024年8月20日印发

A	B	C	D	E	F	G
华南农业大学2024年度校级教学改革项目立项名单						
81	JG2024081	青年项目	马克思主义学院	时间视域下思想政治理论课教学实效性提升研究——以 《中国近现代史纲要》课程为例	孙飞争	钟健、刘晓雷、王超
82	JG2024082	青年项目	电子工程学院（人工智能学院）	基于OBE和云边端协同的DSP技术与应用混合式教学实践研究	高鹏	宋淑然、李震、孙道宗、吕石磊
83	JG2024083	青年项目	园艺学院	《园艺植物生物技术》课程教学的改革与探索	彭泽	张志珂、杨向晖
84	JG2024084	青年项目	动物科学学院	新农科背景下高质量动物科学专业人才培养探索与实践	何小敏	陈志远、邓铭、付晓兰、陈婷
85	JG2024085	青年项目	海洋学院	基于 OBE 理念的大学生心理健康教育课程设计与实践研究	苏婉	祁红、彭金富、杨慧荣、林慷祺
86	JG2024086	自筹项目	工程学院	多维视角下的《工程热力学与传热学》教学：思政教育与工程知识的融合	李成杰	李长友、张烨
87	JG2024087	自筹项目	食品学院	“新工科”视角下基于OBE教学理念的《食品有害物质检测分析》多模式教学探索与实践	王群	曹庸、刘晓娟、苗建银、李梦婷
88	JG2024088	自筹项目	基础实验与实践训练中心	《生物化学实验》教学内容的优化和数字资源的构建与实践	许可	詹福建、许燕珍、母培强、何平
89	JG2024089	自筹项目	公共管理学院	新文科“专创融合”课程的教学改革与实践——以《新文科创新创业思维与就业力提升》课程为例	周毅	申佐佐、贾海薇、余祥、郭雪倩
90	JG2024090	自筹项目	外国语学院	“讲好中国故事”视域下跨文化能力教学改革与实践——以《中外文化比较》课程为例	侯丽娴	文珊、侯金萍、郭圣琳、赵轶哲
91	JG2024091	自筹项目	数学与信息学院、软	“三全育人”背景下《编译原理》课程思政改革与实践	王海燕	方风美

华南农业大学文件

华南农教〔2025〕7号

关于公布华南农业大学2024年度课程思政示范项目立项名单的通知

各学院、部处、各单位:

根据《关于开展2024年度校级课程思政示范建设项目申报工作的通知》,学校组织开展了2024年度课程思政示范项目评选工作。

经项目负责人申请、所在单位遴选推荐、学校组织专家评审、校内公示等程序，决定立项建设华南农业大学2024年度课程思政示范项目91项，包括课程思政试点学院4个、课程思政示范团队6个、课程思政示范课程14门、课程思政示范课堂25个、课程思政典型案例42个（名单详见附件），现予以公布。

本次立项的课程思政示范项目建设期至2026年12月，建设期内，示范项目原则上不允许更换负责人或变更项目团队成员。

各项目负责人要严格按照 2024 年度申报通知要求，及时开展工作，加快推进课程思政改革，确保高质量完成建设目标和任务。

请各学院充分认识课程思政改革的重要意义，认真贯彻《华南农业大学课程思政实施方案》，加强对教师的相关培训、指导、引领和支持，带动教师全员积极参与课程思政教学改革，持续深入抓典型、树标杆、推经验，全面提升本科人才培养质量。

附件：华南农业大学 2024 年度课程思政示范项目立项名单

华南农业大学

2025 年 1 月 24 日

公开方式：主动公开

华南农业大学党政办公室　　2025 年 1 月 24 日印发

附件

华南农业大学 2024 年度课程思政示范项目立项名单

序号	类别	项目名称	所属单位	项目负责人	团队成员（不含负责人）
kcsz2024001	试点学院	课程思政试点学院	动物科学学院	王文策	
kcsz2024069	典型案例	《Linux 系统及程序设计》Linux 发展史及国产化	数学与信息学院、软件学院	钟德祥	李舜鹏
kcsz2024070	典型案例	《复变函数与积分变换》--柯西积分公式	数学与信息学院、软件学院	刘曼莉	
kcsz2024071	典型案例	《生活营造》—中国茶的起源	艺术学院	王小玉	
kcsz2024072	典型案例	《工程热力学与传热学》第三章第 4 节（孤立系统熵增原理）	工程学院	李成杰	
kcsz2024073	典型案例	《数据挖掘与大数据分析》第三章第 2 节 （Seaborn 绘图基础）	经济管理学院	伍敬文	
kcsz2024074	典型案例	《高等数学》第五章第 1 节（定积分的概念）	数学与信息学院、软件学院	郑佳悦	
kcsz2024075	典型案例	《计算机科学绪论》第十三章信息保障与安全	数学与信息学院、软件学院	罗志坚	黄小虎
kcsz2024076	典型案例	《Linux 系统及程序设计》--Linux 程序设计原理	数学与信息学院、软件学院	黄立峰	罗浩宇
kcsz2024077	典型案例	《软件工程导论》第七章 第 7 节（黑盒测试之等价类划分与边界值分析）	数学与信息学院、软件学院	聂笃宪	刘鹏飞

华南农业大学校内公文

本科生院（招办）〔2026〕2 号

关于公布华南农业大学 2025 年度智慧课程认定结果的通知

各学院、部处，各相关单位:

根据《关于做好 2025 年度校级教学质量与教学改革工程项目结题验收工作的通知》要求，学校组织开展了项目的结题验收工作。经项目负责人所在单位组织专家结题、学校组织专家验收、公示等程序，认定《动物营养学》等 69 门校级智慧课程。请各单位高度重视智慧课程建设，以课程建设的智慧化带动专业智慧化升级。各项目负责人应加强项目成果的推广应用，争取获得更好的示范效果。

附件：1.2025 年度校级智慧课程认定名单

2.智慧课程认定标准（2025 年版）

本科生院（招生办公室）

2026 年 1 月 28 日

85280052

33	智慧培育类课程	畜产食品工艺学	郭善广	郭善广，徐振林，艾民珉，郑华，肖南	食品学院
34	智慧培育类课程	信息系统开发综合实践	邓成剑	邓成剑，吴春胤，韦婷婷，刘昌余	数学与信息学院、软件学院
35	智慧培育类课程	数字化运营	张勇威	邓金、骆威、胡焕玲	数学与信息学院、软件学院
36	智慧培育类课程	网络安全技术与实践	张凯	赵丽宁、张建桃、宋歌、韩方珍、杨春	数学与信息学院、软件学院
37	智慧培育类课程	普通昆虫学	王兴民	刘卫欣、王厚帅、陈科伟、何晓芳、岑伊静、王德森、黄嘉	植物保护学院
38	智慧培育类课程	试验统计学	布素红	王少奎、杨维丰、冯发强、陈志雄、黄君、石碧海、张静懿	农学院
39	智慧培育类课程	植物学	白玫	梁祥修、张荣京、孔德鑫、何韩军	生命科学学院
40	智慧培育类课程	《计算智能》AI 课程建设实践	胡春筠	胡春筠，胡洁	电子工程学院（人工智能学院）

41	智慧培育类课程	大学数学 II	周燕	李凤、杨德贵、肖莉、杨志程、夏英俊、刘曼莉、陈银辉、陆琪、何婧、丁仕虹、姚焕城、岑冠军	数学与信息学院、软件学院
42	智慧培育类课程	风景园林植物应用	冼丽铧	翁殊斐、姜春宁、秦新生、胡盛劼、李自若	林学与风景园林学院
43	智慧培育类课程	耕作学	王小龙	祁剑英、陈健文、王媛媛、潘圣刚	农学院
44	智慧培育类课程	抽样调查	杨志程	肖莉、周燕	数学与信息学院、软件学院
45	智慧培育类课程	运筹学	杨振刚	余平祥	数学与信息学院、软件学院
46	智慧培育类课程	计算机组成原理	黄沛杰	王春桃、杨磊、万军洲、肖克辉	数学与信息学院、软件学院
47	智慧培育类课程	机器视觉自动检测技术	杨意	刘金龙，潘哲朗，翁嘉文，杨初平	电子工程学院（人工智能学院）
48	智慧培育类课程	统计学导论	夏英俊	肖莉、徐小红、周燕、李凤、朱玲湘、杨志程、岑冠军	数学与信息学院、软件学院
49	智慧培育类课程	计量经济学	彭泓毅	徐小红，利小玲，夏英俊	数学与信息学院、软件学院
50	智慧培育类课程	解析几何	毛卫华	刘丹，刘木伙，袁利国，黄小虎	数学与信息学院、软件学院
51	智慧培育类课程	高等数学 AI	马立华	方平、古川叶、李倩、曾庆茂、周裕中、朱艳科、文斌	数学与信息学院、软件学院
52	智慧培育类课程	普通化学	刘海峰	刘海峰、肖勇、高琼芝、刘伟鹏、禹筱元	材料与能源学院
53	智慧培育类课程	计算机图形学	廖彬	廖彬，蔡贤资，张连宽，梁茹冰，聂笃宪	数学与信息学院、软件学院
54	智慧培育类课程	插花艺术	李昕悦	李昕悦，范燕萍，玉云祎，岳跃冲	园艺学院
55	智慧培育类课程	场地生态学	李剑	高伟、冼丽铧、陈燕明、胡盛劼	林学与风景园林学院
56	智慧培育类课程	工程热力学与传热学	李成杰	李长友，张烨	工程学院
57	智慧培育类课程	高等数学 BI（经管类）	江雪萍	林利云、王雪琴、赵峰、尤雪莲	数学与信息学院、软件学院
58	智慧培育类课程	音乐鉴赏	胡远慧	叶妮、吴倩晴、佟羽佳、方晓青、刘敏	艺术学院
59	智慧培育类课程	数据分析可视化	古万荣	张大斌，熊俊涛，余平祥，韦婷婷	数学与信息学院、软件学院
60	智慧培育类	善境伦理	高伟	李晖、刘小蓓、古德泉、夏宇、陈	林学与风景园

项目批准号	32401725
申请代码	C1303
归口管理部门	
依托单位代码	51064208A0499-0932

国家自然科学基金

资助项目计划书

（包干制项目）

资助类别：青年科学基金项目

亚类说明：

附注说明：

项目名称：基于烟分析法的稻谷深床干燥能量优化及其模型预测控制研究

资助经费：30万元　　执行年限：2025.01-2027.12

负 责 人：李成杰　　BRID：00807.00.95190

通讯地址：广东省广州市天河区五山路483号华南农业大学

邮政编码：510642　　电　　话：[redacted]

电子邮件：[redacted]

依托单位：华南农业大学

联 系 人：唐家林　　电　　话：020-85280070

填表日期：2024年08月23日

国家自然科学基金委员会制

Version：1.002.396

国家自然科学基金资助项目计划书填报说明

（包干制项目）

一、项目负责人收到《国家自然科学基金资助项目批准通知》（以下简称《批准通知》）后，请认真阅读本填报说明，参照国家自然科学基金相关项目管理办法和新修订的《国家自然科学基金资助项目资金管理办法》（以下简称《资金管理办法》，请查阅国家自然科学基金委员会官方网站首页“政策法规”栏目），按《批准通知》的要求认真填写和提交《国家自然科学基金资助项目计划书》（以下简称《计划书》）。

二、填写《计划书》时要科学严谨、实事求是、表述清晰、准确。《计划书》经国家自然科学基金委员会相关项目管理部门审核批准后，将作为项目研究计划执行、检查和验收的依据。

三、《计划书》各部分填写要求如下：

（一）简表：由系统自动生成。

（二）摘要及关键词：各类获资助项目都应当填写中、英文摘要及关键词。

（三）正文：

1. 青年科学基金项目、青年学生基础研究项目：如果《批准通知》所附“项目评审意见及修改意见表”中“修改意见”栏目没有修改要求的，只需选择“研究内容和研究目标按照申请书执行”即可；如果《批准通知》中上述栏目明确要求调整研究期限或研究内容等的，须选择“根据研究方案修改意见更改”并填报相关修改内容。

2. 国家杰出青年科学基金项目和优秀青年科学基金项目按下列提纲撰写：

（1）研究方向；

（2）结合国内外研究现状，说明研究工作的学术思想和科学意义（限两个页面）；

（3）研究内容、研究方案及预期目标（限两个页面）；

（4）年度研究计划；

四、资助经费相关要求：

1. 资助经费批准时不再区分直接费用和间接费用。

2. 项目负责人在提交计划书时需签署承诺书，承诺尊重科研规律，弘扬科学家精神，遵守科研伦理道德和作风学风诚信要求，认真开展科学研究工作；承诺项目经费全部用于与本项目研究工作相关的支出，不得用于与本项目研究无关的支出。

3. 项目负责人提交计划书时，无需编制项目预算。项目资金由项目负责人自主决定使用，按照《资金管理办法》第九条规定的开支范围列支。有关管理费用的补助支出，由依托单位根据实际管理需要，在充分征求项目负责人意见基础上合理确定。绩效支出由项目负责人根据实际科研需要和相关薪酬标准自主确定，依托单位按照工资制度进行管理。对于青年学生基础研究项目，支付给项目负责人本人的劳务费用，应符合相关比例要求。其余用途经费无额度限制，由项目负责人根据实际需要自主决定使用。

4. 项目结题时，项目负责人根据实际使用情况编制项目经费决算，经依托单位财务、科研管理部门审核后，报自然科学基金委。依托单位应当在单位内部公开非涉密项目立项、主要研究人员、资金使用（重点是间接费用、外拨资金、结余资金使用等）、决算、大型仪器设备购置以及项目研究成果等情况，接受内部监督。
5. 自然科学基金委结合项目管理，对经费使用情况和依托单位管理情况定期开展抽查。

简表

项目负责人信息	姓　　名	李成杰	性 别	男	出生年月	[redacted]	民 族	汉族
	学　　位	博士			职称	副教授		
	是否在站博士后	否			电子邮件	[redacted]cn		
	电　　话	[redacted]			个人网页			
	工 作 单 位	华南农业大学						
	所 在 院 系 所	工程学院						
依托单位信息	名　　称	华南农业大学					代码	51064208A0499
	联 系 人	唐家林			电子邮件	kycjhk@scau.edu.cn		
	电　　话	020-85280070			网站地址	http://kjc.scau.edu.cn/		
合作单位信息	单 位 名 称							
项目基本信息	项 目 名 称	基于㶲分析法的稻谷深床干燥能量优化及其模型预测控制研究						
	资 助 类 别	青年科学基金项目			亚 类 说 明			
	附 注 说 明							
	申 请 代 码	C1303:农业生物系统工程学			C2001:食品原料学			
	基 地 类 别							
	执 行 年 限	2025.01-2027.12						
	资 助 经 费	30万元						

项目摘要

中文摘要：

稻谷干燥过程控制目前主要依赖经验手动、开环操作，无法实现干燥机用能的精准管理，是导致能量利用率低下的重要原因之一，严重阻碍了产地干燥推广。问题的根源在于，现有干燥节能方法仅考虑单一热势场，未能揭示深床干燥热、力多势场协同作用的复杂耦合关系，能量优化效果缺乏保障。前期研究基于㶲分析法初步揭示了稻谷干燥能量传递和转换规律，指明了优化干燥用能的研究方向。本项目拟深入探究稻谷干燥耗能的本质，以㶲驱动为尺度，揭示水分汽化及迁移过程的㶲消耗规律，阐明多势场耦合下㶲传递和转换机制，制定能量优化准则，实现客观㶲的高效利用和主观㶲的合理匹配。同时，以自由能为尺度，解析稻谷物性变化特征并建立定量特征参数，摆脱传递系数限制，构建基于马尔可夫过程的控制模型。最后，融合能量优化准则和控制模型，设计分层模型预测控制器，准确、高效地实现能量优化。研究成果将为解决干燥能量利用率低下的关键共性问题提供理论依据和技术基础。

Abstract：

The current paddy drying process control heavily relies on empirical manual and open-loop operations, preventing precise management of the dryer's energy utilization. This is a significant contributor to low energy efficiency and poses a considerable barrier to the promotion of on-site drying. The core issue lies in the existing drying energy-saving methods, which solely focus on a single thermal potential field, failing to capture the intricate coupling relationships and synergistic effects between thermal and mechanical multi-potential fields in deep-bed drying. This lack of comprehension undermines the effectiveness of energy optimization. Previous research, leveraging exergy analysis, has begun to unveil the laws governing energy transfer and conversion during paddy drying, offering a clear direction for optimizing drying energy usage. This project aims to delve deeper into the essence of energy consumption in paddy drying. By employing exergy drive as a metric, we aim to reveal the patterns of exergy consumption during water vaporization and migration processes. Additionally, we seek to elucidate the mechanisms of exergy transfer and conversion under multi-potential field coupling, establishing energy optimization criteria that enable efficient utilization of objective exergy and rational matching of subjective exergy. Concurrently, using free energy as the metric, the project aims to analyze the physical property changes of paddy, establishing quantitative characteristic parameters. This will enable us to overcome the limitations of transfer coefficients and construct an accurate control model based on Markov processes. Finally, by integrating the energy optimization criteria with the control model, we will design a hierarchical model predictive controller that achieves precise and efficient energy optimization. This will provide both theoretical and technological foundations for addressing the critical and common issue of low drying energy utilization efficiency.

关键词(用分号分开)：干燥处理；工程工艺；稻谷；能量优化；模型预测控制

Keywords(用分号分开)： Drying; Engineering Process; Paddy; Energy Optimization; Model Predictive Control

报告正文

研究内容和研究目标按照申请书执行。

国家自然科学基金项目负责人、依托单位承诺书

国家自然科学基金项目负责人承诺书

本人郑重承诺：我接受国家自然科学基金的资助，严格遵守中共中央办公厅、国务院办公厅《关于进一步加强科研诚信建设的若干意见》《关于进一步弘扬科学家精神加强作风和学风建设的意见》《关于加强科技伦理治理的意见》《科技伦理审查办法（试行）》等规定，和国家自然科学基金委员会关于资助项目管理、项目资金管理等各项规章，在《计划书》填写及项目执行过程中：

（一）按照《批准通知》《国家自然科学基金资助项目计划书填报说明》的要求填写《计划书》，未自行降低、更改目标任务或约定要求，或缩减研究（研制）内容；

（二）树立“红线”意识，严格履行科研合同义务，按照《计划书》负责实施本项目（批准号：32401725），切实保证研究工作时间，按时报送有关材料，及时报告重大情况变动，不违规将科研任务转包、分包他人，不以项目实施周期外或不相关成果充抵交差；

（三）遵守科研诚信、科技伦理规范和学术道德，认真开展研究工作，对资助项目发表的论著和取得的研究成果按规定进行标注，不在非本项目资助的成果或其他无关成果上标注本项目批准号，反对无实质学术贡献者“挂名”，不在成果署名、知识产权归属等方面侵占他人合法权益，并如实报告本人及项目组成员发生的违背科研诚信要求的任何行为；

（四）尊重科研规律，弘扬科学家精神，严谨求实，追求卓越，反对浮夸浮躁、投机取巧，不人为夸大学术或技术价值，不传播未经科学验证的现象和观点；

（五）将项目资金全部用于与本项目研究工作相关的支出，并结合科研活动需要，科学合理安排项目资金支出进度；

（六）做好项目组成员的教育和管理，确保遵守以上相关要求。

如违背上述承诺，本人愿接受国家自然科学基金委员会和相关部门做出的各项处理决定。

项目负责人（签字）：

2024 年 8 月 20 日

国家自然科学基金项目依托单位承诺书

我单位同意承担上述国家自然科学基金项目，将保证项目负责人及其研究队伍的稳定和研究项目实施所需的条件，严格遵守中共中央办公厅、国务院办公厅《关于进一步加强科研诚信建设的若干意见》《关于进一步弘扬科学家精神加强作风和学风建设的意见》《关于加强科技伦理治理的意见》《科技伦理审查办法（试行）》等规定，和国家自然科学基金委员会有关资助项目管理、项目资金管理、科研诚信管理和科技伦理管理等各项规定，并督促实施。

依托单位（公章）：

2024 年 9 月 2 日

国家自然科学基金资助项目签批审核表

本栏目由自然科学基金委填写

科学处审查意见：

同意按计划书内容执行

负责人（签章）：李兴峰

2024年 10月 17日

科学部审查意见：

同意科学处意见

负责人（签章）：吕群燕

2024年 10月 17日

受理编号：c25140500000857

项目编号：2025A1515011276

文件编号：粤基金字〔2025〕10号

广东省基础与应用基础研究基金项目

任务书

项目名称：微波协同热风干燥油茶果爆蒲热湿传递特性及茶蒲失水形变机制

项目类别：广东省自然科学基金-面上项目

项目起止时间：2025-01-01 至 2027-12-31

管理单位（甲方）：广东省基础与应用基础研究基金委员会

依托单位（乙方）：华南农业大学

通讯地址：广东省广州市天河区五山路483号

邮政编码：510642 单位电话：020-85283435

项目负责人：李成杰 联系电话：[redacted]

（广东科技微信公众号） （查看任务书信息） （受理纸质材料二维码）

广东省基础与应用基础研究
基金委员会
二〇二〇年制

填写说明

一、项目任务书内容原则上要求与申报书相关内容保持一致，不得无故修改。

二、项目承担单位通过广东省科技业务管理阳光政务平台下载项目任务书，按要求完成签名盖章后扫描上传到广东省科技业务管理阳光政务平台。

三、签名盖章说明。请分别在单位工作分工及经费分配情况页、人员信息页、签约各方页等地方按要求签字或盖章，签章不合规或错漏将不予受理。其中，人员信息页要求所有参与人员本人亲笔签名，代签或印章无效，漏签将不予受理。

四、本任务书自签字并加盖公章之日起生效，各方均应负本任务书的法律责任，不应受机构、人事变动影响。

五、根据《广东省科学技术厅广东省财政厅关于深入推进省基础与应用基础研究基金项目经费使用“负面清单+包干制”改革试点工作的通知》（粤科规范字〔2022〕2号），2022年度及以后立项资助的全部省基金项目(包括省自然科学基金、省市联合基金、省企联合基金项目等)均适用“负面清单+包干制”，项目提交申请书和任务书时无需编制费用明细科目预算。

一、主要研究内容和要达到的目标

研究内容：

1 微波协同热风加热油茶果物性变化定量特征参数及干燥动力学分析

1）试验和理论考察微波所载能量对茶蒲吸附茶籽水分的热力边界层的微构变化规律、茶蒲形貌特征、组织功能演变机理；

2）分析并考证双场协同干燥动态不可逆过程的去水速率、过程动力、过程阻力的关系；

3）研究微波协同热风不同处理工艺条件下，爆蒲形成的差异性特征及主控因素，微波、热风与油茶果相互作用产生热机制、机械机制以及空化机制与爆蒲形成之间的关系；

4）研究微波加热特征参数值与干燥介质、油茶果介质匹配关系，分析强化传热、加快水分迁移速率及能量损耗，探究爆蒲与应力张量和热通量矢量本构关系，将双场协同干燥系统的主要物理量组合成无量纲的准则数。

2 油茶果热湿传递特性分析及爆蒲机理

1）研究双场协同干燥系统、平衡水分及系统状态参数制约关系，在焓-含湿量图上绘制出量出入的界限线，获得双场协同干燥动力学方程；

2）研究干燥过程茶蒲微观孔道结构发生改变时，其表面裂纹及正剖面区域含水率变化的差异性，分析双场协同作用的效果及差异性；

3）构建干燥过程茶籽与茶蒲结合水分移动模型；

4）应用弹塑性力学分析方法，考察干燥过程茶蒲结合层应力与结构强度的演变规律及影响机制，构建爆蒲模型。

3 茶蒲失水形变机制探究与试验验证

1）考察干燥过程茶蒲应力裂纹形成扩展与各条件因素的作用关系，检测过程的形态变化；

2）分析茶蒲形变量、形变率等力学特征参数受油茶果几何结构、含水率、环境参数和干燥参数等过程要素的影响机制，得到茶蒲撕裂条件理论模型；

3）基于茶蒲的黏弹性体形变特征受时间、温度和含水率的影响机制，构建蠕变型本构方程，结合油茶果的三维几何特征及应力平衡方程，构建茶蒲失水过程的形变预测模型；

4）将水分移动模型与形变预测模型进行耦合并求解，获得油茶果干燥过程应力分布云图，分析整果湿热应力变化规律，揭示完整过程应力形成及演变机理，并进行干燥工艺优化。

要达到的目标：

1）系统剖析茶蒲的力学特性与油茶果在干燥过程中的热湿传递规律、微波能量吸收及其分布特征之间的内在关联，揭示爆蒲的本质机理，并构建精确的爆蒲模型，以实现爆蒲过程的充分性和高效性。

2）全面研究茶蒲完整性受干燥参数、物料物性参数及过程特征等多重因素影响的动态规律，深入揭示茶蒲在失水过程中的形变机制，并建立相应的形变预测模型，以确保爆蒲后籽蒲易于分离，满足产业化的实际需求。

二、项目预期获得的研究成果及形式

论文及专著情况	国家统计源刊物以上刊物发表论文（篇）		3		科技报告（篇）		0	
	其中被SCI/EI/ISTP收录论文数（篇）		2		培养人才（人）		2	
	专著（册）		0		引进人才（人）		0	
专利情况(项)	发明专利		实用新型专利		外观设计专利		国外专利	
	申请	授权	申请	授权	申请	授权	申请	授权
	2	1	0	0	0	0	0	

三、项目进度和阶段目标

（一）项目起止时间： 2025-01-01 至 2027-12-31		
（二）项目实施进度及阶段主要目标:		
开始日期	结束日期	主要工作内容
2025-01-01	2025-12-31	1搭建微波协同热风干燥综合试验台，分析油茶果干燥物性特征参数、热特性参数、动平衡含水率、热力学参数的变化特征，建立干燥动力学模型。 2完善油茶果薄层干燥理论，分析动态过程水分扩散系数、活化能、导热系数的变化规律，并建立拟合方程。 期间，对已获得的部分研究成果进行整理和总结，拟参加国内外相关的学术会议，与同行专家进行交流和探讨。
2026-01-01	2026-12-31	1构建油茶果热风干燥多相解析模型，分析过程要素对干燥状态参数的影响规律，揭示其微波协同热风干燥热质传递特性。 2分析干燥过程力学特征参数的变化规律，得到茶蒲撕裂条件理论解，构建爆蒲模型。 3揭示茶蒲失水过程应力形成及演变机理，构建形变预测模型。 期间，拟与澳大利亚昆士兰科技大学、加拿大英属哥伦比大学相关专家进行学术交流，对试验中取得的进展及遇到的问题进行深入探讨。
2027-01-01	2027-12-31	1搭建油茶果干燥-脱蒲-清选一体化作业装置，分析内外部因素对爆蒲的影响效果及籽蒲分离机制，获得最优干燥参数及分离清选工艺参数，并进行综合验证试验。 2系统总结研究创新成果，进一步确认理论、模型、方法和算法，聘请相关专家和用户代表听取汇报，根据专家意见完善项目成果，做好结题工作，并为下一步的拓展研究做准备。

四、项目总经费及省基金委经费预算

1.省基金委经费下达总额： （大写）壹拾万圆整；（小写 ）10万元；					
2.省基金委经费年度下达计划：					
年度	2025 年	年	年	年	年
经费(万元)	10.00				

五、人员信息

项目负责人								
姓名	证件号码	年龄	性别	职称	学历	在项目中承担的任务	所在单位	签名
李成杰	[redacted]	[redacted]	男	副教授	博士研究生	项目负责人	华南农业大学	李成杰

项目组主要成员								
姓名	证件号码	年龄	性别	职称	学历	在项目中承担的任务	所在单位	签名
李涛	[redacted]	[redacted]	男	副教授	博士研究生	高水分多重结构分析	江西农业大学	李涛
张烨	[redacted]	[redacted]	男	高级工程师	博士研究生	一体化作业装置设计	华南农业大学	张烨
李长友	[redacted]	[redacted]	男	教授	博士研究生	爆蒲及形变理论	华南农业大学	李长友
赵懿琨	[redacted]	[redacted]	女	讲师	博士研究生	微波场能量分布特征研究	华南农业大学	赵懿琨
肖志锋	[redacted]	[redacted]	男	副教授	博士研究生	热湿传递特性分析	江西农业大学	肖志锋
黄建江	[redacted]	[redacted]	男	未取得	本科	物性检测试验	华南农业大学	黄建江
李圣陶	[redacted]	[redacted]	男	未取得	本科	模型验证试验	华南农业大学	李圣陶
徐辉龙	[redacted]	[redacted]	男	未取得	本科	数据采集与处理	江西农业大学	徐辉龙

六、工作分工及财政经费分配

承担/参与单位名称（盖章）	工作分工	省级财政科技资金分配（万元）
华南农业大学	负责项目的整体策划、组织和管理。需要制定详细的项目研究计划和预期成果，确保项目的科学性和可行性。负责整合项目所需的各类资源，包括研究团队、实验设备、资金等。通过与合作伙伴建立紧密的合作关系，确保项目能够顺利推进并取得预期成果。一旦项目获得资助，将承担项目的主要责任，包括项目的执行、监督、评估和结题等各个环节。同时，还需要对项目的成果进行宣传和推广，提高项目的社会影响力和学术价值	7.00
江西农业大学	利用具备的技术或资源优势，为项目提供必要的技术支持和协助。与牵头单位的紧密合作，共同推进项目的进展。为项目提供必要的资源支持，如实验设备、场地、数据等，助于提升项目的整体研究水平。在项目取得成果后，有权分享项目的成果和收益。这有助于激发合作单位的积极性和创造力，促进科研项目的长期发展。	3.00
	合计	10.00

七、任务书条款

第一条 甲方与乙方根据《中华人民共和国民法典》及国家有关法规和规定，按照《广东省自然科学基金及联合基金项目管理实施细则》（粤科规范字〔2024〕5号）《省级科技计划项目任务书管理细则》（粤科规范字〔2022〕8号）等规定，为顺利完成（2025）年微波协同热风干燥油茶果爆蒲热湿传递特性及茶蒲失水形变机制专项项目（项目编号：2025A1515011276）经协商一致，特订立本任务书，作为甲乙双方在项目实施管理过程中共同遵守的依据。

第二条 甲方的权利义务：1.按任务书规定进行经费核拨的有关工作协调。2.根据甲方需要，在不影响乙方工作的前提下，定期或不定期对乙方项目的实施情况和经费使用情况进行检查或抽查。3.根据《广东省科学技术厅科技计划项目科研诚信管理办法》（粤科规范字〔2024〕2号）《广东省基础与应用基础研究基金项目科研不端行为调查处理实施细则（试行）》（粤科规范字〔2023〕1号）等规定对乙方进行科技计划信用管理。

第三条 乙方的权利义务：1.确保落实自筹经费及有关保障条件。2.按任务书规定，对甲方核拨的经费实行专款专用，单独列账，并随时配合甲方进行监督检查。3.经费使用按照广东省级财政科研项目经费使用及省基金项目经费使用“负面清单+包干制”等有关规定进行管理。4.项目依托单位应制定经费使用“负面清单+包干制”内部管理制度并报甲方备案。5.使用财政资金采购设备、原材料等，按照《广东省实施〈中华人民共和国招标投标法〉办法》有关规定，符合招标条件的须进行招标。6.项目任务书任务完成后，或任务书规定的任务、指标及经费投入等提前完成的，乙方可提出验收结题申请，并按甲方要求做好项目验收结题工作。7.若项目发生需要终止结题的情况，乙方须提出终止结题申请，并按甲方要求做好项目终止结题工作。8.在每年规定时间内向甲方如实提交上年度工作情况报告，报告内容包含上年度项目进展情况、经费决算和取得的成果等。9.按照国家和省有关规定，提交科技报告及其他材料。10.利用甲方的经费获得的研究成果，项目负责人和参与者应当注明获得“广东省基础与应用基础研究基金（英文：Guangdong Basic and Applied Basic Research Foundation）（项目编号）”资助或作有关说明。11.乙方要恪守科学道德准则，遵守科研活动规范，践行科研诚信要求，不得抄袭、剽窃他人科研成果或者伪造、篡改研究数据、研究结论；不得购买、代写、代投论文，虚构同行评议专家及评议意见；不得违反论文署名规范，擅自标注或虚假标注获得科技计划（专项、基金等）等资助；不得弄虚作假，骗取科技计划（专项、基金等）项目、科研经费以及奖励、荣誉等；不得有其他违背科研诚信要求的行为。12.确保本项目开展的研究工作符合我国科技伦理管理相关规定。

第四条 在履行本任务书的过程中，如出现广东省相关政策法规重大改变等不可抗力情况，甲方有权对所核拨经费的数量和时间进行相应调整。

第五条 在履行本任务书的过程中，当事人一方发现可能导致项目整体或部分失败的情形时，应及时通知另一方，并采取适当措施减少损失，没有及时通知并采取适当措施，致使损失扩大的，应当就扩大的损失承担责任。

第六条 本项目技术成果的归属、转让和实施技术成果所产生的经济利益的分享，除双方另有约定外，按国家和广东省有关法规执行。

第七条 根据项目具体情况，经双方另行协商订立的附加条款，作为本任务书正式内容的一部分，与本任务书具有同等效力。

第八条 本任务书一式三份，各份具有同等效力。甲、乙方及项目负责人各执一份，三方签字、盖章后即生效，有效期至项目结题后一年内。各方均应负任务书的法律责任，不应受机构、人事变动的影响。

第九条 乙方必须接受甲方聘请的本项目任务书监理单位的监督和管理。监理单位按照甲方赋予的权利对本项目任务书的履行进行审核、进度调查，对项目任务书变更、经费使用情况进行监督管理及组织项目验收。

说明：1.本任务书中，凡是当事人约定无需填写的内容，应在空白处划（/）。

2.委托代理人签订本任务书的，应出具合法、有效的委托书。

八、本任务书签约各方

管理单位（甲方）：　　广东省基础与应用基础研究基金委员会　（盖章）

法定代表人（或法人代理）：　曾路　（签章）

2025 年　03 月　21 日

依托单位（乙方）：　华南农业大学　（盖章）

法定代表人（或法人代理）：　薛红卫　（签章）

联系人（项目主管）姓名：　夏杰　（签章）

Email：　kjcgxk@scau.edu.cn

电话：　020-85285435　/　[redacted]

开户单位名称：　华南农业大学

开户银行名称：　广东广州工行五山支行

开户银行账号：　3602002609000310520

2025 年 4 月 9 日

联系人（项目负责人）姓名：　李成杰　（签名）

Email：　[redacted]

电话：　[redacted]

2025 年 4 月 8 日

任务书编号：2024A04J3960

广州市科技计划项目

任务书

项目名称：	高湿稻谷干燥节能增效机制及递阶智能控制方法研究
承担单位：	华南农业大学
项目负责人：	李成杰
计划类别：	基础研究计划
专题名称：	2024年度基础与应用基础研究专题
支持方向：	青年博士“启航”项目
组织单位：	华南农业大学
起止时间：	2024-01-01 至 2025-12-31
主管处室：	基础研究处

广州市科学技术局制

二〇二四年

填写说明

1.任务书甲方为广州市科学技术局；乙方为项目承担单位；丙方为项目组织单位。

2.任务书基于项目申报书转换而成，请按照“广州科技大脑”提示在线填写核实，若存在不填写内容的栏目，请用“无”表示；任务书中的单位名称应为规范全称，并与单位公章一致。

3.乙方与合作单位的合作协议自动从项目申报书中读取，如需变化调整，须待任务书签订后，按要求及时办理重大变更。

4.乙方完成项目任务书在线填写，依次提交丙方和甲方审核确认后，按要求登录“穗好办”APP完成电子签章。不具备电子签章条件的单位，经与业务主管处室沟通对接后，可下载电子版项目任务书用A4纸双面打印装订签章；一式六份报甲方和丙方签章，其中甲方两份丙方两份，项目承担单位和项目负责人各一份。

5.涉密项目请在“广州科技大脑”下载项目任务书模板，按保密要求离线填写报送。

6.项目申报书是项目任务书填报的重要依据，未经甲方许可，乙方不得修改考核指标，调整主要研究内容。项目任务书将作为项目实施管理、验收结题和监督评估的重要依据。

7.项目任务书中的“备注”，包括重要的必须补充的内容。

8.“广州科技大脑”是项目管理过程中重要通知和文书的电子送达平台。为确保电子送达渠道畅通，乙方和项目负责人应及时更新维护“广州科技大脑”的单位和个人信息。

9.根据相关要求，项目涉及人体临床研究的，项目需经医学伦理委员会审查通过并在任务书附件栏上传相关佐证材料。

一、项目基本信息

项目基本信息	项目名称	高湿稻谷干燥节能增效机制及递阶智能控制方法研究
	申请市财政科技经费	5(万元)
	研究期限	2（年）
项目摘要	高湿稻谷干燥是保障其产后质量安全的重要阶段，干燥过程能耗高是行业亟待解决的问题。由于粮食水分结合能及干燥系统特征函数已揭示并获得了分析解，明确了高湿粮食自身携带有客观干燥势这一事实，继而从质焓驱动机理入手揭示高湿稻谷干燥节能增效机制。本项目拟分析高湿稻谷干燥系统焓传递和转换特征，得到焓匹配准则，并基于递阶策略设计智能控制器以实现高湿稻谷干燥过程客观焓和主观焓的合理匹配，寻求一种干燥节能调控新方法。	

二、项目单位情况

项目承担单位	单位名称	华南农业大学	统一社会信用代码	12440000455416563 4
	注册时间	1952-01-01	单位类型	高等院校
	注册地址	广东省广州市天河区五山路483号		
	办公地址	广东省广州市天河区五山路483号		
	联系人	姓名	倪慧群	
		手机号码	[redacted]	
		电子邮箱	kjcgxk@scau.edu.cn	
	开户银行	广东广州工行五山支行		
	开户户名	华南农业大学		
	银行账号	3602002609000310520		

三、项目负责人信息

姓名	李成杰	证件类型	身份证
证件号码	[redacted]	性别	男
出生日期	[redacted]	民族	汉族
国籍	中国	学历	博士研究生
学位	博士	学位授予国家（或地区）	中国
职务	教师	职称	无
所学专业	农业机械化工程	手机号码	[redacted]
办公电话	020-85280817	电子邮箱	[redacted]

四、项目经费信息

本项目总投入：¥（5）万元，其中，市财政科技经费：¥（5）万元，自筹经费：¥（0）万元。

经费下达计划			
资金来源	小计	市财政科技经费	自筹经费
2024	5	5	0
总计	5	5	0

（单位：万元）

注：本专题纳入“包干制”，市财政科技经费按市科技计划项目经费“包干制”相关规定执行。

五、预期代表性成果

项目负责人在项目实施期内，以该项目作为资助项目获得以下5种情形之一且经费使用符合规定的，由组织单位审核后通过验收。

（一）项目实施期内，以第一作者/通讯作者发表论文1篇或以上（须标注资助项目编号）；

（二）项目实施期内，以第一完成人申请或授权专利、软件著作1项或以上；

（三）项目实施期内，获省级以上科技计划项目或人才项目支持1项或以上；

（四）项目实施期内，获省级以上科技奖励（含列入获奖团队成员名单）1项或以上；

（五）项目实施期内，获得职称晋升。

六、备注

专题补充约定条款：

甲方对未履行勤勉尽责义务的相关责任主体，自作出处理结论之日起，依照法律法规规定或任务书约定实施惩戒5年，取消相关责任主体申报市科技计划项目、申领市科技计划项目经费的资格。

预期代表性成果需在实施期内获得。

项目承担单位（乙方）及项目负责人承诺书

承诺书

本单位/本人作为广州市科技计划项目承担单位/项目负责人，将严格遵守广州市科技计划管理相关规定，严格履行自身责任，加强对项目组人员及合作单位的管理，在此郑重承诺：

（一）确保与本项目有关的全部材料真实、合法、有效，未侵犯其他方知识产权等权利，不存在多头申报、重复申报行为；

（二）严格遵守《广州市科技创新条例》《广州市科技计划项目管理办法》《广州市科技计划项目经费管理办法》《广州市科技计划科技报告管理办法》等相关规定，实施项目和经费管理；

（三）严格遵守国家、省、市关于科研诚信和科技伦理的有关法律、法规，相关政策以及各项规定，加强项目实施过程中的科研诚信及科技伦理管理，恪守科研道德准则。

如有违反，本单位/本人愿意接受相关部门做出的各项处理决定，包括但不限于终止项目、停拨经费、核减经费、追回经费，取消一定期限广州市科技计划项目申报资格，记入科研失信行为数据库，将不良行为向社会公开等。

项目承担单位：华南农业大学

日期：2023年12月16日

项目负责人：李成杰

日期：2023年12月15日

任务书签署

甲乙丙三方根据《广州市科技计划项目管理办法》《广州市科技计划项目经费管理办法》《广州市科技计划科技报告管理办法》等有关文件规定，以及有关法律、政策和管理要求，签署本任务书。

签订地点：广州市越秀区

广州市科学技术局（甲方）：广州市科学技术局
局项目经办人：蒋韬略　　联系电话：83124150
责任处室负责人：麦胜文

2024年01月17日

项目承担单位（乙方）：华南农业大学
二级部门：华南农业大学工程学院
项目负责人：李成杰
项目经费汇入账号
账户名：华南农业大学　　账号：3602002609008810520
开户银行：广东广州工行五山支行
财务负责人：肖斐

2023年12月16日

组织单位（丙方）：华南农业大学
项目经办人：倪慧群

2023年12月18日

88

项目批准号	32171906
申请代码	C1302
归口管理部门	
依托单位代码	51064208A0499-0932

国家自然科学基金

资助项目计划书

（预算制项目）

资助类别：面上项目

亚类说明：

附注说明：测量加工一体化理论方法与技术

项目名称：粮食干燥准则及工艺过程解析理论研究

直接费用：58万元　　执行年限：2022.01-2025.12

负 责 人：李长友

通讯地址：广东省广州市天河区五山路483号

邮政编码：510642　　电　　话：[redacted]

电子邮件：[redacted]

依托单位：华南农业大学

联 系 人：唐家林　　电　　话：020-85280070

填表日期：2021年10月19日

261

国家自然科学基金委员会制

Version：1.015.841

国家自然科学基金资助项目计划书填报说明
（预算制项目）

一、项目负责人收到《国家自然科学基金资助项目批准通知》（以下简称《批准通知》）后，请认真阅读本填报说明，参照国家自然科学基金相关项目管理办法和新修订的《国家自然科学基金资助项目资金管理办法》（以下简称《资金管理办法》，请查阅国家自然科学基金委员会官方网站首页“政策法规”栏目），按《批准通知》的要求认真填写和提交《国家自然科学基金资助项目计划书》（以下简称《计划书》）。

二、填写《计划书》时要科学严谨、实事求是、表述清晰、准确。《计划书》经国家自然科学基金委员会相关项目管理部门审核批准后，将作为项目研究计划执行、检查和验收的依据。

三、《计划书》各部分填写要求如下：

（一）简表：由系统自动生成。

（二）摘要及关键词：各类获资助项目都应当填写中、英文摘要及关键词。

（三）项目组主要成员：计划书中列出姓名的项目组主要成员由系统自动生成，与申请书原成员保持一致，不可随意调整。如果《批准通知》所附“项目评审意见及修改意见表”中“修改意见”栏目有调整项目组成员相关要求的，待项目开始执行后，按照项目成员变更程序另行办理。

（四）资金预算表：根据批准的项目资助额度，按规定调整项目预算，并按照《国家自然科学基金项目计划书预算表编制说明》填报资金预算表和预算说明书。

（五）正文：

1. 面上项目、地区科学基金项目：如果《批准通知》所附“项目评审意见及修改意见表”中“修改意见”栏目没有修改要求的，只需选择“研究内容和研究目标按照申请书执行”即可；如果《批准通知》中上述栏目明确要求调整研究期限或研究内容等的，须选择“根据研究方案修改意见更改”并填报相关修改内容。

2. 重点项目、重点国际（地区）合作研究项目、重大项目、国家重大科研仪器研制项目、原创探索计划项目：须选择“根据研究方案修改意见更改”，根据《批准通知》的要求填写研究（研制）内容，不得自行降低、更改研究目标（或仪器研制的技术性能与主要技术指标、验收技术指标等）或缩减研究（研制）内容。此外，还要突出以下几点：

（1）研究的难点和在实施过程中可能遇到的问题（或仪器研制风险），拟采用的研究（研制）方案和技术路线；

（2）项目主要参与者分工，合作研究单位（如有）之间的关系与分工，重大项目还需说明课题之间的关联；

（3）详细的年度研究（研制）计划。

3. 创新研究群体项目：须选择“根据研究方案修改意见更改”，按下列提纲撰写：

（1）研究方向；

（2）结合国内外研究现状，说明研究工作的学术思想和科学意义（限两个页面）；

（3）研究内容、研究方案及预期目标（限两个页面）；

（4）年度研究计划；

（5）研究队伍的组成情况。

4. 基础科学中心项目：须选择“根据研究方案修改意见更改”，根据《批准通知》的要求和现场考察专家组的意见和建议，进一步完善并细化研究计划，按下列提纲撰写：

（1）五年拟开展的研究工作（包括主要研究方向、关键科学问题与研究内容）；

（2）研究方案（包括骨干成员之间的分工及合作方式、学科交叉融合研究计划等）；

（3）年度研究计划；

（4）五年预期目标和可能取得的重大突破等；

（5）研究队伍的组成情况。

5. 对于其他类型项目，参照面上项目的方式进行选择和填写。

简表

项目负责人信息	姓　　名	李长友	性 别	男	出生年月	[redacted]	民 族	汉族
	学　　位	博士			职称	教授		
	是否在站博士后	否			电子邮件	[redacted]		
	电　　话	020-85280817			个人网页			
	工 作 单 位	华南农业大学						
	所 在 院 系 所	工程学院						
依托单位信息	名　　称	华南农业大学					代码	51064208A0499
	联 系 人	唐家林			电子邮件	kycjhk@scau.edu.cn		
	电　　话	020-85280070			网站地址	http://kjc.scau.edu.cn/		
合作单位信息	单 位 名 称							
项目基本信息	项 目 名 称	粮食干燥准则及工艺过程解析理论研究						
	资 助 类 别	面上项目			亚 类 说 明			
	附 注 说 明	测量加工一体化理论方法与技术						
	申 请 代 码	C1302:农艺农机学			C2001:食品原料学			
	基 地 类 别							
	执 行 年 限	2022.01-2025.12						
	直 接 费 用	58万元						

项目摘要

中文摘要：

粮食干燥关系国计民生和国家发展战略，其生态、经济、社会地位重要。解决干燥系统存在的能耗高，效率低，开环控制，缺少科学、公平、客观评价工艺装备系统能效的标准等共性问题是实施国家乡村振兴战略的重大需求和经济主战场。由于粮食水分结合能及干燥特征函数已经揭示并获得了分析解，克服了基于单一行为描述的质量、热量、动量传递定律没有严格意义数学解的缺陷，肯定了干燥服从马尔科夫过程，这使获得干燥相似准则和基于工艺能力指数得到实际过程理论解成为可能。为此，本研究针对源自于自然环境的有限介质及干燥烟随物系组分迁移状态变化特征，揭示粮食在不同工艺条件下的干燥现象相似准则，研究干燥品质、能耗和过程要素间的制约关系和物理机制，获得干燥准则，得到工艺过程理论解，基于客观烟高效利用和主观烟合理匹配，实现优质、高效节能干燥，基于云服务、远程双向通信、自适应控制技术，实现粮食产地智能干燥，引领绿色干燥技术革新。

Abstract:

Grain drying is the key issue affecting the national economy, people's livelihood and national development strategy, and its ecological, economic and social status is very important. To solve the common problems of drying system, which includes high energy consumption, weak efficiency, open-loop control, lack of scientific, fair and objective evaluation standards of process equipment system energy efficiency, is the major demand and economic main battlefield for the implementation of National Rural Revitalization Strategy. In our previous work, we have revealed the drying characteristic function of grain moisture binding energy and obtained the analytical solution based on the corresponding medium dynamic change, which overcomes the shortcomings of the tradition drying model based on the laws of mass, heat and momentum. The drying process is confirmed to obey the Markov process, which makes it possible to obtain the theoretical solution of drying similarity criterion and actual practical process. Therefore, present work focuses on the variation characteristics of limited medium from the natural environment and the drying exergy with the migration state of system components, aims to reveal the similarity criterion of grain drying phenomenon under different process conditions. The restriction relationship and physical mechanism among drying quality, energy consumption and process factors were also studied. The mathematical expression of the exergy transfer and conversion for physical property change in different drying process was also obtained. The objective of the present work is to solve the bottleneck restricting the intelligent drying in grain producing area and further realize the intelligent drying based on the cloud services. Moreover, based on efficient utilization of objective exergy and reasonable matching of subjective exergy, the another objective is to realize high-quality, efficient and energy-saving drying, expand the scientific frontier, and lead the technological innovation of green energy-saving drying equipment.

关键词(用分号分开)：农机智能化；智能测控与控制算法；干燥工艺装备；农机远程监控；干燥解析理论

Keywords(用分号分开): Intelligent agricultural machinery; Intelligent measurement and control algorithm; Drying equipment; Remote monitoring of agricultural machinery; Analytical theory of drying

项目组主要成员

编号	姓名	出生年月	性别	职称	学位	单位名称	电话	证件号码	项目分工	每年工作时间（月）
1	李长友	[redacted]	男	教授	博士	华南农业大学	[redacted]	[redacted]	项目负责人	6
2	张烨		男	高级工程师	博士	华南农业大学			物性试验	6
3	张永博		男	讲师	硕士	华南农业大学			计算机软件	6
4	李成杰		男	博士生	硕士	华南农业大学			在线检测与智能控制系统	8
5	张雪峰		男	博士生	硕士	华南农业大学			能效评价理论	8
6	黎斌		男	博士生	硕士	华南农业大学			传递和转换理论	8
7	孟敏刚		男	硕士生	学士	华南农业大学			智能控制系统	8
8	黄隽盈		女	硕士生	学士	华南农业大学			试验测定	8

总人数	高级	中级	初级	博士后	博士生	硕士生
8	2	1			3	2

国家自然科学基金预算制项目预算表

项目批准号：32171906　　项目负责人：李长友　　金额单位：万元

序号	科目名称	金额
1	一、基金资助项目直接费用合计	58.0000
2	1、 设备费	0.0000
3	其中：设备购置费	0.0000
4	2、 业务费	39.0000
5	3、 劳务费	19.0000
6	二、 其他来源资金	0.0000
7	三、 合计	58.0000

注：请按照项目研究实际需要合理填写各科目预算金额。

预算说明书

（请按照《国家自然科学基金项目计划书预算表编制说明》等的有关要求，按照政策相符性、目标相关性和经济合理性原则，实事求是编制项目预算。填报时，直接费用应按设备费、业务费、劳务费三个类别填报，每个类别结合科研任务按支出用途进行说明。填报时，对单价≥50万元的设备详细说明，对单价＜50万元的设备费用分类说明，**对合作研究单位资质及资金外拨情况、自筹资金进行必要说明。**）

1.设备费：0万元。

2.业务费：39万元。其中，材料费2万元，测试化验加工费19万元，燃料动力费0万元，差旅/会议/国际合作与交流费10万元，出版/文献/信息传播/知识产权事务费8万元，其他支出0万元。具体支出明细如下：

（1）材料费：2万元。实施6因素，5水平及特定单因素试验，需要进行200次，每次试验需要的试验原料和、辅助耗材、低值测试皿等易耗品计0.01万元，小计2万元。

（2）测试化验加工费：19万元。主要用于课题实施过程中针对主要作物种子，在几何物性（宏观特征）测定的基础上，分为2类，10组，分别测定，迁移组分、水分活度，质构、微观形貌及其动态变化特征、玻璃化转变特性，在测定的基础数据的基础上，对其过程进行能效评价分析。试验测定，4年共需测定2000个样次，每个样次75元，小计15万元；玻璃化转变特性测定，4年共需测试样品200个，150元/个，小计3万元；脂肪酸测定4年共需测试样品500个，每个样品20元，小计1万元。合计19万元。

（3）燃料动力费：0万元。

（4）差旅/会议/国际合作与交流费：10万元。在项目研究过程中开展科学试验、工艺装备产地现场试验考证、学术交流等发生的差旅费及市内交通费用：正高级职称专家出差10人次，往返长途交通费（火车票、机票等）每人次3000元，住宿费每人每天300元。伙食费及市内交通费每人每天80元，每人次出差5天，小计（300元+80元）×5天×10人次+3000元×10人次=4.90万元；副高职称专家出差8人次，每人次出差4天，小计（300元+80元）×4天×8人次+2000元×8人次=2.816万元；中级职称专家出差4人次，往返长途交通费（火车票、机票等）每人次1000元，住宿费每人每天200元，伙食费及市内交通费每人每天80元，每人次出差4天，小计（200元+80元）×4天×4人次+1000元×4人次=0.848万元。研究生参加学术会议，现场试验出差12人次，往返长途交通费（火车票等）每人次600元，住宿费每人每天100元。伙食费及市内交通费每人每天50元，每人次出差4天，小计（100元+50元）×4天×12人次+600元×12人次=1.44万元。合计10.004万元，取整10万元。

（5）出版/文献/信息传播/知识产权事务费：8万元。论文版面费预计最少12篇，平均每篇预计4500元/篇，小计 5.4万元；预计申请发明专利6件，每件专利代理费申请3000元/项，小计1.8万元；国内外查新费4000元/次，委托2次，小计0.8万元；合计8万元。

（6）其他支出：0万元。

3. 劳务费：19万元。其中研究生劳务性费16万元，专家咨询费3万元。具体支出明细如下：

（1）劳务费：16万元。用于研究生的研务费，课题平均每年有3名博士生和2名硕士生参加研究，按4年计算。博士生每人每月平均按0.2万元，年补助按8个月计算，小计3人×4年×8个月×0.2万元=9.6万元，硕士生每人每月平均按0.1万元，年补助按8个月，小计2人×4年×8个月×0.1万元=6.4万元，合计16万元。

（2）专家咨询费：3万元，拟就工艺装备系统能效、能力评价咨询专家15人次，每人次2000元，小计3万元。

报告正文

研究内容和研究目标按照申请书执行。

国家自然科学基金项目负责人、依托单位承诺书

国家自然科学基金项目负责人承诺书

本人郑重承诺：我接受国家自然科学基金的资助，严格遵守中共中央办公厅、国务院办公厅《关于进一步加强科研诚信建设的若干意见》《关于进一步弘扬科学家精神加强作风和学风建设的意见》等规定，及国家自然科学基金委员会关于资助项目管理、项目资金管理等各项规章，在《计划书》填写及项目执行过程中：

（一）按照《批准通知》《国家自然科学基金资助项目计划书填报说明》的要求填写《计划书》，未自行降低、更改目标任务或约定要求，或缩减研究（研制）内容；

（二）树立“红线”意识，严格履行科研合同义务，按照《计划书》负责实施本项目（批准号：32171906），切实保证研究工作时间，按时报送有关材料，及时报告重大情况变动，不违规将科研任务转包、分包他人，不以项目实施周期外或不相关成果充抵交差；

（三）遵守科研诚信、科研伦理规范和学术道德，认真开展研究工作，对资助项目发表的论著和取得的研究成果按规定进行标注，反对无实质学术贡献者“挂名”，不在成果署名、知识产权归属等方面侵占他人合法权益，并如实报告本人及团队成员发生的违背科研诚信要求的任何行为；

（四）尊重科研规律，弘扬科学家精神，严谨求实，追求卓越，反对浮夸浮躁、投机取巧，不人为夸大学术或技术价值，不传播未经科学验证的现象和观点；

（五）将项目资金全部用于与本项目研究工作相关的支出，并结合科研活动需要，科学合理安排项目资金支出进度。

如违背上述承诺，本人愿接受国家自然科学基金委员会和相关部门做出的各项处理决定。

项目负责人（签字）：李云友

2021 年 10 月 30 日

依托单位科研管理部门：	依托单位财务管理部门：
负责人（签章）： 2021 年 11 月 1 日	负责人（签章）： 2021 年 11 月 1 日

国家自然科学基金项目依托单位承诺书

我单位同意承担上述国家自然科学基金项目，将保证项目负责人及其研究队伍的稳定和研究项目实施所需的条件，严格遵守国家自然科学基金委员会有关资助项目管理、项目资金管理和科研诚信管理等各项规定，并督促实施。

依托单位（公章）

2021 年 11 月 1 日

国家自然科学基金资助项目签批审核表

本栏目由自然科学基金委填写

科学处审查意见：

同意按计划书内容执行

负责人（签章）：罗晶

2021年 11月 11日

科学部审查意见：

同意科学处意见

负责人（签章）：徐岩英

2021年 11月 18日

项目名称： 粮食干燥准则及工艺过程解析理论研究

资助类型： 面上项目/测量加工一体化理论方法与技术

申请代码： C1302.农艺农机学

国家自然科学基金项目申请人和参与者科研诚信承诺书

本人**在此郑重承诺**：严格遵守中共中央办公厅、国务院办公厅《关于进一步加强科研诚信建设的若干意见》规定，所申报材料和相关内容真实有效，不存在违背科研诚信要求的行为；在国家自然科学基金项目申请、评审和执行全过程中，恪守职业规范和科学道德，遵守评审规则和工作纪律，杜绝以下行为：

（一）抄袭、剽窃他人科研成果或者伪造、篡改研究数据、研究结论；

（二）购买、代写、代投论文，虚构同行评议专家及评议意见；

（三）违反论文署名规范，擅自标注或虚假标注获得科技计划等资助；

（四）购买、代写申请书；弄虚作假，骗取科技计划项目、科研经费以及奖励、荣誉等；

（五）在项目申请书中以高指标通过评审，在项目计划书中故意篡改降低相应指标；

（六）以任何形式探听尚未公布的评审专家名单及其他评审过程中的保密信息；

（七）本人或委托他人通过各种方式及各种途径联系有关专家进行请托、游说，违规到评审会议驻地游说评审专家和工作人员、询问评审或尚未正式向社会公布的信息等干扰评审或可能影响评审公正性的活动；

（八）向评审工作人员、评审专家等提供任何形式的礼品、礼金、有价证券、支付凭证、商业预付卡、电子红包，或提供宴请、旅游、娱乐健身等任何可能影响评审公正性的活动；

（九）其他违反财经纪律和相关管理规定的行为。

如违背上述承诺，本人愿接受国家自然科学基金委员会和相关部门做出的各项处理决定，包括但不限于撤销科学基金资助项目，追回项目资助经费，向社会通报违规情况，取消一定期限国家自然科学基金项目申请资格，记入科研诚信严重失信行为数据库以及接受相应的党纪政纪处理等。

申请人签字：李洁皮

编号	参与者姓名 / 工作单位名称（应与加盖公章一致）/ 证件号码	签字
1	**张烨** / 华南农业大学 / 4**********2	
2	**张永博** / 华南农业大学 / 6**********6	
3	**李成杰** / 华南农业大学 / 3**********9	
4	**张雪峰** / 华南农业大学 / 5**********9	
5	**黎斌** / 华南农业大学 / 5**********9	
6	**孟敏刚** / 华南农业大学 / 1**********2	
7	**黄隽盈** / 华南农业大学 / 4**********0	
8		
9		

项目名称： 粮食干燥准则及工艺过程解析理论研究
资助类型： 面上项目/测量加工一体化理论方法与技术
申请代码： C1302.农艺农机学

国家自然科学基金项目申请单位科研诚信承诺书

本单位依据国家自然科学基金项目指南的要求，严格履行法人负责制，**在此郑重承诺：**本单位已就所申请材料内容的真实性和完整性进行审核，不存在违背中共中央办公厅、国务院办公厅《关于进一步加强科研诚信建设的若干意见》规定和其他科研诚信要求的行为，申请材料符合《中华人民共和国保守国家秘密法》和《科学技术保密规定》等相关法律法规，在项目申请和评审活动全过程中，遵守有关评审规则和工作纪律，杜绝以下行为：

（一）采取贿赂或变相贿赂、造假、剽窃、故意重复申报等不正当手段获取国家自然科学基金项目申请资格；

（二）以任何形式探听未公开的项目评审信息、评审专家信息及其他评审过程中的保密信息，干扰评审专家的评审工作；

（三）组织或协助项目团队向评审工作人员、评审专家等提供任何形式的礼品、礼金、有价证券、支付凭证、商业预付卡、电子红包等；宴请评审组织者、评审专家，或向评审组织者、评审专家提供旅游、娱乐健身等任何可能影响科学基金评审公正性的活动；

（四）包庇、纵容项目团队虚假申报项目，甚至骗取国家自然科学基金项目；

（五）包庇、纵容项目团队，甚至帮助项目团队采取“打招呼”等方式，影响科学基金项目评审的公正性；

（六）在申请书中以高指标通过评审，在计划书中故意篡改降低相应指标；

（七）其他违反财经纪律和相关管理规定的行为。

如违背上述承诺，本单位愿接受国家自然科学基金委员会和相关部门做出的各项处理决定，包括但不限于停拨或核减经费，追回项目经费，取消一定期限国家自然科学基金项目申请资格，记入科研诚信严重失信行为数据库以及主要责任人接受相应党纪政纪处理等。

依托单位公章：
日期：2021 年 11月 1 日

合作研究单位公章：
日期： 年 月 日

合作研究单位公章：
日期： 年 月 日

子课题编号：2024YFD200010402　　密　　级：公开

国家重点研发计划
子课题任务书

子课题名称：主粮作物移动式烘干机变温精准干燥关键技术研发

所属课题：主粮作物移动式烘干机专用传感器与智能装备创制

所属项目：粮油作物大面积单产提升智能装备创制与智慧系统集成应用

课题牵头承担单位：农业农村部南京农业机械化研究所

子课题承担单位：华南农业大学

子课题负责人：张烨

执行期限：2024 年 12 月 至 2027 年 11 月

2024 年 12 月 11 日

填 写 说 明

一、任务书甲方即课题牵头承担单位，乙方即子课题承担单位。

二、任务书中的单位名称，请按规范全称填写，并与单位公章一致。

三、任务书中文字须用宋体小四号字填写。

四、凡不填写内容的栏目，请用“无”表示。

五、乙方完成任务书的填写，甲方审核确认后，用 A4 纸在线打印、装订、签章。一式六份报课题牵头承担单位签章，其中子课题承担单位一份，子课题负责人一份，作为课题任务书附件四份。

子课题基本信息表

<table>
<tr><td colspan="2">子课题名称</td><td colspan="5">主粮作物移动式烘干机变温精准干燥关键技术研发</td></tr>
<tr><td colspan="2">子课题编号</td><td colspan="5">2024YFD200010402</td></tr>
<tr><td colspan="2">所属课题</td><td colspan="5">主粮作物移动式烘干机专用传感器与智能装备创制</td></tr>
<tr><td colspan="2">所属项目</td><td colspan="5">粮油作物大面积单产提升智能装备创制与智慧系统集成应用</td></tr>
<tr><td colspan="2">密级</td><td colspan="2">■公开 □秘密 □机密</td><td>单位总数</td><td colspan="2">1</td></tr>
<tr><td colspan="2">子课题类型</td><td colspan="5">□基础前沿 □重大共性关键技术 ■应用示范研究 □其他</td></tr>
<tr><td colspan="2">子课题活动类型</td><td colspan="5">□基础前沿 ■应用研究 □试验发展</td></tr>
<tr><td colspan="2">子课题研究所属学科</td><td colspan="5">自然科学相关工程与技术
农业工程</td></tr>
<tr><td colspan="2">子课题成果应用的主要国民经济行业</td><td colspan="5">制造业
专用设备制造业
农、林、牧、渔专用机械制造
机械化农业及园艺机具制造</td></tr>
<tr><td colspan="2">子课题的社会经济目标</td><td colspan="5">农林牧渔业发展
农林牧渔业体系支撑</td></tr>
<tr><td colspan="2">经费预算</td><td colspan="5">总需求 60.00 万元，其中中央财政专项资金需求 60.00 万元</td></tr>
<tr><td colspan="2" rowspan="2">子课题周期节点</td><td>起始时间</td><td>2024 年 12 月</td><td>结束时间</td><td colspan="2">2027 年 11 月</td></tr>
<tr><td>实施周期</td><td>共 36 个月</td><td>预计中期时间点</td><td colspan="2">2026 年 05 月</td></tr>
<tr><td rowspan="9">子课题承担单位</td><td>单位名称</td><td colspan="2">华南农业大学</td><td>单位法定代表人姓名</td><td colspan="2">薛红卫</td></tr>
<tr><td>单位性质</td><td colspan="2">大专院校</td><td>组织机构代码</td><td colspan="2">124400004554165634</td></tr>
<tr><td>单位主管部门</td><td colspan="2">广东省教育厅</td><td>隶属关系</td><td colspan="2">省属高校</td></tr>
<tr><td>单位所属地区</td><td colspan="2">广东省广州市天河区</td><td>地市（市、自治州、盟）</td><td colspan="2">广州市</td></tr>
<tr><td>通信地址</td><td colspan="2">广东省广州市天河区五山路 483 号华南农业大学</td><td>邮政编码</td><td colspan="2">510642</td></tr>
<tr><td>单位开户名称</td><td colspan="5">华南农业大学</td></tr>
<tr><td>开户银行（全称）</td><td colspan="2">中国工商银行股份有限公司广州五山支行</td><td>汇入地点</td><td colspan="2">广州</td></tr>
<tr><td>银行账号</td><td colspan="2">3602 0026 0900 0310 520</td><td>银行机构代码</td><td colspan="2">102581000546</td></tr>
</table>

<table>
<tr><td rowspan="6">子课题负责人</td><td>姓 名</td><td>张烨</td><td>性 别</td><td>■男□女</td><td>出生日期</td><td>[redacted]</td></tr>
<tr><td>证件类型</td><td>身份证</td><td>证件号码</td><td colspan="3">[redacted]</td></tr>
<tr><td>所在单位</td><td colspan="5">华南农业大学</td></tr>
<tr><td>最高学位</td><td colspan="5">■博士 □硕士 □学士 □其他</td></tr>
<tr><td>职 称</td><td colspan="3">□正高级■副高级 □中级 □初级 □其他</td><td>职务</td><td>无</td></tr>
<tr><td>电子邮箱</td><td colspan="2">[redacted]</td><td>移动电话</td><td colspan="2">[redacted]</td></tr>
<tr><td rowspan="3">子课题联系人</td><td>姓 名</td><td>张烨</td><td>电子邮箱</td><td colspan="3">[redacted]</td></tr>
<tr><td>固定电话</td><td>[redacted]</td><td>移动电话</td><td colspan="3">[redacted]</td></tr>
<tr><td>证件类型</td><td>身份证</td><td>证件号码</td><td colspan="3">[redacted]</td></tr>
<tr><td rowspan="3">子课题财务负责人</td><td>姓 名</td><td>肖斐</td><td>电子邮箱</td><td colspan="3">[redacted]</td></tr>
<tr><td>固定电话</td><td>[redacted]</td><td>移动电话</td><td colspan="3">[redacted]</td></tr>
<tr><td>证件类型</td><td>身份证</td><td>证件号码</td><td colspan="3">[redacted]</td></tr>
<tr><td rowspan="2">其他参与单位</td><td>序号</td><td colspan="2">单位名称</td><td>单位性质</td><td colspan="2">组织机构代码</td></tr>
<tr><td></td><td colspan="2">无</td><td></td><td colspan="2"></td></tr>
<tr><td rowspan="2">子课题参加人数</td><td rowspan="2">18 人。其中：</td><td colspan="5">高级职称 3 人，中级职称 2 人，初级职称 0 人，其他 13 人；</td></tr>
<tr><td colspan="5">博士学位 5 人，硕士学位 0 人，学士学位 13 人，其他 0 人。</td></tr>
<tr><td>子课题简介(限 500 字以内)</td><td colspan="6">本子课题为“工厂化农业关键技术与智能农机装备”专项项目“粮油作物大面积单产提升智能装备创制与智慧系统集成应用”课题 4“粮主粮作物移动式烘干机专用传感器与智能装备创制”的子课题。本子课题针对移动式烘干机跨区作业产生的物料水分差异大、产地作业面临的收后水分高、“烂场雨”等极端气候引起的作物与环境湿度大等问题，研究小麦、水稻、玉米三种主粮作物的水分-环境湿度-干燥温度之间的耦合响应机制，温度变化对干燥不均匀度、稻谷爆腰率、玉米裂纹率、玉米热损伤率、小麦湿面筋率的影响机理，提出温度变化耦合响应机制 1 项；研究热风温度超温精准检测及报警技术、热风温度及风量变量调控技术、变温精准干燥控制算法等新技术 3 项，开发热风温度超温精准检测及报警系统 1 个，热风温度及风量变量调控系统 1 个以及变温精准干燥控制系统 1 个，提供应用解决方案 2 套，登记软件著作权 1 项，申请专利 1 件，发表论文 2 篇，培养研究生 2 名。</td></tr>
</table>

一、子课题目标及考核指标、考核方式/方法

1. 子课题目标

本子课题针对移动式烘干机跨区作业产生的物料水分差异大、产地作业面临的收后水分高、“烂场雨”等极端气候引起的作物与环境湿度大等问题，研究小麦、水稻、玉米三种主粮作物的水分-环境湿度-干燥温度之间的耦合响应机制，温度变化对干燥不均匀度、稻谷爆腰率、玉米裂纹率、玉米热损伤率、小麦湿面筋率的影响机理，提出温度变化耦合响应机制 1 项；研究热风温度超温精准检测及报警技术、热风温度及风量变量调控技术、变温精准干燥控制算法等新技术 3 项，开发热风温度超温精准检测及报警系统 1 个，热风温度及风量变量调控系统 1 个以及变温精准干燥控制系统 1 个，提供应用解决方案 1 套，登记软件著作权 1 项，申请专利 1 件，发表论文 2 篇，培养研究生 2 名。

2. 子课题考核指标、考核方式/方法

1）提出温度变化耦合响应机制 1 项；

2）研究热风温度超温精准检测及报警技术、热风温度及风量变量调控技术、变温精准干燥控制算法等新技术 3 项，开发热风温度超温精准检测及报警系统 1 个，热风温度及风量变量调控系统 1 个以及变温精准干燥控制系统 1 个，温度检测精度±0.3℃，控温精度±1.0℃，算法精度≥90%；

3）应用解决方案 2 套；

4）申请软件著作权 1 项，申请专利 1 件，发表论文 2 篇；

5）培养研究生 2 名。

子课题目标、预期成果与考核指标表

子课题	预期成果		对应的课题	考核指标				考核方式（方法）及评价手段
	预期成果名称	预期成果类型		指标名称	立项时已有指标值/状态	中期指标值/状态	完成时指标值/状态	
目标：本子课题主要研究小麦、水稻、玉米三种主粮作物的水分-环境湿度-干燥温度之间的耦合响应机制，提出温度变化耦合响应机制 1 项；研究热风温度超温精准检测及报警技术、热风温度及风量变量调控技术、变温精准干燥控制算法等新技术 3 项，开发热风温度超温精准检测及报警系统 1 个，热风温度及风量变量调控系统 1 个以及变温精准干燥控制系统 1 个，提供应用解决方案 1 套，登记软件著作权 1 项，申请专利 1 件，	12：主粮作物移动式烘干机变温精准干燥智能调控系统	☑新理论 ☑新技术 ☑关键部件 ☑应用解决方案 ☑论文 ☑发明专利	课题 4：主粮作物移动式烘干机专用传感器与智能装备创制	12.1 论著、知识产权数、数据库、新原理方法等指标	无	✧ **提供应用解决方案 1 套** ✧ **登记软件著作权 1 项** ✧ **发表论文 1 篇**	✧ **发表论文 2 篇** ✧ **申请专利 1 件** ✧ **登记软件著作权 1 项** ✧ **提供应用解决方案 2 套** ✧ **提出新理论 1 项**	✧ 论文检索证明 ✧ 专利受理或授权通知书 ✧ 软件著作权登记证书 ✧ 应用解决方案、新理论通过第三方科技成果评价或第三方专家组出具鉴定意见或第三方检测报告
				12.2 技术与应用指标	✧ **现有技术水平：** ①热风温度超温精准检测及报警技术： ✓ 温度检测精度±1.0℃。 ②热风温度及风量变量调控技术： ✓ 控温精度±2.0℃。 ③变温精准干燥控制算法： ✓ 算法精度≥75%。	✧ **开发新技术 3 项，及其配套关键部件 3 套。** ①热风温度超温精准检测及报警技术及其配套系统： ✓ 配套系统达到 TRL5； ✓ 温度检测精度±0.5℃。 ②热风温度及风量变量调控技术及其配套系统： ✓ 配套系统达到 TRL5； ✓ 控温精度±1.5℃。 ③变温精准干燥控制算法： ✓ 算法精度≥80%。	✧ **开发新技术 3 项，及其配套关键部件 3 套。** ①热风温度超温精准检测及报警技术及其配套系统： ✓ 配套系统达到 TRL8； ✓ 温度检测精度±0.3℃。 ②热风温度及风量变量调控技术及其配套系统： ✓ 配套系统达到 TRL8； ✓ 控温精度±1.0℃。 ③变温精准干燥控制算法： ✓ 算法精度≥90%。	✓ 第三方检测报告

发表论文 2 篇，培养研究生 2 名。								

	序号	报告类型[5]	数量	提交时间	公开类别及时限[6]
科技报告考核指标	1	年度执行报告	1	2025.12	延期公开、3 年
	2	年度执行报告	1	2026.12	延期公开、3 年
	3	中期执行情况报告	1	中期检查前	延期公开、3 年
	4	年度执行报告	1	2027.12	延期公开、3 年
	5	综合绩效评价报告	1	项目执行期结束后 6 个月内	延期公开、3 年
	6	最终科技报告	1	项目执行期结束后 6 个月内	延期公开、3 年

其他目标与考核指标完成情况：
培养研究生 2 名

备注：

1.**“子课题目标”**，应从以下方面明确描述：（1）研发主要针对什么问题和需求；（2）将要解决哪些科学问题、突破哪些核心/共性/关键技术；（3）预期成果；（4）成果将以何种方式应用在哪些领域/行业/重大工程等，并拟在科技、经济、社会、环境或国防安全等方面发挥何种的作用和影响。（5）所列主要成果原则上不超过 5 项，如有其他重要成果放在“其他”成果中表述。

2.**“考核指标”**，指相应成果的数量指标、技术指标、质量指标、应用指标和产业化指标等，其中，数量指标可以为专利、产品等的数量，论文代表作应注重质量，不以数量作为评价标准；技术指标可以为关键技术、产品的性能参数等；质量指标可以为产品的耐震动、高低温、无故障运行时间等；应用指标可以为成果应用的对象、范围和效果等；产业化指标可以为成果产业化的数量、经济效益等。同时，对各项考核指标需填写立项时已有的指标值/状态以及子课题完成时要到达的指标值/状态。同时，考核指标也应包括支撑和服务其他重大科研、经济、社会发展、生态环境、科学普及需求等方面的直接和间接效益。如对国家重大工程、社会民生发展等提供了关键技术支撑，成果转让并带动了环境改善、实现了销售收入等。若某项成果属于开创性的成果，立项时已有指标值/状态可填写“无”,若某项成果在立项时已有指标值/状态难以界定，则可填写“/”。

3.**“中期指标”**，各专项根据管理特点，确定是否填写，鼓励阶段目标明确的项目子课题填写中期指标。

4.**“考核方式方法”**，应提出符合相关研究成果与指标的具体考核技术方法、测算方法等。

5.**“科技报告类型”**，包括项目综合绩效评价（验收）前撰写的全面描述研究过程和技术内容的最终科技报告、项目年度或中期检查时撰写的描述本年度研究过程和进展的年度技术进展报告以及在项目实施过程中撰写的包含科研活动细节及基础数据的专题科技报告（如实验报告、试验报告、调研报告、技术考察报告、设计报告、测试报告等）。其中，每个项目在综合绩效评价（验收）前应撰写一份最终科技报告；研究期限超过 2 年（含 2 年）的项目，应根据管理要求，每年撰写一份年度技术进展报告；每个项目可根据研究内容、期限和经费强度，撰写数量不等的专题科技报告。科技报告应按国家标准规定的格式撰写。

6.**“公开类别及时限”**，公开项目科技报告分为公开或延期公开，内容需要发表论文、申请专利、出版专著或涉及技术诀窍的，可标注为“延期公开”。需要发表论文的，延期公开时限原则上在 2 年（含 2 年）以内；需要申请专利、出版专著的，延期公开时限原则上在 3 年（含 3 年）以内；涉及技术诀窍的，延期公开时限原则上在 5 年（含 5 年）以内。涉密项目科技报告按照有关规定管理。

二、子课题研究内容、研究方法及技术路线

（一）子课题的主要研究内容

1. 拟解决的关键科学问题、关键技术问题

①揭示多工况条件下小麦、水稻、玉米等三种主粮作物的含水率与干燥温度耦合响应机制，给出水分-温度-品质特征变化规律的变温精准干燥控制机理模型；

②研发热风温度超温精准检测及报警技术，热风温度及风量变量调控技术及变温精准干燥控制算法，给出变温精准干燥控制和作业参数自适应调整准则。

2. 主要研究内容

①揭示主粮作物的水分-环境湿度-干燥温度之间的耦合响应机制，给出水分-温度-品质特征变化规律的变温精准干燥控制机理模型。

干燥是含湿作物与热风介质之间自发进行地传热传质过程，其水分迁移的发生机理，应由粮食和干燥介质共同决定。对由含湿物料和热风介质两个自然物系共同组成的干燥变量物系开展理论和试验分析，基于粮食平衡含水率方程，以水分活度表征粮食状态，热风温湿度表征介质状态，构建基于主粮作物物性（水分活度、粮食温度及含水率）和热风介质（温度、相对湿度和风速）的六因素粮食干燥系统能量平衡方程，研究主粮作物在动态过程中物性随干燥介质变化的湿热传递特性，揭示其水分-环境湿度-干燥温度之间的耦合响应机制，获得基于主粮作物物性和干燥介质状态的变温干燥机理函数解析式；研究干燥温度对干燥不均匀度、稻谷爆腰率、玉米裂纹率等品质变化的影响机理，给出主粮作物的变温干燥机理模型。

②研发不同主粮、不同烘干条件下的热风温度超温精准检测及报警技术，热风温度及风量变量调控技术，基于变温干燥机理函数解析式，给出变温精准干燥控制算法。

根据小麦、水稻、玉米三种主粮作物的物理特性，分别建立不同主粮的变温干燥控制准则；采用温湿度传感器、测温电缆、远程通讯等设备和技术，研发热风温度超温精准检测及报警技术，并搭建配套系统；基于变温干燥控制准则，研究不同主粮干燥状态和热风温度及风量等干燥介质参数动态变化规律，给出干燥状态变量调控准则，并搭建配套系统；基于变温干燥机理函数解析式，给出不同主粮作物的变温精准干燥控制算法，集成研制变温精准干燥控制系统，降低烘干损失。

（二）子课题采取的研究方法

本课题针对移动式烘干机跨区作业产生的物料水分差异大、产地作业面临的收后水分高、“烂场雨”等极端气候引起的作物与环境湿度大等难题，应用理论解析法和试验验证法结合分析，理论解析研究主粮作物水分-环境湿度-干燥温度之间的耦合响应机制，获得主粮作物变温干燥解析模型，给出水分-温度-品质特征变化规律；试验验证考证，搭建热风温度超温精准检测及报警系统、热风温度及风量变量调控系统和集成的变温精准干燥控制系统，监测干燥过程主粮作物和干燥介质的各项参数，完成数据采集、分析和反馈。通过理论模型和实际数据融合，研究主粮作物物性、干燥介质状态和品质之间的耦合关系，实现主粮作物的变温精准干燥控制，降低烘干损失。

①主粮作物的水分-环境湿度-干燥温度之间的耦合响应机制研究

如图 1 所示为水分-温度-品质的研究思路图。首先，研究主粮作物物性特征在干燥过程的变化，明确水蒸气分压力是干燥去水动力，水分的迁移可以看作是一种能量的迁移，基于能量守恒定理，即可获得主粮作物干燥过程机理模型。其次，基于吉布斯、亥姆赫兹自由能模型，以干燥过程自由能消耗为统一尺度，以水分活度为共同属性，构建主粮作物干燥过程水分迁移特征函数，获得基于主粮作物物性和干燥介质状态的变温干燥机理函数解析式。最后，研究温度与主粮作物品质指标对应关系，揭示作物水分、温度与品质形成之间的耦合机理，构建基于水分-温度-品质特征规律的变温精准干燥控制算法模型。

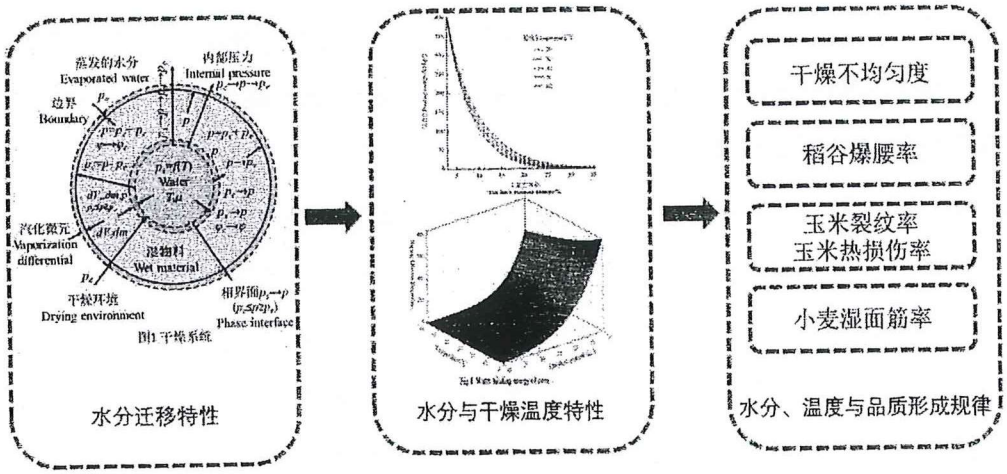

图 1 水分-温度-品质之间的耦合响应机制

②热风温度超温精准检测及报警技术、热风温度及风量变量调控技术和变温精准干燥控制算法及系统研究。

如图 2 所示为热风温度超温精准检测及报警技术、热风温度及风量变量调控技术和

变温精准干燥控制算法及系统的研究思路图。首先，基于变温干燥机理函数解析式，研究了主粮作物在干燥过程中水分和品质随温度变化的相应规律。其次，利用现有互联网+云服务技术，搭建智能干燥系统，包括热风温度超温精准检测及报警系统和热风温度及风量变量调控系统，检测主粮作物的粮食温度、含水率、水分活度与干燥介质温度、湿度、风速等过程参数，结合机理模型，智能识别和判断热风温度是否超温、风温风量匹配是否合理等，实现热风温度超温报警、风温风量变量调控。最后，依托解析模型和控制算法集成变温精准干燥控制系统，研制面向不同主粮作物的变温精准干燥控制系统，降低焦糊、热损伤等造成的烘干损失。

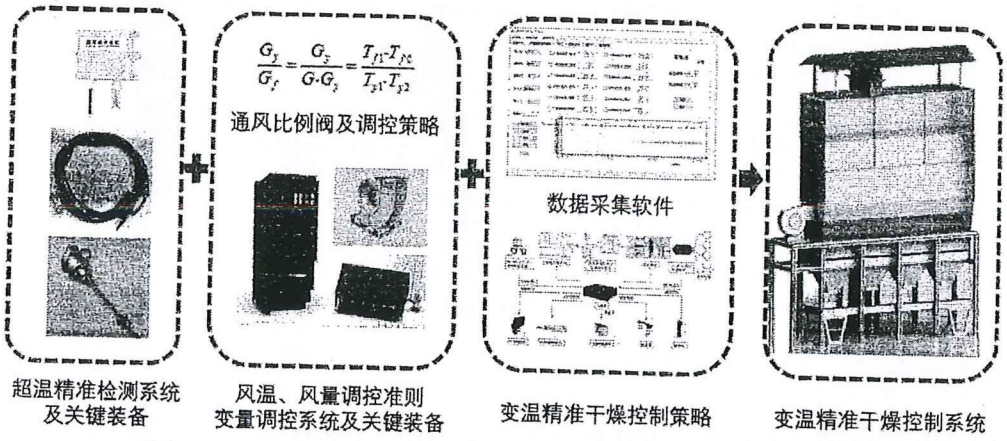

图 2 超温精准检测系统、风温风量调控系统和变温精准干燥系统

（三）技术路线

本子课题的技术路线见图 3。

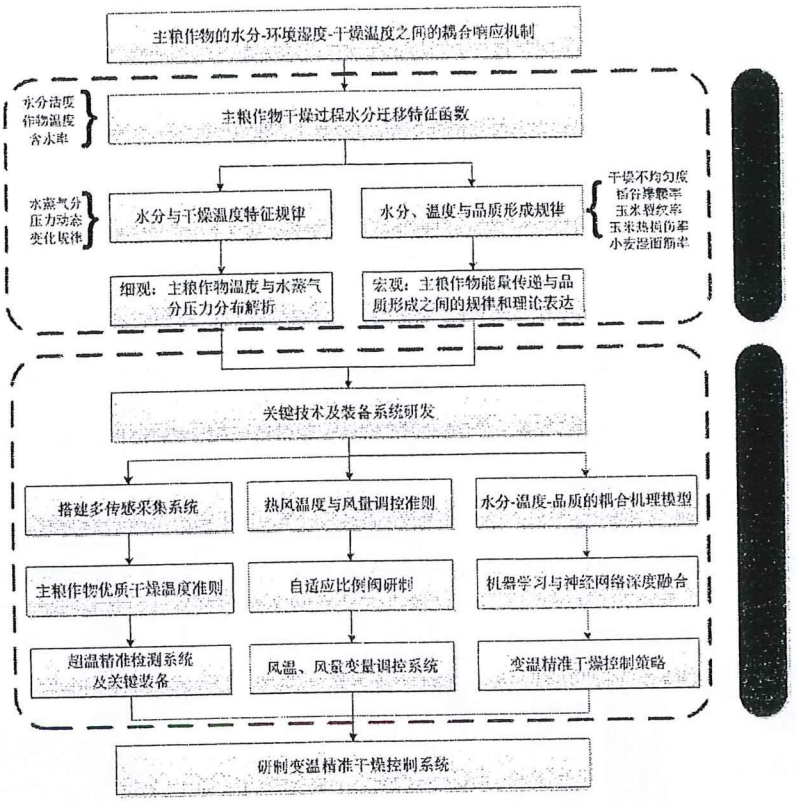

图 3 技术路线

三、主要创新点

①构建主粮作物干燥过程水分迁移特征函数，揭示主粮作物水分与温度之间的耦合响应机理，给出变温精准干燥控制算法。

②基于变温精准干燥控制算法，研发热风温度检测系统、风温及风量变量调控系统和变温精准干燥控制系统，实现精准干燥。

四、预期经济社会效益

1. 课题的科学、技术、产业指标及科学价值

本课题预期达成多方面目标并具多重效益。预期指标涵盖科学研究、技术方法与产业应用。科学研究上，阐明主粮作物含水率与干燥温度耦合响应机制，助力解决移动式烘干产能问题。技术研究揭示主粮作物含水率与干燥温度耦合响应机制，给出变温精准干燥控制机理模型，研发 3 个关键技术及配套系统，登记软件著作权 1 项，申请专利 1 件。产业应用方面，配合课题单位研制移动式智能烘干机关键技术，并开展应用。

2. 科学价值与社会、经济、生态效益

科学价值在于成为粮油作物智能作业技术体系重要部分，填补多作业系统高效协同研究空白。社会效益体现为实现技术替代进口，提升烘干设备机械化与智能化水平推动

农业产业技术升级，保障粮食安全，提高农户积极性。经济效益显著，能快速降粮含水率，减少霉变损失，大幅降低能耗。生态效益表现在精准控制烘干作业能耗，推动农业可持续发展,综合而言对农业各方面发展有着极为重要的推动与支撑作用。

五、子课题年度计划

1. **年度：**2024 年 12 月—2025 年 05 月

任务：开展多工况条件下主粮作物含水率与干燥温度耦合响应机制等关键科学问题开展研究，提出研究方案。

2. **年度：**2025 年 06 月—2025 年 11 月

任务：开展变温精准干燥控制技术研究，针对变温干燥准则及算法等关键技术进行攻关。

考核指标：

①变温烘干新技术 1 项，及其配套关键部件 1 套。

②申请发明专利 1 件，完成年度执行报告 1 份。

成果形式：专利文本或受理通知书。

3. **年度：**2025 年 12 月—2026 年 05 月

任务：基于变温干燥准则，开展热风温度超温精准检测及报警技术、热风温度及风量变量调控技术等新技术研究；开展项目中期检查。

考核指标：

①热风温度超温精准检测及报警技术、热风温度及风量变量调控技术等新技术 2 项，及其配套关键部件 2 套。

②提供移动式烘干机变温精准干燥应用解决方案 2 套。

③登记软件著作 1 件，发表学术论文 1 篇。

④完成中期执行情况报告 1 份。

成果形式： 论文检索或见刊；程序代码。

4. **年度：**2026 年 06 月—2026 年 11 月

任务：制定变温精准控制系统整机搭载测试。

考核指标： 搭建整机测试，完成年度执行报告 1 份。

成果形式：测试平台现场展示。

5. **年度：**2026 年 12 月—2027 年 05 月

任务：完成移动式烘干机变温精准干燥关键技术研发。

考核指标：发表学术论文 1 篇。

成果形式： 论文检索或见刊；定型整机现场展示。

6. **年度：2027 年 06 月—2027 年 11 月**

任务：

①对研究过程进行系统总结。

②撰写课题研究报告及技术总结报告。

③完成课题绩效评价材料。

④组织完成课题、项目绩效评价。

考核指标：

①完成年度执行报告 1 份，完成全部验收资料。

②研究生毕业论文 2 篇；

成果形式： 现场照片与证明；研究生毕业论文；通过农业农村部组织的项目验收。

六、子课题组织实施机制及保障措施

1. 子课题的内部组织管理方式、协调机制等。

建立子课题组织实施机制。子课题负责人对课题的任务分配及进度安排进行组织管理，负责协调解决课题实施中遇到的组织、协调和管理问题；子课题确定任务负责人，负责人及时汇报任务进展。子课题负责人按照课题进度设立岗位及人员，细化任务分工，落实相关责任，确保每项研究任务和目标都落实到人，保证课题实施的质量，定期考核和评估每项研究内容完成情况。

成立子课题内部专家评审小组。子课题内部专家评审小组负责对课题的技术路线、研究方法、实施方案、目标设定等进行论证和审定，并对子课题进展进行监督、指导和必要的调整，全面把控子课题总体进度，协调解决课题研究过程中遇到的关键技术问题。

执行项目联席会议制，控制实施风险。每半年召开子课题联席会议，全方位研讨课题进展情况并解决课题实施中遇到的问题，对前期工作进行综合评判，提出合理的改进意见，并对后续工作进行统一协调安排。每年参加项目组织相关研讨及总结会议。

建立健全财务报表制度，严格监督各参与单位的经费使用情况。子课题资金实行专户存储，专款专用，不允许截留、挪用和串用。课题任务参与单位都将根据本单位的财

务管理制度建立完善清晰的财务明细账表，规范开支范围，定期统计并汇总上报。

2. 子课题实施的相关政策，已有的组织、技术基础，支撑保障条件。

政策支撑条件：2021 年，国务院颁发了《“十四五”推进农业农村现代化规划》，提出要提高农业质量效益和竞争力，强化农业科技和装备支撑，建设智慧农业。2024 年，中央一号文件进一步明确指出，“把粮食增产的重心放到大面积提高单产上”、“实施粮食单产提升工程”。相关政策为本子课题的实施提供了强有力的政策支撑。

组织支撑条件：华南农业大学作为子课题承担单位，拥有优秀的科研团队，研究基础深厚，具有丰富的国家科研项目实施经验，开展了大量的科研与技术应用推广工作，组织支撑优势明显。

资源支撑条件：子课题团队由从农业机械、计算机、控制科学等方面的专业人才构成，专业齐全、结构合理，能够很好地完成项目涵盖的技术研发、设备设计、设备调试等研究任务。

3. 对实现课题总目标的支撑作用，及与课题内其他子课题的协同机制。

项目整体的任务是一个有机整体，在任务分配中相互串联、相互渗透，在项目实施过程中，建立资源共享和快速响应机制，各单位将全力协作、密切配合，最大化地实现信息、技术资源的共享，及时反馈各课题进展情况和存在问题，通过优势互补和默契配合，更有力地推进课题的按期高效实施。子课题研究内容侧重于主粮作物移动式烘干机变温精准干燥关键技术研发，可为课题任务实施提供共性技术与关键技术职称。子课题团队既具有技术产品开发经验，也具有科研试验条件，能够为任务指标的实施，提供良好的支撑。

七、知识产权对策、成果管理及合作权益分配

子课题有关知识产权及成果的管理执行按《中华人民共和国合同法》、《中华人民共和国专利法》、《中华人民共和国著作权法》等相关法律法规以及国家科学技术部《关于加强与科技有关的知识产权保护和管理工作的若干意见》等有关规定执行，将形成的相关研究成果与国家和行业标准发展规划相衔接，为社会服务、实现社会共享。

在子课题实施过程中形成的创新成果，如专利、成果登记和论文等应由子课题主持单位负责相关知识产权的管理。研究期间，各任务获取的相关资料、实验观测数据和文献资料将实行内部共享，促进学术交流和避免重复。涉及本子课题产生的研究数据必须提交课题主持单位，正式发表的论文、论著应注有“国家重点研发专项（课题编号）专

项经费资助”字样。科研成果产权则根据各任务的负责实施情况具体而定，独立完成的成果和形成的知识产权归完成单位拥有；在课题执行期限内，如果由多家单位共同完成，则产权归属于各协作单位共同拥有；因使用双方提供的材料、专利形成的成果，知识产权归属另有规定的，以双方具体协议为准。其他未尽事宜，由双方协商解决。

八、需要约定的其他内容

1.子课题牵头单位华南农业大学，将按照科技计划项目科学数据汇交的有关要求，制定科技资源汇交方案，将科学数据汇交到有关方面认可的科学数据中心并出具汇交凭证。

2.子课题牵头单位华南农业大学，将按照国家重点研发计划项目安全管理的有关要求，切实履行项目安全管理职责，加强人员培训教育，强化科研过程安全管理。

九、子课题参加人员基本情况表

填表说明：
1.专业技术职称：A、正高级　B、副高级　C、中级　D、初级　E、其他；
2.投入本子课题的全时工作时间（人月）是指在子课题实施期间该人总共为子课题工作的满月度工作量；累计是指子课题组所有人员投入人月之和；
3.子课题固定研究人员需填写人员明细；
4.是否有工资性收入：Y、是　N、否；
5.人员分类代码：B、子课题负责人　C、课题/子课题骨干　D、其他研究人员；
6.工作单位：填写单位全称，其中高校要具体填写到所在院系。

序号	姓名	性别	出生日期	证件类型	证件号码	专业技术职称	职务	最高学位	专业	投入本子课题的全时工作时间（人月）	人员分类代码	在子课题中分担的任务	是否有工资性收入	工作单位
1	张烨	男	[redacted]	身份证	[redacted]	副高级	无	博士	农业机械化工程	18	子课题负责人	水稻烘干技术研究	是	华南农业大学工程学院
2	陈震	男	[redacted]	身份证	[redacted]	副高级	无	博士	农业机械化工程	18	项目/课题骨干	稻谷烘干机结构设计	是	华南农业大学工程学院
3	李成杰	男	[redacted]	身份证	[redacted]	中级	无	博士	农业机械化工程	18	项目/课题骨干	采集控制系统集成	是	华南农业大学工程学院
4	赵懿琨	女	[redacted]	身份证	[redacted]	中级	无	博士	农业机械化工程	18	项目/课题骨干	烘干工艺试验优化	是	华南农业大学电子工程学院
5	班华	男	[redacted]	身份证	[redacted]	副高级	无	博士	农业机械化工程	18	项目/课题骨干	采集控制系统集成	是	华南农业大学工程学院

6	李圣陶	男	[redacted]	身份证	[redacted]	其他	无	学士	农机装备工程	18	其他研究人员	自适应控制系统设计	否	华南农业大学工程学院
7	孙懿清	男		身份证		其他	无	学士	农机装备工程	18	其他研究人员	烘干工艺试验优化	否	华南农业大学工程学院
8	陈铸荣	男		身份证		其他	无	学士	农机装备工程	18	其他研究人员	物料变温烘干试验	否	华南农业大学工程学院
9	黄清楷	男		身份证		其他	无	学士	机械工程	18	其他研究人员	物料变温烘干仿真	否	华南农业大学工程学院
10	覃杨	女		身份证		其他	无	学士	农机装备工程	18	其他研究人员	控制系统搭建	否	华南农业大学工程学院
11	黄建江	男		身份证		其他	无	学士	机械工程	18	其他研究人员	配套部件模块化设计	否	华南农业大学工程学院
12	纪思涵	男		身份证		其他	无	学士	控制工程	18	其他研究人员	自适应控制系统设计	否	华南农业大学工程学院
13	陈衍成	男		身份证		其他	无	学士	机械工程	18	其他研究人员	配套部件模块化设计	否	华南农业大学工程学院
14	谢志金	男		身份证		其他	无	学士	机械工程	18	其他研究	排粮部件设计	否	华南农业大学工程学院

			[redacted]		[redacted]						人员			
15	刘仕杰	男		身份证		其他	无	学士	控制工程	18	其他研究人员	自适应控制系统设计	否	华南农业大学工程学院
16	彭智康	男		身份证		其他	无	学士	机械工程	18	其他研究人员	配套部件模块化设计	否	华南农业大学工程学院
17	余展豪	男		身份证		其他	无	学士	机械工程	18	其他研究人员	物料变温烘干试验	否	华南农业大学工程学院
18	谢兆豪	男		身份证		其他	无	学士	机械工程	18	其他研究人员	自适应控制系统设计	否	华南农业大学工程学院
69														
固定研究人员合计										18	/	/	/	/
流动人员或临时聘用人员合计										0	/	/	/	/
累计										18	/	/	/	/

十、经费预算

子课题预算表

表 B1 子课题编号：2024YFD200010402

子课题名称：主粮作物移动式烘干机变温精准干燥关键技术研发

金额单位：万元

序号	预算科目名称	金额
	（1）	（2）
1	一、中央财政专项资金	60.00
2	（一）直接费用	49.00
3	1.设备费	3.00
4	其中：购置设备费	0.00
5	2.业务费	34.00
6	3.劳务费	12.00
7	（二）间接费用（自动计算）	11.00
8	二、其他来源资金	0.00
9	三、合计	60.00

注：1.间接费用无需编制预算说明；2.绩效支出在间接费用中无比例限制。承担单位在统筹安排间接费用时，要处理好合理分摊间接成本和对科研人员激励的关系，绩效支出安排与科研人员在子课题工作中的实际贡献挂钩。

设备费——购置/试制设备预算明细表

表 B2　　子课题编号：2024YFD200010402　　子课题名称：主粮作物移动式烘干机变温精准干燥关键技术研发　　金额单位：万元

填表说明：1.设备分类：购置、试制；
2.购置设备类型：通用、专用；
3.试制设备不需填列本表（9）列、（10）列、（11）列、（12）列；
4.设备单价的单位为万元/台套，设备数量的单位为台套；
5.单价 50 万元以下的设备不用填写；
6.本表只填写中央财政资金购置（试制）的设备。

序号	设备名称	设备分类	功能和技术指标	单价	数量	金额	购置或试制单位	安置单位	购置设备类型	主要生产厂家及国别	规格型号	拟开放共享范围
	（1）	（2）	（3）	（4）	（5）	（6）	（7）	（8）	（9）	（10）	（11）	（12）
单价 50 万元以上购置设备合计							/	/	/	/	/	/
单价 50 万元以上试制设备合计							/	/	/	/	/	/
累计							/	/	/	/	/	/

子课题单位经费预算明细表

表 B3　　子课题编号：　2024YFD200010402　子课题名称：主粮作物移动式烘干机变温精准干燥关键技术研发　　金额单位：万元

填表说明：1.单位类型分子课题承担单位、子课题参与单位；
2.组织机构代码指企事业单位国家标准代码，单位若已三证合一请填写单位统一社会信用代码，无组织机构代码的单位填写“000000000”。

序号	单位名称	组织机构代码-统一社会信用代码		单位类型	任务分工	研究任务负责人	合计	中央财政专项资金		其他来源资金
								小计	其中：间接费用	
	（1）	（2）	（3）	（4）	（5）	（6）	（7）	（8）	（9）	（10）
1	华南农业大学	统一社会信用代码	124400004554165634	子课题承担单位	主粮作物移动式烘干机变温精准干燥关键技术研发	张烨	60.00	60.00	11.00	0.00
累计							60.00	60.00	11.00	0.00

预算说明

一、中央财政资金

预算的编制要坚持任务相关性、政策相符性和经济合理性，实事求是编制提出子课题预算。填报时，直接费用应按设备费、业务费、劳务费三个类别填报，每个类别结合科研任务按支出用途进行说明。除 50 万元以上的设备外，其他费用只提供基本测算说明，不需要提供明细。

本子课题申报中央财政资金 60.00 万元，其中直接费用 49.00 万元，间接费用 11.00 万元。

序号	科目名称	中央财政专项资金（单位：万元）
1	设备费	3.00
2	业务费	34.00
3	劳务费	12.00
4	间接经费	11.00
	合计	60.00

（一）直接费用

1.设备费（是指项目实施过程中购置或试制专用仪器设备，对现有仪器设备进行升级改造，以及租赁外单位仪器设备而发生的费用等。计算类仪器设备和软件工具可在设备费科目编列。填报时，50 万元以上的设备详细说明，50 万元以下的设备费用分类说明）

设备改造费 3.00 万元。

序号	设备名称	数量	单价（万元）	总价（万元）
1	移动式烘干机试验装置改造（改造动力转换、热源回用单元、外壳等）	1	3.00	3.00
	合计			3.00

2.业务费（是指在项目实施过程中消耗的各种材料、低值易耗品等、发生的测试化验加工、燃料动力、出版文献、信息传播、知识产权事务、会议、差旅、国际合作与交流以及其他与项目实施直接相关的各项费用。编报时，对单笔大额支出、对外委托支出重点说明）

业务费总预算 34.00 万元，其中材料费 7.22 万元、测试化验加工费 12.58 万元、燃料动力费 1.20 万元、出版/文献/信息传播/知识产权事务费 8.40 万元、会议/差旅/国际合作交流费 4.60 万元。

2.1 材料费

材料费预算中央财政专项资金 7.22 万元。

序号	材料名称	主要用途	计量单位	数量	单价（万元）	金额（万元）
1	传动机构	主粮作物移动式烘干机变温精准干燥关键技术	套	2	0.66	1.32
2	温度传感器单元		套	20	0.05	1.00
3	水分传感器		个	2	1.00	2.00
4	PLC 控制单元		个	1	0.60	0.60
5	组态软件模块		个	10	0.08	0.80
6	控制柜		个	2	0.75	1.50
	合计					7.22

2.2 测试化验加工费

测试化验加工费预算中央财政专项资金 12.58 万元，主要用于主粮作物移动式烘干机变温精准干燥部件加工及指标检测。

序号	测试化验加工内容	计量单位	数量	单价（万元）	金额（万元）
1	整机预烘干系统增装加工	套	1	3.18	3.18
2	整机控制系统适配改装加工	套	2	2.00	4.00
3	烘干成分品质第三方测试	次	1	2.40	2.40
4	烘干机指标第三方测试	次	1	3.00	3.00
	合计				12.58

2.3 燃料动力费

燃料动力费预算中央财政专项资金 1.20 万元，主要用于烘干试验发生的电、燃油费用。

序号	科目内容	计量单位	数量	单价（元）	金额（万元）
1	电费	千瓦时	4500	0.80	0.36

2	燃油费	升	1200	7.00	0.84
	合计				1.20

2.4 出版/文献/信息传播/知识产权事务费

出版/文献/信息传播/知识产权事务费预算中央财政专项资金 8.40 万元。

序号	科目内容	数量	单价（万元）	金额（万元）
1	论文版面费	3	1.00	3.00
2	软件著作权申请	2	0.50	1.00
3	标准规范	1	2.00	2.00
4	申请专利	4	0.60	2.40
	合计			8.40

2.5 会议/差旅/国际合作交流费

主要用途：用于子课题组组织子课题研讨、交流、评审，中期检查和结题汇报等相关会议召开，参加项目交流讨论、国内相关学术会议等所产生的会议和差旅费用，以及举办干燥机相关技术交流、学术交流和应用示范推广的费用。

其中，子课题执行期间发生的差旅费按照《中央国家机关事业单位差旅费管理办法》（财行〔2013〕531 号）、《关于调整中央和国家机关差旅住宿费标准等有关问题的通知》（财行〔2015〕497 号）及各单位所属地方的相关规定或者各单位内部制定的相关制度。

会议、差旅费中央财政专项资金 4.60 万元。其中会议费 0.60 万元，差旅费 2.00 万元，国际合作交流费 2.00 万元。因未超过直接费用（49.00 万元）的 10%（4.90 万元），因此未对预算内容和资金安排进行具体说明。

2.6 其他支出

暂无。

3.劳务费（是指在项目实施过程中支付给参与项目的研究生、博士后、访问学者以及项目聘用的研究人员、科研辅助人员、科研（财务）助理等的劳务性费用；支付给临时聘请的咨询专家的费用等。项目聘用人员由单位缴纳的社会保险补助

3.1 劳务费

劳务费中央财政专项资金 12.00 万元。

序号	人员类别	标准（万元）	投入本项目工作时间（人日）	金额（万元）
1	项目聘用研究人员	0.15	30	4.50
2	硕士研究生	0.05	90	4.50
3	临时工	0.10	30	3.00
	合计			12.00

3.2 专家咨询费

无。

（二）间接费用

管理费主要用于项目实施中现有仪器设备及房屋，水、电、气、暖消耗，有关管理费用的补助支出；**绩效支出**是任务承担单位为提高科研工作的绩效安排的相关支出，是在对科研工作者进行绩效考核的基础上，结合科研实绩，由所在单位根据国家有关规定统筹安排。子课题间接经费将纳入项目参加单位财务统一管理，统筹安排使用。

间接经费预算中央财政资金 11.00 万元。

二、其他来源资金

对其他来源资金主要用途、支出预算做简要说明。

任务书签署

甲乙双方根据《国务院印发关于深化中央财政科技计划（专项、基金）管理改革方案的通知》（国发〔2014〕64号）、《国务院关于优化科研管理提升科研绩效若干措施的通知》（国发〔2018〕25号）、《国务院办公厅关于改革完善中央财政科研经费管理的若干意见》（国办发〔2021〕32号）、《科技部 财政部关于印发<国家重点研发计划管理暂行办法>的通知》（国科发资〔2017〕152号）、《财政部 科技部关于印发<国家重点研发计划资金管理办法>的通知》（财教〔2021〕178号）、《科学技术活动违规行为处理暂行规定》（科学技术部令第19 号）、科技部财政部关于印发<中央财政科技计划（专项、基金等）监督工作暂行规定>的通知》（国科发政〔2015〕471号）、《科技部自然科学基金委关于进一步压实国家科技计划（专项、基金等）任务承担单位科研作风学风和科研诚信主体责任的通知》(国科发监〔2020〕203号)等有关文件规定，以及有关法律、政策和管理要求，依据课题立项通知，签署本任务书。

同时，本单位和子课题负责人**郑重承诺**：对本子课题所有成果产出（包括但不限于新产品、新技术、标准、论文、专利等）的真实性、与课题（子课题）的关联性等负责，将按要求落实科研作风学风和科研诚信主体责任；项目经费全部用于与本项目研究工作相关的支出，不截留、挪用、侵占，不用于与科学研究无关的支出；严格按照政府采购和保密法律法规规定开展政府采购活动，规范信息公开工作；接受并积极配合相关部门的监督检查。如有违反，本单位和子课题负责人以及相关成果产出者愿接受项目管理专业机构和相关部门做出的各项处理决定，包括但不限于终止子课题执行、追回子课题经费，取消一定期限国家科技计划项目申报资格，记入科研诚信严重失信行为数据库以及主要负责人接受相应党纪政纪处理等。

课题牵头承担单位（甲方）：农业农村部南京农业机械化研究所

法定代表人签字（签章）：周国民

（公章）

年　月　日

课题负责人签字（签章）：丁幼春

年　月　日

子课题承担单位（乙方）：华南农业大学

法定代表人签字（签章）：薛红卫

（公章）

年　月　日

子课题负责人签字（签章）：

2025年10月29日

合同编号：

技术咨询合同

项　目　名　称：种子移动干燥机咨询服务

委托方（甲方）：广州天丁科技有限公司

受托方（乙方）：华南农业大学

签　订　时　间：2025 年 11 月 25 日

签　订　地　点：广东广州

有　效　期　限：2025 年 11 月 25 日-2025 年 12 月 31 日

中华人民共和国科学技术部印刷

填 写 说 明

一、本合同为中华人民共和国科学技术部印制的技术咨询合同示范文本，各技术合同登记机构可推介技术合同当事人参照使用。

二、本合同书适用于一方当事人（受托方）为另一方（委托方）就特定技术项目提供可行性论证、技术预测、专题技术调查、分析评价报告所订立的合同。

三、签约一方为多个当事人的，可按各自在合同关系中的作用等，在“委托方”、“受托方”项下（增页）分别排列为共同委托人或共同受托人。

四、本合同书未尽事项，可由当事人附页另行约定，并可作为本合同的组成部分。

五、当事人使用本合同书时约定无需填写的条款，应在该条款处注明“无”等字样。

技术咨询合同

委托方（甲方）： 广州天丁科技有限公司

住　所　地：广州市天河区灵山东路 5 号大厦 801

法定代表人：许志林

项目联系人：许志林

联系方式

通讯地址：广州市天河区灵山东路 5 号大厦 801

电　　话：[redacted]　传　真：

电子信箱：[redacted]

受托方（乙方）： 华南农业大学

住　所　地：广东省广州市天河区五山路 483 号

法定代表人：薛红卫

项目联系人：张烨

联系方式

通讯地址：广东省广州市天河区五山路 483 号

电　　话：[redacted]　传　真：[redacted]

电子信箱：[redacted]

本合同甲方委托乙方 种子移动干燥机 项目进行技术咨询，并支付咨询报酬。双方经过平等协商，在真实、充分地表达各自意愿的基础上，根据《中华人民共和国民法典》的规定，达成如下协议，并由双方共同恪守。

第一条 乙方进行技术咨询的内容、要求和方式：

1、咨询内容：种子移动干燥机。

2、咨询要求：针对广东省种子品质和环境气候特点提供干燥机的设计和工艺条件。

3、咨询方式：提供一份咨询报告。

第二条 乙方应当按照下列进度要求进行本合同项目的技术咨询工作：在2025年12月31日前，向甲方提供一份种子移动干燥机咨询报告。。

第三条 为保证乙方有效进行技术咨询工作，甲方应当向乙方提供下列协作事项：

1、提供技术资料：

（1）无。

2、提供工作条件：

（1）无。

3、其他：无。

甲方提供上述协作事项的时间及方式：签订合同起3天内完成。

第四条 甲方向乙方支付技术咨询报酬及支付方式为：

1、技术咨询报酬总额为：￥50000.00（人民币伍万元整）

2、技术咨询报酬由甲方一次（一次或分期）支付乙方。

具体支付方式和时间如下：

（1）签订合同后，乙方开具合同款100%的增值税普通发票提供甲方，经甲方审核无误后7天内支付给甲方，即￥50000.00（人民币伍万元整）。

乙方开户银行名称、地址和账号为：

开户银行：广州工行五山支行

地　　址：广东省广州市天河区五山路483号

账　　号：3602002609000310520

第五条 双方确定因履行本合同应遵守的保密义务如下：

甲方：

1、保密内容（包括技术信息和经营信息）：乙方提供给甲方的技术方案。

2、涉密人员范围：能够获取该项目技术资料的所有人员。

3、保密期限：自合同签署日起2年。

4、泄密责任：赔偿由此对乙方造成的一切经济损失。

乙方：

1、保密内容（包括技术信息和经营信息）：甲方透露给乙方的经营策略及一切商业秘密。

2、涉密人员范围：参与该项目及能够获取该项目资料的所有人员。

3、保密期限：自合同签署日起2年。

4、泄密责任：赔偿由此对甲方造成的一切经济损失。

第六条 本合同的变更必须由双方协商一致，并以书面形式确定。但有下列情形之一的，一方可以向另一方提出变更合同权利与义务的请求，另一方应当在30日内予以答复；逾期未予答复的，视为同意：

1、无。

第七条 双方确定，按以下标准和方式对乙方提交的技术咨询工作成果进行验收：

1、乙方提交技术咨询工作成果的形式：提交一份技术咨询报告。

2、技术咨询工作成果的验收标准：咨询报告得到甲方确认。

3、技术咨询工作成果的验收方法：技术咨询验收。

4、验收的时间和地点：2025年12月31日之前，广州。

第八条 双方确定，按以下约定承担各自违约责任：

1、甲方违反本合同第四条约定，应当按每延误一天，按照技术服务费用当期金额的万分之一向乙方支付违约金。（支付违约金或损失赔偿额的计算方法）。

2、乙方违反本合同第二、四、七条约定，应当每延误一天，按照技术咨询费用当期金额的千分之五向乙方支付违约金。（支付违约金或损失赔偿额的计算方法）。

第九条 双方确定，甲方按照乙方符合本合同约定标准和方式完成的技术咨询工作成果作出决策并予以实施所造成的损失，按以下第2种方式处理：

1、乙方不承担责任。

2、乙方承担部分责任。具体承担方式为双方协商。

3、乙方承担全部责任。

第十条 双方确定：

1、在本合同有效期内，甲方利用乙方提交的技术咨询工作成果所完成的新的技术成果，归 双 （甲、双）方所有。

2、在本合同有效期内，乙方利用甲方提供的技术资料和工作条件所完成的新的技术成果，归 双 （乙、双）方所有。

第十一条 双方确定，在本合同有效期内，甲方指定 许志林 为甲方项目联系人，乙方指定张烨为乙方项目联系人，项目联系人承担以下责任：

1、负责双方意见的交流和资料传递；

2、协调双方协助事项。

一方变更项目联系人的，应当及时以书面形式通知另一方。未及时通知并影响本合同履行或造成损失的，应承担相应的责任。

第十二条 双方确定，出现下列情形，致使本合同履行成为不必要或不可能的，可以解除本合同：

1、发生不可抗力；

2、双方协商解除。

第十三条 双方因履行本合同而发生的争议，应协商、调解解决。协商、调解不成的，确定按以下第 2 种方式处理：

1、提交_____仲裁委员会仲裁；

2、依法向人民法院起诉。

第十四条 双方确定：本合同及相关附件中所涉及的有关名词和技术术语，其定义和解释如下：

1、 无。

第十五条 与履行本合同有关的下列技术文件，经双方以 无 方式确认后，为本合同的组成部分：

1、 无 。

第十六条 双方约定本合同其他相关事项为： 无 。

第十七条 本合同一式 陆 份，具有同等法律效力。

第十八条 本合同经双方签字盖章后生效。

甲方：广州天丁科技有限公司（盖章）

法定代表人/委托代理人：（签名）

2025 年 11 月 25 日

乙方：华南农业大学（盖章）

法定代表人/委托代理人：薛红卫（签名）

2025 年 11 月 25 日

印花税票粘贴处：

（以下由技术合同登记机构填写）

合同登记编号：

1、申请登记人：_____

2、登记材料：（1）_____

（2）_____

（3）_____

3、合同类型：_____

4、合同交易额：_____

5、技术交易额：_____

技术合同登记机构（印章）

经办人：

年　月　日


科研空间
欢迎您，李成杰老师
科研动态
我的办公
我的项目
我的经费
我的成果
我的学术交流
我的考核
我的主页
常用下载
项目立项
项目申报（1）
所有项目
职称评定
主持的项目
参与的项目
博硕导评定
主持的项目
参与的项目
项目性质
纵向(4项)
横向(1项)
项目分类
国家自然科学基金项目(1项)
面上项目(1项)
基础与应用基础研究项目（博士青年科技人员类）(1项)
国家重点研发计划子课题(1项)
技术咨询(1项)
参与形式
主持(3项)
参与(2项)
总数:5项 (表中经费单位：万元)
项目名称
查询
新增
删除
导出
全选
项目名称
项目分类
项目成员
起止日期
合同金额
项目状态
审核状态
操作
种子移动干燥机咨询服务
技术咨询
张烨,李成杰
2025-11-25--2025-12-31
5
进行
学校通过
微波协同热风干燥油茶果爆蒲热湿传递特性及茶蒲失水形变机制
面上项目
李成杰
2025-03-07--2027-12-31
10
进行
学校通过
编辑
基于?分析法的稻谷深床干燥能里优化及其模型预测控制研究
国家自然科学基金项目
李成杰
2024-12-01--2027-12-31
30
进行
学校通过
编辑
主粮作物移动式烘干机变温精准干燥关键技术研发
国家重点研发计划子课题
张烨,陈震,李成杰,赵懿琨,班华,李圣陶（学）,孙懿清（学）,陈铸荣（学）,黄清楷（学）,覃杨（学）,黄建江（学）,纪思涵（学）,陈衍成（学）,谢志金（学）,刘仕杰（学）,彭智康（学）,余展豪（学）,谢兆豪（学）
2024-11-01--2027-11-30
60
进行
学校通过
高湿稻谷干燥节能增效机制及递阶智能控制方法研究
基础与应用基础研究项目（博士青年科技人员类）
李成杰
2023-12-18--2025-12-31
5
完成
学校通过
编辑
1/1 共5条
1
技术支持：北京易普拉格科技有限责任公司[科研管理系统] 演示授权版本 信息反馈

SCAULIB202625117

检索证明

根据委托人提供的论文材料，委托人华南农业大学 李成杰(学科类型：自然科学)5篇论文收录情况如下表。

序号	论文名称	发表刊物及发表的年月卷期/页码等	作者排名	论文等级	作者文中单位	收录情况	影响因子	中科院大类分区
1	Hierarchical model predictive control for energy consumption regulation of industrial-scale circulation counter-flow paddy drying process	ENERGY 出版年：2025 出版日期：APR 15 卷期：321 页码：- 文献号：135431 文献类型：Article	第一作者	T2类	华南农业大学 工程学院	SCI	IF2-year=9.4 IF5-year=8.8 (2024)	工程技术 1区 Top 期刊：是 OA 期刊:否 标注：Mega-Journal (2025)
2	Transient thermodynamic analysis and energy optimization of a circulation counter-flow wheat drying system utilizing a closed-loop heat pump configuration	ENERGY CONVERSION AND MANAGEMENT 出版年：2025 出版日期：DEC 15 卷期：346 页码：- 文献号：120508 文献类型：Article	第一作者	T2类	华南农业大学 工程学院	SCI	IF2-year=10.9 IF5-year=10.2 (2024)	工程技术 1区 Top 期刊：是 OA 期刊:否 (2025)
3	油茶果热风干燥爆蒲后茶籽传热传质特性及干燥工艺优化	农业工程学报 出版年：2024 出版日期：2024.12 卷期：40 23 页码：332-341	通讯作者	T2类	华南农业大学 工程学院	EI	无	无

		文献号: 10.11975/j.1ssn.1002-6819.202406126 文献类型：期刊论文						
4	Deep-Learning-Based Model Predictive Control of an Industrial-Scale Multistate Counter-Flow Paddy Drying Process	FOODS 出版年：2024 出版日期：JAN 卷期：13 1页码：- 文献号：43 文献类型：Article	通讯作者	A类	华南农业大学工程学院	SCI	IF2-year=5.1 IF5-year=5.6 (2024)	农林科学 2区 Top 期刊：否 OA 期刊:是 标注：Mega-Journal (2025)
5	基于响应面的白萝卜热风干燥品质及工艺研究	包装工程 出版年：2024 出版日期：2024.11 卷期：45 21 页码：147-157 文献号: 文献类型：期刊论文	通讯作者	A 类	华南农业大学工程学院	北大核心	无	无

说明：论文等级和中科院大类分区按《华南农业大学学术论文评价方案(试行)》划分。

报告免责声明：如未盖章，报告无效

检索员：张进

华南农业大学图书馆

2026-02-28

Energy Conversion and Management 346 (2025) 120508

Contents lists available at ScienceDirect

Energy Conversion and Management

journal homepage: www.elsevier.com/locate/enconman

Research Paper

Transient thermodynamic analysis and energy optimization of a circulation counter-flow wheat drying system utilizing a closed-loop heat pump configuration

Chengjie Li *, Jianjiang Huang, Yancheng Chen, Sihan Ji, Changyou Li, Ye Zhang

College of Engineering, South China Agricultural University, Guangzhou 510642, China

ARTICLE INFO

Keywords:
Drying
Transient analysis model
Wheat
Closed-loop heat pump
Energy optimization

ABSTRACT

Closed-loop heat pump drying of wheat constitutes a dynamic and intricately interconnected composite system, wherein the heat pump and the dryer mutually act as heating sources. During operation, it demonstrates various characteristics, such as large inertia, nonlinearity, and multiple disturbances, which pose considerable challenges to the energy optimization of the system. This study introduces a transient analysis model that deeply delves into the dynamic processes of industrial-scale closed-loop heat pump drying. Subsequently, it facilitates in-depth analysis of transient thermodynamic behaviors and energy utilization patterns throughout the drying process. Results indicate that the mean relative deviations for the predicted wheat moisture content and temperature were 2.66 % and 1.12 %, respectively. Reducing the temperature disparity between the condenser and the drying air alongside decreasing the inlet temperature of the expansion valve markedly enhances the energy efficiency of the system. The study proposes an optimization scheme by designing two regenerators to preheat the drying air twice, resulting in a 26.3 % reduction in compressor power and a 32.5 % reduction in system exergy loss. The research findings offer data and methodological support for optimizing the energy efficiency of closed-loop heat pump drying system and provide mathematical as well as analytical methods for system analysis, state tracking, and dynamic parameter tuning.

1. Introduction

Wheat is major staple crop worldwide, and its drying crucial during postharvest processing to ensure food security and reduce economic losses [1]. The moisture content of stored wheat must be maintained within the range of 0.12–0.14 g water/g wet matter [2]; however, freshly harvested wheat typically exhibits higher moisture level. Delayed or inadequate drying practices can induce mold proliferation, premature germination [3], and carcinogenic aflatoxin generation, all of which degrade grain quality [4,5]. At present, industrial-scale drying predominantly relies on hot air technologies fueled by coal or agricultural straw. These methods often encounter challenges, such as low energy efficiency and high carbon emissions [6,7]. Closed-loop heat pump drying has gained widespread attention for drying food, agricultural products, and industrial materials owing to its high efficiency, energy saving capacity, precise temperature control, and minimal impact on the quality of the dried material [8]. This technology uses a heat pump system to recover and reuse heat from the air within a closed structure, thereby enhancing energy efficiency and reducing external environmental interference during the drying process [9,10]. This makes it particularly suitable for large-scale drying operations of agricultural products.

Closed-loop heat pump drying systems operate on the principle of the reverse Carnot cycle, with the core structure comprising key components such as a drying chamber, evaporator, and condenser. By using the thermodynamic cycle of a refrigerant, this system converts low-grade thermal energy into high-grade thermal energy. This characteristic facilitates markedly higher energy efficiency compared with traditional hot-air drying or open-loop drying systems [11,12]. To further enhance the energy efficiency of system, considerable efforts have been made in existing research. For instance, Duan et al. [13] proposed a two-stage evaporative heat pump drying system designed for graded cooling and dehumidification. This system achieved a 15.5 %–19.3 % increase in coefficient of performance (COP) and a 16.3 %–18.9 % improvement in specific moisture extraction rate (SMER). Osta et al. [14] designed a closed-loop drying system integrating two thermoelectric modules, and their study demonstrated that this system achieves an optimal moisture

* Corresponding author.
E-mail address: chengjie.li@scau.edu.cn (C. Li).

https://doi.org/10.1016/j.enconman.2025.120508
Received 27 May 2025; Received in revised form 30 August 2025; Accepted 7 September 2025
Available online 13 September 2025

Nomenclature

A	Bypass rate, %
c	Specific heat, kJ/kg/°C
COP	Coefficient of performance
d	Humidity ratio, kg/kg
d_s	Saturated humidity ratio, kg/kg
Ex	Exergy, kW
f	Cooling coefficient, h^{-1}
h	Heat transfer coefficient, kg/h/m^2
H	Specific enthalpy, kJ/kg
Δh	Latent heat of condensation, kJ/kg
k	Drying constant, h^{-1}
m	Dehydration rate, kg/h
M	Moisture content, g water/g wet or dry matter
MR	Moisture ratio
MRD	Mean relative deviation
P_c	Compressor power, kW
qm	Mass flow, kg/h
Q	Heat exchange, kW
R	Gas constant, kJ/kg/°C
RH	Relative humidity, %
$RMSE$	Root-mean-square error, g water/g wet matter or °C
S	microelement cross-sectional area
SMER	Specific moisture extraction rate
t	Drying time, h
T	Temperature, °C
v	Flow velocity, m/h
Y_{prej}	Predicted values
Y_{obsj}	Experimental values
z	Bed height, m

Greek letters

ρ	Density, kg/m^3
ε	Heat exchange efficiency
η	Efficiency
$\gamma\alpha$	Effective evaporation area per unit volume, m^2/m^3
μ	Interphase mass transfer coefficient, kg/h/m^2
λ_g	Latent heat of vaporisation of wheat, kJ/kg
$\tau\alpha$	Effective heat transfer area per unit volume, m^2/m^3

Subscripts

a	Drying air
ab	Ambient
c	Cold transfer medium
cr	Condenser
d	Drying
er	Evaporator
ev	Expansion valve
g	Grain
h	Hot transfer medium
r	Refrigerant
ir	Irreversibility
r	Refrigerant
s	Saturated vapour state
wev	Water evaporation
0	Initial

Superscripts

in	Inlet
out	Outlet

Fig. 1. Diagram of 5HP-50-CLHP wheat dryer.

removal rate under high humidity conditions. However, enhancing the energy efficiency of this technology during drying remains a critical challenge, issues such as the evaporator's substantial refrigeration capacity consumption required to handle medium-to-low temperature sensible heat before recovering latent heat from the drying exhaust as well as significant temperature differences between media in the condenser, which exacerbate irreversible losses. These problems severely constrain further enhancement of the system's energy performance.

Closed-loop heat pump drying involves complex heat and mass transfer. It operates through a synergistic coupling mechanism between the refrigerant cycle and the drying air circulation path, wherein the drying chamber and the heat pump system are the mutual heat sources. During drying, fluctuations in any internal parameter or external random disturbances induce transient responses in the system. The use of physical detection methods makes it difficult to accurately obtain

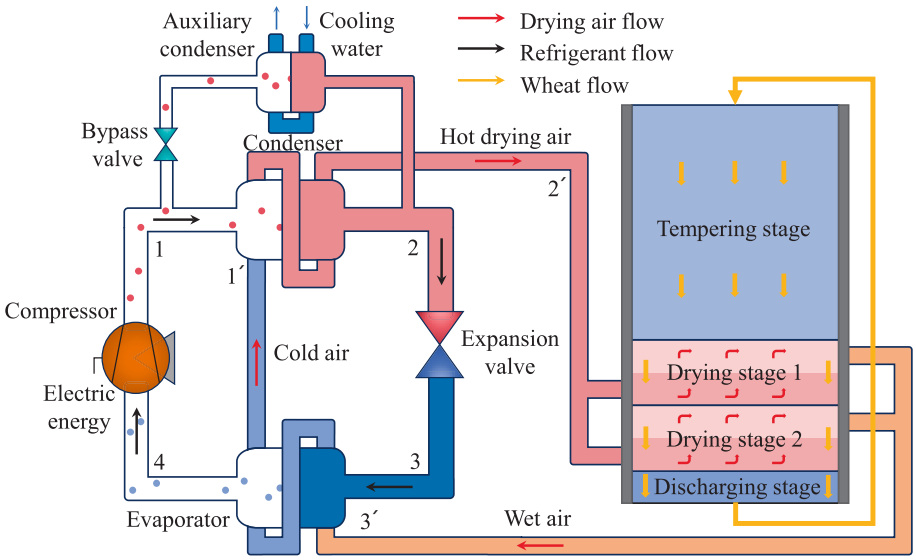

Fig. 2. Physical model of the 5HP-50-CLHP wheat dryer.

transient data of various parameters at specific locations in reality, such as the temperature and humidity of the drying medium, mass flow rate, and material status. This issue is the main reason behind no improvements in the efficiency of closed-loop heat pump drying. To address this, previous researchers have focused on the use of mathematical modeling methods for analyzing the closed-loop heat pump drying process [15,16]. Fu et al. [17] developed thermodynamic models for various closed-loop systems based on steady-state assumptions, analyzed the impact of different parameters on energy performance, and proposed optimization solutions for high-energy consumption links. This led to a 35.59 % increase in SMER. Chen et al. [18] combined a reverse enthalpy–based method with a particle swarm optimization algorithm to develop a quasi-steady-state model for closed-loop heat pump dryers and reported maximum prediction deviations of − 4.72 % for the moisture extraction rate and − 6.50 % for the SMER. Xie et al. [19] developed a transient model based on thermodynamic cycle mechanisms and heat/mass transfer assumptions, achieving model errors within 20 %. They found that increasing wet air velocity enhances heat transfer capacity. However, previous researchers have mainly focused on the development of steady-state models or the use of laboratory-scale drying devices, which makes it difficult to capture the transient response characteristics of industrial-scale equipment and accurately describe real-time energy consumption during the drying process.

In summary, research on the dynamic modeling of industrial-scale closed-loop heat pump drying processes for optimizing the energy efficiency of the system remains unexplored. Building on our previous research [20,21], this study focused on a closed-loop heat pump circulation counter-flow wheat dryer (Model 5HP-50-CLHP) and proposing a novel transient analysis model that deeply delves into the dynamic processes of closed-loop heat pump–based drying. Based on this model, transient thermodynamic and transient energy consumption analyses of the drying process are conducted to identify key stages of system energy loss and optimize the traditional closed-loop heat pump thermodynamic architecture in a targeted manner to enhance the energy efficiency of the entire system.

2. System description

2.1. Drying equipment

Fig. 1 shows a 5HP-50-CLHP wheat dryer installed at the Lifang wheat drying base in Yuncheng, Shanxi Province, China. This dryer mainly consists of a drying chamber, heat pump, cyclone separator, hoist, and control center. It being the system core, the drying chamber is vertically divided into the tempering, drying, and discharging stages. The tempering stage, positioned at the tower apex with a 6-m thickness, facilitates moisture and temperature redistribution within the grain particle. This mitigates the wet and thermal stress types, which are induced by rapid drying and is crucial for preventing kernel rupture, a phenomenon colloquially termed as “waist bursting” [22]. The drying stage comprises two small counter-flow drying stages, of them are 1-m thick. Each small counter-flow drying stage is subdivided into two layers: a lower 0.5-m-thick inlet duct that supplies hot drying air heated by the heat pump condenser and an upper 0.5-m-thick exhaust duct that discharges wet air, which condensed and dehumidified by the heat pump evaporator, releasing latent heat during the process. The drying chamber and heat pump are mutual heat sources within this closed-loop configuration. The discharging stage, located at the bottom of the drying tower with a 0.5-m thickness, does not involve water removal and can be considered as a tempering stage.

2.2. Physical model

Fig. 2 illustrates the physical model of the 5HP-50-CLHP wheat dryer. The physical model framework comprises three cycles: wheat, drying air, and refrigerant. Each cycle possesses distinct transport mechanisms and energy conversion pathways within the system. Before starting the drying process, the drying tower is first loaded with wet wheat, followed by activation of dryer. The grain progressively traverses three distinct operational zones: the tempering, drying, and discharging stages. Upon reaching the base of the tower, the wheat is transported back to the top via a bucket hoist, reentering the tower for continuous circulation. During this process, wheat repeatedly traverses the drying stage, where it interacts with the drying air for the progressive removal of water. In the drying stage, wheat moves in opposite direction to that of the drying air, accommodating the typical pattern of rapid initial drying followed by slower dehydration [23]. As the drying continues, the moisture content of wheat gradually decreases until it reaches the predetermined target value, the point at which point it is finally discharged from the tower.

The drying air cycle operates as described: first, ambient cold air passes through the condenser, where it absorbs heat from the refrigerant and is transformed into hot drying air (state 2́). Subsequently, the hot drying air enters the drying tower, where it interacts with the wheat, absorbing moisture and releasing it as wet air (state 3́). Subsequently, wet air enters into the evaporator, where it gets cooled, causing the

Table 1
Comprehensive delineation of the sensors and instruments.

Devices	Model	Precision	Manufacturer
Air convection oven	LC-101–00	–	Shanghai Lichen Instrument Technology Co., Ltd., China
Infrared thermometer	AM390	0.1 °C	Dongguan Wanchuang Electronic Products Co., Ltd., China
Temperature & humidity sensor	AM2305	0.3 °C & 2 %	Shenzhen Maishida Electronic Technology Co., Ltd., China
Anemometer	QDF-6	0.01 m/s	Shanghai Longtuo Instrument Equipment Co., Ltd., China
Electronic scale	AH-AWC	0.1 g	Shenzhen Anheng Weighing Instrument Electronics Co., Ltd., China

entrained water vapor to condense into liquid water, which is further drained away. This process dehumidifies the air, converting it back into cold air (state 1́) and while releasing latent heat. The resulting cold air is recirculated to the condenser to reabsorb heat, transforming into hot drying air (state 2́) and completing a full drying cycle.

The refrigerant cycle operates as described: the compressor raises the low-pressure, low-temperature gaseous refrigerant to a high-pressure, high-temperature state (state 1). Subsequently, the high-pressure, high-temperature refrigerant flows through the condenser, transferring heat to the drying air and transforming the phase into a medium-temperature, high-pressure liquid (state 2). To enhance condensation efficiency and accurately control condensation temperature, an auxiliary condenser is supplemented to the main condenser. This component uses cooling water to condense the high-temperature, high-pressure refrigerant at the compressor outlet to a set saturation state. The high-pressure liquid refrigerant throttling via the expansion valve reduces the refrigerant's pressure and temperature, converting it into a low-pressure, low-temperature gas–liquid mixture (state 3). Finally, this mixture enters the evaporator. Inside the evaporator, the refrigerant absorbs heat from the wet air discharged by the drying tower, vaporizes into a gaseous refrigerant (state 4), and ultimately returns to the compressor to repeat the cycle.

2.3. Data acquisition

Systematic monitoring and acquisition of crucial process parameters provide mathematical foundations essential for the subsequent analysis of the drying system. The average moisture content of wheat was determined using the standard oven method [24]. The initial wheat temperature was measured using an infrared thermometer. Throughout the drying process, data on air temperature (inlet and outlet) and relative humidity (inlet and outlet) were collected using specific sensors connected to a custom-built data acquisition system and measurements were taken every 10 min. Manual measurements were performed to determine the moisture content and temperature of wheat samples collected from specific locations within the drying tower. The average drying air flow velocity was continuously monitored using an anemometer positioned at the dryer's air inlet, where the air flow was evenly distributed. The average flow velocity of wheat was calculated using an electronic scale. Table 1 presents a comprehensive list of the sensors and instruments used in the field production.

3. Transient analysis model

In this section, a transient analysis model of the circulation counter-flow wheat drying system utilizing a closed-loop heat pump configuration is developed. The following assumptions were made before developing and solving the drying system equations:

1) Wheat deep-bed drying was modeled as a one-dimensional process along the bed height.
2) The water within wheat was diffused to the drying medium in gaseous form.
3) The compression process was assumed to be adiabatic, and the pressure and flow losses of the refrigerant and drying air during the cycle were disregarded.
4) The outlet refrigerant temperatures of the auxiliary condenser and condenser were set equal to the condensing temperature, and energy losses after fluid mixing were ignored.

3.1. Drying stage

3.1.1. Mass conservation equation

A microelement drying system was extracted with boundaries and volume. Within this system, the quality of water evaporated from wheat during a period of time (Δt) is expressed as follows:

$$\Delta m_{wg} = \rho_g S \frac{\partial M_d}{\partial t} \Delta z \Delta t \tag{1}$$

where ρ_g denotes the bulk density of absolute dry wheat; S, cross-sectional area of the microelement; M_d, wheat moisture content on a dry basis; Δz, height of microelement drying system; and t, drying time.

Based on the Meel Van analytical method and the exponential model that describes the thin-layer drying characteristics of wheat, the quality of water evaporated from wheat as it traverses Δz during Δt is calculated as follows:

$$\Delta m_{vw} = \mu \gamma \alpha S (d_s - d) MR \Delta z \Delta t \tag{2}$$

where μ denotes the interphase heat transfer coefficient; $\gamma\alpha$, effective evaporation area of unit volume; d_s, saturated humidity; d, air humidity ratio; and MR, moisture ratio.

The quality of water absorbed by the drying medium as it traverses Δz during Δt is calculated as follows:

$$\Delta m_{aw} = \rho_a v_a S \frac{\partial d}{\partial z} \Delta z \Delta t \tag{3}$$

where ρ_a denotes the drying air density; v_a, drying air flow velocity; and z, bed height.

Factors that contribute to the changes in moisture content in Δz include evaporated water from the wheat and the flow of wheat itself. The change in water quality over the interval Δz during the time period Δt, caused by wheat flow, is calculated as follows:

$$\Delta m_{fw} = \rho_g v_g S \frac{\partial M_d}{\partial z} \Delta z \Delta t \tag{4}$$

where v_g denotes the wheat flow velocity.

Based on the principles of mass migration conservation, Eqs. (5) and (6) were derived from Eqs. (1) to (4):

$$\rho_g \frac{\partial M_d}{\partial t} = v_g \rho_g \frac{\partial M_d}{\partial z} - \mu \gamma \alpha (d_s - d) MR \tag{5}$$

$$\mu \gamma \alpha (d_s - d) MR = v_a \rho_a \frac{\partial \mathrm{d}}{\partial z} \tag{6}$$

3.1.2. Heat conservation equation

The reduced enthalpy of the drying medium as it traverses Δz during Δt is calculated as follows:

$$\Delta Q_a = c_a \rho_a v_a S \frac{\partial T_a}{\partial z} \Delta z \Delta t \tag{7}$$

where c_a denotes the specific heat of drying air and T_a denotes the temperature of drying air.

The heat exchange between the drying medium and wheat as it traverses Δz during Δt is calculated as follows:

$$\Delta Q_{he} = h\tau\alpha S\left(T_a - T_g\right)\Delta z\Delta t \tag{8}$$

where h denotes the heat transfer coefficient; $\tau\alpha$, the effective heat transfer area per unit volume; and T_g, the temperature of wheat.

The heat required to evaporate water in Δz during Δt represents the useful energy, which is calculated as follows:

$$\Delta Q_{hv} = \lambda_g \mu\gamma\alpha S(d_s - d)MR\Delta z\Delta t \tag{9}$$

where λ_g denotes the latent heat of wheat vaporization.

In the drying system, energy loss inevitably occurs in various forms, such as heat loss. Based on previous assumptions, the two primary types of heat loss are the heating wheat-associated heat loss and the exhaust heat loss. The former in Δz during Δt is calculated as follows:

$$\Delta Q_{hh} = c_g \rho_{g,w} S\frac{\partial T_g}{\partial t}\Delta z\Delta t \tag{10}$$

where c_g denotes the specific heat of wheat and $\rho_{g,w}$ denotes the bulk density of wet wheat.

The flow of wheat removes some amount of heat. Therefore, the heat loss in Δz during Δt due to wheat flow is calculated as follows:

$$\Delta Q_{hf} = c_g \rho_{g,w} v_g S\frac{\partial T_g}{\partial t}\Delta z\Delta t \tag{11}$$

The heat conservation equation, represented by Eqs. (12) and (13), is derived from Eqs. (7) to (11):

$$c_a\rho_a v_a\frac{\partial T_a}{\partial z} - v_g c_g \rho_{g,w}\frac{\partial T_g}{\partial z} = c_g\rho_{g,w}\frac{\partial T_g}{\partial t} + \lambda_g\mu\gamma\alpha(d_s - d)MR \tag{12}$$

$$h\tau\alpha\left(T_a - T_g\right) = -c_a\rho_a v_a\frac{\partial T_a}{\partial z} \tag{13}$$

3.2. Tempering stage

During the tempering stage, wheat's internal stress reduces as it moves slowly without losing moisture. Concurrently, the temperature gradually decreases owing to heat loss via convection and radiation. The equations governing heat and mass transfer during moisture redistribution are as follows [20,21]:

$$\frac{\partial M_d}{\partial t} = v_g\frac{\partial M_d}{\partial z} \tag{14}$$

$$\frac{\partial T_g}{\partial t} = v_g\frac{\partial T_g}{\partial z} - f\left(T_g - T_{ab}\right) \tag{15}$$

where f denotes the cooling coefficient and T_{ab} denotes the ambient temperature.

3.3. Heat source

The compressor, which is essential for elevating refrigerant pressure and temperature within the heat pump drying cycle, is characterized by its adiabatic efficiency and power, expressed as follows [25]:

$$\eta_c = \frac{h_s'' - h'}{h'' - h'} \tag{16}$$

$$P_c = q\dot{m}r(h'' - h') \tag{17}$$

where η_c denotes the adiabatic efficiency of the compressor; h_s'', specific enthalpy at the compressor outlet under isentropic compression; h'', actual specific enthalpy at the compressor outlet; h', specific enthalpy at the compressor inlet; P_c, compressor power; and $q\dot{m}r$, mass flow rate of the refrigerant.

The thermodynamic exchange equation for the heat transfer between the drying air and the refrigerant in the condenser is expressed as follows [26]:

$$\dot{Q}_{cr} = q\dot{m}a\left(h_{cr,a}^{out} - h_{cr,a}^{in}\right) = \left(1 - \dot{A}\right)q\dot{m}r\left(h_{cr,r}^{in} - h_{cr,r}^{out}\right) \tag{18}$$

where $h_{cr,a}^{in}$ and $h_{cr,a}^{out}$ denote the specific enthalpies of circulating drying air at the inlet and outlet, respectively; $q\dot{m}a$, mass flow rate of circulating drying air; A, bypass rate; and $h_{cr,r}^{in}$ $h_{cr,r}^{out}$, specific enthalpies of the refrigerant entering and exiting the condenser, respectively.

The bypass rate is expressed as the percentage of heat absorbed by cooling water in the auxiliary condenser relative to the total heat released during the condensation of the refrigerant to a specified temperature.

The mass flow rate of drying air during drying process is calculated as follows:

$$q\dot{m}a = \frac{\dot{m}_d}{d^{out} - d^{in}} \tag{19}$$

where $\dot{m}_d$ denotes the dehydration rate of wheat and d^{in} and d^{out} denote the moisture contents of drying air entering and exiting the drying tower, respectively.

The association between the specific enthalpies of the refrigerant at the inlet and outlet of the expansion valve is expressed as follows [27]:

$$h_{ev,r}^{in} = h_{ev,r}^{out} \tag{20}$$

where $h_{ev,r}^{in}$ and $h_{ev,r}^{out}$ denote the specific enthalpies of the refrigerant entering and exiting the expansion valve, respectively.

The thermodynamic exchange equation for the heat transfer between the drying air and the refrigerant in the evaporator is expressed as follows [28]:

$$\dot{Q}_{er} = q\dot{m}a\left(h_{er,a}^{in} - h_{er,a}^{out}\right) + \dot{m}_d\Delta h = q\dot{m}r\left(h_{er,r}^{out} - h_{er,r}^{in}\right) \tag{21}$$

where $h_{er,a}^{in}$ and $h_{er,a}^{out}$ denote the specific enthalpies of circulating drying air entering and exiting the evaporator, respectively; Δh, the latent heat of condensation of water vapor; and $h_{er,r}^{in}$ and $h_{er,r}^{out}$, specific enthalpies of the refrigerant entering and exiting the evaporator, respectively.

For a wheat drying tower with initial moisture content M_0 and grain temperature $T_{g,0}$, operating under specified initial drying air conditions with temperature $T_{a,0}$ and humidity ratio d_0, the system's initial and boundary conditions are mathematically defined as follows:

Initial condition:

$$\begin{cases} M_{i,0} = M_0 \\ T_{g,i,0} = T_{g,0} \end{cases} \tag{22}$$

Boundary conditions:

$$\begin{cases} d_{0,t} = d_0 \\ T_{a,0,t} = T_{a,0} \end{cases} \tag{23}$$

Where i denotes the i-th layer within the drying system.

3.4. Parameter calculation

Assuming that thin-layer drying follows an exponential model with a drying constant k, the maximum dehydration rate of grain per unit volume in deep-bed drying is $\rho_g k(M_d - M_e)$ and the maximum evaporation rate per unit volume is $\mu\gamma\alpha(d_s - d)MR_{\max}$. By setting $MR_{\max} = 1$, the maximum drying rate of grain equals the maximum interfacial evaporation rate, resulting in the following equation:

$$\mu\gamma\alpha = \frac{\rho_g k(M_d - M_e)}{(d_s - d)} \tag{24}$$

By integrating both sides of Eq. (13) with respect to z, the following equation can be obtained:

Table 2
Equations and parameter values used in the transient analysis model.

Parameter	Value/Equation	Units	Ref
λ_g	$\lambda_g = [2500 - 2.386(T_g + 273.15)][1 + 23\exp(-40M_d)]$	kJ/kg	[29]
c_g	$c_g = 1.11 + 0.045\frac{M_d}{1+M_d}$	kJ/kg/℃	[30]
ρ_g	$\rho_g = \frac{1}{1+M_d}(-5.9M_d + 763.9)$	kg/m^3	[30]
H	$H = 1.005T_a + d(2501 + 1.86T_a)$	kJ/kg	[31]
P_s	$P_s = 133.322\exp\left(18.751 - \frac{4075.16}{236.516 + Ta}\right)$	Pa	[32]
d	$d = 0.622\cdot\frac{RHaP_s}{P_b - RHaP_s}$	kg/kg	[11]
M_e	$M_e = \left[\frac{-\ln(1-RH)}{1.23\times10^{-5}(T_a+63.346)}\right]^{\frac{1}{2.558}}$	%d.b.	[29]
k	$k = 0.0388T_{a,in} - 1.046$	h^{-1}	[33]
c_a	1.004	kJ/kg/℃	–

$$h\tau\alpha\left(\int_0^z T_a\partial z - \int_0^z T_g\partial z\right) = -c_a\rho_a v_a\int_{T_{a,out}}^{T_{a,in}}\partial T_a \tag{25}$$

According to the mean value theorem of integrals:

$$\int_0^z T_a\partial z = \overline{T_a}z \tag{26}$$

$$\int_0^z T_g\partial z = \overline{T_g}z \tag{27}$$

where $\overline{T_a}$ denotes the qualitative drying air temperature and $\overline{T_g}$ denotes the qualitative grain temperature.

These qualitative temperatures reflect the average properties of the drying medium and the grain within the drying layer, with their values defined as the arithmetic mean of the temperatures at the inlet and outlet.

By simultaneously solving Eqs. (25) to (27), the following equation can be obtained:

$$h\tau\alpha = v_a c_a\rho_a\frac{T_{a,in} - T_{a,out}}{z(\overline{T_a} - \overline{T_g})} \tag{28}$$

During the tempering stage, the cooling rate of the grain is relatively slow. Assuming that the left-hand side term of Eq. (15) is ~zero, the following equation can be obtained:

$$v_g\frac{\partial T_g}{\partial z} \approx f(T_g - T_{ab}) \tag{29}$$

By integrating both sides of Eq. (29) with respect to z and applying the mean value theorem for integrals, the following equation can be obtained:

$$f \approx \frac{v_g(T_{g,in} - T_{g,out})}{z(\overline{T_g} - \overline{T_{ab}})} \tag{30}$$

where $\overline{T_{ab}}$ denotes the average ambient temperature.

Some other equations and parameter values used in the transient analysis model are presented in Table 2.

4. Energetic evaluation index

The energy utilization characteristics of the drying system are examined from the energy and exergy perspectives. Energy efficiency is determined by the ratio of energy effectively used for water evaporation ($\dot{Q}_{wev}$) within the drying tower to the total energy supplied ($\dot{Q}_{in}$) to the tower [34]:

$$\eta_{en} = \frac{\dot{Q}_{wev}}{\dot{Q}_{in}} \tag{31}$$

$\dot{Q}_{wev}$ and $\dot{Q}_{in}$ are calculated using Eqs. (32) and (33), respectively [35]:

$$\dot{Q}_{wev} = \dot{m}_d\lambda_g \tag{32}$$

$$\dot{Q}_{in} = q\dot{m}aH_{in} \tag{33}$$

where H_{in} denotes the specific enthalpy of drying air.

The exergy for dehydration ($\dot{E}_{x,wev}$), exergy of discharged wheat ($\dot{E}_{x,g}$), and irreversibility exergy destruction ($\dot{E}_{x,ir}$) in the drying tower are calculated using Eqs. (34) to (36), respectively [36,37]:

$$\dot{E}_{x,wev} = \left(1 - \frac{T_{ab}}{T_g}\right)\dot{Q}_{wev} \tag{34}$$

$$\dot{E}_{x,g} = \left(1 - \frac{T_{ab}}{T_g}\right)\dot{Q}_g \tag{35}$$

$$\dot{E}_{x,ir} = \left(\dot{Q}_{wev} + \dot{Q}_g\right)T_{ab}\left(\frac{T_{ab} - T_g}{T_{ab}T_g}\right) \tag{36}$$

where $\dot{Q}_g$ denotes the energy expended for grain heating, calculated as follows (37) [38]:

$$\dot{Q}_g = c_g\dot{m}_g(T_{g,out} - T_{ab}) \tag{37}$$

where $\dot{m}_g$ denotes the weight flow rate of grain.

For the closed-loop heat pump aspect, this study employed the COP, SMER, and P_c as evaluation metrics for the energy performance. The COP is expressed as the ratio of heat absorbed by circulating drying air in the heat pump ($\dot{Q}_{h,a}$) to the P_c [39]:

$$COP = \frac{\dot{Q}_{h,a}}{P_c} \tag{38}$$

SMER is expressed as the ratio of the quantity of water removed during the drying process to the P_c [40]:

$$SMER = \frac{\dot{m}_d}{P_c} \tag{39}$$

5. Data analysis

5.1. Statistical analysis

Herein, two metrics were used to evaluate the precision of the transient analysis model when used in the circulation counter-flow wheat drying system utilizing a closed-loop heat pump configuration: root-mean-square error (RMSE), defined in Eq. (40) [41], and mean relative deviation (MRD), defined in Eq. (41) [42]:

Table 3
Uncertainties of the experimental measurements and total uncertainties for predicted values.

Parameter	Unit	Value
Experimental measurements		
Moisture content	g water/g wet matter	±0.050
Wheat temperature	°C	±1.134
Air temperature	°C	±0.308
Air relative humidity	–	±2.227 %
Air flow velocity	m/s	±0.015
Mass of the product	g	±1.387
Predicted measurements		
Compressor power	kW	±1.21 %
Coefficient of performance	–	±1.87 %
Specific moisture extraction ratio	kg/kWh	±2.13 %
Exergy loss	kJ/kg water	±3.73 %

$$RMSE = \left[\frac{1}{n}\sum_{j=1}^{n}\left(Y_{prej} - Y_{obsj}\right)^2\right]^{0.5} \quad (40)$$

$$MRD = \left[\frac{1}{n}\sum_{j=1}^{n}\left(\frac{Y_{prej} - Y_{obsj}}{Y_{obsj}}\right)^2\right]^{0.5} \times 100 \quad (41)$$

where Y_{prej} and Y_{obsj} denote the predicted and observed values, respectively, for the j-th data point and n denotes the total number of measurements taken in each experiment.

5.2. Uncertainty analysis

Herein, the experimental uncertainties were determined through repeated measurements using the following equation [43]:

$$U_F = \left[\left(\frac{\partial F}{\partial x_1}u_1\right)^2 + \left(\frac{\partial F}{\partial x_2}u_2\right)^2 + \ldots\ldots + \left(\frac{\partial F}{\partial x_n}u_n\right)^2\right]^{0.5} \quad (42)$$

where U_F denotes the uncertainty in the outcome; u_1, u_2, …, u_n, the uncertainty in the independent variables; x_1, x_2, …, x_n, the independent variables; and F, the function of the independent variables.

6. Results and discussion

6.1. Model validation

Table 3 presents the findings of the uncertainty analysis. According to previous researchers [44,45], an error of less than 5 % is acceptable. The calculated experimental measurement uncertainties and overall predicted value uncertainties all fall within this range.

To validate the accuracy and reliability of the transient analysis model proposed in this study, wheat drying experiments were conducted on June 7, 2023. The experimental material was Jinmai 91, a conventional variety of indica wheat, was obtained from a farm in Yuncheng, Shanxi Province, China, with freshly harvested wheat demonstrating an initial moisture content of 0.186 g water/g wet matter. For this batch of wheat drying, the condensing temperature was set at 70 °C and the drying air temperature at 60 °C. Field measurements showed an average drying air velocity of 1620 m/h and an average wheat flow velocity of 3.8 m/h. The actual drying air temperature ranged from 59.4 °C to 62.2 °C, averaging to 61 °C. The ambient air data for this location on the day of drying illustrated in Fig. S1 (Supplementary Material). Throughout the testing phase, the ambient temperature averaged 23.9 °C with relative humidity of 66.5 %. These measured ambient parameters were subsequently input into a bespoke program using linear interpolation to predict temporal variations in the moisture content and temperature profiles of the discharged grain during the drying process.

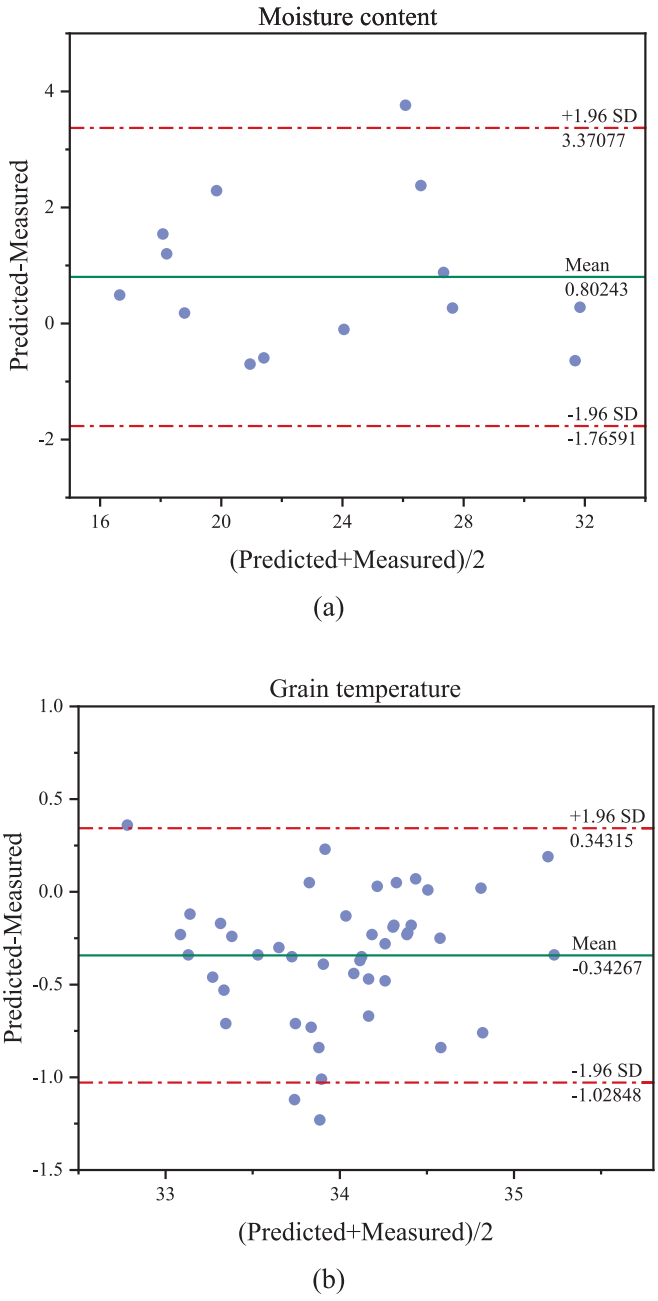

Fig. 3. Bland-Altman analysis of measured and predicted values: (a) Moisture content, (b) Grain temperature.

The accuracy of model predictions was rigorously evaluated using the Bland–Altman method. As shown in Fig. 3, the Bland–Altman analysis conducted on the predicted wheat moisture content and temperature revealed a mean difference close to zero, with the majority of data points falling within the 95 % limit of agreement. This outcome demonstrates a strong consistency between the predicted and measured values. Validation under dynamic drying conditions further confirmed the precision of the model. The predicted moisture content and outlet wheat temperature closely matched the actual measurements, as shown in Fig. 4, achieving low RMSE values of 0.0045 g water/g wet matter for moisture and 0.37 °C for temperature, along with an MRD of 2.66 % and 1.12 %, respectively. Previous studies have reported that an MRD below 15 % is acceptable [46], indicating high accuracy of the model.

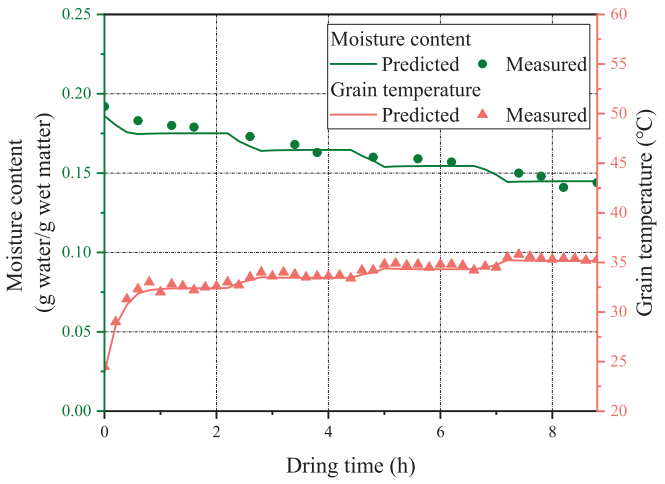

Fig. 4. Comparison between predicted and measured values of outlet grain moisture content and temperature.

Table 4
Baseline drying parameters for simulating the wheat drying process.

Parameter	Value
Ambient temperature, ℃	23.5
Relative humidity, %	21
Wheat initial weight, kg	50,000
Wheat initial moisture content, g water/g wet matter	0.22, **0.26**, 0.30
Wheat target moisture content, g water/g wet matter	0.14
Drying air flow velocity, m/h	2500
Grain flow velocity, m/h	1.03, **1.53**, 2.01
Wheat initial temperature, ℃	23.5
Drying air temperature, ℃	50, **60**, 70
Condensing temperature, ℃	**60**, 63, 66, 69
Terminal temperature difference, ℃	4, **5**, 6
Compressor adiabatic efficiency, %	80

Note: Bold values represent the baseline values used for this variable parameter in simulation.

6.2. Transient thermodynamic analysis

This section presents a thermodynamic analysis of the wheat drying process using a transient model, which accurately captures transient response characteristics that cannot be analyzed by traditional steady-state models. The study systematically investigated the spatial and temporal changes in the moisture and temperature gradients within the drying tower while elucidating the influence of three key operational factors: drying air temperature, initial moisture content, and grain flow velocity.

This study employs a single-factor control method in the transient simulation to prevent interference from the interactions of multiple factors on the result interpretation. Concurrently, R134a was selected as the refrigerant for the closed-loop heat pump drying system. During the transient simulation, the baseline values used for estimating various drying variable parameters are detailed in Table 4.

With all the drying parameters held at baseline values, Fig. 5 illustrates the spatiotemporal distribution characteristics of the moisture content and temperature fields of wheat throughout the tower. As influenced by the tempering stage, the moisture content evolution demonstrated a stepwise decline pattern. When wheat enters the air inlet zone of the first drying stage, the convective heat transfer between the wheat and hot drying air leads to a sharp temperature increase and rapid moisture loss. Advancing to the tempering zone of the second stage, moisture diffusion and heat conduction create a stable moisture plateau while lowering grain temperature. Upon entering the drying zone of the second stage, intense convective heat transfer is re-

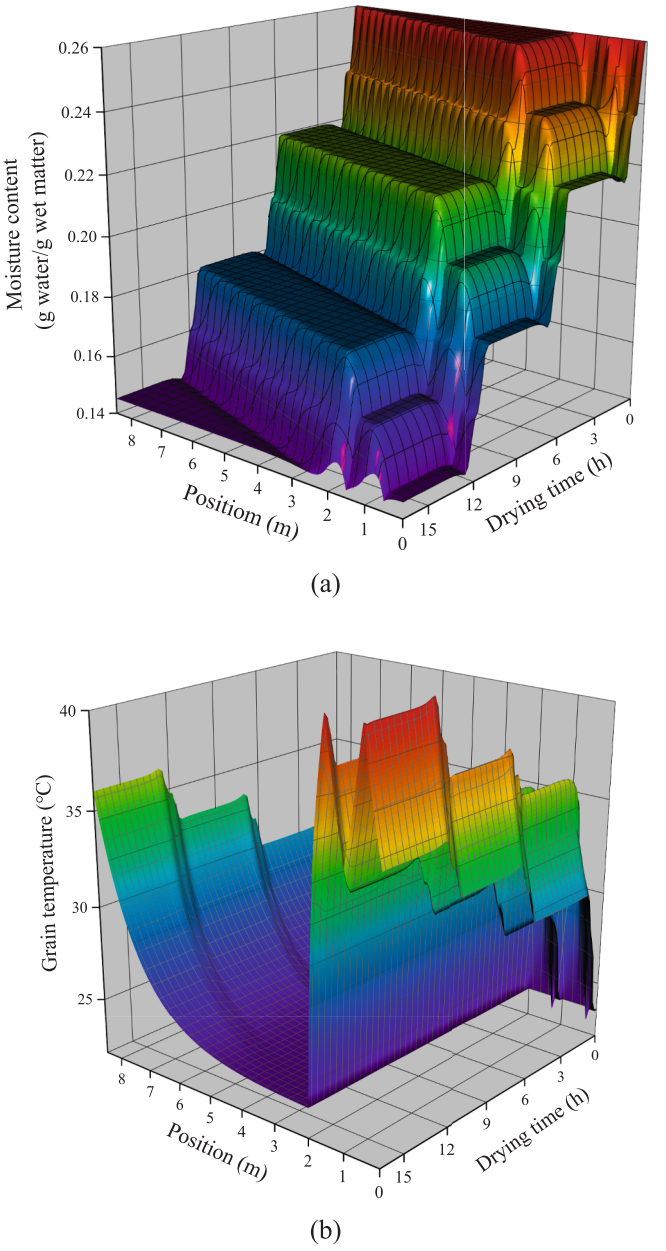

Fig. 5. Spatiotemporal distribution characteristics in the drying tower: (a) moisture content, and (b) grain temperature.

established, causing secondary temperature elevation and steep moisture reduction. Finally, wheat advances to the discharging stage and is recirculated via a hoist for prolonged tempering, where the grain temperature gradually decreases and the moisture content achieves renewed stability. In addition, the grain temperature gradient during mid-to-late drying phases markedly exceeds that during early-to-mid phases, a phenomenon caused by increased energy requirements to dislodge bound water from the solid matrix as the moisture content declines. This results in more heat being converted to grain temperature increase rather than latent heat consumption [32]. This finding is consistent with the drying temperature characteristics reported by researchers in paddy [31] and tea drying experiments [47].

6.2.1. Drying air temperature

With all the other drying parameters held at baseline values, except for a condensing temperature of 70 ℃, the impact of different drying air temperatures on the wheat drying process was elucidated via numerical

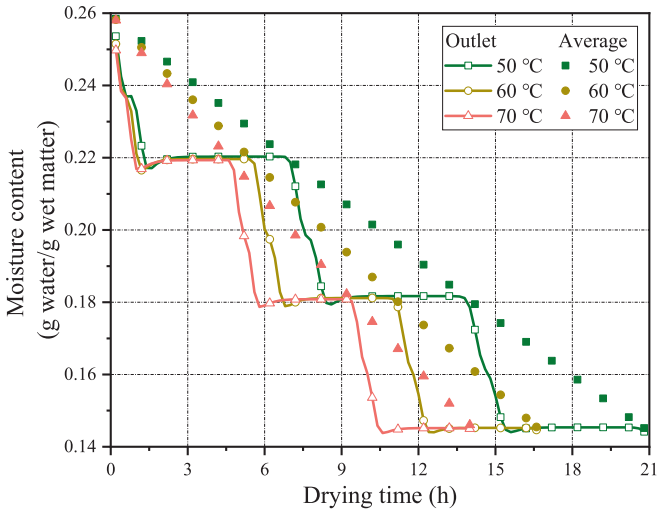

Fig. 6. Changes in outlet and average moisture content of drying tower at different drying air temperatures.

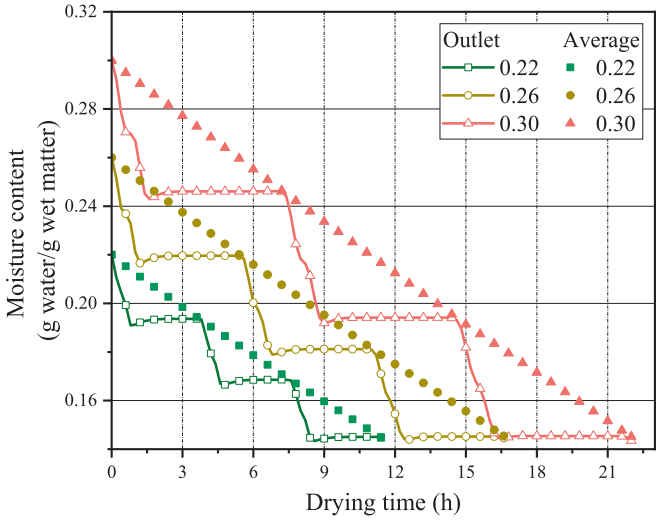

Fig. 7. Changes in outlet and average moisture content of drying tower at different initial moisture contents.

simulation. Fig. 6 presents the moisture content curves at the discharging stage outlet and average moisture content under these conditions. The impact of varying drying air temperatures is most pronounced during the second and third circulation cycles, reaching its peak in the later stage of drying. This finding supports the conclusion by Li et al. [32] regarding grain binding energy. As drying continues, the amount of free water decreases and bound water increases, raising the binding energy required for evaporation. This increased energy demand demands for stronger thermodynamic forces to overcome the water–matrix adsorption interactions, thereby promoting efficient moisture evaporation [48]. Under identical drying conditions, a higher drying air temperature exerts a dual effect by providing an additional influx of thermal energy. First, it ensures the presence sufficient energy for evaporation. Second, it disrupts water–matrix bonds, accelerating water migration onto the surface. Experimental data indicate that upon elevating the drying air temperature to 70 °C, the drying rate reaches 0.0081 g water/g wet matter/h. This represents a 48 % and 18 % increase compared with the drying rates at 50 °C and 60 °C, respectively.

6.2.2. *Initial moisture content*

With all the other drying parameters held at baseline values, the impact of different initial moisture contents on the wheat drying process was elucidated via numerical simulation. Fig. 7 presents the moisture content curves at the discharging outlet and the average moisture content under these conditions. All drying curves for various initial moisture content levels demonstrated multistage decline patterns, which are similar to those observed under different drying air temperatures. Following 8 h of continuous drying, samples with initial moisture contents of 0.30 and 0.26 g water/g wet matter, achieved average moisture content declines of 0.082 and 0.079 g water/g wet matter, respectively. These declines are considerably greater than the decline of 0.064 g water/g wet matter observed in the sample with an initial moisture content of 0.22 g water/g wet matter. During the initial 0–2 h of the drying phase, the average drying rates for the initial moisture contents of 0.30 and 0.26 g water/g wet matter exceeded those of the 0.22 g water/g wet matter by 5.71 % and 4.74 %, respectively. Li [49] observed a similar trend in the study conducted on polygonati rhizoma extract drying. Wheat with a higher initial moisture content contains a greater proportion of free water. The binding energy between free water and the solid matrix is relatively low, which allows it to rapidly respond to external thermal energy and facilitate prompt evaporation. However, opposite results have been obtained in some drying devices, such as in experiments with Soybean [50] and strawberry [51].

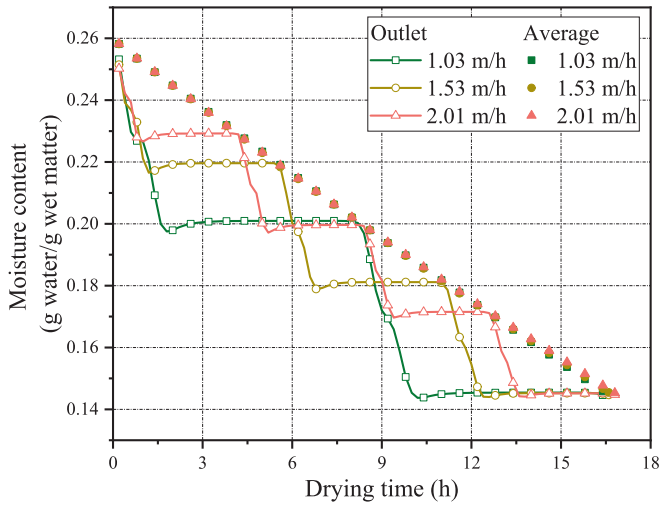

Fig. 8. Changes in outlet and average moisture content of drying tower at different wheat flow velocities.

6.2.3. *Grain flow velocity*

To explore the effects of different grain flow velocities on wheat drying with all the other drying parameters held at baseline values, numerical simulation was conducted. Fig. 8 presents moisture content curves at the discharging outlet and average moisture content under these conditions. The results indicated that wheat subjected to lower flow velocity experiences greater reduction in moisture content during drying, as prolonged contact with the drying air promotes dehydration. However, although the water removal efficiency considerably varies for individual wheat grains at different flow velocities, the overall difference in average moisture content across the drying tower is relatively small. This observation indicates that, although wheat has a shorter residence time in the drying stage at higher flow velocities, the overall average water removal efficiency remains comparable with that observed at lower flow velocities. This phenomenon mainly stems from the heightened throughput of wheat passing through the drying stage per unit time at an elevated flow velocity, which effectively compensates for the reduced contact time.

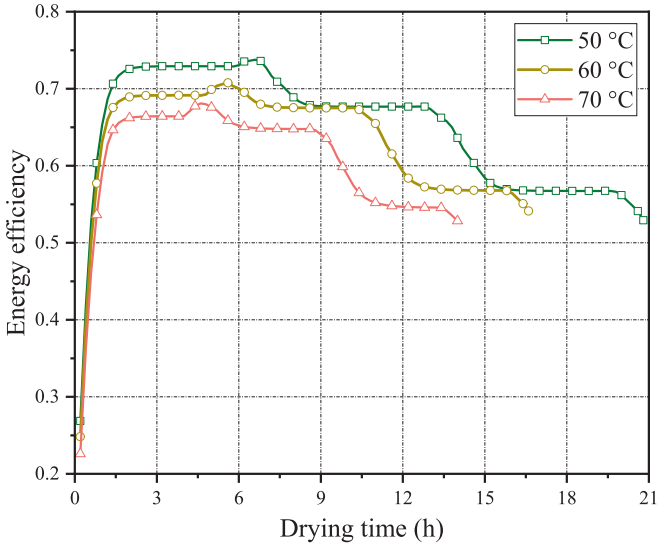

Fig. 9. Transient energy efficiency of wheat drying system under different drying air temperatures.

6.3. Transient energy consumption analysis

Owing to the inherently dynamic nature of the heat pump–assisted drying process, traditional steady-state analysis methods cannot accurately describe real-time energy consumption during the drying process. Therefore, in this section, a transient analysis model is used to precisely capture the system's transient energy performance and identify stages with high-energy consumption or low efficiency throughout the drying cycle. This approach facilitates targeted optimization of drying operations and enhances the overall energy performance.

6.3.1. Drying air temperature

Fig. 9 presents the transient energy efficiency of wheat drying at different drying air temperatures. The transient energy efficiency sharply increases for all drying air temperatures during the first 1.5 h. This rapid increase occurs when the system begins with ambient conditions as the initial parameters. At this stage, the enthalpy of the drying air entering the system is relatively low. Consequently, heating the ambient air to the target drying temperature requires substantial energy consumption, resulting in relatively low energy efficiency in the initial phase.

The influence of drying air temperature on system's energy efficiency demonstrates distinct phased characteristics. During the early drying phase, lower drying air temperature exhibits a higher transient energy efficiency, as less energy is required to overcome the evaporation threshold. This enables efficient water removal without excessive convective heat loss that usually occurs at higher temperatures. However, in the mid-to-late phases, the differences in energy efficiency across various temperature conditions decrease to within 5 %. Consistent with the trend observed in fixed bed wheat drying by Yan et al. [52]. This convergence is attributed to the higher binding energy required for the evaporation of bound water, coupled with a reduced internal humidity gradient that lowers the concentration driven evaporation rate. This observation highlights the need to implement a staged temperature control strategy in industrial drying processes. To maintain sufficient drying rates while maximizing energy efficiency, lower air temperatures should be applied during the initial stage when the moisture content is high. Subsequently, transitioning to a higher temperature during the deceleration drying phase can effectively address the mass transfer bottleneck in water migration, thereby resulting in considerable operational cost savings.

During the drying process, the association between drying air

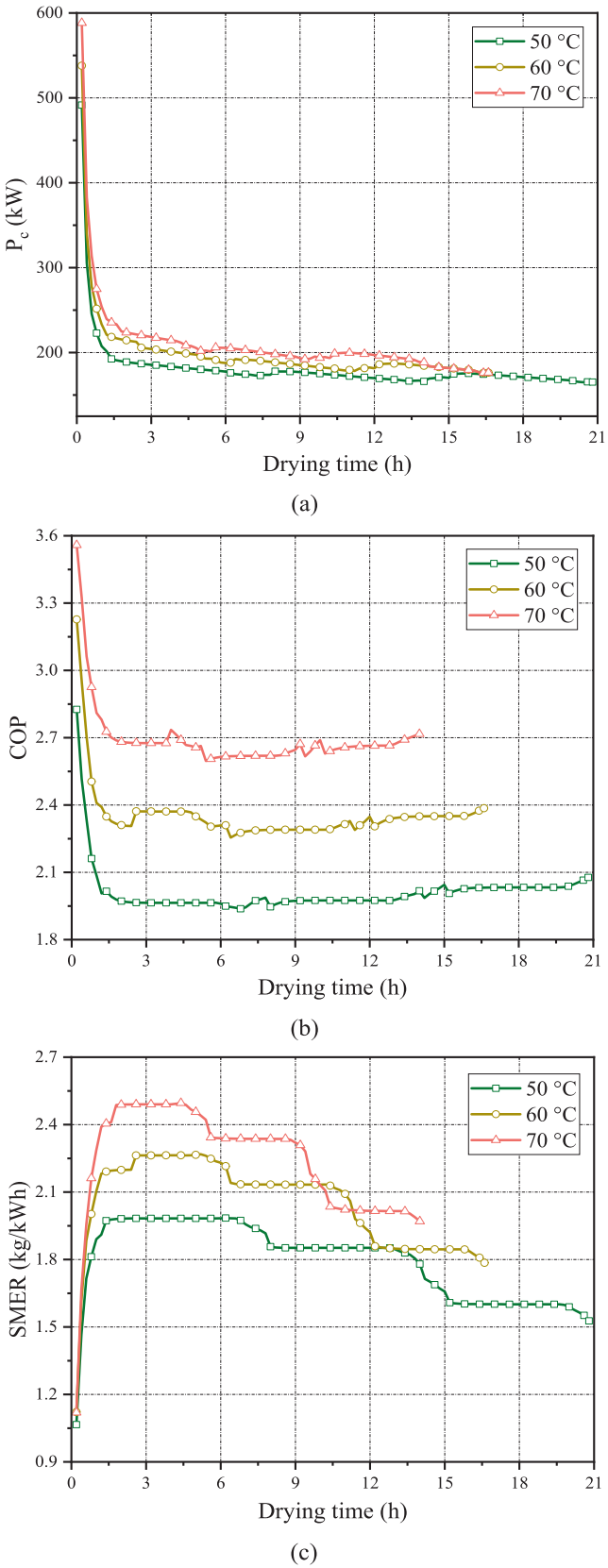

Fig. 10. Transient energy characteristics of wheat drying system under different drying air temperatures: (a) P_c, (b) COP, and (c) SMER.

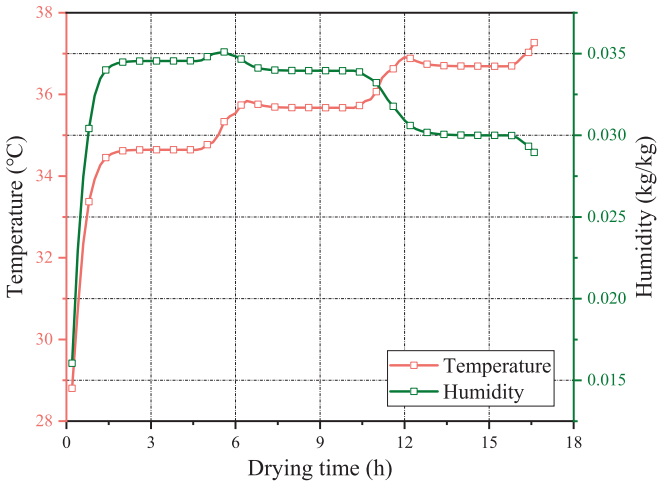

Fig. 11. Exhaust drying air state of the drying tower at a drying air temperature of 60 ℃.

temperature and energy efficiency exhibits nonlinear characteristics. Although increasing the drying air temperature from 50 °C to 70 °C reduces drying time by 32.7 %, the energy saved by such a reduction is insufficient to compensate for the extra energy required for maintaining higher temperatures. Consequently, the average energy efficiency decreases with increasing drying air temperature. For example, at 70 °C, the average energy efficiency reaches 0.613, representing 88.5 % and 94.1 % of the efficiencies observed at 50 °C and 60 °C, respectively. Notably, although the average efficiency of closed-loop heat pump drying systems at 70 °C is lower, it exceeds that of traditional hot-air drying [53] at the same temperature by 27.7 %, highlighting the inherent energy efficiency advantages of closed heat pump drying systems.

Fig. 10 presents the impact of different drying air temperatures on the transient energy characteristics of the closed-loop cycle heat pump drying system, with all the other drying parameters held at baseline values except for a condensing temperature of 70 °C. As illustrated in Fig. 10(a) and (b), the drying system exhibits high transient COP and P_c during the first 1.5 h after startup, followed by a rapid decline into a stable operational phase. During the initial phase, the drying system requires considerable energy to elevate ambient air to the target drying temperature owing to the low ambient conditions at the start, which increases the heating capacity and transient COP. In addition, the low humidity of the inlet drying air at the initial stage, combined with the limited moisture removal capacity, exists the exhaust drying air from the drying tower to reach markedly lower temperature and humidity than that in the stable operational phase, along with a correspondingly reduced dew point temperature, as illustrated in Fig. 11. To ensure effective dehumidification, the refrigerant temperature at the evaporator outlet is maintained low to ensure adequate difference in heat exchange temperature, which increases compressor workload and reduces the transient SMER value during this phase, as illustrated in Fig. 10(c). As the drying process progresses, the drying system stabilizes, with the dew point temperature of the exhaust drying air reaching steady-state conditions. Concurrently, the operating temperature of the evaporator stabilizes, suggesting that after the drying air flows through the evaporator, the temperature and humidity reach equilibrium. The enthalpy of the drying air before and after it flows through the evaporator remains relatively constant, and the heating capacity stabilizes, resulting in a consistent trend for transient COP and P_c.

As presented in Fig. 10(b) and (c), increasing the drying air temperature at a constant condensing temperature markedly enhances the COP and SMER. For example, at 70 °C, the drying system reaches the average COP and SMER values of 2.69 and 2.24 kg/kWh, respectively. These values are 1.34 and 1.14 times higher than those at 50 °C, and

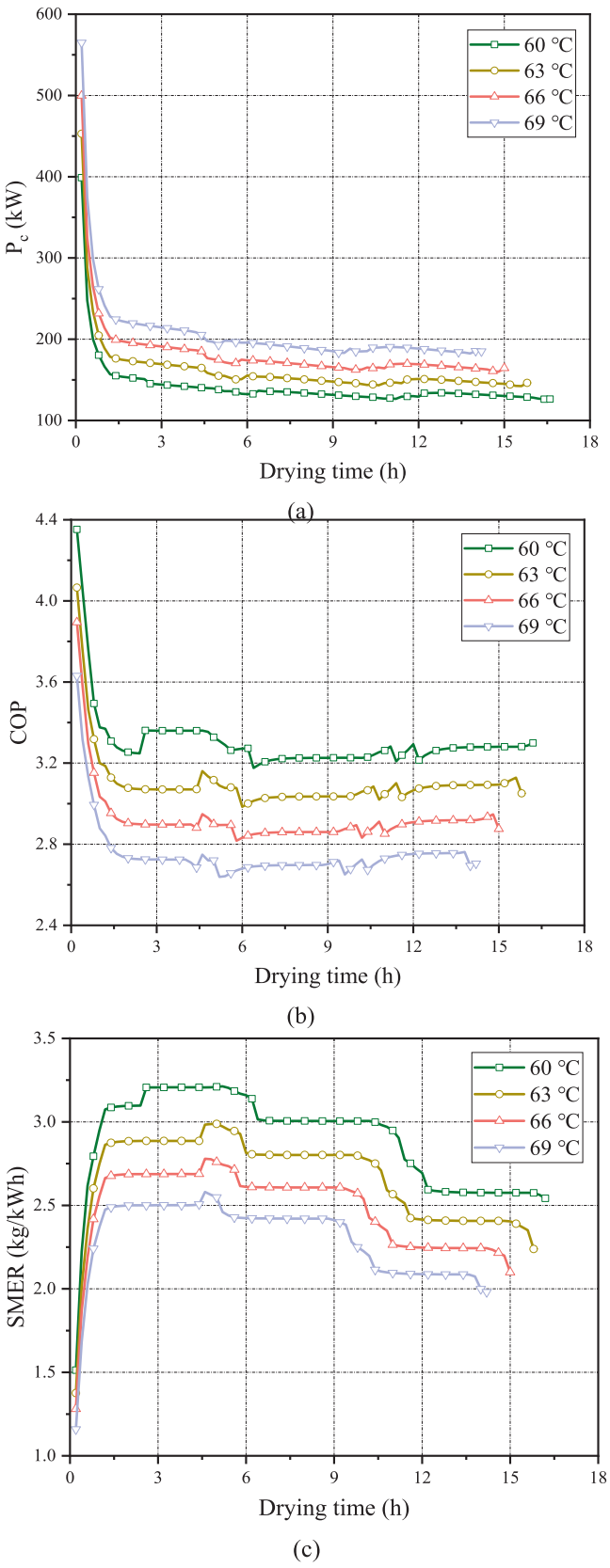

Fig. 12. Transient energy characteristics of wheat drying system under different condensing temperatures: (a) P_c, (b) COP, and (c) SMER.

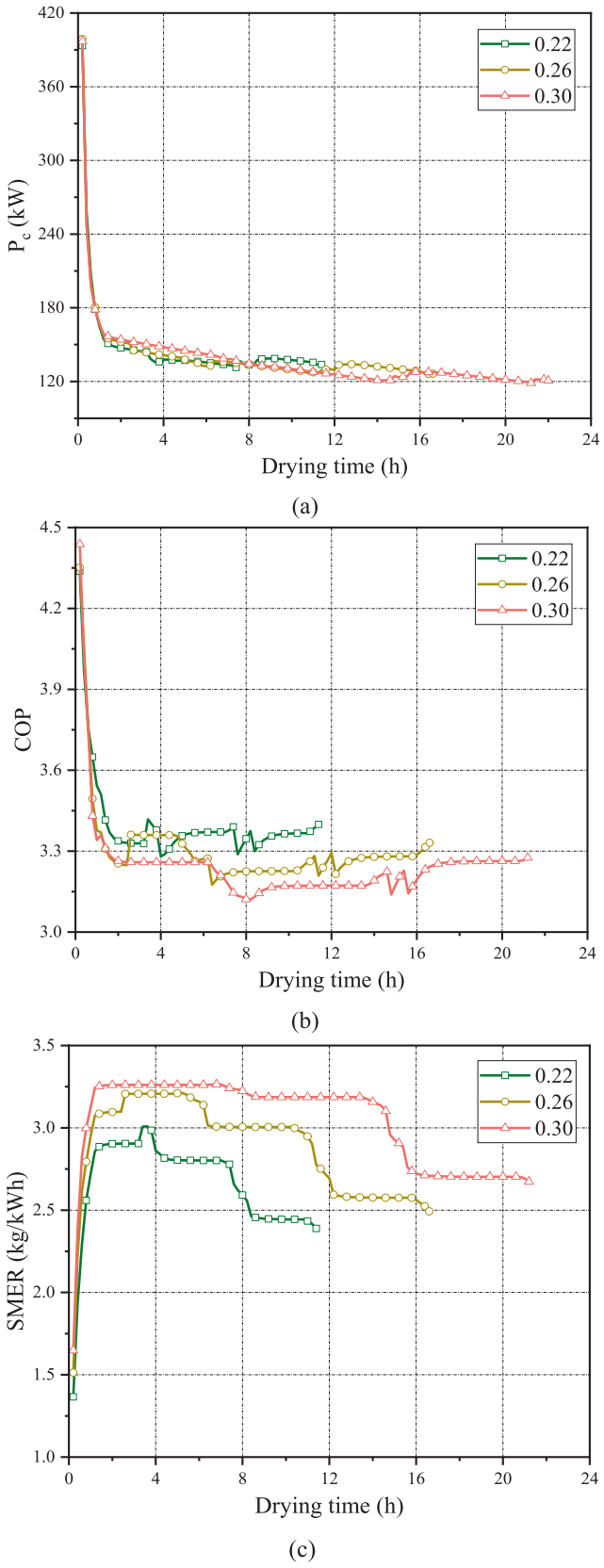

Fig. 13. Transient energy characteristics of wheat drying system under different initial moisture contents: (a) P_c, (b) COP, and (c) SMER.

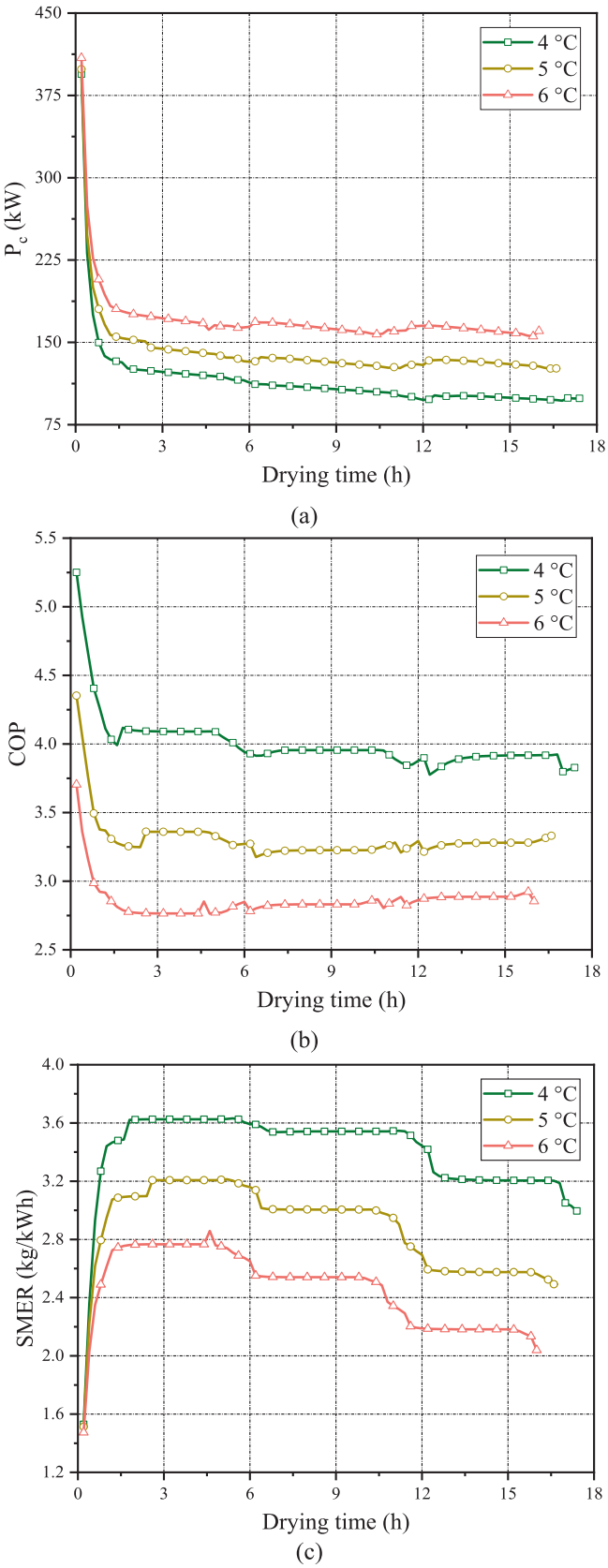

Fig. 14. Transient energy characteristics of wheat drying system under different terminal temperature differences: (a) P_c, (b) COP, and (c) SMER.

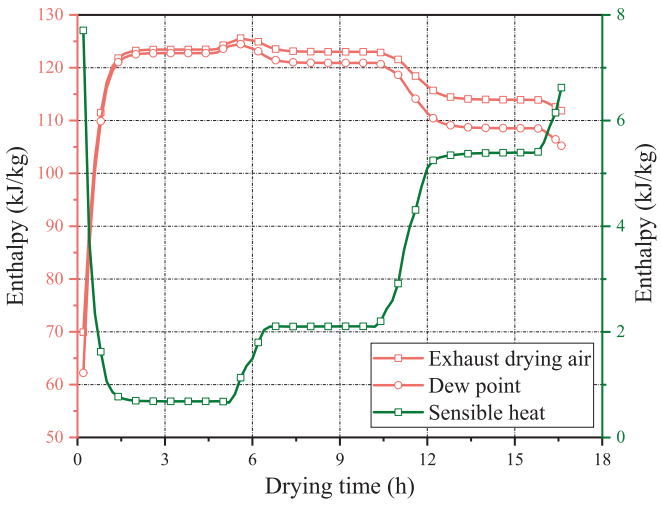

Fig. 15. Changes in sensible heat of exhaust drying air with wheat drying process.

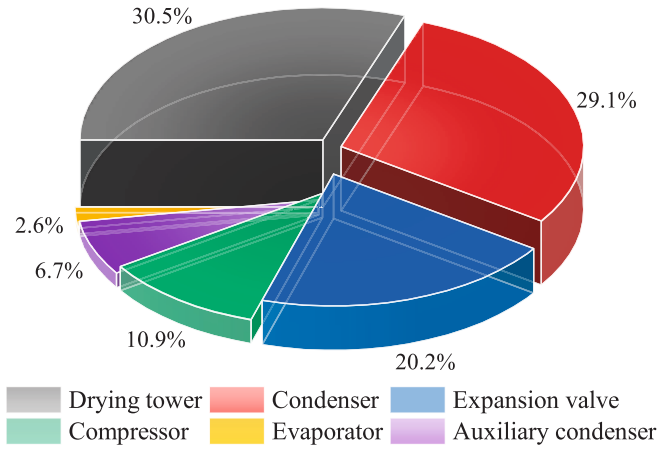

Fig. 16. Exergy loss percentages of each component.

1.25 and 1.09 times higher than those at 60 °C. This phenomenon indicates that reducing the difference between the drying air and condensing temperatures can enhance the overall energy utilization performance. Similar results were reported for the closed-loop heat pump drying of dishwasher [54]. Notably, while theoretically reducing the condensing temperature could further enhance the energy performance and practical operation requires maintenance of adequate temperature difference between the hot refrigerant and cold air for an efficient heat exchange. Consequently, the condensing temperature must not fall below the drying air temperature. Under optimal conditions, the energy performance of the drying system reaches its peak when the condensing temperature aligns with the drying air temperature.

6.3.2. Condensing temperature

To elucidate the influence of drying air and condensing temperatures on the system's energy performance, Fig. 12 shows the interactive effects of concurrent adjustments in these temperatures on the transient energy behavior of the closed-loop heat pump drying system, with all the other drying parameters held at baseline values. The trends for the COP, SMER, and P_c under diverse temperature conditions consistently align with those in Fig. 10. With the increase in both the temperatures, P_c shows an upward trend, whereas the COP and SMER demonstrate a downward trend. This phenomenon indicates that the negative impact of increased condensing temperature on the COP and SMER outweighs the positive effects with increased drying air temperature. Specifically, an increase in condensing temperature increases the internal system pressure, requiring more work by compressor during refrigerant compression, thereby increasing the overall energy consumption, as illustrated in Fig. 12(a). Therefore, simultaneous increases in both the temperatures reduce the SMER. For example, elevating the drying air temperature to 69 °C yields an average water removal rate of 470.04 kg/h, which is only 1.21 times that at 60 °C. Contrarily, when the condensing temperature increases to 69 ℃, the average P_c reaches 207 kW, which is 1.55 times that at 60 ℃. Zhang et al. [55] reported similar results in the study of closed and semi closed- loop heat pump drying systems. However, several studies report conflicting results [17].

6.3.3. Initial moisture content

Fig. 13 illustrates the impact of the different initial moisture contents of wheat on the transient energy characteristics of the closed-loop cycle heat pump drying system, with all the other drying parameters held at baseline values. During the initial 1.5 h of the drying phase, the influence of initial moisture content on transient energy performance aligns with the patterns observed at different drying air temperatures. As illustrated in Fig. 13(a), wheat with higher initial moisture content demonstrates a higher P_c at the early stage of drying. This occurs because a higher initial moisture content corresponds to greater average drying rate, enabling the removal of a considerable amount of moisture within the same timeframe. The enhanced moisture evaporation increases the humidity of the exhaust drying air during the drying stage, thereby increasing its dew point temperature. When a constant temperature difference is maintained between the dew point of the exhaust drying air and the evaporator, the evaporator temperature rises in conjunction with the dew point of the exhaust drying air. Theoretically, this condition enables the compressor to operate at a lower pressure difference, reducing the P_c. However, to effectively dehumidify the high-temperature, high-humidity exhaust drying air, the evaporator must provide additional refrigeration capacity, which requires increased refrigerant flow. The decrease in P_c caused by the increase in evaporator temperatures is insufficient to compensate for the power increase caused by a higher refrigerant mass flow rate. Consequently, wheat with higher initial moisture content demonstrates greater P_c in the early drying phase. Xu et al. [56] reported similar findings in their study on alfalfa seed drying. Following the passage of drying air through the evaporator, its temperature increase reduces the difference between the drying air and condensing temperatures. Such a reduction diminishes the heating capacity of the heat pump for drying air, resulting in lower COP at a higher initial moisture content, as illustrated in Fig. 13(b). For example, the average COP is 3.4 at an initial moisture content of 0.22 g water/g wet matter and 3.24 at 0.30 g water/g wet matter. Alternatively, the growth rate of moisture removal with increasing initial moisture content exceeds that of P_c. This disparity leads to higher SMER for higher initial moisture content, a trend opposite to that of COP, as illustrated in Fig. 13 (c). For example, the average SMER is 2.66 kg/kWh at an initial moisture content of 0.22 g water/g wet matter, which increases to 3.02 kg/kWh at 0.30 g water/g wet matter.

6.3.4. Terminal temperature difference

Fig. 14 illustrates the impact of different terminal temperature differences on the transient energy characteristics of the closed-loop cycle heat pump drying system, with all the other drying parameters held at baseline values. During the initial 1.5 h of the drying phase, the influence of terminal temperature difference on transient energy performance aligns with the patterns observed at different drying air temperatures and initial moisture contents. When the initial parameters of the drying air at the drying stage inlet are constant, the dew point temperature of the exhaust drying air remains stable. However, variations in the terminal temperature difference alter the evaporator's operating conditions. A larger terminal temperature difference results in

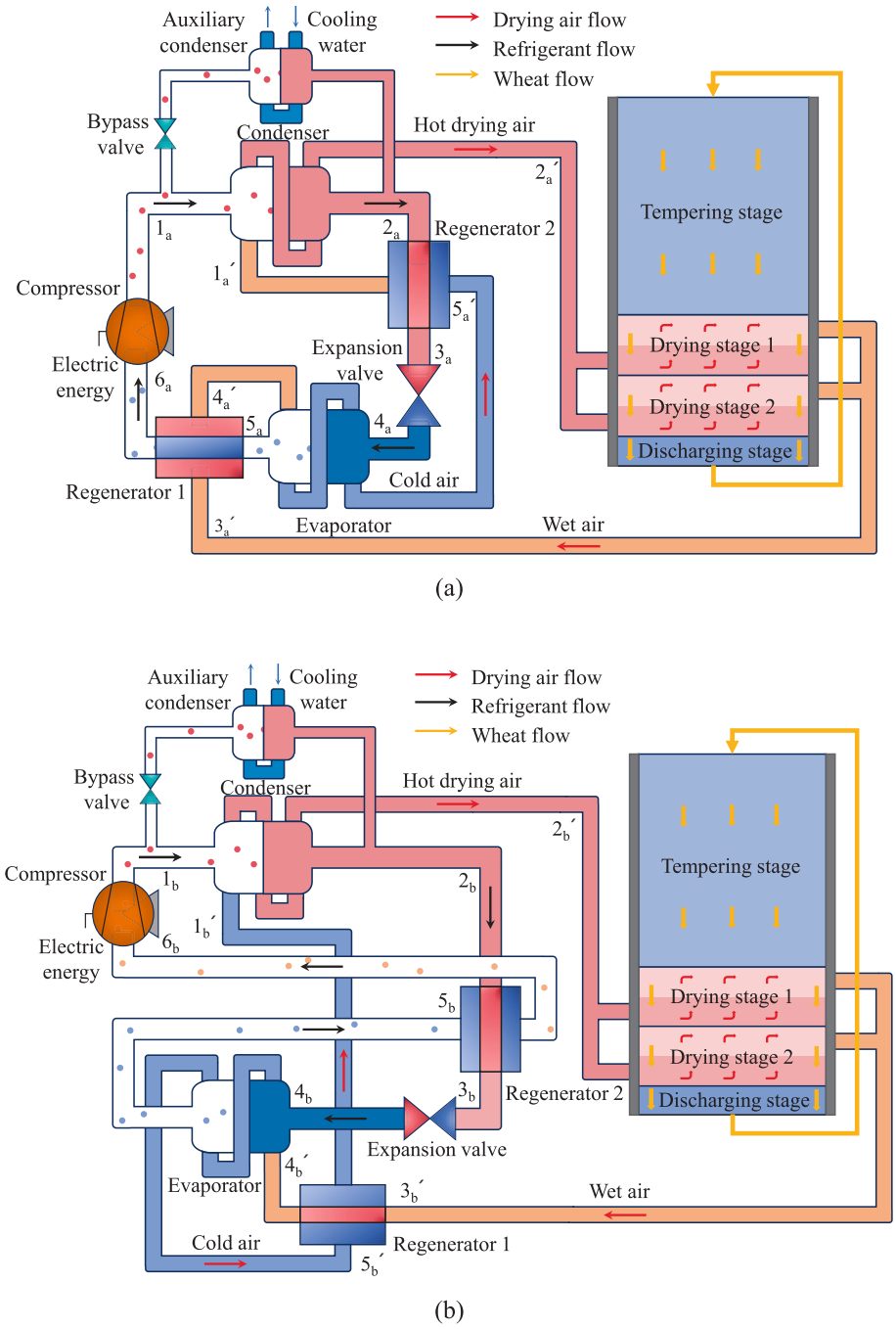

Fig. 17. Schematic diagram of three heat recovery schemes: (a) Scheme A, (b) Scheme B, and (c) Scheme C.

lower refrigerant temperature and pressure at the evaporator outlet [57]. This requires the compressor to operate under a higher pressure difference, which increases the P_c. In addition, a larger terminal temperature difference enhances the evaporator's heat transfer efficiency, enabling sufficient heat absorption from the drying air with a lower refrigerant mass flow rate. Although the reduced refrigerant flow may partly reduce the P_c, such a reduction cannot fully compensate for the additional power increase caused by the lower evaporator temperature. Consequently, the overall P_c increases with larger terminal temperature difference, as shown in Fig. 14(a). The lower operating temperature of the evaporator means that the drying air passing through it reaches a lower temperature, thereby increasing the difference between the drying air and condensing temperatures and enhancing the heating capacity. However, as the heating capacity growth rate lags behind that of the P_c, the COP decreases with the increase in the terminal temperature difference, as shown in Fig. 14(b). For example, at a 6 °C terminal temperature difference, the average COP and Pc are 2.86 and 171.14 kW, respectively, compared with 4 and 115.32 kW at 4 °C. Moreover, under an atmospheric pressure, the drying air at lower temperature demonstrates reduced humidity, accelerating the drying process. However, the moisture removal growth rate induced by this humidity reduction is slower than the P_c growth rate. This reduces the SMER at a larger terminal temperature difference, as illustrated in Fig. 14(c). Although a smaller terminal temperature difference increases the COP and SMER while reducing the P_c, an excessively low terminal temperature difference may impair evaporator efficiency by hindering moisture

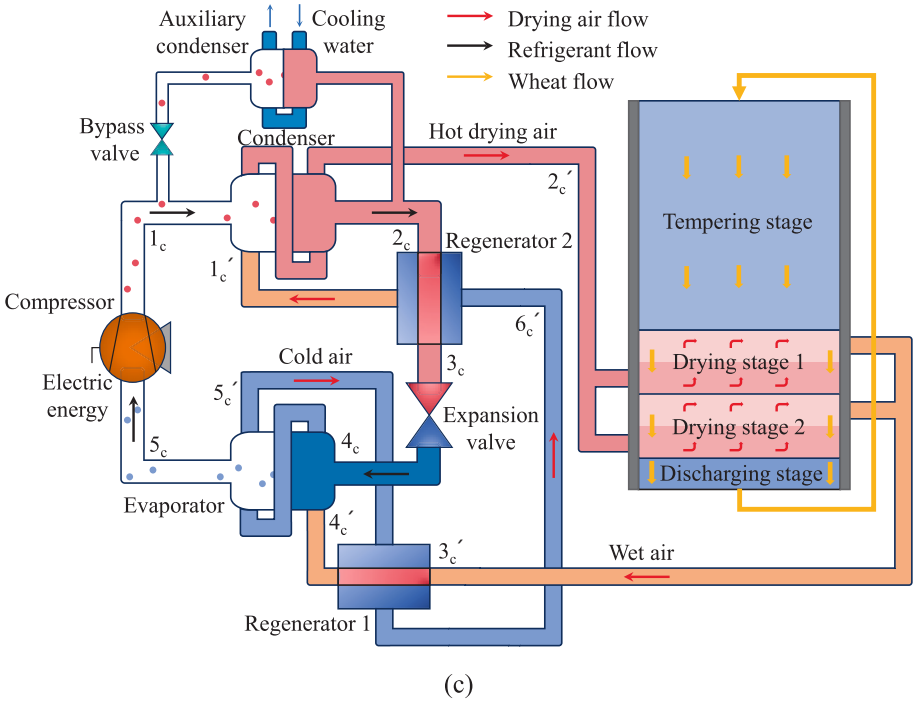

Fig. 17. (*continued*).

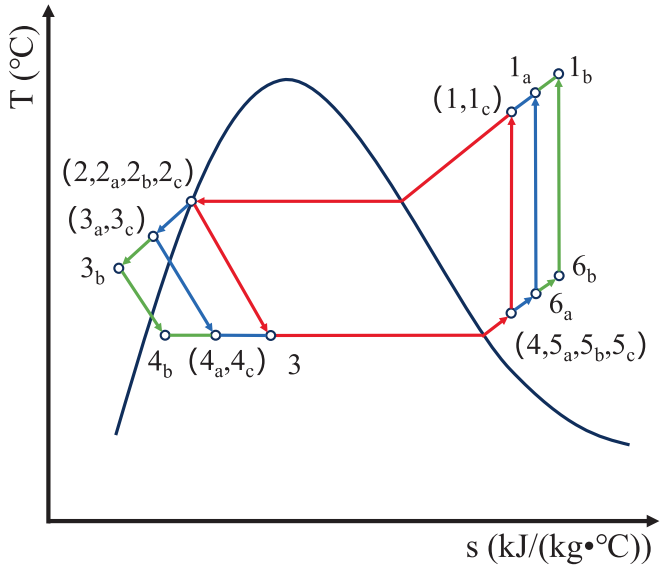

Fig. 18. T-s diagram of refrigerant.

Table 5
Function of regenerator in three heat recovery schemes.

Scheme	Regenerator 1		Regenerator 2	
	pre-cool	pre-heat	pre-cool	pre-heat
A	wet air	evaporator outlet refrigerant	condenser outlet refrigerant	cold air
B	wet air	cold air	condenser outlet refrigerant	evaporator outlet refrigerant
C	wet air	cold air	condenser outlet refrigerant	cold air

transfer from the drying air to the evaporator surface. Therefore, appropriate terminal temperature difference settings are crucial to ensure high efficiency and stable operation of the heat pump drying system.

6.4. System optimization

6.4.1. Problem description

Fig. 15 presents the variation trend of sensible heat content in the exhaust drying air, under the conditions where all the drying parameters are maintained at their baseline values. As the drying process progresses, the sensible heat of the exhaust drying air gradually increases, requiring the evaporator to provide additional refrigeration capacity to manage the sensible heat carried by the drying air to achieve effective moisture removal. Under fixed terminal temperature difference conditions, maintaining the required refrigeration effect leads to an increase in refrigerant mass flow rate, thereby exacerbating the overall exergy loss of the drying system.

Furthermore, the exergy loss of each component in the drying system was calculated using Equations (31) to (37). The average exergy loss of the entire drying system amounts to 107.89 kW; the exergy loss percentages for each component are illustrated in Fig. 16. The proportion of exergy loss at the drying tower is 30.5 %, whereas the total exergy loss attributable to the heat pump is 69.5 %. In the heat pump drying system, exergy loss is predominantly concentrated in three key components, namely, the condenser, expansion valve, and compressor, accounting for 60.2 % of the total exergy loss of the drying system. In these system components, phase change processes occur. Notably, in the condenser, a considerable temperature difference between the dry air and condensation temperature promotes intensive heat transfer. Concurrently, the refrigerant undergoes phase change, resulting in substantial exergy loss. Furthermore, exergy loss in the auxiliary condenser and compressor is inevitable and irrecoverable, representing a considerable proportion of the total loss. These observations reveal two important optimization pathways for traditional closed-loop heat pump drying systems. First, a notable temperature difference exists in the refrigerant between the condenser and the expansion valve. Second, distinct temperature gradients persist among the media within the condenser itself.

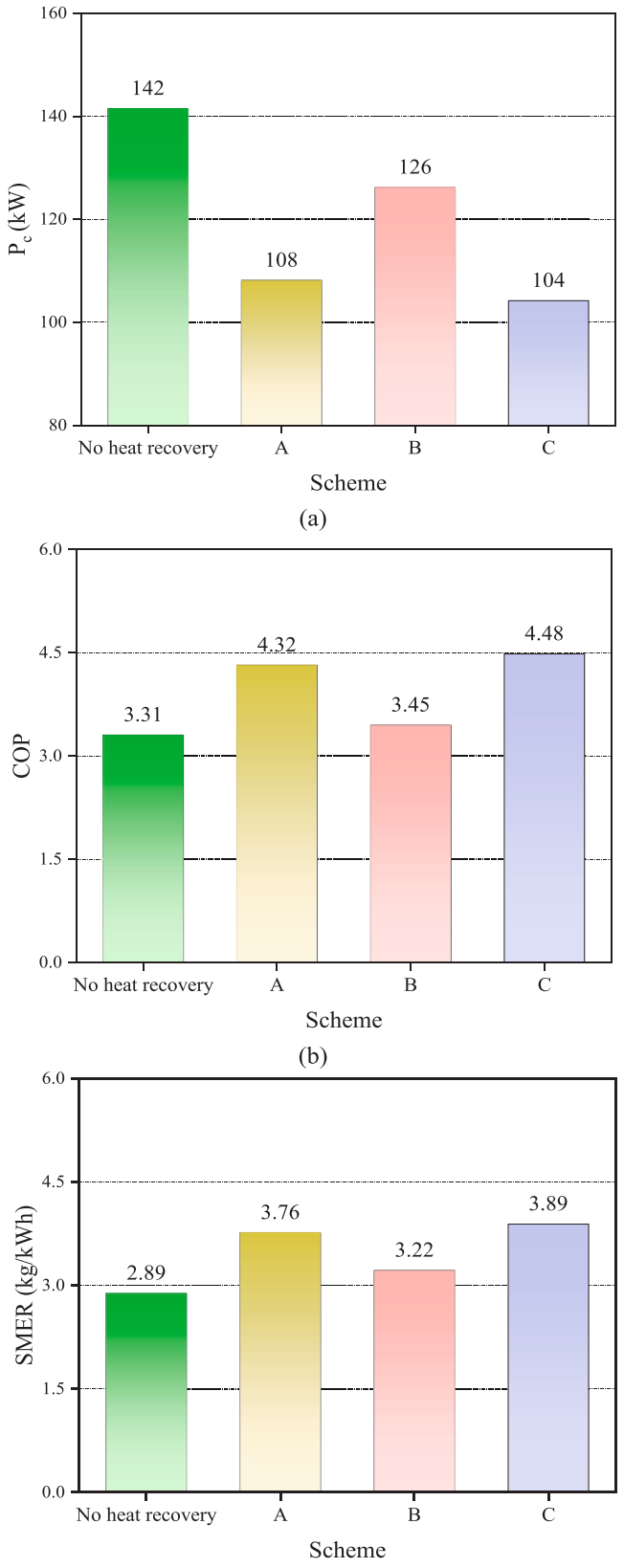

Fig. 19. Comparison of energy characteristics for wheat drying system employing different heat recovery schemes: (a) P_c, (b) COP, and (c) SMER.

6.4.2. Optimization schemes

To mitigate exergy losses in the previously described closed-loop heat pump drying system, this study proposes the integration of a regenerator as an optimization strategy to enhance the overall energy performance of the drying system. The integration of the regenerator only requires adjustments to the pipeline system, eliminating the need to redesign the heat pump cycle, thereby simplifying the transformation process. Moreover, all the core components are commercially available and mature, which helps control costs and ensures high engineering feasibility. The specific strategies are as follows: 1) precool the wet air discharged from the drying stage using the regenerator 1 to a temperature that approaches, slightly exceeds, the dew point by 0.5 °C. This prevents moisture condensation within the regenerator while maximizing refrigeration capacity utilization, thereby enhancing the dehumidification efficiency and 2) utilize regenerator 2, with an efficiency set to 0.8, to lower the refrigerant temperature at the expansion valve inlet. This mitigates vaporization induced by pressure reduction across the valve, thereby enhancing the evaporator's cooling performance.

To quantify the disparity between the actual heat transfer performance and theoretical limits, the regenerator efficiency parameter is introduced. This parameter quantifies the ratio of the actual heat transfer to the theoretical maximum heat transfer, which is calculated as follows [20]:

$$\varepsilon = \frac{c_{ph} q_{mh} \left(T_h^{in} - T_h^{out}\right)}{\left(c_p q_m\right)_{\min} \left(T_h^{in} - T_c^{in}\right)} = \frac{c_{pc} q_{mc} \left(T_c^{out} - T_c^{in}\right)}{\left(c_p q_m\right)_{\min} \left(T_h^{in} - T_c^{in}\right)} \tag{43}$$

where c_{ph} and c_{pc} denote the specific heat capacities at a constant pressure for the hot and cold fluids, respectively; q_{mh} and q_{mc}, the mass flow rates of hot and cold fluids, respectively; T_h^{in} and T_c^{in}, the inlet temperatures of hot and cold fluids, respectively; T_h^{out} and T_c^{out}, the outlet temperatures of hot and cold fluids, respectively; and $(c_p q_m)_{\min}$, the smaller value between the products of mass flow rate and specific heat capacity at a constant pressure for hot and cold fluids.

Based on the above considerations, this study proposed three distinct heat recovery schemes to optimize energy flow within the drying system, aiming to enhance the overall energy efficiency, as illustrated in Fig. 17. All three schemes employ regenerator-based techniques. As illustrated in Fig. 18, the T-s diagrams depict the refrigerant's thermodynamic behavior across these schemes. Table 5 presents the function of the regenerator in three heat recovery schemes.

6.4.3. Result and analysis

With all the drying parameters held at baseline values, Fig. 19 presents a comparative analysis of the energy utilization characteristics of different heat recovery schemes. The results indicate that the use of regenerators markedly enhance system's energy performance. In a closed-loop heat pump drying system with heat recovery schemes under identical drying conditions, P_c markedly reduces compared with scenarios without heat recovery. This improvement mainly stems from two factors: first, all the heat recovery schemes effectively control sensible heat and enhance the evaporator's dehumidification efficiency. They markedly decrease the refrigerant mass flow rate, resulting in a substantial reduction in the P_c and second, these schemes effectively decrease the expansion valve inlet refrigerant temperature. This minimizes vaporization within the valve and further enhances the evaporator's cooling capacity. Notably, Scheme B exhibits the smallest reduction in the P_c among the three schemes, whereas Schemes A and C show more pronounced decreases, as illustrated in Fig. 19(a). For instance, the P_c of Scheme C is 104.23 kW, representing a notable decrease of 26.3 % compared with 141.51 kW that is observed without the heat recovery system. Contrarily, the P_c of Scheme B decreased by 10.8 %. This difference occurs as Scheme B only preheats the compressor inlet refrigerant, whereas Schemes A and C preheat the drying air. As illustrated in Fig. S2 (Supplementary Material), the energy performances of all the heat recovery schemes improve with an increase in the efficiency of

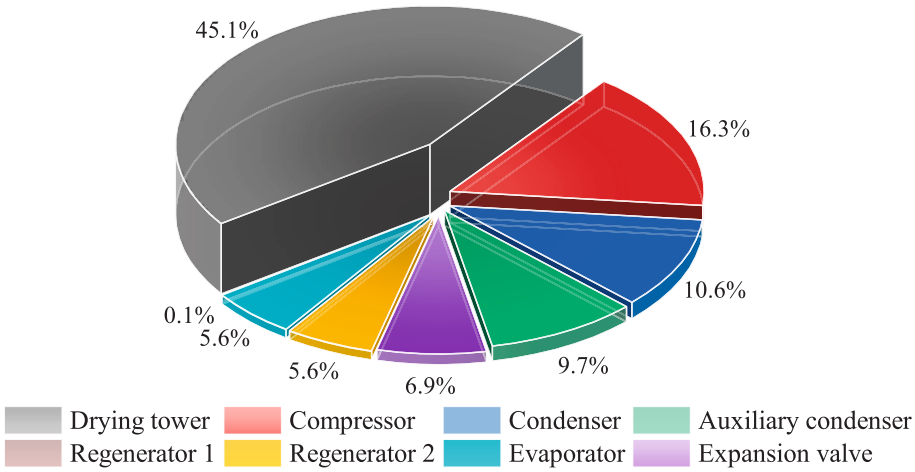

Fig. 20. Exergy loss percentages of each component in Scheme C.

regenerator 2. Such an improvement directly increases the compressor inlet refrigerant temperature for Scheme B; however, the resulting gain in energy performance is not significant. Moreover, the energy performance of Scheme C surpasses that of Scheme A, indicating that reducing the temperature difference between the drying air and the condensing temperature is far more effective in enhancing the system's energy performance than increasing the compressor inlet refrigerant temperature. As illustrated in Fig. 19(b) and (c), the COP and SMER increased for all the heat recovery schemes, particularly in Schemes A and C. For example, the average COP for Schemes A and C increased to 4.32 and 4.48, whereas the average SMER increased to 3.76 and 3.89 kg/kWh, respectively. Compared with systems without heat recovery, the COP for Schemes A and C increased by 33.4 % and 35.3 %, whereas the SMER increased by 30.1 % and 34.6 %, respectively. These findings indicate that Scheme C outperforms Schemes A and B across all performance metrics, including P_c, COP, and SMER.

With all the drying parameters held at baseline values, Fig. 20 shows the percentage distribution of exergy loss for each component within Scheme C. The average exergy loss of the entire drying system is 72.75 kW, indicating a 32.5 % reduction compared with the system without heat recovery. The primary exergy losses occur in unavoidable and nonrecoverable components, particularly the drying stage, compressor, and auxiliary condenser. When compared with the percentages in Fig. 15, the exergy loss percentages are substantially lower at the condenser and expansion valve. The integration of the regenerator enables effective control of irreversible losses at these crucial components, confirming the effectiveness of the design of Scheme C. By implementing a two-stage preheating process for the drying air through regenerators placed between the drying stage and evaporator, as well as between condenser and expansion valve, the difference between the drying air and condensing temperatures is minimized. Such an optimization enhances the overall energy performance, highlighting the role of the condenser as a key component. This conclusion aligns with the findings of Erbay [58] regarding the condenser's function in the heat pump system.

7. Conclusion

This study proposed a transient analysis model for a circulation counter-flow wheat drying system utilizing a closed-loop heat pump configuration, performing transient thermodynamic analysis and energy optimization. The key outcomes of this study are as follows:

(1) The predictions for discharged wheat moisture content and temperature aligned well with the actual measurements, achieving an RMSE of 0.0045 g water/g wet matter and 0.37 °C as well as MRD of 2.66 % and 1.12 %, respectively.
(2) At the start of drying phase, a lower drying air temperature is applied to grains with high free water content. During the mid-to-late stages of drying, the temperature is increased to overcome the binding energy between water and the solid matrix of the grains. This two-stage strategy enhances energy efficiency while ensuring optimal drying rates.
(3) Maintaining stable condensing temperature while elevating the drying air temperature narrows the difference between them, enhancing the energy performance of the drying system. In contrast, the initial moisture content of wheat has no notable effect on energy performance.
(4) The implementation of dual-stage preheating of the drying air through a regenerator can considerably enhance the energy performance of the drying system. With all the drying parameters held at baseline values, Scheme C achieves a 26.3 % reduction in the P_c, a 35.3 % increase in the COP, and a 34.6 % increase in the SMER compared with systems without heat recovery. In addition, it results in a 32.5 % reduction in exergy loss, demonstrating optimal performance across various energy efficiency metrics.

The transient analysis model proposed in this study provides reliable groundwork for exploring adaptive control strategies in the drying process and shows potential for application to agricultural products, such as paddy and barley, warranting further exploration. Moreover, the dual-regenerator optimization scheme introduced here offers notable advantages in energy conservation and consumption reduction in industrial-scale closed-loop heat pump drying systems. Future research will focus on the deployment and practical application of this optimization scheme in the field of engineering.

CRediT authorship contribution statement

Chengjie Li: Writing – original draft, Supervision, Software, Methodology, Investigation, Funding acquisition. **Jianjiang Huang:** Validation, Software, Methodology, Investigation, Data curation. **Yancheng Chen:** Validation, Investigation. **Sihan Ji:** Validation, Software, Data curation. **Changyou Li:** Resources, Methodology, Conceptualization. **Ye Zhang:** Writing – review & editing, Validation, Investigation, Funding acquisition.

Declaration of competing interest

The authors declare that they have no known competing financial interests or personal relationships that could have appeared to influence

the work reported in this paper.

Acknowledgements

This work was supported by the National Natural Science Foundation of China (No.32401725 and No.32171906), the National Key Research and Development Program of China (No.2024YFD200010402), the Guangdong Basic and Applied Basic Research Foundation (No.2025A1515011276), and the Guangzhou Science and Technology Plan Project (No.2024A04J3960).

Appendix A. Supplementary data

Supplementary data to this article can be found online at https://doi.org/10.1016/j.enconman.2025.120508.

Data availability

Data will be made available on request.

References

[1] Yan J, Wei H, Wu H, You Z, Xie H. Thermodynamics and non-uniformity in convective reversing drying wheat. Appl Therm Eng 2023;231:120948. https://doi.org/10.1016/j.applthermaleng.2023.120948.
[2] Aranha ACR, Ferrari AL, Bissaro CA, Matias GS, Defendi RO, Paschoal SM, et al. Mathematical modelling of wheat drying by fractional order and assessment of transport properties. Can J Chem Eng 2024;102(2):996–1006. https://doi.org/10.1002/cjce.25081.
[3] Chen P, Fan M, Zhu W, Liu Y, Jiang M, Wang Y, et al. Numerical simulation of hot air drying of wheat grain piles based on CFD-DEM and experimental research. Dry Technol 2024;42(2):199–211. https://doi.org/10.1080/07373937.2023.2283877.
[4] Tian Y, Tian X, Yang B, Ma J, Shan J, Xing F. Analysis of the impact of drying on common wheat quality and safe. Heliyon 2024;10(12):e33163. https://doi.org/10.1016/j.heliyon.2024.e33163.
[5] Jiang M, Wu P, Xing H, Li L, Jia C, Chen S, et al. Water migration and diffusion mechanism in the wheat drying. Dry Technol 2021;39(6):738–51. https://doi.org/10.1080/07373937.2020.1716001.
[6] Jimoh KA, Hashim N, Shamsudin R, Man HC, Jahari M, Onwude D. Recent advances in the drying process of grains. Food Eng Rev 2023;15(3):548–76. https://doi.org/10.1007/s12393-023-09333-7.
[7] Yao M, Li M, Zhang Y, Wang Y, Li G, Zhang Y. Performance, Energy and exergy analysis of solar-assisted heat pump drying system with heat recovery: a comprehensive experimental study. Renew. Energ 2025;122665. https://doi.org/10.1016/j.renene.2025.122665.
[8] Babu AK, Kumaresan G, Surya SBV, Raj VAA, Singh AP, Bonsa KB. Drying characteristics of eggplant drying in a heat pump dryer. Int J Syst Assur Eng 2024;15(6):2634–44. https://doi.org/10.1007/s13198-024-02285-z.
[9] Ren Y, Chen Z, Wu W, Wang H, Yang Y, Yang Q. Study on the effect of circulating air volume on the performance of closed loop heat pump drying system. Appl Therm Eng 2022;210:118362. https://doi.org/10.1016/j.applthermaleng.2022.118362.
[10] Zou L, Liu Y, Yu M, Yu J. A review of solar assisted heat pump technology for drying applications. Energy 2023;283:129215. https://doi.org/10.1016/j.energy.2023.129215.
[11] Lee Y, Kim S, Han C, Lee D, Kim Y. Comparative analysis of drying performances of various types of heat pump tumble dryers at different climate regions. Case Stud Therm Eng 2025;68:105866. https://doi.org/10.1016/j.csite.2025.105866.
[12] Gao L, Fix A, Seabourne T, Pei Y, Adegbaye P, Hwang Y, et al. A comprehensive review of heat pump wood drying technologies. Energy 2024;311:133241. https://doi.org/10.1016/j.energy.2024.133241.
[13] Duan S, Wang L, Nie D. Performance analysis of a two-stage evaporation heat pump drying system for graded cooling/dehumidification. Appl Therm Eng 2024;247:122965. https://doi.org/10.1016/j.applthermaleng.2024.122965.
[14] Osta MH, Yakut K, Köksal H. Experimental performance assessment of two-stage thermoelectric system in a closed-cycle drying process. Appl Therm Eng 2025:127451. https://doi.org/10.1016/j.applthermaleng.2025.127451.
[15] Zhao H, Dai J, Wu K. Simulation of coupled heat-mass transfer in sea cucumbers with heat pump drying. Appl Sci 2022;12(11):5508. https://doi.org/10.3390/app12115508.
[16] Guangbin L, Kaixuan X, Qichao Y, et al. Flow field and drying process analysis of double-layer drying chamber in heat pump dryer. Appl Therm Eng 2022;209:118261. https://doi.org/10.1016/j.applthermaleng.2022.118261.
[17] Fu H, Shi J, Yuan J, Zhang X, Sun L. Heat recovery scheme design and thermodynamic analysis of closed-cycle heat pump drying system. Energ Convers Manage 2023;286:117034. https://doi.org/10.1016/j.enconman.2023.117034.
[18] Chen Z, Guo Y, An L, Liang Y, Zhao J, Shan L, et al. R290 closed-cycle heat pump tumble clothes dryer: simulation model solving and multi-objective optimization based on intelligent algorithms. Appl Therm Eng 2025;127611. https://doi.org/10.1016/j.applthermaleng.2025.127611.
[19] Xie Y, Wu J, Miao Z, Zhou L, Liu S. Coupled investigation of dynamic moist air dehumidification and heat pump drying in a close-cycle dishwasher. Appl Therm Eng 2025;261:125153. https://doi.org/10.1016/j.applthermaleng.2024.125153.
[20] Li C, Fang Z, Zhong J, Li B, Li C. Evaluating the dynamic characteristics and energetic performance of a paddy multistage counter-flow dryer. Biosyst Eng 2022;221:208–23. https://doi.org/10.1016/j.biosystemseng.2022.07.003.
[21] Li C, Ren J, Seth A, Zhang Y, Huang J, Li C, et al. Hierarchical model predictive control for energy consumption regulation of industrial-scale circulation counter-flow paddy drying process. Energy 2025;321:135431. https://doi.org/10.1016/j.energy.2025.135431.
[22] Leal AF, Coradi PC, Moraes RS, Müller E, Teodoro PE, Teodoro LPR, et al. Tempering time and air temperature relationships for real-scale paddy drying and their effects on the physical, physicochemical, and morphological qualities of polished rice. Dry Technol 2023;41(11):1878–92. https://doi.org/10.1080/07373937.2023.2199834.
[23] Zhang Y, Fang Z, Li C, Li C. Deep-learning-based model predictive control of an industrial-Scale multistate counter-flow paddy drying process. Foods 2023;13(1):43. https://doi.org/10.3390/foods13010043.
[24] Jain S. A comparative study of oven drying method and microstrip moisture sensor for determination of moisture content of soil and analysis of bulking of sand phenomenon. Wirel Pers Commun 2024;139(3):1659–67. https://doi.org/10.1007/s11277-024-11684-1.
[25] Zhang Y, Liang T, Yang K. An integrated energy storage system consisting of compressed carbon dioxide energy storage and organic rankine cycle: Exergoeconomic evaluation and multi-objective optimization. Energy 2022;247:123566. https://doi.org/10.1016/j.energy.2022.123566.
[26] Liu S, Li X, Song M, Li H, Sun Z. Experimental investigation on drying performance of an existed enclosed fixed frequency air source heat pump drying system. Appl Therm Eng 2018;130:735–44. https://doi.org/10.1016/j.applthermaleng.2017.11.068.
[27] Liu Z, Liu B, Guo J, Xin X, Yang X. Conventional and advanced exergy analysis of a novel transcritical compressed carbon dioxide energy storage system. Energ Convers Manage 2019;98:111807. https://doi.org/10.1016/j.enconman.2019.111807.
[28] Li Z, Wu W, Wang J, Wang H, Yu X. Effect of compressor speeds on performance of a closed loop heat pump drying system. Appl Therm Eng 2021;195:117220. https://doi.org/10.1016/j.applthermaleng.2021.117220.
[29] Li C. Analytical theory study on latent heat coefficient of grain water vaporization. Dry Technol 2021;39(6):803–19. https://doi.org/10.1080/07373937.2020.1720224.
[30] Li C. Analysis of Grain Drying. Beijing, China: Science Press; 2018.
[31] Li T, Li C, Li B, Li C, Fang Z, Zeng Z, et al. Characteristic analysis of heat loss in multistage counter-flow paddy drying process. Energy Rep 2020;6:2153–66. https://doi.org/10.1016/j.egyr.2020.08.006.
[32] Li C, Mai Z, Fang Z. Analytical study of grain moisture binding energy and hot air drying dynamics. Trans Chin Soc Agric Eng 2014;30(7):236–42. https://doi.org/10.3969/j.issn.1002-6819.2014.07.028.
[33] Li C, Kamide J. Studies on drying mechanism of wheat-Theoretical analysis of drying process. Trans Chin Soc Agric Eng 1993;01:83–91.
[34] Li R, Zhang G, Zhang Q, Yuan T, Wang N, Li X, et al. Energy contribution and loss of greenhouse-type drying chamber in multi-energy drying system: Heat distribution and exergy efficiency. Renew Energ 2024;237:121652. https://doi.org/10.1016/j.renene.2024.121652.
[35] Beigi M, Tohidi M, Torki-Harchegani M. Exergetic analysis of deep-bed drying of rough rice in a convective dryer. Energy 2017;140:374–82. https://doi.org/10.1016/j.energy.2017.08.100.
[36] Aziz M, Oda T, Kashiwagi T. Enhanced high energy efficient steam drying of algae. Appl Energy 2013;109:163–70. https://doi.org/10.1016/j.apenergy.2013.04.004.
[37] Nazghelichi T, Kianmehr MH, Aghbashlo M. Thermodynamic analysis of fluidized bed drying of carrot cubes. Energy 2010;35(12):4679–84. https://doi.org/10.1016/j.energy.2010.09.036.
[38] Mellalou A, Riad W, Bacaoui A, Outzourhit A. Impact of the greenhouse drying modes of two-phase olive pomace on the energy, exergy, economic and environmental (4E) performance indicators. Renew Energ 2023;10:229–50. https://doi.org/10.1016/j.renene.2023.04.074.
[39] Zhang L, Jiang L, Xu Z, Zhang X, Fan Y, Adnouni M, et al. Optimization of a variable-temperature heat pump drying process of shiitake mushrooms using response surface methodology. Renew Energ 2022;198:1267–78. https://doi.org/10.1016/j.renene.2022.08.094.
[40] Ismaeel HH, Yumrutaş R. Thermal performance of a solar-assisted heat pump drying system with thermal energy storage tank and heat recovery unit. Int J Energ Res 2020;44(5):3426–45. https://doi.org/10.1002/er.4966.
[41] Mohammadi I, Tabatabaekoloor R, Motevali A. Effect of air recirculation and heat pump on mass transfer and energy parameters in drying of kiwifruit slices. Energy 2019;170:149e58. https://doi.org/10.1016/j.energy.2018.12.099.
[42] Mondal MHT, Hossain MA, Sheikh MAM, Akhtaruzzaman M, Sarker MSH. Energetic and exergetic investigation of a mixed flow dryer: a case study of maize grain drying. Dry Technol 2021;39(4):466e80. https://doi.org/10.1080/07373937.2019.1709077.
[43] Sun Z, Wang Q, Yuan Y, Wang D, Zhou Q, Xu C, et al. Experimental analysis of a CO2 closed heat pump drying system combined with rotary dehumidification for drying banana slices drying. Int J Refrig 2024;160:76–87. https://doi.org/10.1016/j.ijrefrig.2024.01.017.

[44] Khanali M, Aghbashlo M, Rafiee S. Exergetic performance assessment of plug flow fluidised bed drying process of rough rice. Int J Exergy 2013;13(3):387–408. https://doi.org/10.1504/IJEX.2013.057357.
[45] Aghbashlo M, Mobli H, Rafiee S, Madadlou A. Energy and exergy analyses of the spray drying process of fish oil microencapsulation. Biosyst Eng 2012;111(2):229–41. https://doi.org/10.1016/j.biosystemseng.2011.12.001.
[46] Zare D, Chen G. Evaluation of a simulation model in predicting the drying parameters for deep-bed paddy drying. Comput Electron Agr 2009;68(1):78e87. https://doi.org/10.1016/j.compag.2009.04.007.
[47] Zeng Z, Han C, Li H, Chen T, Zeng J, Fang Z, et al. Modeling and evaluation in transient analysis of industrialized counter-flow tea drying system. Case Stud Therm Eng 2024;53:103781. https://doi.org/10.1016/j.csite.2023.103781.
[48] Wang H, Li S, Zhang Y, Ali KAM, Wu W, Li C. The analytical theory of water activity in the paddy rice drying process. Agronomy 2024;14(8):1728. https://doi.org/10.3390/agronomy14081728.
[49] Li Y, Gao H, Wan Q, Qiu X, Qi Y, Wu Z. Investigation of water variation and surface crust of Polygonati Rhizoma extract during vacuum drying. LWT 2024;207:116623. https://doi.org/10.1016/j.lwt.2024.116623.
[50] Defendi RO, Nicolin DJ, Paraíso PR, Jorge LM. Assessment of the initial moisture content on soybean drying kinetics and transport properties. Dry Technol 2016;34(3):360–71. https://doi.org/10.1080/07373937.2015.1055496.
[51] Akpinar EK. Thermodynamic analysis of strawberry drying process in a cyclone type dryer. J Sci Ind Res (India) 2007;66:152e61. http://nopr.niscair.res.in/handle/123456789/1160.
[52] Yan J, Xie H, Hu Z, Wei H, You Z, Xue H. Simulation and process optimization of upward and downward reversing ventilating drying by fixed bed. Trans Chin Soc Agric Eng 2015;31(22):292e300. https://doi.org/10.11975/j.issn.1002-6819.2015.22.040.
[53] Li C, Chen Y, Zhang X, Mozafari G, Fang Z, Cao Y, et al. Exergy analysis and optimisation of an industrial-scale circulation counter-flow paddy drying process. Energy 2022;251:123901. https://doi.org/10.1016/j.energy.2022.123901.
[54] Yang J, Miao Z, Wu J, Yu X, Liu C, Liu S. Dishwasher's closed drying process investigation based on heat pump system. Energ Effi 2023;16(5):45. https://doi.org/10.1007/s12053-023-10126-4.
[55] Zhang W, Fan Y, Zhang J. Sensitivity analysis of closed and semi-closed heat pump drying systems. JPCS 2025;2932(1):012061. https://doi.org/10.1088/1742-6596/2932/1/012061.
[56] Xu K, Liu G, Wang T, Li L. Study on thermal performance of closed heat pump seed drying system. Trans Chin Refri Air Cond 2019;19(07):72–6. https://doi.org/10.3969/j.issn.1009-8402.2019.07.015.
[57] Zhang X, Wang D, Yuan J, Deng Z, Qin B, Sun L. Design and thermodynamic analysis of heat recovery method for closed-cycle heat pump drying system. Trans Chin J Chin Agric Mech Chem 2024;45(12):216–23. https://doi.org/10.13733/j.jcam.issn.2095-5553.2024.12.032.
[58] Erbay Z, Hepbasli A. Application of conventional and advanced exergy analyses to evaluate the performance of a ground-source heat pump (GSHP) dryer used in food drying. Energ Convers Manage 2014;78:499–507. https://doi.org/10.1016/j.enconman.2013.11.009.

Energy 321 (2025) 135431

Contents lists available at ScienceDirect

Energy

journal homepage: www.elsevier.com/locate/energy

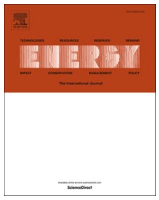

Hierarchical model predictive control for energy consumption regulation of industrial-scale circulation counter-flow paddy drying process

Chengjie Li [a,*,1], Jiayang Ren [b,1], Arpan Seth [c], Ye Zhang [a], Jianjiang Huang [a], Changyou Li [a], Yankai Cao [b,**]

[a] College of Engineering, South China Agricultural University, Guangzhou, 510642, China
[b] Department of Chemical and Biological Engineering, University of British Columbia, Vancouver, V6T1Z3, Canada
[c] Evonik Corporation, Trexlertown, PA, 18195, USA

ARTICLE INFO

Handling editor: Isabel Soares

Keywords:
Paddy drying
Model predictive control
Industrial-scale
Energy optimization
Exergy efficiency

ABSTRACT

Paddy drying is an energy-intensive process that involves complex interaction such as inertia, nonlinearity, and random disturbances. Real-time energy consumption regulation is challenging due to the interplay of these factors. This study proposes a two-level hierarchical model predictive control (MPC) strategy for industrial-scale circulation counter-flow paddy drying process. The first-level optimizer encompasses an energetic optimizer, engineered to minimize energy consumption. This optimizer integrates drying mathematical and energetic models, as well as drying and ambient data. It operates at a low frequency of once every 180 s to handle computational complexity and slow-changing ambient conditions. To handle high-frequency disturbances, a second-level MPC operates at 2.25 s intervals, relying exclusively on drying mathematical model and tracking ideal trajectory established by first-level optimizer. Experiments show that first-level optimizer reduces total energy consumption by 12.8 % compared to previous proposed static ventilation strategy. Hierarchical MPC strategy consistently achieves lower relative average deviations (0.70 %, 0.79 %, and 0.81 %) from ideal trajectory under varying disturbance fluctuation rates (±60 %, ±80 %, and ±100 % respectively). These deviations are markedly lower (by 1.58 %, 15.67 %, and 19.52 % respectively) than those observed when applying first-level optimizer under noisy conditions. These findings underscore the enhanced energy-saving and disturbance-suppression capabilities of proposed hierarchical MPC strategy.

Nomenclature

ARD	Average relative deviation
c	Specific heat (kJ/(kg·°C))
C	Output matrix
d	Humidity ratio (kg/kg)
DR	g water/(g wet matter h)
ex	Specific exergy (kJ/kg)
En	Energy rate (kW)
Ex	Exergy rate (kW)
f	Cooling coefficient (h^{-1})
f(•)	Drying mathematical model
g	Heating coefficient (h^{-1})
G	Total mass of grain (kg)
h	Heat transfer coefficient (kJ/(h·m^2·°C))
H	Enthalpy (kJ/kg)

(*continued on next column*)

(*continued*)

J	Objective function
k	Time step
m	Mass flow rate (kg/h)
M	Moisture content (g water/g wet or dry matter)
MR	Moisture ratio
MRD	Mean relative deviation
N_c	Second-level MPC control horizon
$N_{ex,ir}$	Dimensionless normalized exergy destruction rate of irreversibility
N_f	First-level optimizer control horizon
N_p	Second-level MPC prediction horizon
P	Pressure (Pa)
Q	Energy rate (kW)
r	Drying constant (h^{-1})
R	Gas constant (kJ/(kg·°C))

(*continued on next page*)

* Corresponding author.
** Corresponding author.
E-mail addresses: chengjie.li@scau.edu.cn (C. Li), yankai.cao@ubc.ca (Y. Cao).
[1] These authors contributed equally to this work and should be considered co-first authors.

https://doi.org/10.1016/j.energy.2025.135431
Received 8 January 2024; Received in revised form 22 January 2025; Accepted 2 March 2025
Available online 5 March 2025

(*continued*)

RAD	Relative average deviation
RH	Relative humidity (%)
RMSE	Root-mean-square error (g water/g wet matter or °C)
S	Area (m^2)
t	Drying time (h)
T	Temperature (°C)
u	Control inputs
V	Flow velocity (m/h or m/s)
x	System states
y	System outputs
z	Bed height (m)
Greek letters	
$\gamma\alpha$	Effective evaporation area per unit volume (m^2/m^3)
δ	Measurement disturbance
Δ	Deviation
ε_r	Radiator emissivity
λ_g	Latent heat of vaporisation of paddy (kJ/kg)
η	Efficiency
μ	Interphase mass transfer coefficient ($kg/(h{\cdot}m^2)$)
ρ	Density (kg/m^3)
σ	Blackbody radiation constant ($W/(m^2{\cdot}°C^4)$)
$\tau\alpha$	Effective heat transfer area per unit volume (m^2/m^3)
ω	Productivity ($kg\ h^{-1}$)
Subscripts	
a	Drying air
ab	Ambient
d	Dry basis
g	Grain
h	Heating grain
in	Inlet
ir	Irreversibility
out	Outlet
r	Flue gas pipe
ref	Reference trajectory
v	Vapour
we	Water evaporation

1. Introduction

Paddy, recognized as a pivotal food crop indispensable for human survival and development [1,2], necessitates prompt treatment due to its intrinsically high moisture content, typically exceeding 0.3 g water/g wet matter, and the frequently concurrent occurrence of its harvest period with typhoon season. Failure to address this promptly can result in rapidly mildew and deterioration of the wet paddy under high temperature, humidity, and rainfall, ultimately affecting product quality [3,4]. Industrial-scale drying occupies a crucial position in safeguarding the quality of paddy during the post-harvest phase, holding substantial ecological, economic, and social significance. However, drying processes are typically energy-intensive, accounting for a significant portion of global energy usage ranging from 12 % to 25 %, with agricultural product drying alone contributing 3.62 % [5,6]. In light of the increasingly urgent environmental challenges and the limited availability of fossil fuels, the high energy consumption associated with paddy drying emerges as a pivotal factor that hinders sustainable human development [7]. Hence, minimizing energy consumption during the paddy drying process in the post-harvest phase possesses considerable practical importance.

Energy consumption during drying is influenced by multiple factors, with energy generation and supply mode, ventilation parameters, and ambient conditions being the most significant. Researchers have investigated energy conservation strategies through innovative drying methods, such as hot air-assisted radio frequency drying [8], solar-assisted heat pump drying [9], and microwave-assisted hot air drying [10]. However, these methods, which require high-grade energy, may not be economically viable for small-scale farmers, thereby limiting their widespread adoption in the agricultural industry. Consequently, research has shifted towards studying the influence of ventilation parameters on energy consumption [11,12], proposing structural improvements to enhance energy utilization [13,14], and developing energy optimization models [15,16]. Techniques such as response surface methodology [17], variable ventilation parameters method [18], and waste-heat recovery [19] are commonly employed in these studies. These investigations primarily focus on analysing and optimizing the transfer and transformation characteristics of drying energy or exergy within systems, taking into account the complexities arising from both internal factors (such as process mode, mechanical structure, and physical property changes) and external conditions (like drying air temperature and flow velocity, and grain initial moisture content).

In the context of a specific grain dryer operating in a given environment, the energy conveyed by the drying air originates from the heat absorbed by a specific volume of ambient air in the heat source. Therefore, the energy consumption during the drying process of grain with a particular initial state is closely related to ambient conditions. However, existing research has overlooked the impact of dynamically changing ambient conditions on the energy utilization characteristics of drying systems. Specifically, there is a notable lack of studies that integrate energy conservation with real-time energy consumption regulation during the drying process. This limitation has hindered the advancement of energy-saving drying equipment upgrades.

Model Predictive Control (MPC) is an effective method for addressing this challenge. It leverages a system model and the current state to predict future system behaviour. At each time step, it computes the optimal control actions by considering the control objectives, system constraints, and potential disturbances [20]. Compared to PID control, fuzzy control, and intelligent control, MPC is regarded as the most effective approach for grain drying, receiving substantial attention and application in this domain [21]. Song et al. [22] proposed an MPC drying strategy for paddy, aiming to maximize head paddy yield through real-time optimization. Simulations and experiments showed MPC outperformed constant temperature drying, demonstrating its feasibility and potential for real-time optimization. Bottari et al. [23] proposed an MPC method for continuous cross-flow paddy dryers. Through simulations, it was found that the control system could rapidly determine optimal drying parameters under external random disturbances, significantly improving the performance of traditional closed-loop drying control structures. Zhang et al. [24] utilized deep learning techniques to fit the original drying MPC algorithm, enabling rapid regulation of the moisture content of discharged grain in a multistage counterflow paddy dryer. This work demonstrated the potential of MPC in addressing the time-consuming task of online optimization in deep-bed grain drying. However, implementing classical MPC for energy consumption regulation in paddy drying involves solving a complex optimization problem at each time step. This results in significant computational costs, making online implementation challenging, especially in the presence of disturbances.

Hierarchical MPC, in contrast, provides a promising approach to reducing computational complexity and enhancing real-time responsiveness. It achieves this by decomposing the complex optimization problem into a serial of smaller subproblems, which are solved individually and then integrated into a cohesive framework. Hierarchical MPC has been widely applied in various energy optimization processes, including greenhouse management [25], fuel cells [26], and electric vehicles [27]. However, to the best of our knowledge, no prior research has investigated the use of hierarchical MPC for designing energy optimization strategies in industrial-scale paddy drying. This paper aims to address this gap by proposing a hierarchical MPC framework that optimizes energy consumption while mitigating disturbances in the context of paddy drying.

In this study, we focus on industrial-scale circulation counter-flow paddy drying, a prevalent batch drying technique [28]. This process involves gradually dehydrating wet paddy in a thin layer using low-temperature drying air to create mild drying conditions. Subsequently, the paddy is conveyed back to the drying chamber via an elevator for additional circulation and drying until it attains a desired

moisture level. Compared to large-scale continuous drying processes, circulation counter-flow drying boasts flexibility, cost-effectiveness, and ease of operation [29]. Consequently, it is popular in regions with widespread but high-volume paddy production, such as southern China, Japan, South Korea, and certain Southeast Asian nations. However, like other industrial-scale drying processes, energy consumption is a significant concern that must be addressed to ensure the method's industrial viability and promotion.

In summary, research on energy consumption regulation in industrial-scale paddy drying processes using MPC technology remains limited due to high computational costs, particularly in environments with significant disturbances. Building on our previous study [18], this paper introduces a novel hierarchical MPC strategy tailored for the industrial-scale circulation counter-flow paddy drying process with disturbances. The proposed approach addresses computational challenges by decomposing the complex energy optimization problem into two interconnected levels of MPC subproblems, enhancing the feasibility of online implementation and reducing computational costs.

The first level controller serves as an energetic optimizer to minimize energy consumption while adhering to the system constrains. It integrates both drying mathematical and energetic models with drying and ambient data as system states. Given its computational complexity and the slow-changing nature of ambient conditions, this first level operates at a low frequency of once every 180 s in our experiments. To handle high-frequency disturbances occurring between the updates of the first-level optimizer, a second-level MPC controller is proposed based on the drying mathematical model solely, operating at a higher frequency of 2.25 s. This controller is designed to accurately track the ideal trajectory generated by the first-level optimizer while suppressing disturbances. Our experiments demonstrate the enhanced energy-saving and disturbance-suppression capabilities of our proposed hierarchical MPC strategy, providing a foundation and technical support for advancing innovation in energy-efficient drying equipment during the grain post-harvest phase.

The remainder of this paper is organized as follows. Section 2 presents the system model. Section 3 introduces the energetic analysis. Section 4 describes the MPC controller design. Section 5 reports the results and discussions. Section 6 concludes the key ideas of this paper.

2. System model

2.1. Equipment description and physical model

Fig. 1 shows the scene graph of a type of circulation counter-flow paddy dryer, 5HP-20, which is developed by our laboratory. This drying system consists of three sections: heat source, drying chamber, and dedusting device. The heat source primarily consists of a cost-effective combustion chamber, which utilizes paddy hull as its fuel. The combustion chamber is connected to the drying chamber via a heat exchanger. Within the drying chamber, the paddy flows sequentially from top to bottom through the tempering stage, preheating stage, drying stage, and discharging stage. The tempering and drying stage employ counter flows of ambient and drying air, respectively. The preheating stage primarily comprises four tubular infrared radiators inserted into this stage, which utilize waste heat carried by a portion of the flue gas emitted from combustion chamber to preheat paddy. The discharging stage consists of a reciprocating grain discharging device. The exhaust gas from drying chamber and flue gas emitted by the radiators are directed into a cyclone separator under the action of the induced fan (Model Y4-73, Shandong Shuntong Blower co., Ltd). The 5HP-20 paddy dryer has been implemented at a farm in Leizhou, Guangdong Province, China.

Fig. 2 depicts the physical model that elucidating the flow dynamics and interaction between wet paddy and drying air within a 5HP-20 circulation counter-flow paddy dryer. The controlled object is described as follows: Initially, the drying tower is completely filled with wet paddy, characterized by an initial moisture content (M_{in}). Subsequently, the induced fan, heat source, and grain discharging device are sequentially activated. Under the influence of gravity, wet paddy flows steadily from the top to the bottom of the dryer at a predefined flow velocity ($V_{g,in}$). Upon reaching the discharging stage, the paddy, now with a moisture content denoted as M_{out}, is conveyed back to the top of the drying tower via an elevator for subsequent circulation. Throughout multiple circulation processes within the dryer, the paddy undergoes heat and mass transfer with the drying air. Ultimately, once the desired moisture content is attained, the paddy is discharged from the dryer. Meanwhile, ambient air passes through a heat exchanger, where it undergoes a temperature increases (from T_{ab} to $T_{a,in}$) upon heating. Driven by the induced fan, this heated air enters the dryer from the bottom to the top. The drying air subsequently comes into contact with the wet paddy, effectively extracting excess moisture, and is subsequently

Fig. 1. Diagram of 5HP-20 industrial-scale circulation counter-flow paddy dryer.

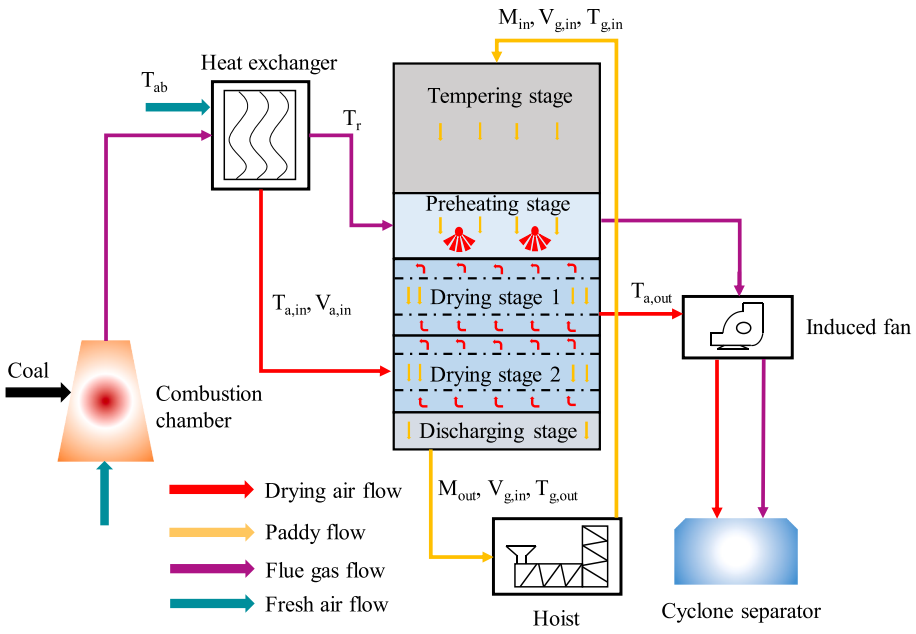

Fig. 2. Physical model of circulation counter-flow paddy drying system.

expelled from the drying system through a cyclone separator, at which point its temperature is denotes as $T_{a,out}$.

Based on the physical model, the fundamental components of the paddy drying system comprise ambient air, flowing paddy, and drying air. Among these components, the uncontrollable factors include the ambient state, characterized by temperature T_{ab} and relative humidity (RH), as well as the initial state of the paddy, defined by its moisture content M_{in} and inlet temperature $T_{g,in}$. Notably, the actual state of the drying paddy, specifically its moisture content (M) and temperature (T_g) can be manipulated by adjusting the drying air temperature ($T_{a,in}$), drying air flow velocity ($V_{a,in}$), and paddy flow velocity ($V_{g,in}$). These adjustments are facilitated through alterations in the power of the heating system, the frequency of the induced fan, and the frequency of the discharging motor, respectively. Consequently, the inputs of the paddy drying system are identified as $T_{a,in}$, $V_{a,in}$, and $V_{g,in}$, whereas the outputs consist of the moisture content (M_{out}) and temperature ($T_{g,out}$) of the paddy exiting the discharging stage. As illustrated in Fig. 3, the drying system can be conceptualized as a thermodynamic open system, characterized by flowing material with the drying chamber wall serving as the boundary.

2.2. System constraints

2.2.1. State constraints

To mitigate the adverse impacts of inertial drying on product quality, the present study establishes a target average moisture content for the paddy that is marginally elevated compared to the safe moisture content

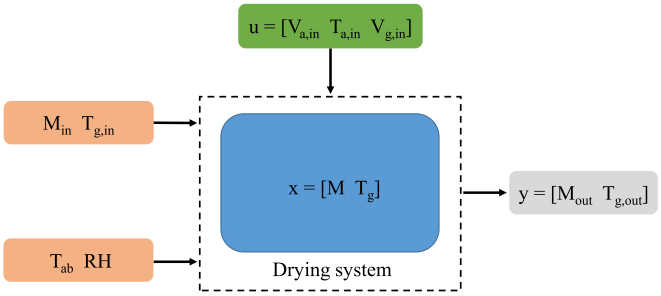

Fig. 3. Description of input and output parameters of drying system.

for storage (M_{saf}), which is defined as 0.14 g water/g wet matter [30]. This specific constraint can be formulated as follows:

$$M_{out}(t_f) = M_{saf} \tag{1}$$

where t_f is the time at the end of drying.

The primary concerns in industrial-scale grain drying pertain to the crack ratio and rice taste, which constitute the foremost quality indicators of significance. By drawing upon the mechanism of fissure formation in paddy kernels based on glass transition theory [31] and the influence of drying air on rice taste characteristics [32], it is imperative to confine the drying state of paddy within the safe-quality zones throughout the entire drying tower. These safe-quality zones can be delineated using Equation (2) and Equation (3), which represent the state constraints pertaining to drying quality [18,33,34]:

$$T_g - 53.63 + 88 \cdot M \geq 0 \tag{2}$$

$$5.021 - \ln T_g - 5.8 \cdot M \leq 0 \tag{3}$$

The drying rate (DR) quantifies the rate of change in paddy moisture content per hour throughout the drying process. Maintaining an adequate drying rate is crucial to fulfill the minimum requirements for production efficiency. To guarantee drying productivity and comply with the production index, it is imperative that the drying rate does not decrement below a specified minimum threshold value:

$$DR \geq DR_{min} \tag{4}$$

2.2.2. Input constraints

Following the determining the process mode and mechanical structure of the paddy dryer, it is necessary to confine the input variables of the drying control system within prescribed ranges. Consequently, the constraints of the drying control system can be formulated as outlined below:

$$T_{a,in,min} \leq T_{a,in} \leq T_{a,in,max} \tag{5}$$

$$V_{a,in,min} \leq V_{a,in} \leq V_{a,in,\max} \tag{6}$$

$$V_{g,in,min} \leq V_{g,in} \leq V_{g,in,max} \tag{7}$$

where $T_{a,in}$ is the inlet drying air temperature, $V_{a,in}$ is the inlet drying air

flow velocity, $V_{g,in}$ is the paddy flow velocity, $T_{a,in,max}$ and $T_{a,in,min}$ are the lower and upper bounds of $T_{a,in}$, $V_{a,in,max}$ and $V_{a,in,min}$ are the lower and upper bounds of $V_{a,in}$, $V_{g,in,max}$ and $V_{g,in,min}$ are the lower and upper bounds of $V_{g,in}$.

To minimize wear and tear on mechanical components, such as fans and discharging motors, it is essential to restrict the rate of change of operating parameters. Therefore, the change rate of the input variables must be confined within a specific range, as detailed below:

$$\left|\frac{dT_{a,in}}{dt}\right| \le l_1 \tag{8}$$

$$\left|\frac{dV_{a,in}}{dt}\right| \le l_2 \tag{9}$$

$$\left|\frac{dV_{g,in}}{dt}\right| \le l_3 \tag{10}$$

where l_1, l_2, and l_3 are the thresholds for change rates of $T_{a,\,in}$, $V_{a,\,in}$, and $V_{g,in}$, respectively.

2.3. Drying mathematical model

Given the primary distinctions in process characteristics among various serial stages stemming from variations in ventilation parameters, the paddy drying process investigated in this study can be represented by a simplified schematic diagram, as depicted in Fig. 4 [33]. Fig. 4 (a) depicts the drying stage, wherein the drying air flows from the bottom to the top. Fig. 4 (b) illustrates the preheating stage, with the flue gas pipe traversing through the stage. Fig. 4 (c) shows either the tempering stage or the discharging stage, depending on the air flowing through, which is ambient air in both cases.

In industrial-scale grain drying, people often focus on the state distribution in batches of grain instead of state of single kernel. Therefore, in the context of the circulation counter-flow drying process examined in this study, it is essential to select a spatial node within the above-mentioned stages as the fundamental research unit for synthesizing the overall system state. Specifically, the micro-element ΔZ, as indicated in Fig. 4, which represents a drying system with a defined boundary and volume, has been chosen as the primary research system for this purpose. Detailed description for modeling this micro-element can be found in Supplementary materials A. After modeling the micro-element ΔZ, an analytical model of the entire circulation counter-flow drying system can be derived by synthesizing the global states, based on the variations in the process characteristics at each stage.

2.3.1. Drying stage model

To numerically model the micro-space node depicted in Fig. 4 (a), the fundamental mathematical model introduced in References [18,33] is employed in this study. This model can be encapsulated in the following partial differential equations (PDEs). During the drying stage, alterations in heat and mass of the micro-space node arise due to both drying and paddy flow. The corresponding heat and mass balance equation can be formulated as:

$$\rho_g \frac{\partial M_d}{\partial t} - V_g \rho_g \frac{\partial M_d}{\partial z} = -\mu\gamma\alpha(d_s - d)MR \tag{11}$$

$$c_g \rho_{g,w} \frac{\partial T_g}{\partial t} + V_g c_g \rho_{g,w} \frac{\partial T_g}{\partial z} = -h\tau\alpha\left(T_a - T_g\right) - \lambda_g \mu\gamma\alpha(d_s - d)MR \tag{12}$$

$$V_a \rho_a \frac{\partial d}{\partial z} = \mu\gamma\alpha(d_s - d)MR \tag{13}$$

$$c_a \rho_a V_a \frac{\partial T_a}{\partial z} = -h\tau\alpha\left(T_a - T_g\right) \tag{14}$$

where ρ_g is the bulk density of absolute dry paddy, M_d is the paddy moisture content, on a dry basis, t is the drying time, z is the bed height, μ is the interphase heat transfer coefficient, γα is the effective evaporation area of unit volume, d_s is the saturated humidity, d is the air humidity ratio, MR is the moisture ratio, c_g is the specific heat of paddy, $\rho_{g,w}$ is the bulk density of wet paddy, h is the heat transfer coefficient, τα is the effective heat transfer area per unit volume, λ_g is the latent heat of vaporisation of paddy, ρ_a is the air density, and c_a is the specific heat of dry air.

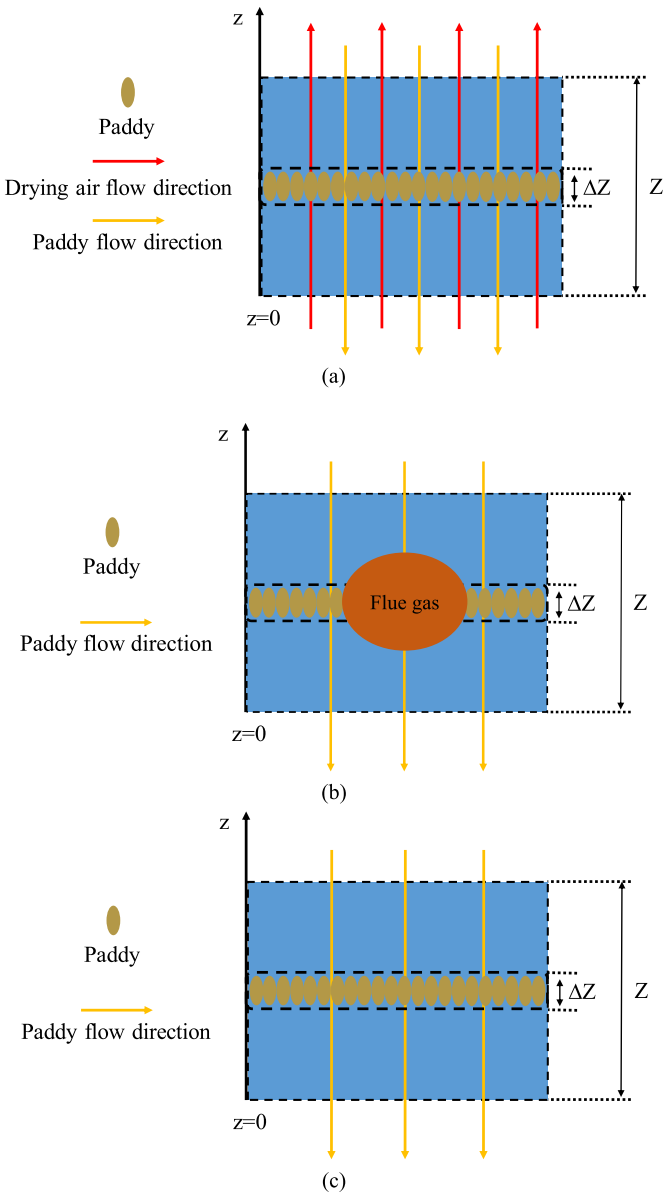

Fig. 4. Diagram of the drying, preheating, and tempering stage in industrial-scale grain drying system: (a) Drying stage, (b) preheating stage, and (c) tempering stage.

2.3.2. Tempering stage model

For the tempering and discharging stage illustrated in Fig. 4 (b), the variation in moisture content within the micro-space node is solely attributed to paddy flow. Simultaneously, heat gradually dissipates into the ambient environment through convection and radiation. Consequently, the heat and mass balance equation for the tempering and discharging stage can be formulated as:

$$\frac{\partial M_d}{\partial t} = V_g \frac{\partial M_d}{\partial z} \tag{15}$$

$$\frac{\partial T_g}{\partial t} = V_g \frac{\partial T_g}{\partial z} - f(T_g - T_{ab}) \tag{16}$$

where f is the cooling coefficient and T_{ab} is the ambient temperature.

2.3.3. Preheating stage model

Analogous to the tempering stage, paddy does not undergo dehydration during the preheating stage, and changes in the moisture content of the micro-space node are exclusively driven by paddy flow. Heat transfer to the paddy occurs via radiation from the flue gas pipe, resulting in alterations in the heat content of the micro-space node. Consequently, the heat and mass balance equation for the preheating stage can be expressed as:

$$\begin{cases} \frac{\partial M_d}{\partial t} = V_g \frac{\partial M_d}{\partial z} \\ \frac{\partial T_g}{\partial t} = V_g \frac{\partial T_g}{\partial z} + g(T_r - T_g) \end{cases} \tag{17}$$

where g is the heating coefficient, and T_r is the temperature of flue gas pipe.

To solve above PDEs, following initial and boundary conditions should be given [18]:

Initial conditions:

$$\begin{cases} M_{i,0} = M_0 \\ T_{g,i,0} = T_{g,0} \end{cases} \tag{18}$$

Boundary conditions:

$$\begin{cases} d_{0,t} = d_0 \\ T_{a,0,t} = T_{a,0} \end{cases} \tag{19}$$

where M_0 is the initial moisture content of paddy, $T_{g,0}$ is the initial temperature of paddy, $T_{a,0}$ is the temperature of inlet drying air, d_0 is the absolute humidity of inlet drying air, and i is the ith layer of drying system divided in z-direction.

2.3.4. Model performance analysis

In our previous studies [18,33], we conducted a paddy drying experiment to validate the performance of the mathematical model. Detailed experimental procedures are provided in Supplementary material B. Essential drying data collected at the drying site, including ambient and ventilation parameters as well as initial state parameters of the paddy, were substituted into the mathematical model to calculate real-time paddy drying states. The calculated real-time paddy moisture content and temperature were compared with measured values. To quantify the performance of the calculation model, we employed two evaluation indicators: the root mean square error (RMSE) and the average relative deviation (ARD). Results demonstrated that RMSE for real-time paddy moisture content and temperature at discharging outlet were 0.98 % w.b. and 0.49 °C, respectively, while the ARD were 5.5 % and 1.42 %, respectively. The reasonable values of these performance evaluation indicators confirmed the accuracy of the calculation model. Therefore, the calculation model can be utilized as a tool for energy consumption regulation in the industrial-scale circulation counter-flow paddy drying process studied in this paper.

3. Energetic analysis

3.1. Energy analysis

Based on the physical model of the circulation counter-flow paddy drying system, depicted in Fig. 2, the input energy of the thermodynamic open system comprising the drying chamber primarily consists of the energy transported by the drying air and waste gases within the flue gas pipe. A portion of this input energy is allocated to the removal of moisture, another portion to the heating of the paddy, while the remainder is expelled from the system via waste air. Consequently, in accordance with the first law of thermodynamics, the energy balance equation for the controlled object under investigation in this paddy drying process can be formulated as follows [34]:

$$\dot{m}_{a,in} H_{in} + \dot{Q}_g = \dot{m}_{a,out} H_{out} + \dot{Q}_{we} + \dot{Q}_h \tag{20}$$

where $_{a,in}$ is the mass flow rate of drying air, H is the specific enthalpy of drying air, $_g$ is the energy transfer rate by flue gas pipe, $_{we}$ and $_h$ are the energy transfer rate for water evaporation and heating paddy, respectively.

The equation for calculating $_{a,in}$ is as follows [35]:

$$\dot{m}_a = \frac{101.35}{0.287 T_{ab}} V_a S \tag{21}$$

where S is the cross-sectional area of inlet air pipe.

$_g$, $_{we}$, and $_h$ are calculated using Equation (22)–(24), respectively [36–38]:

$$\dot{Q}_g = \sigma \varepsilon_r T_r^4 S_r \tag{22}$$

$$\dot{Q}_{we} = \dot{m}_{we} \lambda_g \tag{23}$$

$$\dot{Q}_h = c_g \dot{m}_g (T_{g,out} - T_{ab}) \tag{24}$$

where σ is the blackbody radiation constant, ε_r is the radiator emissivity, S_r is the surface area of flue gas pipe, $_{we}$ is the water evaporation rate, and $_g$ is the mass flow rate of paddy.

3.2. Exergy analysis

Upon deriving the energy balance equation and incorporating the principles of the second law of thermodynamics, the exergy balance equation for the controlled object can be formulated as Equation (25) [39]:

$$\dot{m}_{a,in} ex_{in} + \dot{E}x_g = \dot{m}_{a,out} ex_{out} + \dot{E}x_{we} + \dot{E}x_h + \dot{E}x_{ir} \tag{25}$$

where ex is the specific exergy of drying air, x_g is the exergy transfer rate by flue gas pipe, x_{we} and x_h are the exergy transfer rate for water evaporation and heating grain, respectively, and x_{ir} is the exergy destruction rate of irreversibility.

The equation utilized for calculating specific exergy of drying air at both the inlet and outlet of the drying chamber (ex) is provided as follows [40]:

$$ex = (c_a + dc_v)(T_a - T_{ab}) - T_{ab}\left[(c_a + dc_v)\ln\left(\frac{T_a}{T_{ab}}\right) - (R_a + dR_v)\ln\left(\frac{P_a}{P_b}\right)\right] + T_{ab}\left[(R_a + dR_v)\ln\left(\frac{1 + 1.6078 d_{ab}}{1 + 1.6078 d}\right) + 1.6078 dR_a \ln\left(\frac{d}{d_{ab}}\right)\right] \tag{26}$$

where c_v is the specific heat of vapour, R_a is the gas constant of drying air, R_v is the gas constant of vapour, P_a is the pressure of drying air, the atmospheric pressure P_b is 101,325 Pa in this study, and d_{ab} is the humidity ratio of ambient air.

The transfer rate of exergy carried by waste gas in flue gas pipe (x_g) is calculated using Equation (27) [41]:

$$\dot{E}x_g = \sigma T_r^4 \left(\varepsilon_r + \frac{1}{3}\left(\frac{T_{ab}}{T_r}\right)^4 - \frac{4}{3}\varepsilon_r^{-0.75}\left(\frac{T_{ab}}{T_r}\right)\right) \tag{27}$$

The transfer rate of exergy for dehydration (x_{we}) and heating paddy (x_h), as well as the exergy destruction rate of irreversibility (x_{ir}) are calculated using Equation (28)–(30), respectively [42,43]:

$$\dot{E}x_{we} = \dot{Q}_{we}\left(1 - \frac{T_{ab}}{T_g}\right) \tag{28}$$

$$\dot{E}x_h = \dot{Q}_h\left(1 - \frac{T_{ab}}{T_g}\right) \tag{29}$$

$$\dot{E}x_{ir} = (\dot{Q}_h + \dot{Q}_{we})T_{ab}\left(\frac{T_a - T_{ab}}{T_a T_{ab}}\right) \tag{30}$$

The equation for calculating transient energy consumption rate (n_{in}) and drying efficiency (η_{en}) are Equation (31) and (32), respectively [44]:

$$\dot{E}n_{in} = \dot{Q}_g + \dot{m}_{a,in}H_{in} \tag{31}$$

$$\eta_{en} = \frac{\dot{Q}_{we}}{\dot{Q}_g + \dot{m}_{a,in}H_{in}} \tag{32}$$

Exergy efficiency (η_{ex}) is calculated using Equation (33) [39]:

$$\eta_{ex} = \frac{\dot{E}x_{we}}{\dot{E}x_g + \dot{m}_{a,in}ex_{in}} \tag{33}$$

Productivity is usually adopted as an intuitive indicator to evaluate the working capacity of grain dryers, and it is calculated using Equation (34) [45]:

$$\omega = \frac{G_0(1 - M_0)}{t_{tol}(1 - M_{fn})} \tag{34}$$

where G_0 is the total mass of wet paddy feeding into dryer, M_0 is the initial moisture content of paddy, M_{fn} is the moisture content of dried paddy, and t_{tol} is the total drying time.

4. MPC controller design

This section introduces a hierarchical MPC framework designed to optimize energy consumption while mitigating disturbances in industrial-scale paddy drying processes. As illustrated in Fig. 5, the framework consists of two interconnected levels: a low-frequency first-level optimizer and a high-frequency second-level MPC controller. This hierarchical design ensures a balance between computational efficiency and real-time responsiveness, while effectively coordinating energy-saving objectives and disturbance mitigation.

The first-level optimizer integrates the drying mathematical model (Section 2.3) and the energetic model (Section 3) to serve as an energetic optimizer. Its primary inputs include ambient data, including ambient temperature and relative humidity, as well as system outputs from the dryer. It minimizes energy consumption while adhering to system constraints and provides an optimal reference trajectory for the second-level controller. Given the computational complexity of this optimization and the slow-varying nature of ambient conditions, the first-level optimizer operates at a low frequency to reduce computational demands, updating its outputs every 180 s in our experiments.

The second-level MPC controller focuses on real-time control and disturbance suppression, utilizing solely the drying mathematical model. It uses the reference trajectory provided by the first-level optimizer as input. Additionally, it takes real-time measurements from the dryer, such as the moisture content (M_{out}) and temperature ($T_{g,out}$) of the discharged paddy from the outlet of the discharging stage. The second-level controller generates control inputs to track the reference trajectory and counteract disturbances. By operating at this higher frequency (e.g., every 2.25 s), it effectively suppresses system disturbances and ensures precise control.

This hierarchical structure leverages the complementary strengths of both levels. The first-level optimizer provides an energy-saving trajectory based on slow-changing system states, while the second-level MPC controller ensures fine-tuned, real-time adjustments to maintain process stability and energy efficiency under disturbances.

4.1. First-level optimizer

To facilitate the representation within control systems frameworks, we provide a detailed elaboration on the discrete-state space formulation of the drying mathematical model, which is denoted as Equation (35):

$$\begin{cases} \boldsymbol{x}(k+1) = f(\boldsymbol{x}(k), \boldsymbol{u}(k)) \\ \boldsymbol{y}(k) = C\boldsymbol{x}(k) \end{cases} \tag{35}$$

where k is the discrete sampling time point, $\mathbf{x} = [M, T_g]$ is the system state (moisture content and temperature of whole tower of paddy, measuring using sensors [46] placed inside each stage), $\mathbf{u} = [T_{a,in}, V_{a,in}, V_{g,in}]$ is the input (inlet air temperature, inlet air velocity, and paddy flow velocity), $\mathbf{y} = [M_{out}, T_{g,out}]$ is the output (moisture content and temperature of discharged paddy). This corresponds to the last layer of paddy in the dryer and is extracted as the last element of the state vector $\mathbf{x}$. Consequently, the output matrix C is in the form of [0, 0, 0, …, 0, 1]. f (•) is the drying mathematical model outlined in Section 2.3 (Equations (11)–(19)).

In the context of the first-level optimizer, our focus is on investigating various optimization strategies for paddy drying, with the primary objective of minimizing energy consumption while concurrently ensuring that productivity and product quality remain within acceptable limits. Utilizing the drying mathematical and energetic model, the optimal control inputs $\mathbf{u}_{ref}$ and system outputs $\mathbf{y}_{ref}$, which correspond to different optimization objectives, are computed under dynamically changing ambient conditions. These computed values are then transmitted to the second-level MPC for trajectory tracking. The subsequent

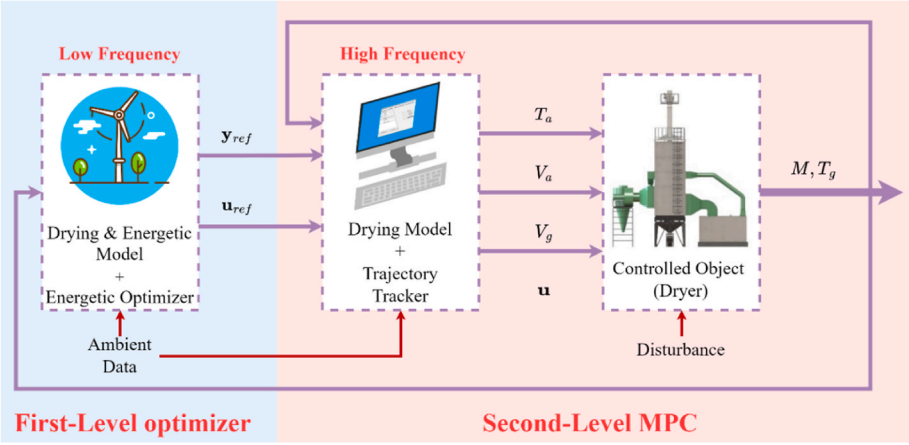

Fig. 5. Diagram of hierarchical control system of paddy drying.

sections delve into the formulation of the pertinent optimization problems.

4.1.1. Strategy 1

Paddy drying represents a unit operation characterized by substantial energy consumption. The primary objective of Strategy 1 is to optimize the process by minimizing the overall energy expenditure associated with drying, which can be mathematically formulated as depicted in Equation (36):

$$J_1(\mathrm{k}) = \sum_{i=k}^{k+N_f-1} \left(Q_g(\mathrm{i}) + m_{a,in}(\mathrm{i})H_{in}(\mathrm{i})\right) \tag{36}$$

where k is the current step, and N_f is the final time step of optimization horizon, respectively.

4.1.2. Strategy 2

In the context of paddy drying, optimizing energy consumption necessitates a holistic approach that not only considers the total input energy but also emphasizes minimizing heat losses. This implies a focus on maximizing energy utilization efficiency during the drying process. Consequently, Strategy 2, in contrast to Strategy 1, incorporates an additional requirement related to heat loss minimization. This objective can be mathematically articulated as shown in Equation (37):

$$J_2(\mathrm{k}) = \sum_{i=k}^{k+N_f-1} \left(Q_g(\mathrm{i}) + m_{a,in}(\mathrm{i})H_{in}(\mathrm{i}) + m_{a,out}(\mathrm{i})H_{out}(\mathrm{i}) + Q_h(\mathrm{i})\right) \tag{37}$$

4.1.3. Strategy 3

Given that exergy analysis accounts for the quality of energy, it provides a more comprehensive insight into the irreversibility and efficiency losses during energy conversion and utilization compared to traditional energy analysis. Consequently, exergy analysis offers deeper guidance for system optimization, such as enhancing equipment exergy efficiency and reducing exergy losses. In this study, the objective of Strategy 3 is to minimize exergy losses while simultaneously ensuring the lowest possible energy consumption. The control method aligned with this optimization strategy is generally regarded as the optimal drying control approach. This can be mathematically expressed as follows:

$$J_3(\mathrm{k}) = \sum_{i=k}^{k+N_f-1} \left(Q_g(\mathrm{i}) + m_{a,in}(\mathrm{i})H_{in}(\mathrm{i}) + m_{a,out}(\mathrm{i})ex_{out}(\mathrm{i}) + Ex_h(\mathrm{i}) + Ex_{ir}(\mathrm{i})\right) \tag{38}$$

The reference control inputs $\mathbf{u}_{\mathrm{ref}}$ remains constant throughout the entire update period of the first-level optimizer (e.g., 180 s in our experiment) and is determined by solving the following optimizing problem:

$$\begin{aligned} &\boldsymbol{u}_{ref}(\mathrm{k}) = \mathrm{argmin}\ J_1(\mathrm{k})\ or\ J_2(\mathrm{k})\ or\ J_3(\mathrm{k}) \\ &s.t.\ Drying\ mathematic\ model\ (35) \\ &Energetic\ model\ (20)-(31) \\ &System\ constraints\ (1)-(10) \\ &\boldsymbol{x}(0) = measured\ system\ states\ at\ time\ k. \end{aligned} \tag{39}$$

The reference system outputs, denoted as $\mathbf{y}_{\mathrm{ref}}$, are generated by applying the reference control inputs $\mathbf{u}_{\mathrm{ref}}$ to the disturbance-free drying mathematical during the current updates period, using the current measured states from the actual dryer as initial system states.

4.2. Second-level MPC

Due to the disturbances in paddy drying process, the actual paddy drying state often deviates from the reference trajectory $\mathbf{y}_{\mathrm{ref}}$ when using the optimal input $\mathbf{u}_{\mathrm{ref}}$ obtained from the first-level optimizer. The second-level MPC is designed to mitigate the effects of these disturbances, ensuring that the drying process continuously tracks the reference trajectory.

The second-level employs a closed-loop control approach to achieve precise reference trajectory tracking utilizing the measured system states. The corresponding objective function is expressed in Equation (40):

$$\begin{aligned} J_{\mathrm{m}}(\mathrm{k}) = &\sum_{i=1}^{N_p} (\Delta\boldsymbol{y}(k+i))^T D_y(\Delta\boldsymbol{y}(k+i)) + \\ &\sum_{i=0}^{N_c-1} (\Delta\boldsymbol{u}(k+i))^T D_u(\Delta\boldsymbol{u}(k+i)) \end{aligned} \tag{40}$$

where $\mathrm{N_p}$ and $\mathrm{N_c}$ are the prediction and control horizon, respectively. $\mathrm{D_y}$ and $\mathrm{D_u}$ are the weights of $\mathbf{y}$ and $\mathbf{u}$, respectively. $\Delta\mathbf{y}$ is the system output deviation, $\Delta\mathbf{u}$ is the control input deviation used to compensate for state deviation caused by disturbances. $\Delta\mathbf{y}$ and Δu can be expressed as follows:

$$\Delta\boldsymbol{y}(k+i) = \boldsymbol{y}(k+i) - \boldsymbol{y}_{ref}(k+i) \tag{41}$$

$$\Delta\boldsymbol{u}(k+i) = \boldsymbol{u}(k+i) - \boldsymbol{u}_{ref}(k) \tag{42}$$

where $\mathbf{u}_{\mathrm{ref}}$(k) is the latest reference input from the first-level optimizer at time k. $\mathbf{y}_{\mathrm{ref}}$(k + i) is the ith reference system output obtained by applying $\mathbf{u}_{\mathrm{ref}}$(k) to the drying mathematical model with the initial system state $\mathbf{x}$ (k). The essence of MPC in second-level is to solve the following optimization problem:

$$\begin{aligned} &\Delta\boldsymbol{u}^*(k) = \mathrm{argmin}J_m(k) \\ &s.t.\ Drying\ mathematic\ model\ (35), \\ &System\ constraints\ (1)-(10), \\ &\boldsymbol{x}(\mathrm{k}) = measured\ system\ states\ at\ time\ k. \end{aligned} \tag{43}$$

The control input $\Delta\mathbf{u}^*(k)$ obtained by solving Equation (43) is a sequence that depends on the current measured system states. However, measurement values after time k cannot influence the current states, which means that external disturbances and model mismatch information contained in future measurements are not reflected in the current states. To address this issue, MPC retains only the first action of $\Delta\mathbf{u}^*(k)$ as the input and discards the rest of the sequence. Specifically, assuming the optimization problem in Equation (43) has a solution, the optimal sequence can be expressed as $\Delta\mathbf{u}^*(k) = [\Delta\mathbf{u}(k), \Delta\mathbf{u}(k+1), \Delta\mathbf{u}(k+2), \ldots, \Delta\mathbf{u}(k + \mathrm{N_c}\text{-}1)]^{\mathrm{T}}$. By retaining only the first element $\Delta\mathbf{u}$(k) from this solution sequence, the control input applied to the system at the current time step k can be represented as:

$$\boldsymbol{u}(k) = \boldsymbol{u}_{ref}(k) + \Delta\boldsymbol{u}(k) \tag{44}$$

At time k+1, the updated system states are used as the initial states to predict the system output over the prediction horizon $\mathrm{N_p}$, and the corresponding optimization problem (Equation (43)) is solved again. As the process advances, the prediction horizon rolls forward, allowing for continuous adjustment and ensuring effective control over the entire drying process.

5. Results and discussions

5.1. Simulation parameters of controller

The focus of this study's simulation is 5HP-20 circulation counterflow paddy dryer, as depicted in Fig. 1. As illustrated in Fig. 6, the drying tower possesses a total height of 5.5 m. The primary drying process occurs within a 2-m-high drying stage. The tempering and preheating stages measure 2 m and 1 m in height, respectively, while the discharging stage spans 0.5 m. The volume of entire dryer is 32.5 m^3, capable of accommodating approximately 18–22 t of wet paddy.

The finite difference method is employed to solve the drying mathematical model, with the calculation process illustrated in Fig. 7. Table 1

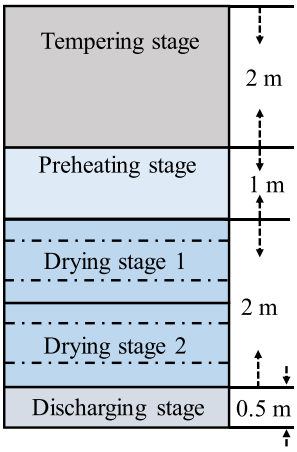

Fig. 6. Size distribution of drying tower.

presents a selection of the thermodynamic equations and corresponding values utilized during the computational process. Furthermore, Tables 1 and 2 collectively provide essential property values and thermodynamic equations that are crucial for the calculation process in both energy and exergy analyses.

For the simulation of the drying controller, the reference basis for the state of paddy and drying air was derived from on-site measured data. Based on our previous research [18], the initial moisture content and temperature of the paddy were established as 0.242 g water/g wet matter and 28.6 °C, respectively. The real-time ambient data from the drying site, as depicted in Fig. 8, was utilized to simulate the real-time ambient state. The data presented in Fig. 8 represents the ambient conditions during a complete operating cycle of paddy drying conducted in Leizhou, Guangdong Province, in May 2021. During the test period, the average ambient temperature and relative humidity were 29.9 °C and 80.27 %, respectively.

In our experimental setup, the closed-loop system incorporates a sampling period of 2.25 s. The first-level optimizer operates at a lower frequency, executing once every 180 s. Conversely, the second-level MPC operates at a higher frequency, cycling every 2.25 s in our experiment. The control and prediction horizons for the first-level optimizer are both configured to span 5 sampling periods, whereas the second-level MPC has a horizon of 2 sampling periods. The parameters, including state constraints, input constraints, control horizon, and prediction horizon, are outlined in Table 3.

To quantify the tracking performance of the hierarchical MPC for a reference trajectory, indicators including relative average deviation (RAD) and maximum relative deviation (MRD) were introduced. These indicators measure the deviation degree of the paddy drying process between the hierarchical MPC system and the reference trajectory. Specifically, RAD was utilized to evaluate the overall tracking effect, whereas MRD was employed to assess the tracking effect at the worst tracking point. RAD and MRD were calculated using Equation (45) and Equation (46), respectively:

Table 1
Thermodynamic equations and property values used in calculation process.

Parameters	Equations/Values	Units
P_s	$P_s = 133.322\exp\left(18.751 - \frac{4075.16}{236.516 + T_{ab}}\right)$	Pa
d	$d = 0.622\frac{RH \cdot P_s}{P_b - RH \cdot P_s}$	kg/kg
MR	$MR = \frac{M_d - M_e}{M_0 - M_e}$	–
M_e	$M_e = \left[\frac{-\ln(1-RH)}{1.919\times10^{-5}(T_a+51.161)}\right]^{\frac{1}{2.445}}$	g water/g dry matter
ρ_a	1.293	kg/m^3
c_a	1.005	kJ/(kg·K)
ρ_g	$\rho_g = \frac{1}{1+M_d}(2.073M_d + 508.5)$	kg/m^3
c_g	$c_g = 1.11 + 0.045\frac{M_d}{1+M_d}$	kJ/(kg·°C)
λ_g	$\lambda_g = [2500 - 2.386(T_g + 273)][1 + 2.556\exp(-20.176M_d)]$	kJ/kg
$\mu\gamma\alpha$	$\mu\gamma\alpha = \frac{\rho_g r(M_d - M_e)}{(d_s - d)}$	kg/(h·m^3)
r	$r = 0.0153T_{a.in} - 0.215$	1/h
$h\tau\alpha$	$h\tau\alpha = V_a c_a \rho_a \frac{T_{a.in} - T_{a.out}}{Z(\overline{T_a} - \overline{T_g})}$	kJ(h·m^3·°C)

Note: r denotes the drying constant, and the equation utilized for its calculation is sourced from Reference [47].

Table 2
Property values and thermodynamic equations used in calculation process.

Parameter	Values/Equations	Units
H	$H = 1.005T_{ab} + d(2501 + 1.86T_{ab})$	kJ/kg
A	0.126	m^2
σ	5.67×10^{-8}	W/(m^2·°C^4)
ε_r	0.9	–
A_r	8.3	m^2
c_v	1.872	kJ/(kg·°C)
R_a	0.287	kJ/(kg·°C)
R_v	0.462	kJ/(mol·°C)

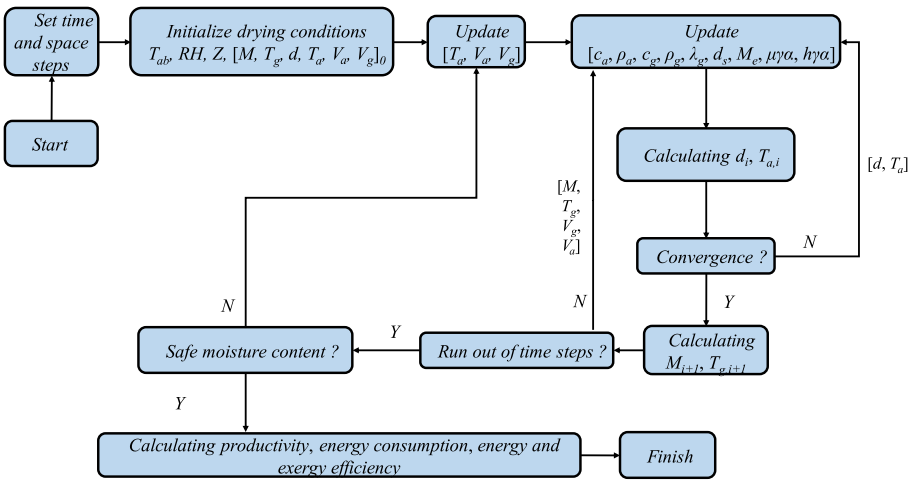

Fig. 7. Solving process based on the finite difference method.

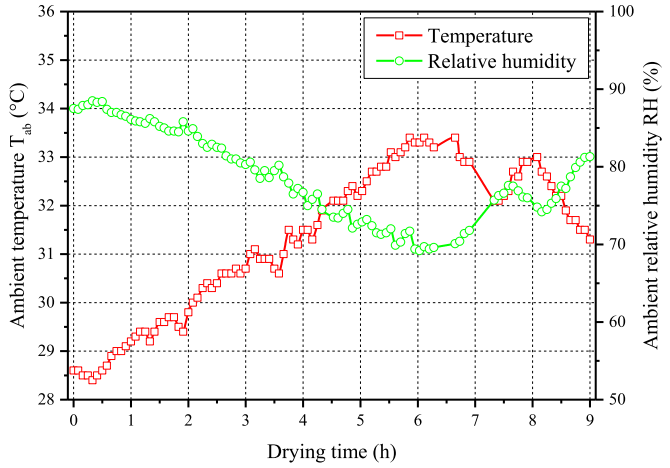

Fig. 8. Real-time temperature and relative humidity of ambient air.

Table 3
Simulation parameters.

Variable	Value	Unit
M_{saf}	0.145	g water/g wet matter
DR_{min}	0.01	g water/(g wet matter h)
$T_{a,in,min}$	60	°C
$T_{a,in,max}$	80	°C
$V_{a,in,min}$	0.56	m/s
$V_{a,in,max}$	0.83	m/s
$V_{g,in,min}$	1.5	m/h
$V_{g,in,max}$	3.5	m/h
k_1	0.02	°C/s
k_2	0.02	m/s^2
k_3	0.001	m/(h·s)
N_p	2	–
N_c	2	–
D_x	100	–
D_u	1	–

$$RAD = \frac{1}{N}\sum_{i=1}^{N}\left|\frac{x_m(i)-x_r(i)}{x_r(i)}\right| \tag{45}$$

$$MRD = \max\left(\left|\frac{x_m(i)-x_r(i)}{x_r(i)}\right|\right) \tag{46}$$

where x_m is the measurement value, x_r is the trajectory value, and N is the sampling point.

The 'fmincon' function, which is part of the MATLAB 2017b Optimization Toolbox, is employed to address optimization problems characterized by nonlinear constraints. The chosen optimization algorithm for this purpose is the interior point algorithm. The implementation of this process is executed on a laptop with Intel i5 CPU running at 3.2 GHz.

5.2. Optimization and analysis

5.2.1. Optimal input

Under the constraint imposed by objective function of Strategy 1, the input results computed by the optimization system are depicted in Fig. 9. Specifically, Fig. 9 (a) reveals that, initially during the drying process (≤3 h), the drying air temperature was predominantly maintained at a relatively low level of 60 °C. Conversely, for the majority of middle and later stages, the drying air temperature was elevated. The primary determinant of paddy drying was the interplay between water and dry matter, which decreased the partial pressure of water vapour at the water surface, subsequently reducing the free energy of water. This reduction in free energy was quantitatively equivalent to the binding energy required to remove 1 kg of water from the material [48]. Given

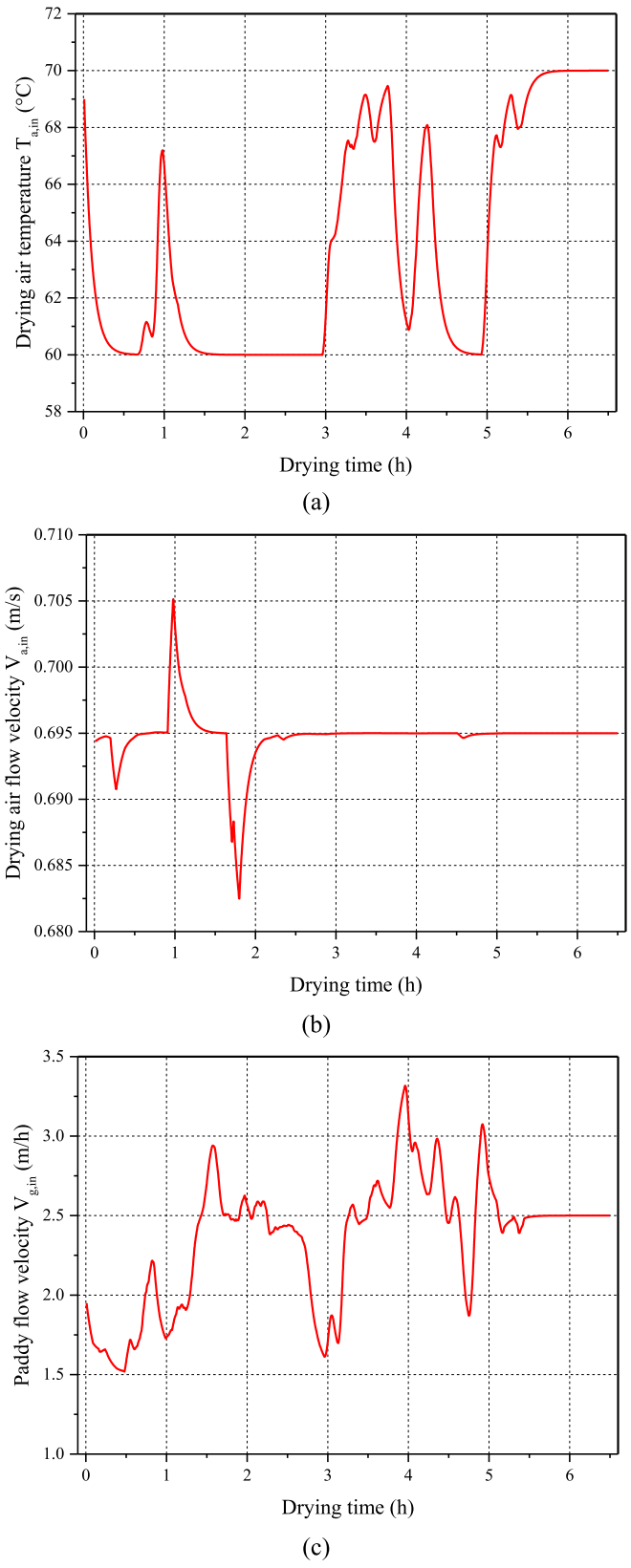

Fig. 9. Variation of input under Strategy 1: (a) Drying air temperature, (b) drying air flow velocity, and (c) paddy flow velocity.

that both depth of water migration and the proportion of removed adsorbed bound water increased as paddy moisture content decreased, the binding energy that needed to be overcome during the water migration process inevitably rose. Consequently, to guarantee a high drying rate, a slight increase in drying air temperature was observed during the later stage of drying (≥3.5 h). This finding also validated the accuracy of the variation curve of binding energy between dry matter and water during paddy the drying process, as calculated in our previous research [18].

Regarding the drying air flow velocity, except for minor fluctuations at specific points, it remained relatively constant at 0.69 m/s throughout the entire drying process. Related research [49] has indicated that the water vaporized within the drying system is transported by the flowing drying air, thereby maintaining the thermal and wet potential difference within the system. However, the constant drying air flow velocity, as constrained by the objective function of Strategy 1, suggests that, in comparison to the drying air temperature, the influence of drying air flow velocity on the drying process was not the primary factor governing transient energy consumption and drying rate. Fig. 9 (c) illustrates that the paddy flow velocity exhibited a pattern where the later stage (2.61 m/s) was greater than the early stage (2.13 m/s). In the later stage of drying, the rapid increase in paddy temperature led to a significantly large heat loss of heating paddy compared to the early stage, often accounting for more than 60 % of the total [50]. Therefore, to adhere to the low energy consumption constraint of Strategy 1, the heat loss of heating paddy was mitigated in this stage by augmenting the paddy flow velocity.

Under the constraints imposed by the objective functions of Strategy 2 and Strategy 3, the input results obtained through the optimization system are depicted in Figs. 10 and 11, respectively. To attain a superior energy/exergy efficiency throughout the drying process, the drying air temperature was promptly reduced from its preset initial value to the lowest level of 60 °C and maintained at this temperature throughout the entire drying duration. With regard to the drying air flow velocity, Strategy 2 and Strategy 3 exhibited a relatively similar trend overall. However, within the first 2.5 h of the drying range, the average drying air flow velocity of Strategy 3 (0.56 m/s) was observed to be lower than that of Strategy 2 (0.61 m/s). Sinha et al. [51], in their research on vibro fluid bed tea drying system, reported that exergy destruction of irreversibility comprised the largest proportion of the total in the early stage of drying. This was attributed to the rapid decrease in the thermal gradient between the drying air and the material surface. Consequently, during this initial stage, Strategy 3′ adoption of a lower drying air flow velocity in to gradually diminish the thermal gradient emerged as an effective approach to mitigate exergy loss and sustain a high level of exergy utilization in the drying process. This conclusion was further corroborated by Yu et al. [39] through their analysis of a hot air circulation convection carrot drying process.

5.2.2. *Drying kinetics*

Fig. 12 illustrates the real-time drying state of paddy at the discharging outlet throughout the drying process, under three distinct strategies. Fig. 12 (a) reveals that the moisture content of the paddy at the discharging outlet exhibited a fluctuating pattern in tandem with variations in input. Overall, a gradual decrease in moisture content was observed as the drying process progressed. This trend marked a notable departure from the real-time drying state observed under constant drying conditions, which exhibited a characteristic step-wise decline [45]. Fig. 12 (b) demonstrates that, due to the constraints imposed by the optimization function, the temperature of the paddy at the discharging outlet was significantly elevated under Strategy 1 compared to Strategy 2 and Strategy 3. Notably, this elevation was accompanied by pronounced fluctuations. During the mid-stage of the drying process, however, the temperatures of the paddy at the discharging outlet under Strategy 2 and Strategy 3 remained relatively stable, without significant fluctuations. Regarding drying efficiency, Strategy 1 achieved a drying

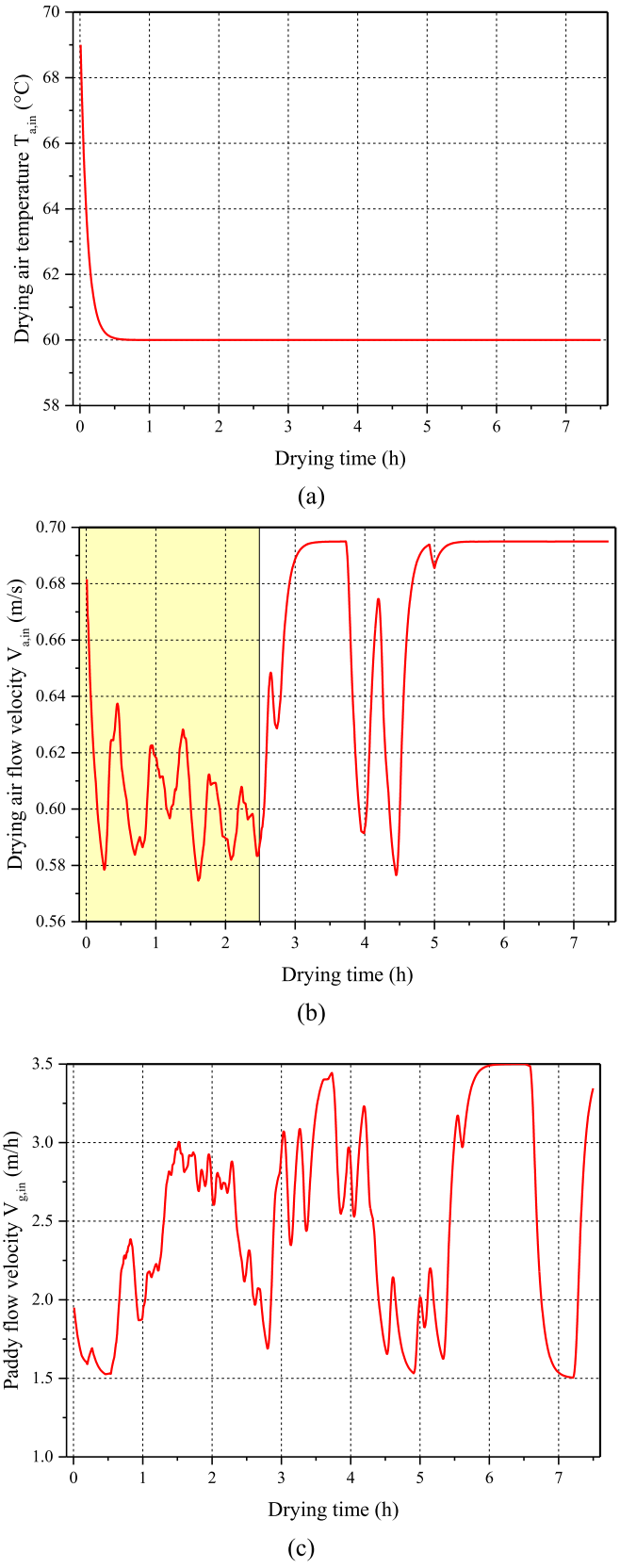

Fig. 10. Variation of input under Strategy 2: (a) Drying air temperature, (b) drying air flow velocity, and (c) paddy flow velocity.

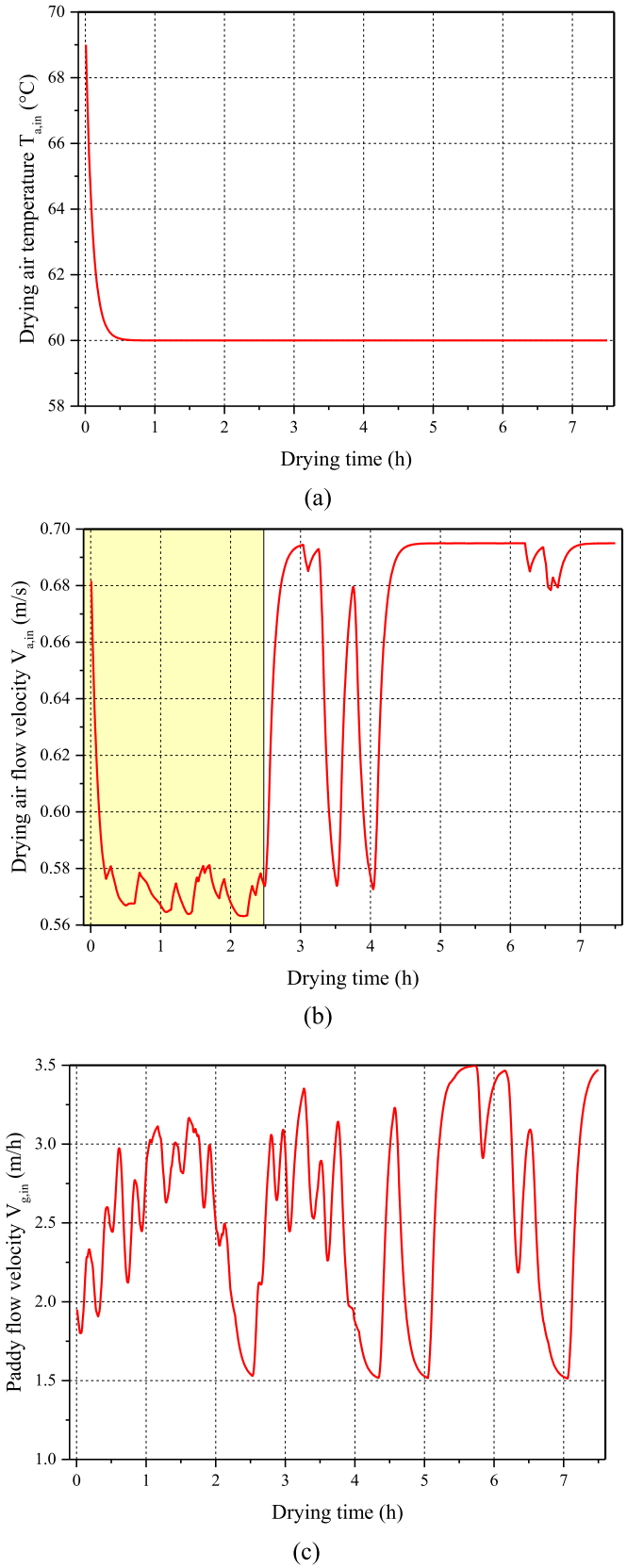

Fig. 11. Variation of input under Strategy 3: (a) Drying air temperature, (b) drying air flow velocity, and (c) paddy flow velocity.

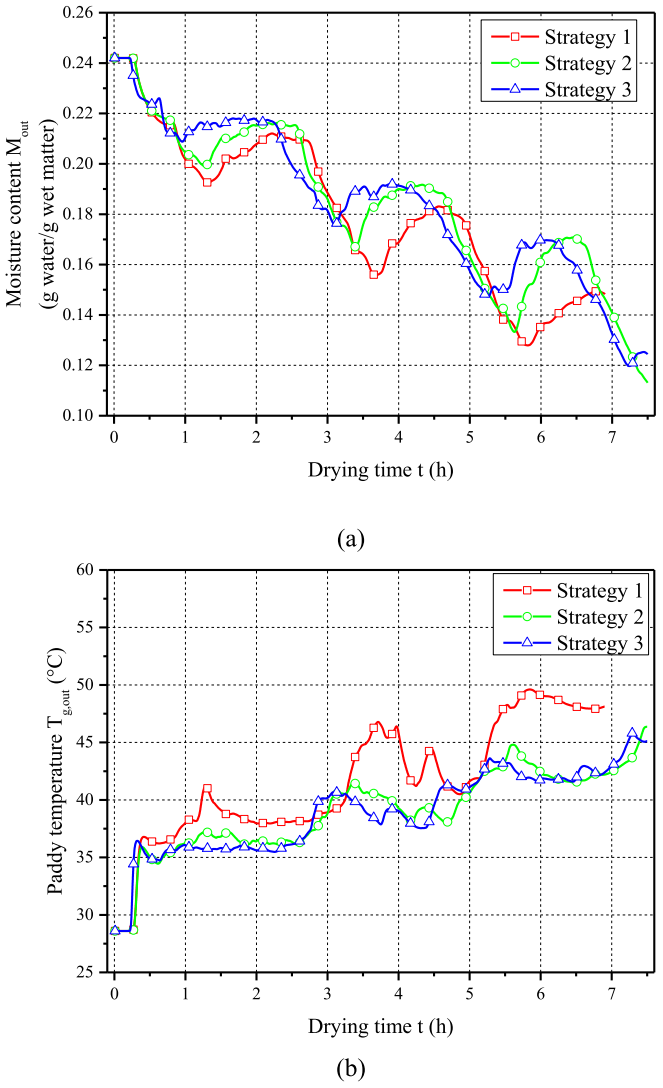

Fig. 12. Real-time drying state of paddy at discharging outlet under three strategies: (a) moisture content and (b) temperature.

time of 6.9 h, corresponding to a productivity of 1899.1 kg/h. Conversely, both Strategy 2 and Strategy 3 required a drying time of 7.5 h, with a productivity of 1747.2 kg/h.

Fig. 13 depicts the variations in the average moisture content and temperature of paddy under three distinct optimization strategies, along with the curves representing the glass transition and taste characteristics. Given the current equipment parameters and their corresponding drying conditions, and under the influence of state constraints, the drying kinetics curves obtained under all three strategies were positioned above the glass transition curve (indicating a rubber state). This finding suggests that the drying process did not traverse the glass transition phase. Based on the fissure formation mechanism in paddy kernels, which is rooted in the glass transition theory as proposed by Zhao et al. [31], when the state of the paddy remains unchanged during the drying process, the rate of additional fissuring can be effectively minimized. Furthermore, the drying kinetics curves obtained under all three strategies were situated within the safe taste area, well below the taste curve and far removed from the taste destruction zone. This observation indicates that the implementation of reasonable temperature control during the drying process can stabilize the paddy in an ideal taste state [32]. The results of the aforementioned analysis confirm the effective guarantee provided by the designed optimizer in terms of product quality.

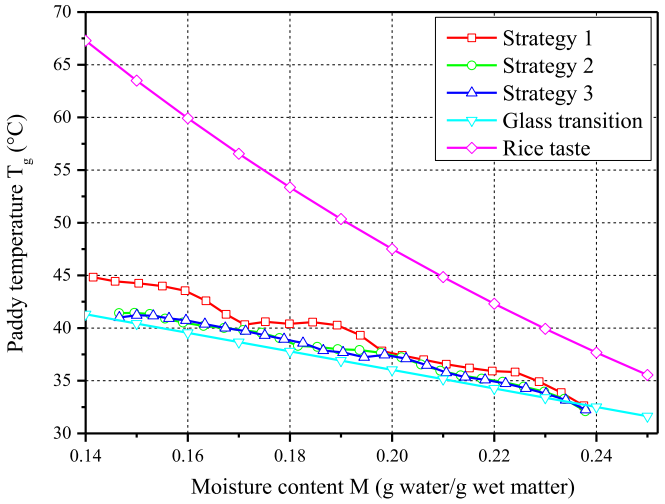

Fig. 13. Variations in average moisture content and temperature of paddy under three strategies.

5.2.3. Energy and exergy analysis

Fig. 14 presents the variation curves of transient energy and exergy efficiency during the drying process under three different optimization strategies. As illustrated in Fig. 14 (a), the transient energy efficiency exhibits a gradual downward trend as the drying process progresses. During the initial drying stage, the water evaporation from the paddy surface resembles the evaporation from a free water surface [52], facilitating the removal of water within the paddy kernel. Consequently, a significant amount of heat is effectively utilized during this phase, leading to decreased temperatures of both the discharged paddy and waste air, and consequently, reduced heat loss for both. However, as the drying process continues, the removal of water becomes increasingly challenging [48], resulting in a substantial amount of heat not being effectively utilized and instead being discharged from the drying system. Additionally, the heated paddy also transfers some heat externally, contributing to the gradual decline in transient energy efficiency. When compared to Strategy 2 and Strategy 3, which incorporated energy efficiency indicators, Strategy 1 exhibited significantly lower transient energy efficiency. The ranges of transient energy efficiency under the three strategies were 45.4%–67 %, 46.2%–71.1 %, and 49%–71.6 %, respectively. The average energy efficiencies were 58.2 %, 62.2 %, and 63.2 % for Strategy 1, Strategy 2, and Strategy 3, respectively. Similar trends in energy efficiency variations have also been observed in studies on the drying of pears [11], bananas [53], and tomato paste [54].

As for the exergy aspect, Fig. 14 (b) shows that the transient exergy efficiency for Strategy 1, Strategy 2, and Strategy 3 ranged from 24.7% to 42.2 %, 26.7%–45.8 %, and 28.3%–43 %, respectively. According to Equation (33), exergy efficiency is proportional to the water evaporation rate. During the initial drying stage, dehydration occurs without requiring substantial exergy, as less energy is needed to remove loosely bound water. As drying progresses, more exergy is consumed to overcome the increasing binding energy between water molecules and dry matter. In the final drying stage, removing tightly bound water becomes significantly more difficult, leading to a reduced dehydration rate and lower dehydration efficiency. Combined with the analysis of transient energy efficiency in the previous paragraph, we found that the binding energy between water and dry matter is the key internal factor determining efficient water removal and energy utilization. Drying air, in contrast, serves as an external factor that provides energy and facilitates the removal of water. The latent heat of vaporisation supplied to the paddy is ultimately converted into internal energy, highlighting the role of drying air as an external energy source. To gain a theoretical understanding of the complex interactions within the paddy drying system, it is essential to derive an analytical solution of the dynamic drying process

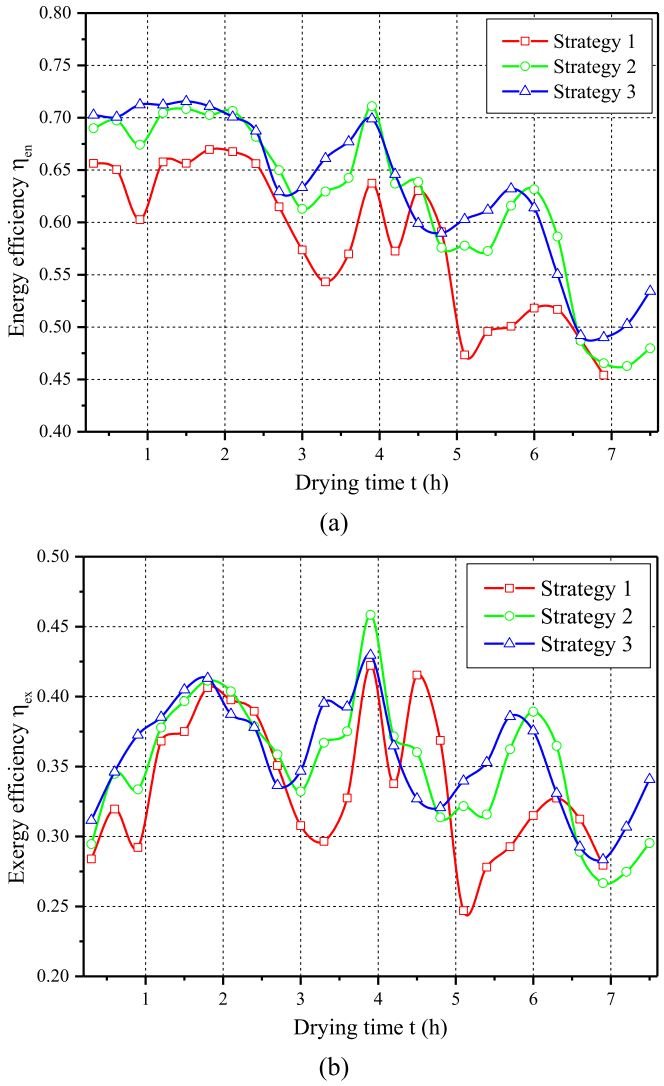

Fig. 14. Transient energy (a) and exergy (a) efficiency of paddy drying process under three strategies.

based on the energy properties driving material state changes. This approach offers a pathway to move beyond reliance on empirical transfer coefficients based on heat and mass transfer laws and enables process-adaptive control. Consistent with the results for energy efficiency, Strategy 3, which incorporates an exergy utilization indicator, achieved higher transient exergy efficiencies compared to Strategy 1 and Strategy 2. The average exergy efficiencies for the three strategies were 33.5 %, 35 %, and 35.7 %, respectively. Similar trends in exergy efficiency have been observed in the drying of tomato paste [54], corn [55], and carrots [56].

The primary distinction between Strategy 2 and Strategy 3 resides in their distinct handling of heat loss and exergy loss within their respective objective functions. Exergy signifies the utmost useful work attainable when a thermodynamic system undergoes reversible transformations from an arbitrary state to a state of equilibrium with its surroundings. By incorporating the exergy concept, we gain profound insights into energy losses within the drying system, the value of energy, and losses across diverse sectors. This concept acts as a holistic framework for optimizing energy utilization [57]. The outcomes of optimizing exergy consumption under Strategies 2 and 3 are delineated in Fig. 15. It is apparent that Strategy 3 achieves reductions in exergy losses associated with exhaust air, heating paddy, and irreversibility, when benchmarked against Strategy 2. Notably, the decrement in exergy loss of

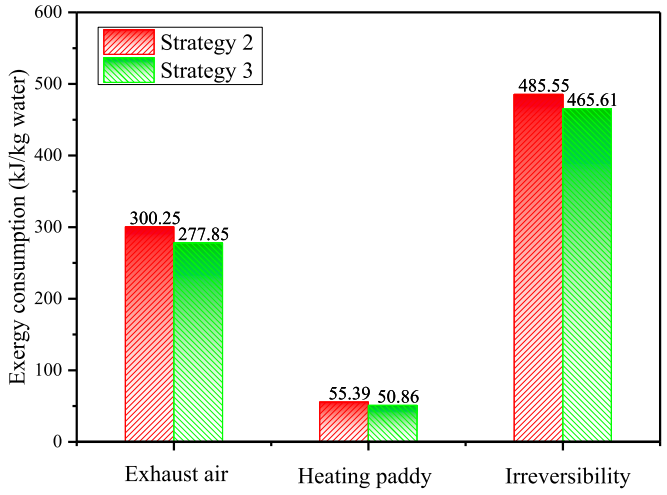

Fig. 15. Comparison of exergy consumption in each component of present paddy drying processes under Strategy 2 and Strategy 3.

exhaust air constitutes 47.8 % of the overall reduction, whereas exergy loss due to irreversibility comprises 42.5 %. These reductions are primarily attributed to the reduced drying airflow velocity during the initial drying phase in Strategy 3, as elaborated in Section 5.2.1. The decreased drying airflow velocity facilitates the moist paddy, which harbors higher moisture levels, to maximize the utilization of energy conveyed by the drying air, thereby minimizing heat loss in the exhaust [58]. Furthermore, the diminution in the thermal gradient contributes to a decrease in irreversibility-related exergy loss [51]. Hence, when compared to a focus solely on heat loss, an objective function that encompasses exergy loss not only optimizes energy utilization but also achieves a remarkable equilibrium between the heat and mass transfer characteristics of paddy drying. It considers both the direction and quality of optimizing energy usage during the drying process. Consequently, this approach possesses broader implications in terms of optimization and utilization, underscoring its significant value in enhancing the overall efficiency of the drying system.

The transient energy consumption rate variation curves for three distinct strategies are depicted in Fig. 16. Despite all three optimization strategies effectively constraining transient energy consumption, Strategy 1 failed to constrain energy utilization efficiency, leading to a faster drying process (approximately 0.6 h quicker than Strategy 2 and Strategy 3). Consequently, the transient energy consumption rate of Strategy 1 remained significantly higher than Strategy 2 and Strategy 3 throughout the entire drying process. The average energy consumption rates for the three strategies were 408.7 kW, 333.9 kW, and 328.6 kW, respectively. Table 4 presents a comparative analysis of energetic performance under various optimization strategies. Notably, the strategy presented in the last row of the table was previously proposed in our research [18] and is referred to as the 'static ventilation strategy'. In comparison to the static ventilation strategy, Strategy 1, Strategy 2, and Strategy 3 in this study achieved energy consumption reductions of 0.2 %, 11.4 %, and 12.8 %, respectively. Additionally, significant improvements were observed in energy efficiency, exergy efficiency, and energy consumption rate. Furthermore, Strategy 3 reduced total energy consumption by 12.6 % and 1.6 % compared to Strategy 1 and Strategy 2, respectively. By comparing the energy optimization results under the different strategies and considering the aforementioned analysis of productivity and quality characteristics, it can be conclusively stated that the input corresponding to Strategy 3 was the optimal strategy.

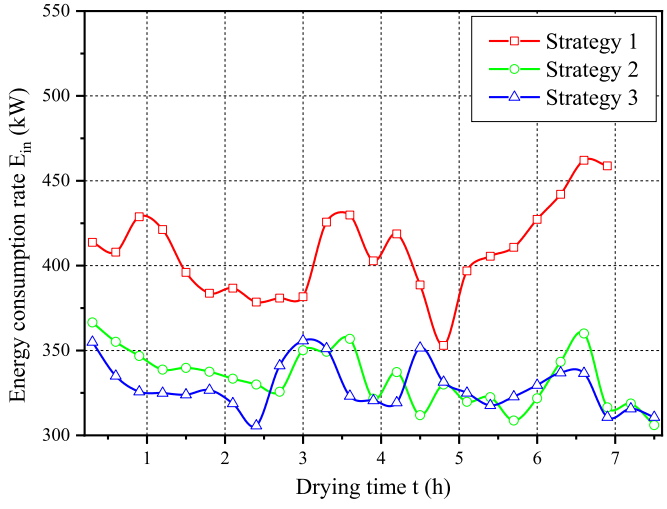

Fig. 16. Transient energy consumption rate of paddy drying process under three strategies.

To elucidate the exergy utilization characteristics of the paddy drying process under the optimal strategy and to examine the exergy losses and destruction in each critical section, a Sankey diagram depicting the exergy components of the paddy drying process under Strategy 3 is presented in Fig. 17. When considering the ambient state as the reference point, Fig. 17 reveals that a total exergy rate of 95.13 kW was supplied to the drying system. Among this, 33.97 kW was effectively utilized for water removal. The remaining portions included an exergy utilization rate of 21.44 kW in the exhaust air, 3.8 kW for heating the paddy, and 35.95 kW due to irreversibility. To quantify the exergy utilization level of the drying system, the dimensionless exergy destruction of irreversibility ($N_{ex,ir}$) was calculated. The results indicated that $N_{ex,ir}$ in Strategy 3 was 1.06. This value, along with the reasonable exergy utilization level index, further validates the effectiveness of the proposed optimization strategy and underscores the beneficial energy utilization performance of the dryer.

5.3. Control results and analysis

In this section, we examine the capability of the proposed hierarchical MPC system to manage disturbances and track the reference trajectory. For the first-level optimizer, Strategy 3 is selected. To emulate the abnormal drying conditions that may arise due to model mismatches or unforeseen disturbances during the actual drying process, disturbances with maximum fluctuation rates of ±60 %, ±80 %, and ±100 % are randomly introduced to the moisture content and temperature of the paddy at the discharging outlet of the 5HP-20 dryer. In the presence of these disturbances, the moisture content of the paddy at the discharging outlet of the dryer typically exhibits irregular high-frequency fluctuations during its decline. Consequently, paddy drying without a corrective strategy will inevitably deviate from the ideal drying state, resulting in a diminished energy utilization level and decreased uniformity in moisture content distribution.

Fig. 18 presents statistical data on the computation time for each optimization step of the first-level optimizer and the second-level MPC. Overall, it is evident that the first-level optimizer, which incorporates both the drying mathematical model and the energetic model, exhibits a longer computation time (with an average of 3.69 s) compared to the second-level MPC, which solely considers the drying mathematical

Table 4
Comparison of energetic performance under different optimization strategies.

	η_{en}	η_{ex}	E_{in} (kW)	E_{tot} (MJ)
Strategy 1	58.2 %	33.5 %	408.7	8871.55
Strategy 2	62.2 %	35 %	333.9	9015.05
Strategy 3	**63.2 %**	**35.7 %**	**328.6**	**10152.63**
Static ventilation strategy	54.3 %	32.8	471.1	10174.68

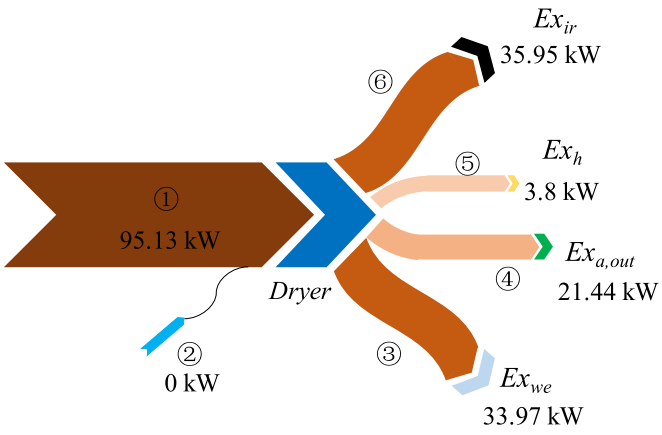

Fig. 17. Sankey diagram depicting the exergy flowing through paddy drying process in Strategy 3.

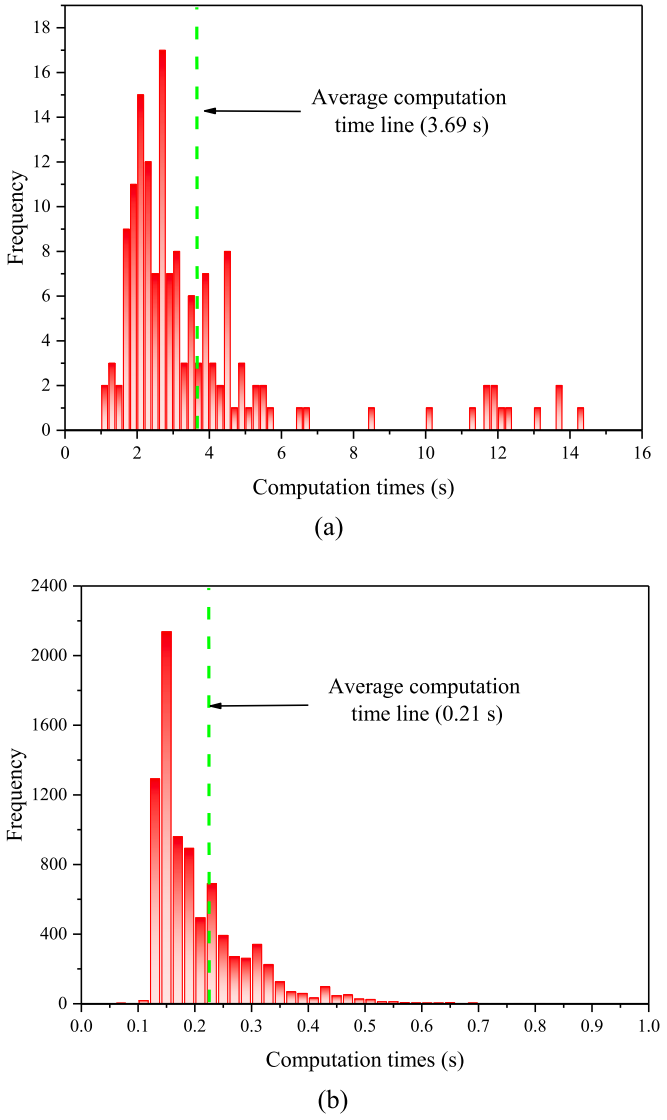

Fig. 18. Statistics for the computation times of first-level optimizer (a) and second-level MPC (b).

model and has an average computation time of 0.21 s. Notably, the sampling period in this study is 2.25 s. For the first-level optimizer, over 72 % of the total optimization steps have computation times exceeding 2.25 s, with the maximum computation time reaching over 14 s in our experiments. Therefore, setting a sufficiently low control frequency for the first-level optimizer (every 180 s in this study) ensures that computations can be completed appropriately within each period while satisfying the ambient conditions. Regarding the second-level MPC, all computation times are below 1 s (less than the 2.25-s sampling period). Consequently, the set frequency of every 2.25 s for the second-level MPC is sufficient to complete each optimization process and provides ample time to address any high time-consuming situations that may arise. The above discussions affirm the rationale behind our two-level hierarchical MPC approach, which balances computational efficiency and control precision to optimize the paddy drying process.

Fig. 19 (a) illustrates the tracking performance of hierarchical MPC system compared to the reference trajectory under ±60 % disturbances. As described in Section 4.1, the reference trajectory is obtained by applying $\mathbf{u}_{ref}$, determined by the first level optimizer, to the disturbance-free drying mathematical model. Conversely, the feedforward control trajectory is generated by directly applying $\mathbf{u}_{ref}$ to the drying system in the presence of disturbances. Lastly, the hierarchical MPC trajectory is obtained by applying the second-level control input ($\mathbf{u}$) to the drying

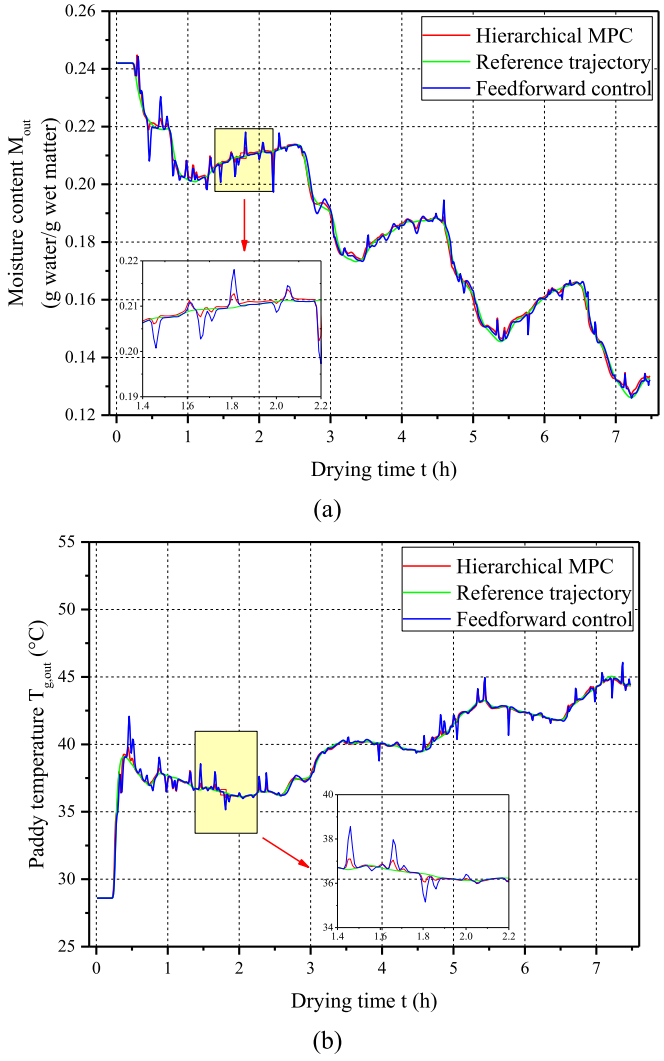

Fig. 19. Comparison of feedforward control and hierarchical MPC under ±60 % disturbances: (a) moisture content and (b) temperature of paddy at discharging outlet of dryer.

system under the same disturbed conditions.

For the reference trajectory, the moisture content of paddy at discharging outlet showed a stable declining trend. While the moisture content curve under the feedforward control system generally followed the reference trajectory, it displayed significant high-frequency fluctuations throughout the drying process, deviating from the ideal drying state. In contrast, the moisture content curve under the hierarchical MPC system closely aligned with the reference trajectory and was less affected by the disturbances. Fig. 19 (b) shows the temperature curves of paddy at discharging outlet. Like moisture content curves, the temperature curve adjusted by hierarchical MPC showed strong consistency with the reference trajectory, outperforming the feedforward control in accuracy and stability. Comparable results were also observed under ±80 % and ±100 % disturbances, as illustrated in Fig. S2 and Fig. S3 in the Supplementary materials C.

The quantitative results of tracking performance for both feedforward control and hierarchical MPC under various disturbances are presented in Table 5. Considering the moisture content of paddy at the discharging outlet as an illustrative example, when the system disturbances exhibited maximum fluctuation rates of ±60 %, ±80 %, and ±100 %, respectively, the RAD under hierarchical MPC was 0.70 %, 0.79 %, and 0.81 %, respectively. In comparison, the RAD values under feedforward control were 0.72 %, 0.93 %, and 1.008 %, respectively, indicating a reduction in RAD by 2.78 % (approximately 1.58 percentage points), 15.67 %, and 19.52 % when employing hierarchical MPC. For the MRD, hierarchical MPC achieved reductions of 18.60 % (from 6.66 % to 5.42 %), 36.49 % (from 11.57 % to 7.35 %), and 39.12 % (from 13.11 % to 7.98 %) across the respective disturbance levels. Similarly, the control effect of hierarchical MPC on paddy temperature exhibited comparable results, suggesting that the hierarchical MPC system demonstrated superior tracking performance compared to feedforward control. These findings underscore the efficacy of the hierarchical MPC approach in enhancing the tracking performance of the paddy drying process.

Table 5
Quantitative results of hierarchical MPC's tracking performance for ideal states.

	Feedforward control		MPC	
	RAD	MRD	RAD	MRD
M_{60}(%)	0.72 %	6.66 %	0.70 %	5.42 %
Tg_{60}(%)	0.51 %	8.44 %	0.34 %	5.92 %
M_{80}(%)	0.93 %	11.57 %	0.79 %	7.35 %
Tg_{80}(%)	0.67 %	9.66 %	0.40 %	8.28 %
M_{100}(%)	1.01 %	13.11 %	0.81 %	7.98 %
Tg_{100}(%)	0.84 %	33.66 %	0.38 %	7.86 %

The subscripts '60′, '80′, and '100′ in this table indicate that the corresponding values represent the results obtained under system disturbances with maximum fluctuation rates of ±60 %, ±80 %, and ±100 %, respectively.

6. Conclusions

In this study, we conducted a comprehensive analysis of energy consumption optimization and control in an industrial-scale circulation counter-flow paddy drying process operating under randomly fluctuating ambient conditions. This analysis was facilitated through system identification, numerical simulation, theoretical analysis, and structural design. The key findings of this study are summarized as follows.

(1) The primary factor influencing paddy drying was identified as the binding energy between water and dry matter. As the drying process progressed and moisture content decreased, the binding energy that needed to be overcome during water migration gradually increased. To maintain the drying rate, increasing the drying air temperature in the later stages was found to be beneficial. In contrast, the drying air flow velocity was not a dominant factor in transient energy consumption or drying rate.
(2) Under three different optimization strategies, the real-time moisture content of paddy at the discharging outlet exhibited fluctuating increases, while the temperature displayed declining trends. The corresponding drying kinetics curves were consistently positioned above the glass transition curve and below the safety taste curve, confirming the effectiveness of the proposed optimization strategies in ensuring product quality.
(3) The transient exergy efficiency varied within ranges of 24.7%–42.2 %, 26.7%–45.8 %, and 28.3%–43 % under the three optimization strategies, respectively. When compared to the traditional artificial two-stage drying strategy, Strategy 1, and Strategy 2, Strategy 3 reduced total energy consumption by 12.8 %, 12.6 %, and 1.6 %, respectively. Notably, the $N_{ex,ir}$ for Strategy 3 was 1.06, further validating the effectiveness of this optimization strategy in rationalizing energy consumption.
(4) When system disturbances were subjected to maximum fluctuation rates of ±60 %, ±80 %, and ±100 %, the RAD of paddy moisture content between the hierarchical MPC system and the reference trajectory was 0.70 %, 0.79 %, and 0.81 %, respectively. These values represented reductions of 1.58 %, 15.67 %, and 19.52 % compared to feedforward control, indicating the superior tracking performance of the proposed hierarchical MPC system.

Above results demonstrate the enhanced energy-saving and disturbance-suppression capabilities of our proposed hierarchical MPC strategy. In future research endeavors, the emphasis will be placed on augmenting the hardware capabilities of the control system for industrial-scale circulation counter-flow paddy dryers, thereby facilitating the practical deployment of the hierarchical MPC strategy in real-world applications. Furthermore, the deployment of the controller introduced in this study onto multistage counterflow drying systems presents considerable promise and warrants further exploration.

CRediT authorship contribution statement

Chengjie Li: Writing – original draft, Validation, Software, Methodology, Investigation, Funding acquisition, Data curation. **Jiayang Ren:** Writing – original draft, Validation, Software, Methodology, Investigation. **Arpan Seth:** Writing – review & editing, Validation, Methodology, Investigation. **Ye Zhang:** Validation, Software, Data curation. **Jianjiang Huang:** Validation, Software, Data curation. **Changyou Li:** Resources, Funding acquisition, Conceptualization. **Yankai Cao:** Writing – review & editing, Validation, Supervision, Methodology, Investigation.

Declaration of competing interest

The authors declare that they have no known competing financial interests or personal relationships that could have appeared to influence the work reported in this paper.

Acknowledgments

This work was supported by the National Natural Science Foundation of China (No.32401725 and No.32171906), the Guangzhou Science and Technology Plan Project (No.2024A04J3960), and Specific University Discipline Construction Project (No.2023B10564002).

Appendix. ASupplementary data

Supplementary data to this article can be found online at https://doi.org/10.1016/j.energy.2025.135431.

Data availability

Data will be made available on request.

References

[1] Chokphoemphun S, Hongkong S, Chokphoemphun S. Artificial neural network for drying behavior prediction of paddy in developed chamber fluidized–bed dryer. Comput Electron Agric 2024;220:108888. https://doi.org/10.1016/j.compag.2024.108888.

[2] Jin Z, Yue R, Ma Z, Cheng S, Khan MN, Nie L. Effect of water and nitrogen coupling on energy balance and production efficiency in rice production. Energy 2024;288:129739. https://doi.org/10.1016/j.energy.2023.129739.

[3] Guan X, Wang Y, Li M, Li A, Zhou X, Yang J, Liang Z. Research on the performance of heat pump drying system with rock thermal energy storage. Energy 2025:134510. https://doi.org/10.1016/j.energy.2025.134510.

[4] Mondal MHT, Sarker MSH. Comprehensive energy analysis and environmental sustainability of industrial grain drying. Renew Sustain Energy Rev 2024;199:114442. https://doi.org/10.1016/j.rser.2024.114442.

[5] César LVE, Lilia CMA, Octavio GV, Orlando SS, Alfredo DN. Energy and exergy analyses of a mixed-mode solar dryer of pear slices (Pyrus communis L). Energy 2021;220:119740. https://doi.org/10.1016/j.energy.2020.119740.

[6] Nejad AM. A new drying approach deploying solid-solid phase change material: a numerical study. Energy 2021;232:120990. https://doi.org/10.1016/j.energy.2021.120990.

[7] Arias DM, García-Valladares O, Besagni G, Markides CN. A vision of renewable thermal technologies for drying, biofuels production and industrial waste, gas or water recovery. Appl Therm Eng 2023;223:120022. https://doi.org/10.1016/j.applthermaleng.2023.120022.

[8] Ren L, Zheng Z, Fu H, Yang P, Xu J, Yang D. Hot air–assisted radio frequency drying of corn kernels: the effect on structure and functionality properties of corn starch. Int J Biol Macromol 2024;267:131470. https://doi.org/10.1016/j.ijbiomac.2024.131470.

[9] Yahya M, Fahmi H, Hasibuan R, Fudholi A. Development of hybrid solar-assisted heat pump dryer for drying paddy. Case Stud Therm Eng 2023;45:102936. https://doi.org/10.1016/j.csite.2023.102936.

[10] Okeyo AA, Luthra K, Vazquez AR, Atungulu GG. Quality characteristic of instant rice produced using microwave-assisted hot air drying. Cereal Chem 2024;101(3):641–53. https://doi.org/10.1002/cche.10770.

[11] Li K, Zhang Y, Wang YF, El-Kolaly W, Gao M, Sun W, Li M. Effects of drying variables on the characteristic of the hot air drying for gastrodia elata: experiments and multi-variable model. Energy 2021;222:119982. https://doi.org/10.1016/j.energy.2021.119982.

[12] Panda BK, Mishra G, Panigrahi SS, Shrivastava SL. Microwave-assisted parboiling of high moisture paddy: a comparative study based on energy utilization, process economy and grain quality with conventional parboiling. Energy 2021;26:121011. https://doi.org/10.1016/j.energy.2021.121011.

[13] Singh P, Mahanta P, Kalita P. Experimental investigation of paddy drying characteristics in a slitless rotary fluidized-bed dryer. Dry Technol 2022;40(15):3262–72. https://doi.org/10.1080/07373937.2021.2018700.

[14] Wincy WB, Edwin M. Experimental energy, exergy, and exergoeconomic (3E) analysis of biomass gasifier operated paddy dryer in parboiling industry. Biomass Convers Bior 2022. https://doi.org/10.1007/s13399-021-02156-8.

[15] Zhang LZ, Jiang L, Xu ZC, Zhang XJ, Fan YB, Adnouni M, Zhang CB. Optimization of a variable-temperature heat pump drying process of shiitake mushrooms using response surface methodology. Renew Energy 2022;198:1267–78. https://doi.org/10.1016/j.renene.2022.08.094.

[16] Sami S, Deymi-Dashtebayaz M, Gholizadeh M, Khutornaya J, Sergienko O. Potential of an internal combustion engine as an energy supplier for the drying process: a thermo-economic analysis with multi-objective optimization. Energy 2024;291:130429. https://doi.org/10.1016/j.energy.2024.130429.

[17] Das HJ, Saikia R, Mahanta P. Thermo-economic assessment of bubbling fluidized bed paddy dryers. Energy 2023;263:125668. https://doi.org/10.1016/j.energy.2022.125668.

[18] Li C, Chen Y, Zhang X, Mozafari G, Fang Z, Cao Y, Li C. Exergy analysis and optimization of an industrial-scale circulation counter-flow paddy drying process. Energy 2022;251:123901. https://doi.org/10.1016/j.energy.2022.123901.

[19] Choi Y, Chen Y, Ozaki A, Lee H, Arima Y. Advancing sustainable laundry practices utilizing waste heat from commercial laundry facilities. Appl Therm Eng 2024;247:123136. https://doi.org/10.1016/j.applthermaleng.2024.123136.

[20] Khan MIH, Sablani SS, Joardder MUH, Karim MA. Application of machine learning-based approach in food drying: opportunities and challenges. Dry Technol 2022;40(6):1051–67. https://doi.org/10.1080/07373937.2020.1853152.

[21] Khan MIH, Sablani SS, Nayak R, Gu Y. Machine learning-based modeling in food processing applications: state of the art. Compr Rev Food Sci F 2022;21(2):1409–38. https://doi.org/10.1111/1541-4337.12912.

[22] Song Q, Wei X, Sun W, Li D. Model predictive control strategy of head rice yield in paddy rice intermittent drying. Dry Technol 2022;40(14):2941–51. https://doi.org/10.1080/07373937.2021.1979032.

[23] Bottari A, Braccia L. Optimal control structure selection based on economics for continuous cross-flow grain dryer. Dry Technol 2023;41(10):1605–19. https://doi.org/10.1080/07373937.2021.1979032.

[24] Zhang Y, Fang Z, Li C, Li C. Deep-Learning-based model predictive control of an industrial-scale multistate counter-flow paddy drying process. Foods 2023;13(1):43. https://doi.org/10.3390/foods13010043.

[25] Lin D, Dong Y, Ren Z, Zhang L, Fan Y. Hierarchical optimization for the energy management of a greenhouse integrated with grid-tied photovoltaic–battery systems. Appl Energy 2024;374:124006. https://doi.org/10.1016/j.apenergy.2024.124006.

[26] Wei Z, Song R, Ji D, Wang Y, Pan F. Hierarchical thermal management for PEM fuel cell with machine learning approach. Appl Therm Eng 2024;236:121544. https://doi.org/10.1016/j.applthermaleng.2023.121544.

[27] Gao H, Zhang X, Zeng X, Yang D, Song D, Zhou L. Predictive cruise control for hybrid electric vehicles based on hierarchical convex optimization. Energy Convers Manag 2024;299:117883. https://doi.org/10.1016/j.enconman.2023.117883.

[28] Chen K, Zuo Y, Li H, Qi C, Liu H, Ben Z. Design and experiment of heat pump low-temperature circulating grain dryer control system. Trans Chin Soc Agric Mach 2021;52(5):316–23. https://doi.org/10.6041/j.issn.1000-1298.2021.05.035.

[29] Luo H, Li C, Zhang Y. Design and experimental study of 5HP-25 type grain dryer. Trans Chin Soc Agric Mach 2021;37(1):279–89. https://doi.org/10.11975/j.issn.1002-6819.2021.01.033.

[30] Akhtaruzzaman M, Mondal MHT, Sarker MSH, Biswas M, Shanta SA, Sheikh MAM. Evaluation of drying characteristics, energy consumption and quality of parboiled paddy: two stage drying. J Agr Food R 2022;8:100284. https://doi.org/10.1016/j.jafr.2022.100284.

[31] Zhao L, Yang J, Wang S, Wu Z. Investigation of glass transition behavior in a rice kernel drying process by mathematical modeling. Dry Technol 2020;38(8):1092–105. https://doi.org/10.1080/07373937.2019.1612427.

[32] Zheng X, Zhao X, Chen L. Effect of drying conditions of paddy on rice taste & quality. Trans Chin Soc Agric Eng 2000;16(4):126–8. https://doi.org/10.3321/j.issn.1002-6819.2000.04.033.

[33] Fang Z, Li C, Zhao Y. Transient mathematical modeling of circulation counter-flow rice drying system. Trans Chin Soc Agric Eng 2019;35(23):286–95. https://doi.org/10.11975/j.issn.1002-6819.2019.23.035.

[34] Mugi VR, Chandramohan VP. Energy, exergy, economic and environmental (4E) analysis of passive and active-modes indirect type solar dryers while drying guava slices. Sustain Energy Techn 2022;52:102250. https://doi.org/10.1016/j.seta.2022.102250.

[35] Tunçkal C, Direk M, Doymaz İ, Göksel Z, Atak A. Drying kinetics and energy-exergy analysis of an experimental heat pump dryer utilized horseshoe heat recovery heat pipes for drying different grapes. Therm Sci Eng Prog 2022;36:101487. https://doi.org/10.1016/j.tsep.2022.101487.

[36] Li C. Engineering thermodynamics and heat transfer. Beijing: China Agricultural University Press; 2012.

[37] Beigi M, Tohidi M, Torki-Harchegani M. Exergetic analysis of deep-bed drying of rough rice in a convective dryer. Energy 2017;140:374–82. https://doi.org/10.1016/j.energy.2017.08.100.

[38] Mellalou A, Riad W, Bacaoui A, Outzourhit A. Impact of the greenhouse drying modes of two-phase olive pomace on the energy, exergy, economic and environmental (4E) performance indicators. Renew Energy 2023;210:229–50. https://doi.org/10.1016/j.renene.2023.04.074.

[39] Yu X, Zielinska M, Ju H, Mujumdar AS, Duan X, Gao Z, Xiao H. Multistage relative humidity control strategy enhances energy and exergy efficiency of convective drying of carrot cubes. Int J Heat Mass Tran 2020:119231. https://doi.org/10.1016/j.ijheatmasstransfer.2019.119231. 149.

[40] Yildirim N, Genc S. Energy and exergy analysis of a milk powder production system. Energy Convers Manag 2017;149:698–705. https://doi.org/10.1016/j.enconman.2017.01.064.

[41] Dolgun GK, Aktaş M, Dolgun EC. Infrared convective drying of walnut with energy-exergy perspective. J Food Eng 2021;306:110638. https://doi.org/10.1016/j.jfoodeng.2021.110638.

[42] Aziz M, Oda T, Kashiwagi T. Enhanced high energy efficient steam drying of algae. Appl Energy 2013;109:163–70. https://doi.org/10.1016/j.apenergy.2013.04.004.

[43] Nazghelichi T, Kianmehr MH, Aghbashlo M. Thermodynamic analysis of fluidized bed drying of carrot cubes. Energy 2010;35(12):4679–84. https://doi.org/10.1016/j.energy.2010.09.036.

[44] Fudholi A, Sopian K, Bakhtyar B, Gabbasa M, Othman MY, Ruslan MH. Review of solar drying systems with air based solar collectors in Malaysia. Renew Sustain Energy Rev 2015;51:1191–204. https://doi.org/10.1016/j.rser.2015.07.026.

[45] Li C, Fang Z, Zhong J, Li B, Li C. Evaluating the dynamic characteristics and energetic performance of a paddy multistage counter-flow dryer. Biosyst Eng 2022;221:208–23. https://doi.org/10.1016/j.biosystemseng.2022.07.003.

[46] Li C, Zhang X, Meng M, Li B, Li C. Capacitive online corn moisture content sensor considering porosity distributions: modeling, design, and experiments. Appl Sci-basel 2021;11(16):7655. https://doi.org/10.3390/app11167655.

[47] Motohashi K, Hosokawa A. An application of forced air drying theory to the deep bed drying of rough rice (I). J Jap Soc Agri Mach 1979;40(4):557–64. https://doi.org/10.11357/jsam1937.40.557.

[48] Li C, Mai Z, Fang Z. Analytical study of grain moisture binding energy and hot air drying dynamics. Trans Chin Soc Agric Eng 2014;30(7):236–42. https://10.3969/j.issn.1002-6819.2014.07.028.

[49] Dorneles LDNS, Goneli ALD, Cardoso CAL, da Silva CB, Hauth MR, Oba GC, Schoeninger V. Effect of air temperature and velocity on drying kinetics and essential oil composition of Piper umbellatum L. leaves. Ind Crop Prod 2019;142:111846. https://doi.org/10.1016/j.indcrop.2019.111846.

[50] Li T, Li C, Li B, Li C, Fang Z, Zeng Z, Ou W, Huang J. Characteristic analysis of heat loss in multistage counter-flow paddy drying process. Energy Rep 2020;6:2153–66. https://doi.org/10.1016/j.egyr.2020.08.006.

[51] Sinha A, Gupta R, Pandey KM, Dey SK. Exergy analysis of coal fired tea drying furnace. Int J Exergy 2015;17(1):54–73. https://doi.org/10.1504/IJEX.2015.069318.
[52] Li C. Characteristic functions of drying material system and its theoretical solution. Trans Chin Soc Agric Eng 2020;36(12):286–95. https://doi.org/10.11975/j.issn.1002-6819.2020.12.034.
[53] Singh A, Sarkar J, Sahoo RR. Experimental energy, exergy, economic and exergoeconomic analyses of batch-type solar-assisted heat pump dryer. Renew Energy 2020;156:1107–16. https://doi.org/10.1016/j.renene.2020.04.100.
[54] Hadibi T, Boubekri A, Mennouche D, Benhamza A, Kumar A, Bensaci C, Xiao HW. Effect of ventilated solar-geothermal drying on 3E (exergy, energy, and economic analysis), and quality attributes of tomato paste. Energy 2021;26:122764. https://doi.org/10.1016/j.energy.2021.122764.
[55] Li C, Li B, Huang J, Li C. Energy and exergy analyses of a combined infrared radiation-counterflow circulation (IRCC) corn dryer. Appl Sci-basel 2020;10(18):6289. https://doi.org/10.3390/app10186289.
[56] Aktaş M, Khanlari A, Amini A, Şevik S. Performance analysis of heat pump and infrared–heat pump drying of grated carrot using energy-exergy methodology. Energy Convers Manag 2017;132:327–38. https://doi.org/10.1016/j.enconman.2016.11.027.
[57] Liu Z, Quan Z, Zhang N, Wang Y, Yang M, Zhao Y. Energy and exergy analysis of a novel direct-expansion ice thermal storage system based on three-fluid heat exchanger module. Appl Energy 2023;330:120371. https://doi.org/10.1016/j.apenergy.2022.120371.
[58] Kosasih EA, Zikri A, Dzaky MI. Effects of drying temperature, airflow, and cut segment on drying rate and activation energy of elephant cassava. Case Stud Therm Eng 2020;19:100633. https://doi.org/10.1016/j.csite.2020.100633.

foods

MDPI

Article

Deep-Learning-Based Model Predictive Control of an Industrial-Scale Multistate Counter-Flow Paddy Drying Process

Ye Zhang [1], Zhuangdong Fang [2], Changyou Li [1] and Chengjie Li [1,*]

[1] College of Engineering, South China Agricultural University, Guangzhou 510642, China; zhangye@scau.edu.cn (Y.Z.); lichyx@scau.edu.cn (C.L.)
[2] Shanwei Academy of Agricultural Sciences, Shanwei 516600, China; zhuangdongfang@outlook.com
* Correspondence: chengjie.li@scau.edu.cn; Tel.: +86-020-85280817

Abstract: In practical industrial-scale paddy drying production, manual empirical operation is still widely used for process control. This often leads to poor uniformity in the moisture content distribution of discharged grains, affecting product quality. Model Predictive Control (MPC) is considered the most effective control method for paddy drying, but its implementation in industrial-scale drying is hindered by its high computational cost. This study aims to address this challenge by proposing a deep-learning-based model predictive control (DL-MPC) strategy for paddy drying. By establishing a mapping relation between the inlet and outlet paddy moisture content and paddy flow velocity, a DL-MPC strategy suitable for multistage counter-flow paddy drying systems is proposed. DL-MPC systems are developed using long short-term memory (LSTM) neural networks and trained using datasets from single-drying-stage and multistage drying systems. Simulation and analysis are conducted, followed by verification experiments on a 5HNH-15 multistage counter-flow paddy dryer. The results show that the DL-MPC system significantly improves computational speed while achieving satisfactory control performance. The predicted paddy flow velocity exhibits a smooth variation and matches field data obtained from multiple transition points, confirming the effectiveness of the designed DL-MPC system. The mean absolute error between the predicted and actual paddy moisture content under the DL-MPC system is 0.190% d.b., further supporting the effectiveness of the control system.

Keywords: paddy drying; industrial-scale drying; model predictive control; computational cost; deep-learning

Citation: Zhang, Y.; Fang, Z.; Li, C.; Li, C. Deep-Learning-Based Model Predictive Control of an Industrial-Scale Multistate Counter-Flow Paddy Drying Process. *Foods* **2024**, *13*, 43. https://doi.org/10.3390/foods13010043

Academic Editor: J. A. Cárcel

Received: 15 November 2023
Revised: 17 December 2023
Accepted: 20 December 2023
Published: 21 December 2023

1. Introduction

China, as a major grain-producing country, primarily focuses on paddy cultivation [1]. In 2022, national paddy production reached 208.49 million tons [2]. The drying process is crucial for post-harvest paddy processing. However, each year in China, approximately 21 billion kilograms of grains are lost due to drying issues, resulting in spoilage and excessive fungal toxin contamination. Among these issues, the unreliable control systems and low efficiency of dryers significantly contribute to an uneven moisture distribution in dried products [3]. Addressing the global challenge of implementing an effective and reliable process control in paddy drying is crucial for minimizing post-harvest losses and ensuring food security worldwide.

Freshly harvested wet paddy often exhibits a significant variation in moisture content, causing fluctuations in grain moisture feeding in industrial-scale continuous drying equipment and making real-time prediction challenging [4–6]. Current control methods commonly used in practical paddy drying production still rely on manual empirical operation, which is subjective and requires specialized operators. The three main approaches for automatic control of paddy drying are feedback control, computer simulation control, and model predictive control (MPC). Feedback control, represented by proportional,

integral, and derivative (PID) tuning, adjusts the drying process in real-time based on the detected grain moisture to reduce deviations [7,8], but it may not align well with the independent events of the inlet grain, drying conditions, and outlet grain in paddy drying. Computer simulation control involves modeling and solving nonlinear processes using artificial intelligence (AI) algorithms [9,10], but obtaining effective coefficients is difficult due to the randomness in field drying. Researchers have developed Boltzmann coefficient generators [11,12] that can generate real-time coefficients based on field measurements. However, this approach significantly increases control costs and presents challenges in accurately measuring data online, especially in the presence of large-scale dynamic disturbances. MPC establishes an analytical model of the drying system, utilizes disturbance information through online optimization, and calculates optimal future inputs based on the current state [13,14]. It addresses time delay effects and is suitable for controlling paddy drying that features high inertia, nonlinearity, and multiple disturbances during the dehydration process.

Researchers have developed MPC strategies specifically for grain drying, focusing on predicting and controlling the process based on heat and mass transfer mechanisms. Wu et al. [15] proposed an MPC method using temperature, humidity, and other coupled parameters represented as the equivalent moisture potential accumulation in the drying process, based on an equivalent moisture potential accumulation model. Jin et al. [16] used a data-driven approach with a back-propagation neural network to design an MPC controller that predicted the moisture content of discharged grain and adjusted the grain flow velocity to regulate the drying process. Additionally, there are hybrid MPC methods that integrate classical control approaches with data-driven strategies [17–19]. Despite a successful implementation in laboratory-scale drying research, applying MPC to industrial-scale drying processes is still challenging due to the high computational cost of solving the online optimization problem in real-time. This challenge arises from the nonlinear dynamic models and multi-parameter coupling involved in grain drying.

The computational cost of large-scale MPC in industrial applications is a challenge due to the need to solve nonconvex optimization problems with updated information at each prediction step [20,21]. Despite efforts to improve computational tractability [22], latency remains a limiting factor for MPC-based grain drying systems. The computational overhead can also reduce the economic benefits of investing in grain drying equipment. One potential solution to this challenge is approximating the original MPC law using function approximation techniques like deep neural networks (DNNs) [23]. By employing DNNs, the online implementation of the approximated MPC law simplifies function evaluation and significantly reduces the computational burden. Fast MPC designs using DNNs have been successful in areas like battery management [24], vehicle dynamics [25], and chemical technology [26]. However, to the best of our knowledge, there have been no previous studies that specifically explore the application of fast MPC for designing control systems in paddy deep-bed drying processes.

Multistate counter-flow paddy drying is commonly used for the centralized drying of freshly harvested wet grains [6]. It involves the grains flowing from top to bottom through multiple stages of the dryer, undergoing drying–tempering processes until they reach the desired moisture content and are discharged. This method offers benefits like energy efficiency, high productivity, and low grain breakage [27]. The height of the multistage dryer results in an extended residence time for the grains inside the drying tower. This prolonged residence time is mainly due to the need for the grains to travel through all stages of the drying process from top to bottom. It is important to carefully manage and optimize this residence time to ensure that the grains reach the desired moisture content without excessive drying or other negative impacts on their quality. When applying MPC for process control, the system needs to predict the state of the grains entering the drying system based on ambient conditions and drying parameters, including changes in inlet grain moisture content. This results in a significant computational burden for the online optimization process, which affects the real-time performance of the drying MPC system.

To address the research gap in efficient process control for multistate counter-flow paddy drying systems, this study introduces deep-learning-based MPC. Firstly, a dataset generated from classical drying MPC is used to train a deep-learning neural network that approximates the original MPC law. This approach aims to replace the optimization process of classical MPC, reducing computational costs and improving efficiency. Secondly, simulations are conducted to verify the performance of the designed controller for both single-drying stages and the multistage system. Thirdly, field experiments using a 5HNH-15 multistage counter-flow dryer validate the control performance of the proposed method. The presented paddy drying control method has practical significance for enhancing intelligent grain drying equipment in terms of transformation and upgrading.

2. Description of Controlled Object

Due to the interaction between the initial point of the counter-flow hot air and the final point of wet paddy, which corresponds to the interaction between the final point and the initial point of wet paddy, it satisfies the drying heat matching requirement where the binding energy with the moisture content decreases. This results in a better energy utilization efficiency and higher drying intensity. However, improper operation can lead to product quality issues. To alleviate internal stress in the paddy kernel and prevent breakage, a counter-flow drying process should include multiple tempering stages. Therefore, a paddy multistage counter-flow drying process often consists of multiple drying stages and tempering stages connected in series. The schematic diagram of the multistage counter-flow drying process is shown in Figure 1.

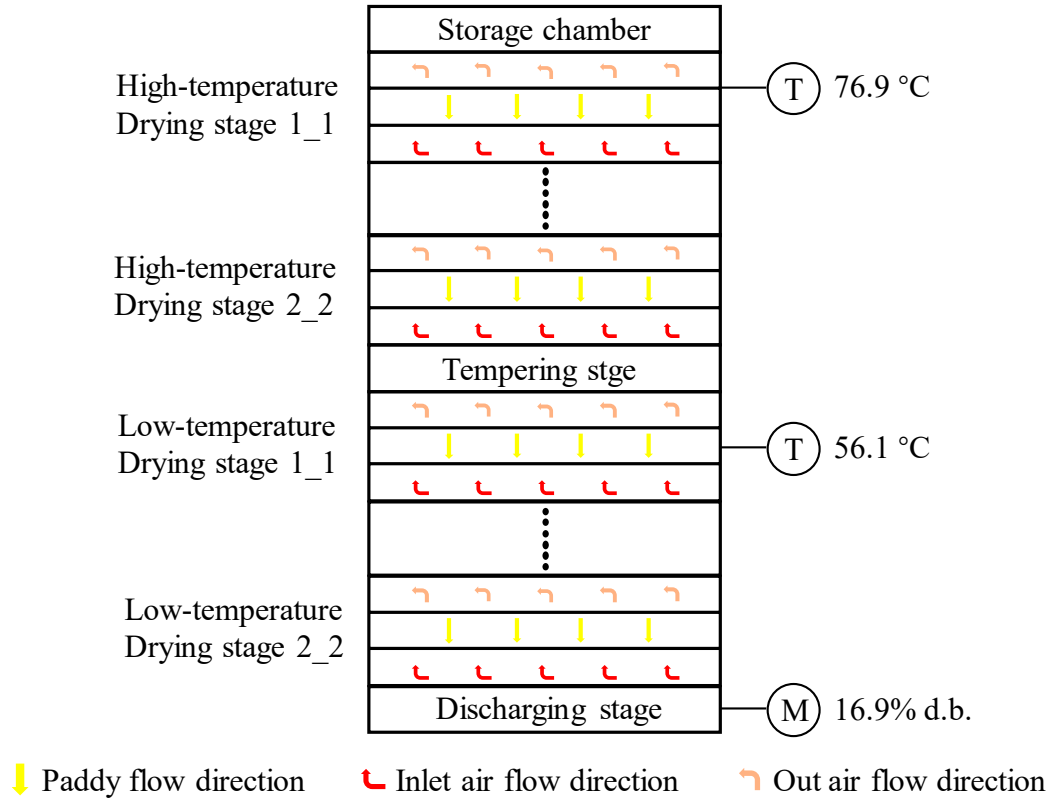

Figure 1. Schematic diagram of multistage counter-flow drying process.

In this study, the industrial-scale multistate counter-flow paddy dryer (Model: 5HNH-15), designed by our laboratory and applied in Haina Grain Processing Center in Changsha, Hubei Province, China, was adopted as an experimental setup. The diagram of the dryer is shown in Figure 2. The total height and volume of the dryer are 14.32 m and 145.8 m^3, respectively, and the capacity is about 90 t. The detailed drying process is as follows: Before drying, the

freshly harvested wet paddy was fed into multistate counter-flow dryer by the hoist. Then, the induced fan, conveyor belt, elevator, and discharging motor were started in turn after the drying chamber was first filled with wet paddy. Paddy flowed from top to bottom of the dryer under gravity and sequentially passed through two high-temperature drying stages (with a thickness of 2 m) and two low-temperature drying stages (with a thickness of 2 m), accompanied by four tempering stages (with a thickness of 1.58 m). Finally, paddy that reached the safe moisture content was discharged from the dryer at the discharging stage.

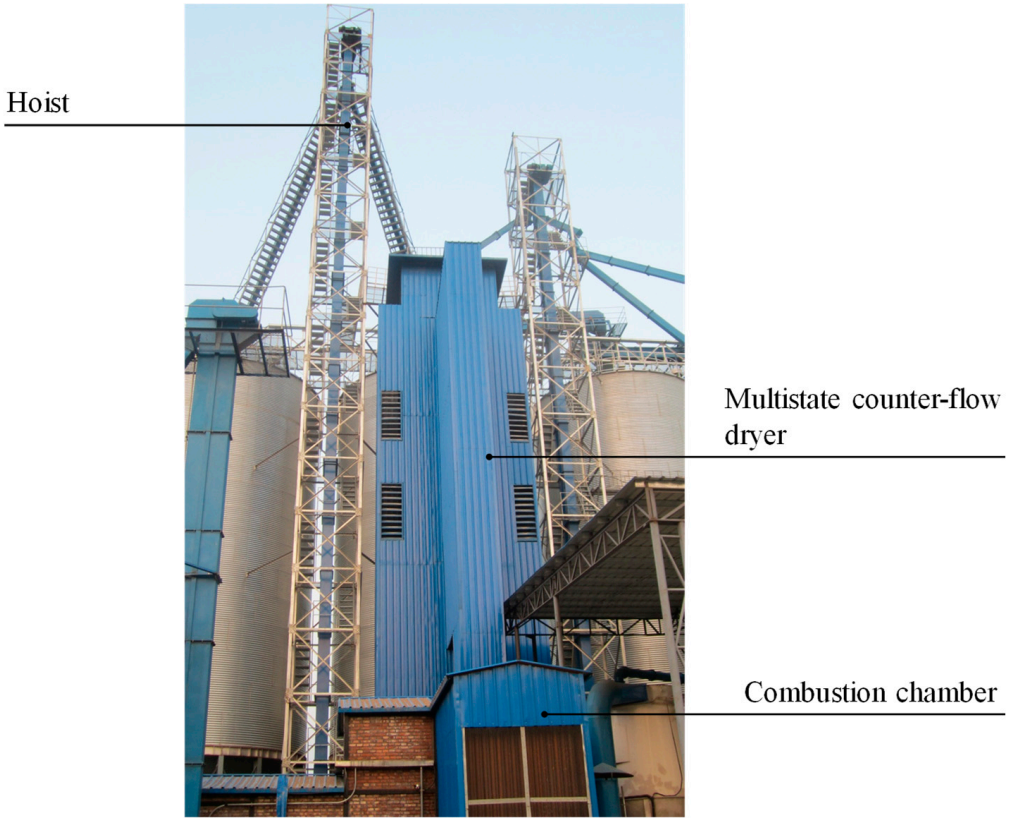

Figure 2. Diagram of the 5HNH-15 industrial-scale multistate counter-flow paddy dryer.

As an aspect of the drying condition, under the action of induced fans (Model: Y4-73, Shandong Shuntong Blower Co., Ltd., Heze, China) equipped in the high- and low-temperature drying stages, low-temperature ambient air rose to the pre-set temperature after being heated by the heat exchanger, and was then fed into two drying stages, respectively. As the paddy flows downwards in the dryer, the drying air comes into contact with it and removes excess water. This moisture-laden air is then expelled from the drying system, while the partially dried paddy continues its journey towards reaching the desired moisture content.

Wet paddy undergoes a comprehensive drying process inside the dryer, which allows it to reach a safe moisture content. Throughout this period, the operator adjusts the frequency of the discharging motor in response to real-time ambient conditions, initial paddy states, drying air parameters, and operational knowledge. This adjustment modifies the paddy flow velocity, thereby changing the real-time moisture content of the discharged paddy. A detailed description of sensors and instruments that measured air temperature and humidity, paddy moisture content and temperature, and ambient state can be found in Table 1.

Table 1. Detailed description of the sensors and instruments.

Devices	Model	Precision	Manufacturer
Air convection oven	DHG070B	-	Shanghai Anting Scientific Instrument Factory, Shanghai, China
Infrared thermometer	62 MAX+	1 °C	Fluke Testing Instruments (Shanghai) Co., Ltd., Shanghai, China
Temperature and humidity sensor	AM2305	0.3 °C and 2%	Guangzhou Aosong Electronics Co., Ltd., Guangzhou, China
Anemometer	AS8336	±0.01 m/s	Guangzhou Ximarui Electronics Co., Ltd., Guangzhou, China
Electronic scale	DY-718	±1 g	Jinhua Furuisi Electronics Co., Ltd., Jinhua, China

3. Construction of Controller

3.1. Framework of Model Predictive Control

The MPC implementation process can be briefly summarized in the following three steps: Firstly, the prediction model and current system state $y_{act,i}$ are utilized to predict the output $y_{act,i+1}$, $y_{act,i+2}$, …, $y_{act,tp-1}$, $y_{act,tp}$ of the future time domain t_p. Secondly, under system constraints, a specific optimization method is adopted to determine an input sequence u_{i+1}, u_{i+2}, …, u_{tc-2}, u_{tc-1} that satisfies the objective function within a control time domain, aiming to achieve an actual output that closely approximates the objective output y_{obj} in future time domain t_p. Thirdly, the first element of the obtained input sequence, u_{i+1}, is applied to the control system to obtain the system state at time i + 1. Then, the current time is set as i, and the above steps are repeated. As the control system operates, the prediction time domain continuously rolls forward to achieve control over the entire operation process. Specifically, the above optimization problem can be illustrated in Equation (1) [28]:

$$J = \sum_{i=1}^{t_p} Q(y_{obj} - y_{act,i})^2 + \sum_{i=1}^{t_p} R\Delta u_i{}^2 \quad (1)$$

where Q and R are the weighting matrices.

The above description for MPC illustrates that the essence of MPC is to obtain the future input based on a prediction model and measured system state data, wherein the actuator is the selected optimizer. To address the computational burden of classical MPC systems and enable their practical application in the field, the mapping relation between measurable state variables and control inputs can be established. This approach replaces the online optimization process in the classical MPC system, making it a more intuitive means of implementing MPC in field applications. Based on establishing a complete and accurate mechanistic simulation model for the drying system [6,29], a deep learning method can establish a mapping relation from state to action using a large amount of simulation data. This allows MPC to be implemented without the need for online optimization. The principle and primary implementation method are shown in Figure 3. The output in typical MPC (M in Figure 3a) is selected as the input of the deep-learning model, and the input in typical MPC (v_g in Figure 3a) is selected as the output. Finally, a deep-learning-based optimizer, as shown in Figure 3b, can be obtained to replace the MPC in Figure 3a.

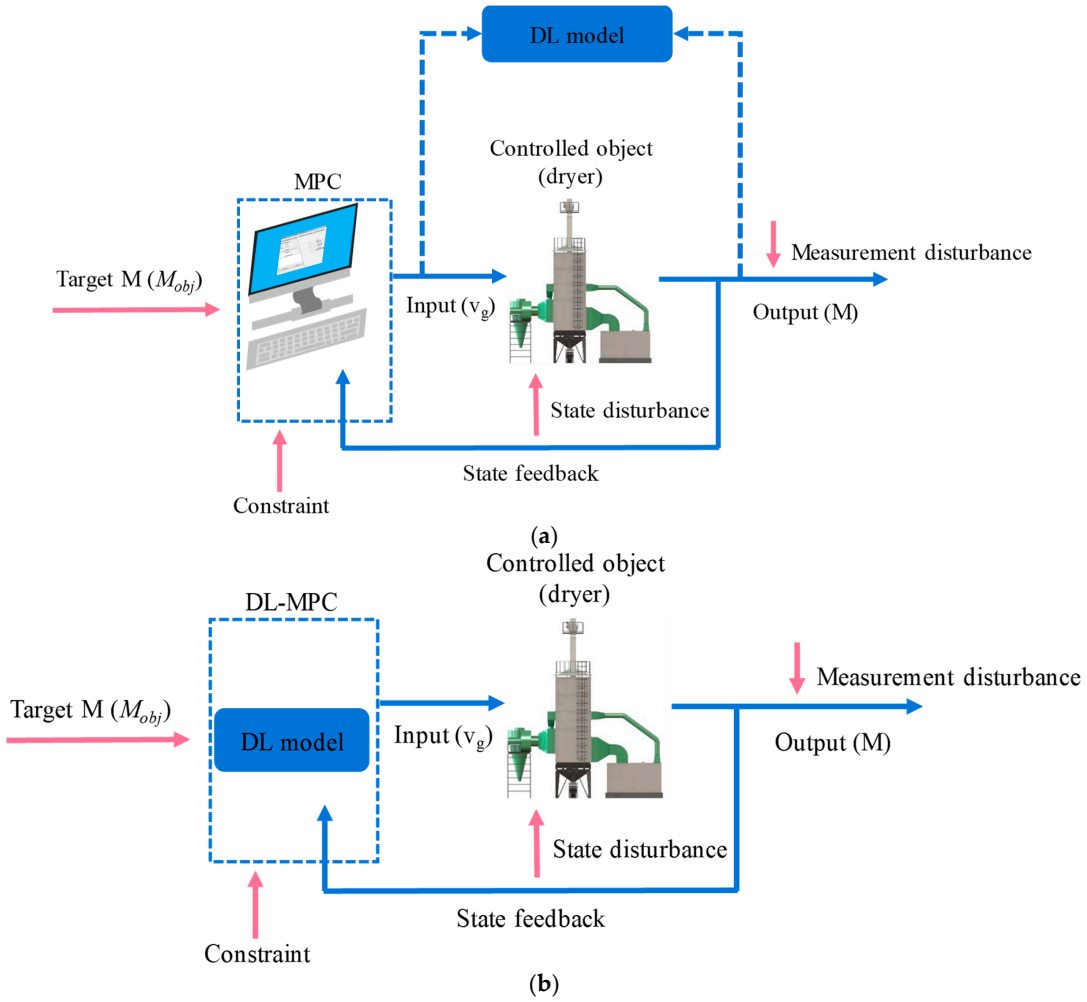

Figure 3. Schematic diagram of multistage counter-flow drying process: (**a**) train process and (**b**) application process.

3.2. Deep-Learning-Based MPC

During the paddy drying process, the moisture content of the paddy discharged from the dryer is affected by fluctuations in the ambient state, drying air state, and machine operation. These factors influence the paddy as it flows through the complete drying tower. Therefore, the output, which is the moisture content of the discharged paddy, at a given time is not solely determined by the current input factors such as the ambient or drying air state. It also depends on past inputs that have occurred over a certain period. As a result, modeling a paddy drying system using data-driven approaches can be considered as modeling time series data, considering the temporal dependencies and patterns in the system. The Recurrent Neural Network (RNN), incorporating temporal dependence into the traditional feedforward neural network, introduces the previous output as an input to the next hidden layer. This unique structure gives the RNN short-term memory capabilities and preserves the relations among data, making it suitable for analyzing time series data [30]. The long short-term memory (LSTM) model, a variant of the RNN, addresses issues such as gradient vanishing/exploding and limited long-term memory capacity [31].

The application process of the LSTM-based predictive controller is illustrated in Figure 4. It involves taking a time-sliding window of system state variables and input variables, f(3, N), which are collected in a preserved time sequence order and fed into an LSTM network as inputs to predict the next moment's system input, $v_g(N + 1)$, where N represents the length of the time series. As the drying progresses, the sliding window

moves forward continuously, capturing f′(3, N), f″(3, N), and so on. The LSTM utilizes the input data to calculate the output for the next moment and transfers it to the drying system, completing the predictive control process. In this study, the selected system state variables are the inlet moisture content (M_{in}) and outlet moisture content (M_{out}), while the input variable is the paddy flow velocity (v_g). In this framework, adjusting the paddy flow velocity takes into account not only the current system state but also the historical states and inputs within a specified time period. This approach goes beyond a simple one-to-one correspondence between input and output at a single moment. By considering a broader range of information, it allows for a more comprehensive, extensive, and accurate understanding of the system dynamics.

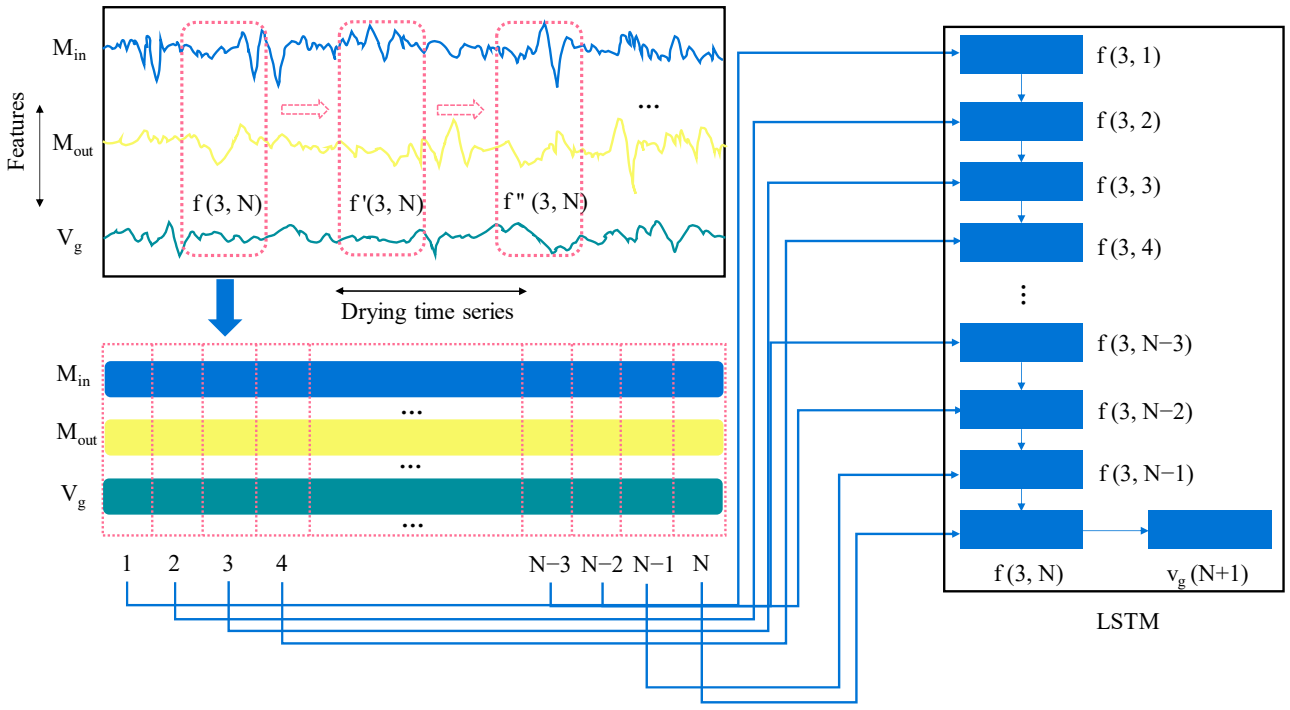

Figure 4. Diagram and application process of paddy drying LSTM predictive controller.

3.3. Analytical Model for Data Generation and Collection

This study combines numerical simulation and experimental research to obtain a comprehensive dataset for constructing DL-MPC. Specifically, an analytical model based on heat and mass transfer mechanisms is adopted to simulate various drying conditions in paddy drying processes. It should be noted that the predictive reliability of the mathematical model needs to be validated. In our previous research [6,32], we developed a mathematical model for paddy drying based on the spatial description method, which was successfully applied to analyze the process of the paddy multistage counter-flow dryer, the focus of this study. For the drying stage where water removal occurs, the mathematical model can be represented by the following set of partial differential equations:

$$\rho_g \frac{\partial M_d}{\partial t} - v_g \rho_g \frac{\partial M_d}{\partial Z} = -\mu\gamma\alpha(d_s - d)\frac{M_d - M_e}{M_0 - M_e}, \tag{2}$$

$$c_g \rho_{g,w} \frac{\partial T_g}{\partial t} + v_a c_g \rho_{g,w} \frac{\partial T_g}{\partial Z} = -h\tau\alpha(T_a - T_g) - \lambda_g \mu\gamma\alpha(d_s - d)\frac{M_d - M_e}{M_0 - M_e}, \tag{3}$$

$$v_a \rho_a \frac{\partial d}{\partial Z} = \mu\gamma\alpha(d_s - d)\frac{M_d - M_e}{M_0 - M_e}, \tag{4}$$

$$c_a \rho_a v_a \frac{\partial T_a}{\partial Z} = -h\tau\alpha(T_a - T_g) \tag{5}$$

where ρ_g is the bulk density of absolute dry paddy, M_d is the paddy moisture content, on a dry basis, t is the drying time, v_g is the paddy flow velocity, Z is the bed height, μ is the interphase heat transfer coefficient, $\gamma\alpha$ is the effective evaporation area of unit volume, d_s is the saturated humidity, M is the moisture content on a dry basis, c_g is the specific heat of paddy, v_a is the drying air flow velocity, T is temperature, λ_g is the latent heat of vaporization of paddy, ρ_a is the air density, h is the heat transfer coefficient, $\tau\alpha$ is the effective heat transfer area per unit volume, and $\rho_{g,w}$ is the bulk density of wet paddy.

The tempering stage that facilitates the even distribution of temperature and water in a kernel can be represented by the following mathematical model:

$$\frac{\partial M_d}{\partial t} = v_g \frac{\partial M_d}{\partial Z}, \tag{6}$$

$$\frac{\partial T_g}{\partial t} = v_g \frac{\partial T_g}{\partial Z} - S(T_g - T_{ab}) \tag{7}$$

where S is the cooling coefficient.

The numerical solution method is employed to solve the aforementioned mathematical model. The initial and boundary conditions can be represented as follows.

Initial conditions:

$$\begin{cases} M_{i,0} = M_0 \\ T_{g,i,0} = T_{g,0} \end{cases} \tag{8}$$

Boundary conditions:

$$\begin{cases} d_{0,t} = d_0 \\ T_{a,0,t} = T_{a,0}\ , \end{cases} \tag{9}$$

where i refers to the ith layer of the mesh divided in the z-direction.

Some property values and equations used in the solving process are listed in Table 2. We have conducted multiple model validation experiments in our previous research [32], and the results showed that the root-mean-square error (RMSE) for predicting paddy drying moisture content and temperature is 0.98% d.b. and 0.49 °C, respectively. The mean relative deviation (MRD) is 5.5% for paddy moisture content and 1.42% for temperature. These reasonable reliability indicators demonstrate the effectiveness of the mathematical model in analyzing actual paddy processes.

Table 2. Thermodynamic equations and property values used in calculation process.

Meters	Equations/Values	Units
P_s	$P_s = 133.322 \exp(18.751 - \frac{4075.16}{236.516 + T_{ab}})$	Pa
d	$d = 0.622 \cdot \frac{RH \cdot P_s}{P_b - RH \cdot P_s}$	kg/kg
M_e	$M_e = [\frac{-\ln(1-RH)}{1.919 \times 10^{-5}(T_a + 51.161)}]^{\frac{1}{2.445}}$	g water/g dry matter
ρ_a	1.293	kg/m^3
c_a	1.005	kJ/(kg·°C)
ρ_g	$\rho_g = \frac{1}{1+M_d}(2.073M_d + 508.5)$	kg/m^3
c_g	$c_g = 1.11 + 0.045\frac{M_d}{1+M_d}$	kJ/(kg·°C)
λ_g	$\lambda_g = [2500 - 2.386(T_g + 273)][1 + 2.556\exp(-20.176M_d)]$	kJ/kg
$\mu\gamma\alpha$	$\mu\gamma\alpha = \frac{\rho_g r(M_d - M_e)}{(d_s - d)}$	kg/(h·m^3)
r	$r = 0.0153T_{a,in} - 0.215$	1/h
$h\tau\alpha$	$h\tau\alpha = V_a c_a \rho_a \frac{T_{a,in} - T_{a,out}}{Z(\overline{T_a} - \overline{T_g})}$	kJ/(h·m^3·°C)

Note: The atmospheric pressure P_b is 101,325 Pa in this study. R is drying constant. The equation for calculating r is quoted from the research by Motohashi and Hosokawa [33].

3.4. Statistical Analysis

In this study, the mean absolute error (MAE), defined in Equation (10), was adopted to evaluate the predictive accuracy of DL-MPC to paddy flow velocity when applied in the multistate counter-flow dryer:

$$MAE = \frac{1}{n}\sum_{i=1}^{n}\left|y_{pre} - y_{obsj}\right| \quad (10)$$

where y_{pre} and y_{obsj} are the predicted and experimental values, respectively, and n is the number of measurements for each experiment.

4. Simulation

4.1. Simulation of Single-Drying Stage

The drying stage is the key phase in a multistage counter-flow dryer, where the primary focus is reducing moisture content during the paddy drying process. The tempering stage primarily regulates the paddy kernel temperature and does not involve moisture removal; it functions as an auxiliary stage. In this section, we focus on studying a single drying stage. We simulate the paddy drying process in a single-core counter-flow drying stage. The objective is to observe the response capability of the DL-MPC system when there are changes in the inlet paddy moisture content. States of the ambient conditions, drying system, wet paddy, and drying air are listed in Table 3. It should be noted that the variations in process parameters occur after the system reaches a steady state, i.e., after the wet paddy that has not undergone the complete drying process in the first tower has been discharged from the drying system.

Table 3. Parameters of drying system.

Parameters	Values	Units
Thickness of drying stage	0.5	m
Thickness of tempering stage (air outlet)	0.5	m
Target moisture content	14.61	% d.b.
Paddy initial temperature	20	°C
Ambient temperature	20	°C
Ambient relative humidity	50	%
Drying air temperature	60	°C
Drying air flow velocity	2300	m/h
Controllable range of paddy flow velocity	1–5	m/h

The variation in inlet paddy moisture content is the crucial factor affecting the drying efficiency of multistage counter-flow dryers. To provide sufficient information for training a neural network controller, this study defines an inlet moisture content signal sequence based on actual drying experimental data and past field operation experience, as shown in Figure 5. The defined inlet moisture content signal sequence (M_{in}) has a duration of 100 h with a sampling period of 0.01 h, generating 10,000 data points within the range of 19–23% d.b. It thoroughly analyzes practical process disturbances, including step changes, sinusoidal variations, and noise, to deliver valuable identification information. Under the designed classic MPC system (Figure 3a), the discharging paddy moisture content is controlled to approach the target moisture content by continuously adjusting the paddy flow velocity (Figure 5b). As shown in Figure 5a, compared with the uncontrolled moisture content curve (M_{uc}), the MPC-controlled moisture content curve (M_{mpc}) is primarily distributed around the target moisture content curve (M_{obj}), with an MAE of 0.132% d.b.

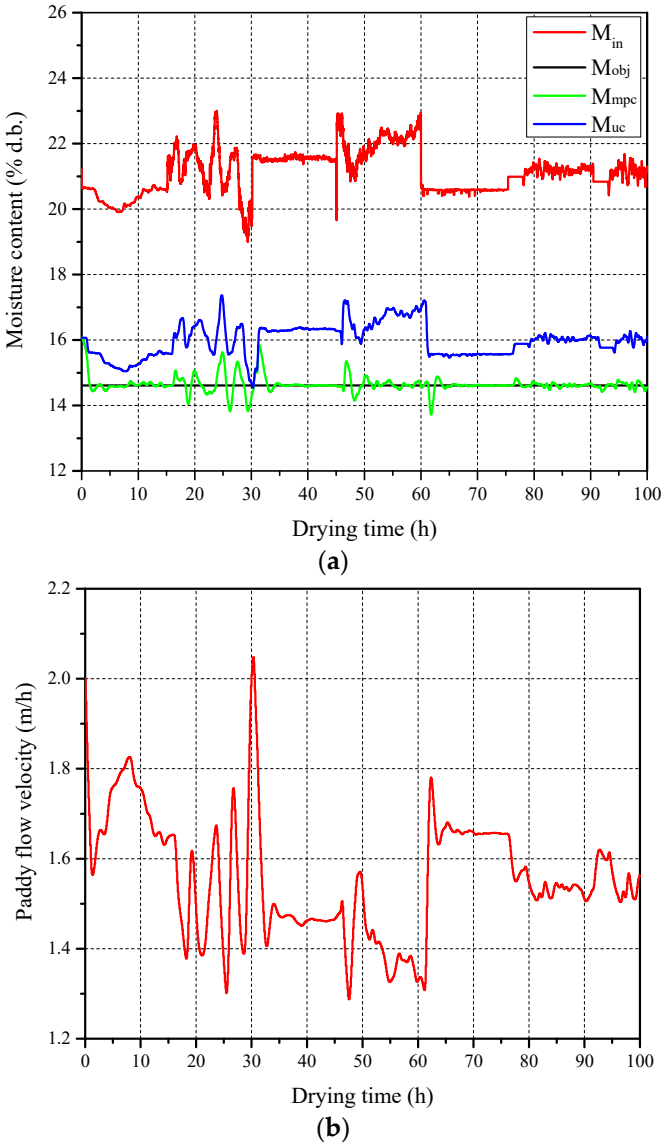

Figure 5. Dataset for building DL-MPC: (**a**) Paddy moisture content and (**b**) flow velocity.

After standardizing the dataset obtained from the classical MPC system, the data consisting of 10,000 samples were divided into training and test sets in an 8:2 ratio. The training set was employed to fit a neural network, while the test set was used for evaluating the model's generalization capability. The input for the LSTM model, developed using the Keras library in Python's TensorFlow 2.0 deep-learning framework, consisted of the inlet paddy moisture content, paddy flow velocity, and outlet paddy moisture content in the preceding 10 time steps (N = 10). The model output was the predicted paddy flow velocity for the subsequent time step. Specifically, the LSTM architecture for forecasting paddy flow velocity in a single counter-flow drying stage comprised two layers, with each layer comprising 50 units. During the model training process, the Adam optimization algorithm was utilized with a batch size of 20, a dropout rate of 0.2, and a time step length of 30.

Upon reaching 11 epochs, the neural network prediction model exhibited a stable mean square error (MSE) and determination coefficient (R^2) values. After completing 30 epochs, training concluded with an MSE below 0.0005 and an R^2 exceeding 0.98. Utilizing this trained model, predictions were made on the test set and compared to actual values of paddy flow velocity in Figure 6. The curves of predicted and actual values closely aligned, indicating a strong resemblance. The mean absolute error (MAE) was 0.006 m/h, while

R^2 was 0.937, showcasing the LSTM neural network's high accuracy in forecasting and its generalizability.

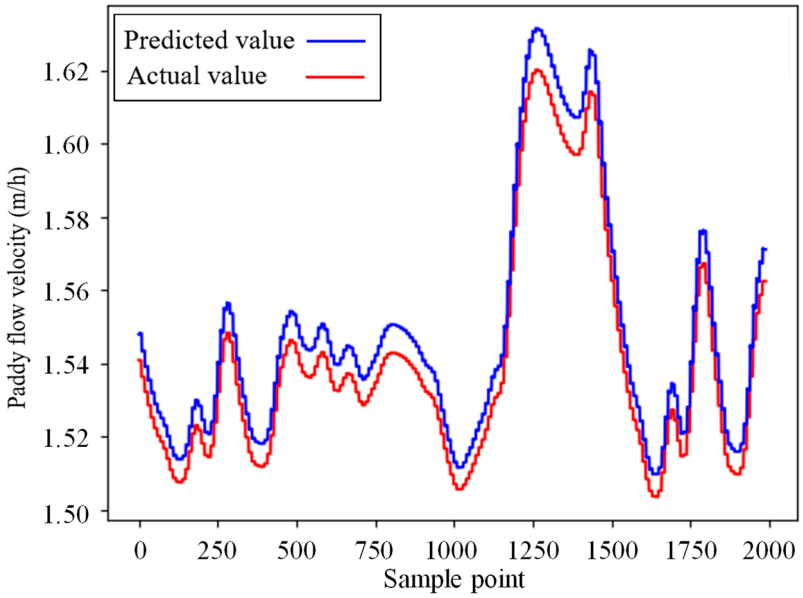

Figure 6. Prediction results of model on the test set of single-drying stage simulation.

The obtained LSTM neural network model was imported into the MATLAB 2017b environment to replace the optimization process of the classical MPC and to construct a DL-MPC simulation system. This system was used to observe the response capability of the DL-MPC system to variations in paddy initial moisture content. The basic parameters for the ambient state, drying system, paddy, and initial state of drying air were taken from Table 2. The simulation results are presented in Figure 7. It can be observed that the DL-MPC system made corresponding adjustments whenever there was a sudden change in the inlet paddy moisture content. The simulation time for the DL-MPC system, running on the simulation software and hardware platform (Intel(R) Core CPU i5-11320 running at 3.2 GHz) under the drying conditions corresponding to a drying time of 10 h, was 7.245 s. In contrast, the simulation time for the classical MPC system under the same drying conditions was 144.889 s. This demonstrates that compared with the classical MPC, the DL-MPC system significantly improves computational speed while ensuring the completion of control tasks, making it more suitable for online processes.

4.2. Simulation of Multiple-Drying Stage

Based on the construction and simulation of the single-stage DL-MPC system, a similar approach can be used to build a multistage counter-flow drying DL-MPC system. By extending the methodology to multiple stages, we can develop a comprehensive control system that optimizes the drying process across all stages in the counter-flow dryer. This allows for improved control and efficiency throughout the entire drying operation. In this section, the response capability of the DL-MPC system to variations in the inlet paddy moisture content is observed during the paddy drying process in the multistage counter-flow drying system shown in Figure 1. Table 4 presents the fundamental parameters of the ambient state, drying system, paddy, and initial state of the drying air. Similarly, changes in process parameters occur after the system reaches a steady state.

In the multistage counter-flow drying system, the paddy drying process is more complex and influenced by numerous factors. Thus, compared with a single drying stage, more data are required to construct a training set with abundant features. As shown in Figure 8a, a fluctuating signal sequence of inlet paddy moisture content was defined for 200 h with a sampling interval of 0.01 h, resulting in 20,000 data points within the range of

25–29% d.b. amplitude. From Figure 8b, it can be observed that the classical MPC system, when faced with variations in the inlet paddy moisture content, can continuously adjust the paddy flow velocity to maintain the outlet paddy moisture content around the target value, with an MAE of 0.161% d.b.

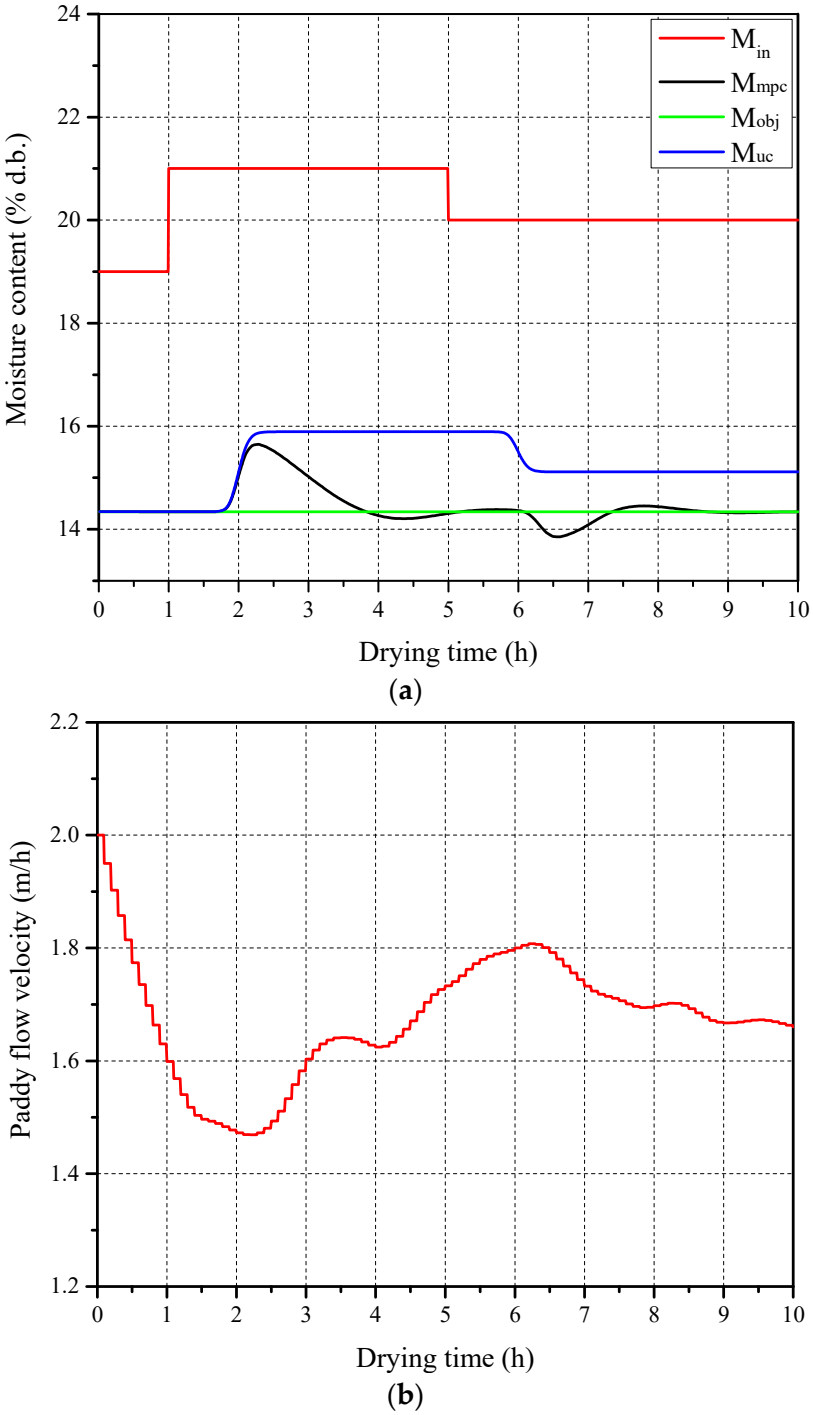

Figure 7. Test result of DL-MPC of single drying stage: (**a**) Paddy moisture content and (**b**) flow velocity.

Table 4. Parameters of multistage counter-flow drying system.

Parameters	Values	Units
Thickness of drying stage	0.5	m
Thickness of tempering stage (air outlet)	0.5	m
Thickness of tempering stage	1.58	m
Target moisture content	14.01	% d.b.
Paddy initial temperature	20	°C
Ambient temperature	20	°C
Ambient relative humidity	50	%
Drying air temperature in high-temperature drying stage	70	°C
Drying air temperature in low-temperature drying stage	50	°C
Drying air flow velocity in high-temperature drying stage	1924.5	m/h
Drying air flow velocity in low-temperature drying stage	1154.2	m/h
Controllable range of paddy flow velocity	1–5	m/h

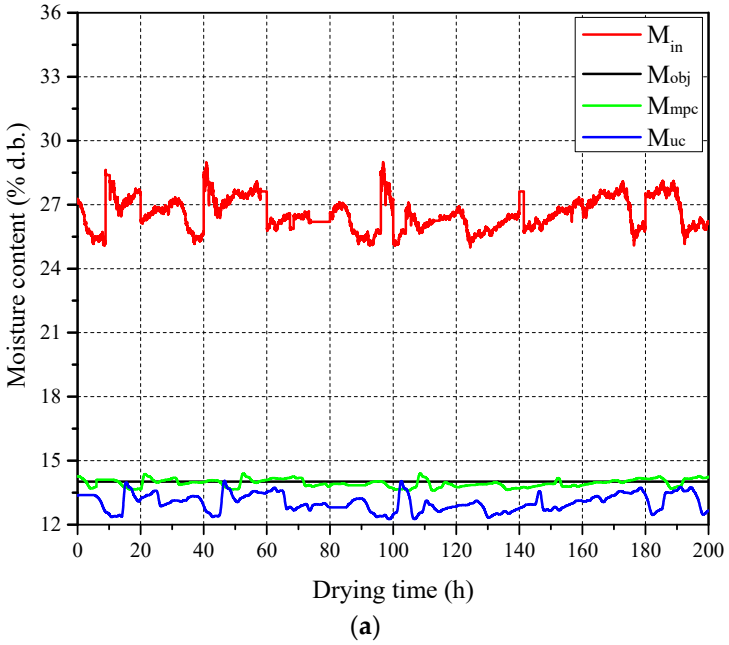

Figure 8. Dataset for constructing DL-MPC of multistage counter-flow drying system: (**a**) Paddy moisture content and (**b**) flow velocity.

After standardizing the database obtained from the classical MPC system, a similar approach as the single drying stage was used to train an LSTM network. In the model training process, N was set to 70. The LSTM network consisted of two layers, each with 50 units. The Adam optimization algorithm was utilized for model training, with a batch size of 20, a dropout rate of 0.2, and a time step length of 30. After reaching 13 epochs, the neural network prediction model's MSE and R^2 tended to stabilize. By the time the training reached 30 epochs, the training was completed, with an MSE below 0.0005 and an R^2 exceeding 0.98. The trained neural network model was then used to predict the data on the test set, and the predicted paddy flow velocity was compared with the actual values, as shown in Figure 9. It can be seen that the predicted and actual curves of the paddy flow velocity closely overlap. The MAE was found to be 0.0058 m/h, and the R^2 was 0.9980, indicating that the established LSTM neural network demonstrated high prediction accuracy and good generalization capability.

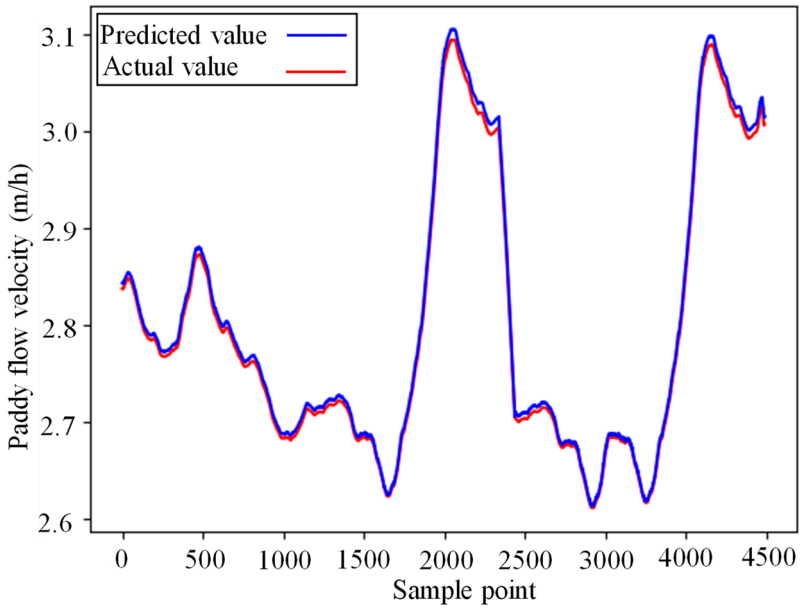

Figure 9. Prediction results of model on the test set of multiple-drying stage simulation.

The LSTM neural network model was imported into the MATLAB environment to replace the optimization process of classical MPC, creating a DL-MPC simulation system for paddy multistage counter-flow drying. The DL-MPC system's response to variations in the inlet paddy moisture content was observed using the basic parameters provided in Table 3 for the ambient state, drying system, paddy, and initial state of the drying air. Figure 10 presents the simulation results which demonstrate that the DL-MPC system made appropriate adjustments whenever there was a sudden change in the inlet paddy moisture content. The simulation period for the DL-MPC system was 22.499 s for a drying time of 30 h, while the classical MPC took 15,120 s under the same drying conditions. This significant improvement in computational speed enables the DL-MPC system to effectively accomplish control tasks in online processes, making it more suitable for such applications.

Furthermore, from Figure 10a, it can be observed that, due to the single adjustment control method used in this study and the larger height of the multistage counter-flow drying system, the system's adjustment time is longer. When the drying air parameters and paddy flow rate are adjusted simultaneously, the system's adjustment time might be shorter. Therefore, in future research, the utilization of multiple adjustment control variables will be explored. This includes simultaneously adjusting variables such as drying air temperature, drying air flow velocity, and paddy flow velocity, with the aim of constructing a multi-variable DL-MPC controller.

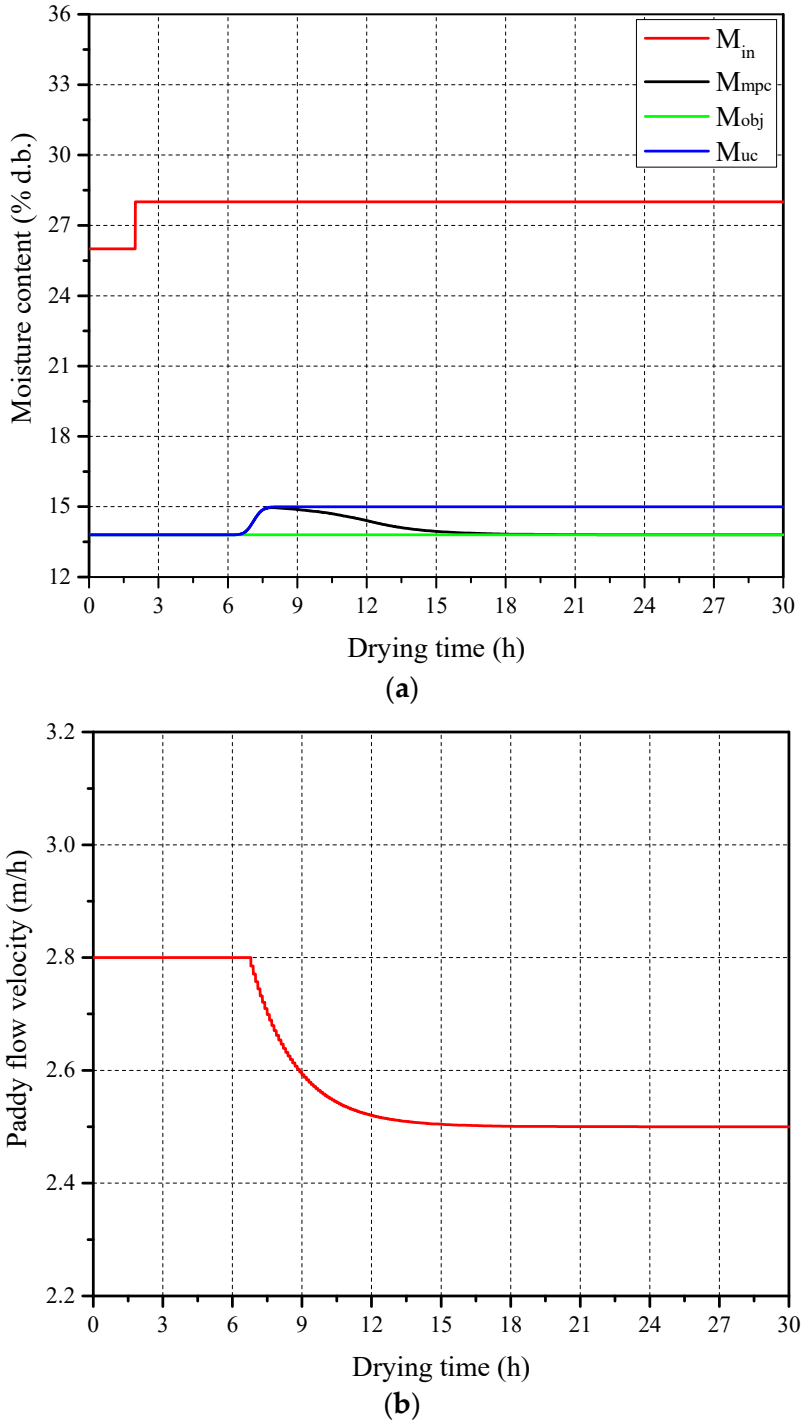

Figure 10. Test result of DL-MPC of multistate drying: (**a**) paddy moisture content and (**b**) flow velocity.

5. Experiment

In this section, the performance of the designed DL-MPC system was analyzed through experiments using the 5HNH-15 laboratory-designed multistage counter-flow dryer shown in Figure 2. The structural parameters of the 5HNH-15 dryer, as well as the data acquisition system and sensor parameters, are provided in Section 2. The experimental paddy sample used was Guangliangyouxiang 66. During the data collection period, the average ambient temperature and relative humidity were 9.6 °C and 66.6%, respectively. The average inlet air temperature in high- and low-temperature stages were 76.9 °C and 56.1 °C, respectively. Over the 40 h test period, real-time measurements of the inlet paddy moisture content,

outlet paddy moisture content (M_{out}), and frequency of the grain discharging motor (f_g) are shown in Figure 11.

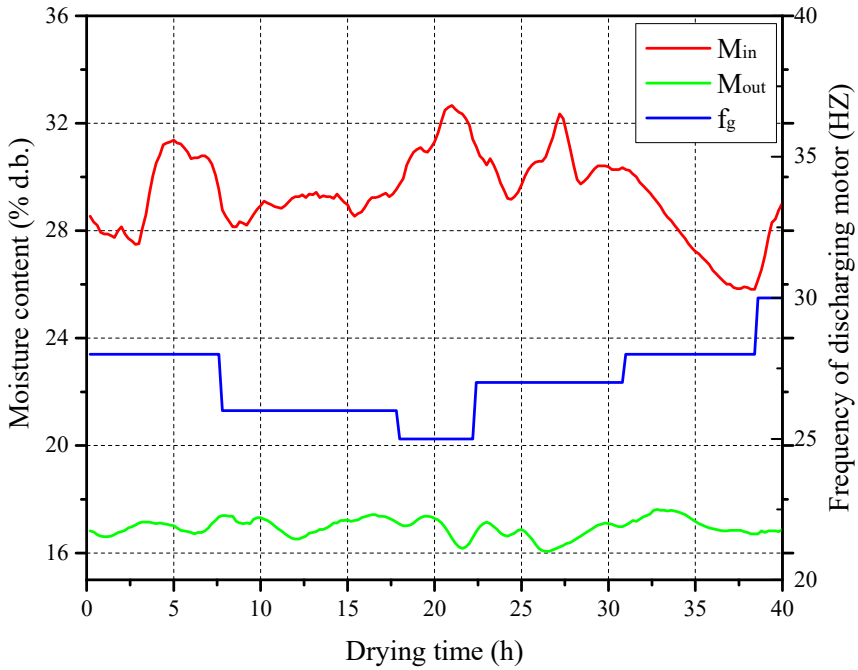

Figure 11. Real-time moisture content of inlet and outlet grain and frequency of grain discharging motor during drying process.

During the construction of the training dataset for the DL-MPC system, to reduce data quantity and facilitate the feasibility testing of the proposed method, it was assumed that the ambient state and ventilation parameters remained constant (taken as the average measured values). Based on field experimental data, the inlet paddy moisture content dataset was generated. The DL-MPC system was then constructed using the controller design method described in Section 3, followed by simulation. The predicted paddy flow velocity was compared with the actual frequency of the discharging motor. The results are shown in Figure 12. It can be observed that compared with the actual frequency of the discharging motor obtained from the field, the predicted paddy flow velocity exhibits a smooth variation and shows the same changing trend as the actual frequency of the discharging motor at multiple transition points (highlighted in blue boxes in Figure 12), indicating the effectiveness of the designed DL-MPC system. However, since the DL-MPC system ignores the variations in the ambient state and fluctuations in the inlet drying air conditions, the paddy flow velocity under DL-MPC strictly follows the changes in inlet paddy moisture content, resulting in some differences between the predicted data trends and the field data.

The predicted outlet paddy moisture content ($M_{out,mpc}$) obtained from the DL-MPC system is compared with the actual values ($M_{out,act}$), and the results are shown in Figure 13. It can be observed that compared with the actual outlet paddy moisture content, the predicted values are distributed more consistently around the target moisture content, with smaller variations as the inlet paddy moisture content changes. This is because the DL-MPC system has a higher adjustment frequency and more precise control than manual adjustments. The MAE between the predicted and actual values of the outlet paddy moisture content is 0.19% d.b.

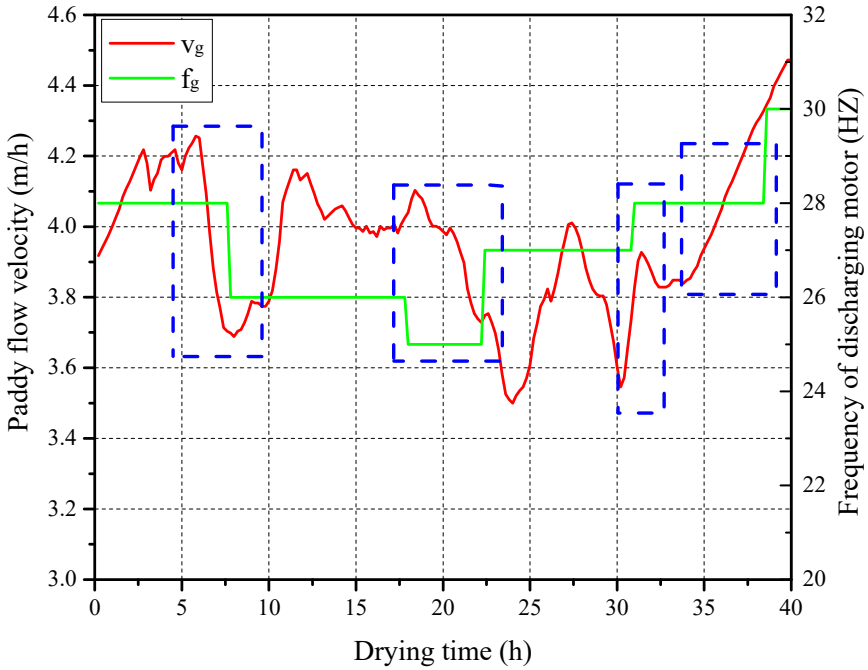

Figure 12. Predicted grain flow velocity and frequency of grain discharging motor.

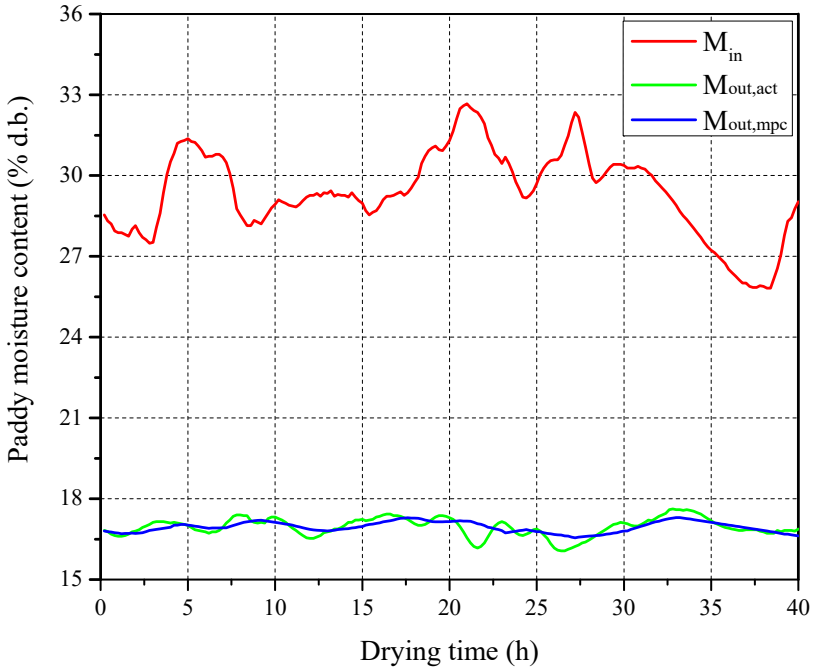

Figure 13. Comparison between predicted and actual moisture content.

6. Discussions

When the goal is to maintain a safe moisture content in paddy drying systems, the control problem can be addressed by rejecting disturbances and ensuring zero steady-state error in the system output. However, the significant lag response characteristics of drying systems limit the effectiveness of relying solely on output feedback control [34,35]. By considering the overall system state and incorporating modern control techniques like state observation, optimal state estimation, and system model parameter identification, it is possible to achieve disturbance rejection control in drying systems using model predictive control principles. Our DL-MPC control system stands out for its ability to provide a rapid response by replacing the optimization process in MPC with a deep-learning-based data

mapping function. Through simulation experiments, we demonstrate that the calculation of input parameters for drying processes lasting over 10 h can be completed within 10 s. In contrast to previous approaches primarily using data-driven models instead of mechanistic models for controller optimization, which still rely on iterative processes [36,37], our method offers a different perspective. Jin et al. [38] proposed an approach integrating LSTM neural networks to approximate the actual drying process and constructed an LSTM-MPC controller for dryer control, with a response time of 1150 s. Dai et al. also attempted to design grain drying controllers using machine learning methods, such as genetic optimization algorithms [39] and support vector machines [40]. While these small-sample modeling approaches improve computational speed to some extent, their control precision heavily relies on the accuracy of the data-driven model. In contrast, our DL-MPC system achieves an acceptable accuracy in controlling the target moisture content, with a MAE of 0.19% d.b. Another study conducted by Li et al. [14] proposed an NARX-based PSO-MPC controller for counter-current flow grain dryers, achieving an acceptable control accuracy of 0.52%, but this approach also faces challenges related to high data dependency. Similar results have been reported in MPC drying experiments with agricultural products like sawdust [41], corn [42], and red maple [43].

On the other hand, the unique material properties of paddy make its deep-bed drying process different from that of vegetables, fruits, and other agricultural products. It should be noted that the significant time delay characteristic of drying systems poses an important challenge in designing a paddy drying controller [6,44]. Although the controller designed for the multistage counter-flow dryer can achieve accurate process regulation, the adjustment time is excessively long, possibly exceeding 6 h. Figure 14 illustrates the transient response characteristics of paddy drying with step changes in grain moisture content at different paddy flow velocities, focusing on a single drying stage mentioned in Section 4.1. The figure shows that when the drying time is 0.2 h, the paddy moisture content jumps from 35% d.b. to 40% d.b., and the system transitions from one steady-state point to another, with a delay before the output begins to respond. For a paddy flow velocity of 1 m/h, the delay time is 0.4 h, the time for paddy to flow within the layer is 0.5 h, and the transition time is 0.6 h. Increasing the paddy flow velocity to 2 m/h reduces the delay time to 0.2 h, the flow time within the layer to 0.25 h, and the transition time to 0.3 h. Similarly, a paddy flow velocity of 4 m/h further decreases the delay time to 0.1 h, the flow time within the layer to 0.125 h, and the transition time to 0.15 h. In the step change process of grain moisture input, the transition time is greater than the flow time, which in turn is greater than the delay time. Additionally, higher paddy flow velocities require shorter delay and transition times. This analysis reveals that the flow-layer drying system exhibits pure lag characteristics, where information propagation is influenced by the time it takes for paddy to pass through the drying layer. Slower paddy flow velocities result in slower information propagation and longer system output delays. Relying solely on output feedback control for a system with pure lag characteristics leads to a significant overshoot, longer adjustment time, and poor control performance [45]. These findings align with previous studies that concluded that output feedback PID controllers [46,47] are not suitable for deep-bed flow-layer drying systems.

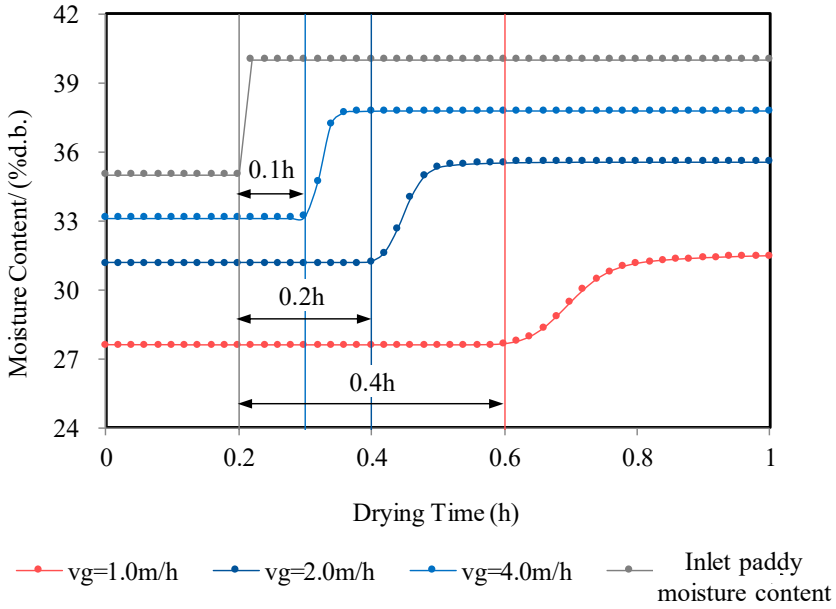

Figure 14. Transient response of counter-flow drying system with inlet paddy moisture content step change.

7. Conclusions

This study addresses the high computational cost challenge of applying classical MPC to industrial-scale paddy drying. A deep-learning-based model predictive control strategy suitable for paddy multistage counter-flow drying systems is proposed and designed through numerical simulation and optimization design. The controller's performance is validated through online and field experiments, leading to the following conclusions:

(1) For a single-drying stage, the DL-MPC system achieves a simulation time of 7.245 s, significantly improving computational speed compared to classical MPC (144.889 s). This makes DL-MPC more suitable for online processes while ensuring effective control.

(2) In multistage combined continuous drying, DL-MPC reduces the control time from 15,120 s to 22.499 s. However, due to the tall height of the control object, the adjustment time is longer compared to a single-drying stage, indicating the pure lag characteristics of the paddy deep-bed drying system.

(3) Field validation experiments demonstrate that the predicted paddy flow velocity follows the discharge motor frequency trend and exhibits a smoother variation. This indicates that the designed DL-MPC controller offers a higher adjustment frequency and more precise control compared to manual adjustments. The MAE between the predicted and actual outlet paddy moisture content is 0.19% d.b., confirming the effectiveness of the DL-MPC controller.

Considering the significant time delay characteristics in multistage counter-flow drying systems, future research will explore the utilization of multiple adjustment control variables, such as simultaneously adjusting the drying air temperature, drying air temperature flow velocity, and paddy flow velocity, to construct a multi-variable DL-MPC controller.

Author Contributions: Y.Z.: Methodology, Investigation, Results Analysis, Data Curation, Writing—Original Draft Preparation. Z.F.: Conceptualization, Methodology, Experimental Tests, Results Analysis, Writing—Original Draft Preparation. C.L. (Changyou Li): Conceptualization, Resources, Results Analysis, Supervision, Funding Acquisition. C.L. (Chengjie Li): Methodology, Investigation, Modeling, Experimental Tests, Results Analysis, Validation, Data Curation, Writing—Original Draft Preparation. All authors have read and agreed to the published version of the manuscript.

Funding: This work was supported by the National Natural Science Foundation of China (No.32171906) and the Guangzhou Science and Technology Plan Project (2024A04J3960).

Data Availability Statement: Data are contained within the article.

Acknowledgments: The authors would like to thank the editors and reviewers for their valuable and constructive comments.

Conflicts of Interest: The authors declare that they have no known competing financial interests or personal relationship that could have appeared to influence the work reported in this paper.

References

1. Cai, S.; Zhao, X.; Pittelkow, C.M.; Fan, M.; Zhang, X.; Yan, X. Optimal nitrogen rate strategy for sustainable rice production in China. *Nature* **2023**, *615*, 73–79. [CrossRef] [PubMed]
2. Liu, C.; Chen, S.; Xiao, S.; Ma, L.; Zhang, Y.; Chen, S. Process research and performance verification of variable temperature homogeneous drying device for paddy. *Trans. Chin. Soc. Agric. Mach.* **2023**. Available online: https://link.cnki.net/urlid/11.1964.S.20230925.0912.012 (accessed on 25 September 2023).
3. Mesterházy, Á.; Oláh, J.; Popp, J. Losses in the grain supply chain: Causes and solutions. *Sustainability* **2020**, *12*, 2342. [CrossRef]
4. Du, Y.; Yan, J.; Wei, H.; Xie, H.; Wu, Y.; Zhou, J. Drying kinetics of paddy drying with graphene far-infrared drying equipment at different IR temperatures, radiations-distances, grain-flow, and dehumidifying-velocities. *Case Stud. Therm. Eng.* **2023**, *43*, 102780. [CrossRef]
5. Mujumdar, A.S.; Menon, A.S. Drying of solids: Principles, classification, and selection of dryers. In *Handbook of Industrial Drying*; CRC Press: Boca Raton, FL, USA, 2020; pp. 1–39.
6. Li, C.; Fang, Z.; Zhong, J.; Li, B.; Li, C. Evaluating the dynamic characteristics and energetic performance of a paddy multistage counter-flow dryer. *Biosyst. Eng.* **2022**, *221*, 208–223. [CrossRef]
7. EL-Mesery, H.S.; EL-Seesy, A.I.; Hu, Z.; Li, Y. Recent developments in solar drying technology of food and agricultural products: A review. *Renew. Sustain. Energy Rev.* **2022**, *157*, 112070. [CrossRef]
8. Flor, O.; Palacios, H.; Suárez, F.; Salazar, K.; Reyes, L.; González, M.; Jiménez, K. New Sensing Technologies for Grain Moisture. *Agriculture* **2022**, *12*, 386. [CrossRef]
9. Khan, M.I.H.; Sablani, S.S.; Joardder, M.U.H.; Karim, M.A. Application of machine learning-based approach in food drying: Opportunities and challenges. *Dry. Technol.* **2022**, *40*, 1051–1067. [CrossRef]
10. Khan, M.I.H.; Sablani, S.S.; Nayak, R.; Gu, Y. Machine learning-based modeling in food processing applications: State of the art. *Compr. Rev. Food Sci. Food Saf.* **2022**, *21*, 1409–1438. [CrossRef]
11. Noé, F.; Olsson, S.; Köhler, J.; Wu, H. Boltzmann generators: Sampling equilibrium states of many-body systems with deep learning. *Science* **2019**, *365*, eaaw1147. [CrossRef]
12. Dibak, M.; Klein, L.; Krämer, A.; Noé, F. Temperature steerable flows and Boltzmann generators. *Phys. Rev. Res.* **2022**, *4*, L042005. [CrossRef]
13. Arroyo, J.; Manna, C.; Spiessens, F.; Helsen, L. Reinforced model predictive control (RL-MPC) for building energy management. *Appl. Energy* **2022**, *309*, 118346. [CrossRef]
14. Li, H.; Chen, S. A neural-network-based model predictive control scheme for grain dryers. *Dry. Technol.* **2019**, *38*, 1079–1091. [CrossRef]
15. Wu, W.; Liu, Z.; Han, F.; Zhang, Y.; Chen, J. Dual Drive Mutual Window Control Method for Continuous Grain Drying Based on Equivalent Water Potential Product. Patent No. CN113778153A, 29 September 2021.
16. Jin, Y.; Wong, K.W.; Yang, D.; Zhang, Z.; Wu, W.; Yin, J. A neural network model used in continuous grain dryer control system. *Dry. Technol.* **2022**, *40*, 1901–1922. [CrossRef]
17. Bai, H.; Chu, Z.; Wang, D.; Bao, Y.; Qin, L.; Zheng, Y.; Li, F. Predictive control of microwave hot-air coupled drying model based on GWO-BP neural network. *Dry. Technol.* **2023**, *41*, 1148–1158. [CrossRef]
18. Salehi, F. Recent applications of heat pump dryer for drying of fruit crops: A review. *Int. J. Fruit Sci.* **2021**, *21*, 546–555. [CrossRef]
19. Reis, F.R.; Marques, C.; de Moraes, A.C.S.; Masson, M.L. Trends in quality assessment and drying methods used for fruits and vegetables. *Food Control* **2022**, *142*, 109254. [CrossRef]
20. Karamanakos, P.; Liegmann, E.; Geyer, T.; Kennel, R. Model predictive control of power electronic systems: Methods, results, and challenges. *IEEE Open J. Ind. Appl.* **2020**, *1*, 95–114. [CrossRef]
21. Karamanakos, P.; Geyer, T. Guidelines for the design of finite control set model predictive controllers. *IEEE Trans. Power Electron.* **2019**, *35*, 7434–7450. [CrossRef]
22. Drgoňa, J.; Arroyo, J.; Figueroa, I.C.; Blum, D.; Arendt, K.; Kim, D.; Ollé, E.; Oravec, J.; Wetter, M.; Vrabie, D.L.; et al. All you need to know about model predictive control for buildings. *Annu. Rev. Control* **2020**, *50*, 190–232. [CrossRef]
23. Kamilaris, A.; Prenafeta-Boldú, F.X. Deep learning in agriculture: A survey. *Comput. Electron. Agric.* **2018**, *147*, 70–90. [CrossRef]
24. Li, Y.; Wang, Y.; Chen, Y.; Lu, Y.; Hua, K.; Ren, J.; Mozafari, G.; Lu, Q.; Cao, Y. Deep-Learning-Based Predictive Control of Battery Management for Frequency Regulation. *Ind. Eng. Chem. Res.* **2022**, *61*, 8432–8442. [CrossRef]

25. Zhang, X.; Bujarbaruah, M.; Borrelli, F. Near-optimal rapid MPC using neural networks: A primal-dual policy learning framework. *IEEE Trans. Control Syst. Technol.* **2021**, *29*, 2102–2114. [CrossRef]
26. Vaupel, Y.; Hamacher, N.C.; Caspari, A.; Mhamdi, A.; Kevrekidis, I.G.; Mitsos, A. Accelerating nonlinear model predictive control through machine learning. *J. Process Contr.* **2020**, *92*, 261–270. [CrossRef]
27. Li, T.; Li, C.; Li, B.; Li, C.; Fang, Z.; Zeng, Z.; Ou, W.; Huang, J. Characteristic analysis of heat loss in multistage counter-flow paddy drying process. *Energy Rep.* **2020**, *6*, 2153–2166. [CrossRef]
28. Kamali, S.; Ward, V.C.; Ricardez-Sandoval, L. Closed-loop operation of a simulated recirculating aquaculture system with an integrated application of nonlinear model predictive control and moving horizon estimation. *Comput. Electron. Agric.* **2023**, *209*, 107820. [CrossRef]
29. Chen, Y.; Huang, Y.; Zhang, Z.; Wang, Z.; Liu, B.; Liu, C.; Huang, C.; Dong, S.; Pu, X.; Wan, F.; et al. Plant image recognition with deep learning: A review. *Comput. Electron. Agric.* **2023**, *212*, 108072. [CrossRef]
30. Yu, Y.; Si, X.; Hu, C.; Zhang, J. A review of recurrent neural networks: LSTM cells and network architectures. *Neural. Comput.* **2019**, *31*, 1235–1270. [CrossRef]
31. Sherstinsky, A. Fundamentals of recurrent neural network (RNN) and long short-term memory (LSTM) network. *Phys. D* **2020**, *404*, 132306. [CrossRef]
32. Fang, Z.; Li, C.; Zhao, Y. Transient mathematical modeling of circulation counter-flow rice drying system. *Trans. Chin. Soc. Agric. Eng.* **2019**, *35*, 286–295. [CrossRef]
33. Motohashi, K.; Hosokawa, A. An application of forced air drying theory to the deep bed drying of rough rice (I). *J. Jpn. Soc. Agric. Mach.* **1979**, *40*, 557–564. [CrossRef]
34. Song, Q.; Wei, X.; Sun, W.; Li, D. Model predictive control strategy of head rice yield in paddy rice intermittent drying. *Dry. Technol.* **2022**, *40*, 2941–2951. [CrossRef]
35. Xu, X.; Zhao, T.; Ma, J.; Song, Q.; Wei, Q.; Sun, W. Application of Two-Stage Variable Temperature Drying in Hot Air-Drying of Paddy Rice. *Foods* **2022**, *11*, 888. [CrossRef] [PubMed]
36. Chokphoemphun, S.; Chokphoemphun, S. Moisture content prediction of paddy drying in a fluidized-bed drier with a vortex flow generator using an artificial neural network. *Appl. Therm. Eng.* **2018**, *145*, 630–636. [CrossRef]
37. Jha, A.; Tripathy, P.P. Optimization of process parameters and numerical modeling of heat and mass transfer during simulated solar drying of paddy. *Comput. Electron. Agric.* **2021**, *187*, 106215. [CrossRef]
38. Jin, Y.; Xie, H.; Yin, J.; Zhang, Z. Research on intelligent control method of grain drying based on LSTM-MPC. *Sci. Technol. Cereals Oils Foods* **2023**, *31*, 25–34. [CrossRef]
39. Dai, A.; Zhou, X.; Liu, X.; Liu, J.; Zhang, C. Intelligent control of a grain drying system using a GA-SVM-IMPC controller. *Dry. Technol.* **2018**, *36*, 1413–1435. [CrossRef]
40. Dai, A.; Zhou, X.; Dang, H.; Sun, M.; Wu, Z. Intelligent modeling method for a combined radiation-convection grain dryer: A support vector regression algorithm based on an improved particle swarm optimization algorithm. *IEEE Access* **2018**, *6*, 14285–14297. [CrossRef]
41. Eh, S.H.; Choi, Y.S.; Nam, Y.S.; Lee, C.G.; Lee, S.Y.; Oh, K.C.; Oh, J.H.; Kim, D.H. Development of a real-time drying control system for a pneumatic conveying dryer for sawdust in pellet production. *Energy* **2018**, *161*, 10–16. [CrossRef]
42. Han, F.; Zuo, C.; Wu, W.; Li, J.; Liu, Z. Model predictive control of the grain drying process. *Math. Probl. Eng.* **2012**, *2012*, 584376. [CrossRef]
43. Li, J.; Xiong, Q.; Wang, K.; Shi, X.; Liang, S. A recurrent self-evolving fuzzy neural network predictive control for microwave drying process. *Dry. Technol.* **2016**, *34*, 1434–1444. [CrossRef]
44. Wang, D.; Wang, J.; Qiu, S.; Zhan, T.; Tao, D.; Zhang, B. Optimization and experimental study of tempering process parameters during hot air drying of paddy rice. *Trans. Chin. Soc. Agric. Mach.* **2021**, *37*, 285–292. [CrossRef]
45. Shen, L.; Zhu, Y.; Liu, C.; Wang, L.; Liu, H.; Kamruzzaman, M.; Liu, C.; Zhang, Y.; Zheng, X. Modelling of moving drying process and analysis of drying characteristics for germinated brown rice under continuous microwave drying. *Biosyst. Eng.* **2020**, *195*, 64–88. [CrossRef]
46. Chen, J.; Zhang, M.; Xu, B.; Sun, J.; Mujumdar, A.S. Artificial intelligence assisted technologies for controlling the drying of fruits and vegetables using physical fields: A review. *Trends Food Sci. Technol.* **2020**, *105*, 251–260. [CrossRef]
47. Abhigna, R.; Sharma, A.; Kavya, K.; Sharma, P.; Salkuti, S.R.; Rajesh Kumar, M.; Naidu, R.C.; Sreekeessoon, B. Genetically Optimized PID Controller for a Novel Corn Dryer. In *Soft Computing for Problem Solving. Lecture Notes in Networks and Systems*; Thakur, M., Agnihotri, S., Rajpurohit, B.S., Pant, M., Deep, K., Nagar, A.K., Eds.; Springer: Singapore, 2023; Volume 547. [CrossRef]

《中文核心期刊要目总览》收录
Ei Compendex(核心版)收录
百种中国杰出学术期刊
RCCSE中国权威学术期刊

ISSN 1002-6819
CN 11-2047/S
CODEN NGOXEO
www.tcsae.org

农业工程学报

农业工程学报

NONGYE GONGCHENG XUEBAO | TRANSACTIONS OF THE CHINESE SOCIETY OF AGRICULTURAL ENGINEERING

2024年 第40卷 VOL. 40 23

二〇二四年十二月 第四十卷 第二十三期 中国农业工程学会

农 业 工 程 学 报

2024 年 12 月第 23 期 （总第 496 期） 第 40 卷

目 次

·农业生物环境与能源工程·

·土地保障与生态安全·

·农产品加工工程·

期刊基本参数：CN 11-2047/S*1985*s*16*360*zh*P* ¥ 80.00*290*36*2024-12

✦✻✦✻✦✻✦✻✦✻✦✻✦✻✦✻✦✻✦✻✦✻✦✻✦✻✦✻

致谢：感谢中国农业大学何雄奎教授团队提供的封面图片“数智农田智能作业装备系统”。

《农业工程学报》:与时俱进，追求卓越

《农业工程学报》(以下简称《学报》)创刊于1985年，现为半月刊，全年24期，大16开面向国内外公开发行。《学报》是由中国科学技术协会主管、中国农业工程学会主办的全国性专业学术期刊。读者对象为农业工程学科及相关领域的科研、教学及生产科技人员、技术管理及推广人员和高等院校师生。刊稿内容涵盖了农业装备工程与机械化、农业航空工程、农业水土工程、农业信息与电气技术、农业生物环境与能源工程、土地保障与生态安全、农产品加工工程等学科专业领域。

《学报》始终坚持“双为”方向和“双百”方针的办刊宗旨及“内容为王，质量为本”的办刊理念。拥有国内外农业工程相关领域各专业的知名专家学者组成的编委会，其中两院院士30余人。本刊坚持专家办刊，编委在稿件同行评审把关中发挥重要作用。

《学报》是中国农业工程领域的领军期刊，在行业具有很高的学术影响力，被EI Compendex（核心版）、 Scopus、 CA、CSA、CAB Abstracts、CSCD、《中文核心期刊要目总览》、《中国科技核心期刊目录》、《中国农林核心期刊概览2020》等国内外多个权威数据库收录。中国科学技术信息研究所2024年最新影响因子2.785。

我们愿与广大农业工程同仁携手并肩，共同奋斗，与时俱进，对标一流，追求卓越，创建国际知名品牌，引领学科发展，培养人才，激励创新，为全面推进乡村振兴，加快建设农业强国，推进农业农村现代化，为建设社会主义现代化强国作出新贡献！

期刊荣誉：多项位列农业工程类期刊榜首

- ✧ 国家新闻出版广电总局“双效期刊”
- ✧ 国家新闻出版广电总局“百强报刊”
- ✧ 中国科技期刊卓越行动计划-领军期刊
- ✧ 百种中国杰出学术期刊
- ✧ 中国精品科技期刊
- ✧ TOP5%中国最具国际影响力学术期刊
- ✧ RCCSE 中国权威学术期刊（A+）
- ✧ 科技期刊数字影响力 100 强
- ✧ 世界学术影响力指数 WAJCI-Q1 区期刊（为本学科唯一入选中文刊）
- ✧ Google Scholar 学术期刊影响力排名位列高被引中文刊第四名
- ✧ 中国农林领域高质量科技期刊分级目录第一区（T1）
- ✧ 中国科协精品科技期刊工程项目资助期刊

對標一流
追求卓越

ISSN 1002-6819
CN 11-2047/S
国内邮发代号：18-57
海外发行代号：BM3335
国内定价：80元

ISSN 1002-6819
9 771002 681245 23>

· 农产品加工工程 ·

油茶果热风干燥爆蒲后茶籽传热传质特性及干燥工艺优化

黄建江[1]，郭子洋[1]，李圣陶[1]，张 烨[1]，李长友[1]，李 涛[2]，李成杰[1※]

（1. 华南农业大学工程学院，广州 510642；2. 江西农业大学工学院，南昌 330000）

摘 要：为深入挖掘油茶果热风干燥爆蒲后茶籽内部水分和温度变化规律，找到一种低耗、高效的干燥工艺参数，该研究通过试验测定了油茶籽导热系数、密度等物性参数，计算得出油茶籽有效水分扩散系数的 Arrhenius 关系式，引入传热传质的数学建模理念建立了油茶籽传热传质模型，模型预测值与试验数据吻合较好，最大误差不超过 8.5%。基于上述模型，研究了油茶籽的变温干燥工艺，经过响应面优化后的干燥参数为前期风温 63.7 ℃、水分转换点 38.5%、后期风温 74.8 ℃，在此干燥条件下，单位能耗为 5.040 kJ/g，干燥速率为 0.048 g/(g·h)，与试验指标的回归模型预测结果相比，其相对误差分别为 7.4% 和 12.1 %。该研究提出的干燥工艺参数可为油茶果干燥爆蒲方法的产业化推广提供理论依据和应用参考。

关键词：工艺优化；模型；油茶；爆蒲；传热传质；热风干燥

doi：10.11975/j.issn.1002-6819.202406126

中图分类号：TS222.1 **文献标志码：**A **文章编号：**1002-6819(2024)-23-0332-10

黄建江，郭子洋，李圣陶，等. 油茶果热风干燥爆蒲后茶籽传热传质特性及干燥工艺优化[J]. 农业工程学报，2024，40(23)：332-341. doi: 10.11975/j.issn.1002-6819.202406126 http://www.tcsae.org

HUANG Jianjiang, GUO Ziyang, LI Shengtao, et al. Heat and mass transfer characteristics and drying process optimization of *Camellia oleifera* seeds after hot air drying and shelling of the fruits[J]. Transactions of the Chinese Society of Agricultural Engineering (Transactions of the CSAE), 2024, 40(23): 332-341. (in Chinese with English abstract) doi: 10.11975/j.issn.1002-6819.202406126 http://www.tcsae.org

0 引 言

油茶是中国特有木本食用油料植物，其产出的茶油含有丰富的不饱和脂肪酸，还含有皂苷、酚类、角鲨烯等多种功能活性成分，具有良好的抗氧化、抗癌及降血压等作用，营养价值极高[1]。油茶果脱蒲（又称脱壳）是其产后加工的必要工序，目前采用的方法主要有自然晾晒、机械脱蒲、干燥爆蒲 3 种[2–4]。自然晾晒方法难以应对天气变化、场地制约、人工翻晒等给油茶果造成爆蒲均匀度较差的现实，影响后期清选效率，且霉变、生虫等因素极易使后期产油品质受到影响，再加上较强的人工依赖性，使得这种脱蒲方法与油茶产业发展的需求严重不符[5–7]。机械脱蒲方法一定程度上提高了生产效率并降低了人工劳动强度，但这种方法容易使脱蒲不充分或形成碎蒲末，后期清选难度较大，且机械方式极易损伤茶籽，造成碎籽现象，严重影响最终出油率[8–9]；此外，机械脱蒲方法未考虑油茶青果采摘后过程生命活体内油脂含量的进一步积累，也可能会影响最终出油率[10–12]。热风干燥爆蒲是近年来出现的脱蒲新方法，油茶果受热后，茶蒲逐渐自动破裂爆开，完全爆蒲后的油茶果轻轻搅动即可实现蒲籽分离，完成脱蒲过程。热风干燥过程中，茶籽亦得到充分干燥，处于安全水分的茶籽质地均匀完整，既保证了榨油原料的品质，又延长了榨油期，迎合了油茶产业发展的本质需求[13]。然而，油茶果在经过爆蒲后，茶籽干至安全储藏水分仍需较长时间，期间干燥参数难以准确调控，极易导致过干或欠干等情况，影响后期出油量和出油品质。因此，需要对油茶果热风干燥爆蒲后茶籽的传热传质特性进行深入研究，以优化实际干燥工艺 过程，进而促进干燥爆蒲方法的产业化推广。

干燥爆蒲是一种新型的脱蒲技术，目前国内外相关机理研究较少，油茶果热风干燥爆蒲后茶籽的传热传质特性研究尚处于空白。基于上述事实，本文以油茶果爆蒲后的茶籽干燥为研究对象，测定其物性参数，基于传热传质控制方程建立油茶籽干燥数学模型，模拟热风干燥过程中油茶籽的干燥特性，并将该模型运用于油茶籽干燥工艺的优化，以期得到低耗、高效的工艺方案，为油茶果爆蒲方法的产业化推广提供理论依据和数据支持。

1 材料与方法

1.1 传热传质数学模型

1.1.1 模型假设

为了构建和求解热风干燥过程油茶籽的传热和传质模型，对爆蒲后的茶籽进行如下基本假设：1）油茶籽为各向同性的均匀体，内部初始温度和水分分布均匀；2）水分迁移相对于油茶籽中心对称；3）油茶籽表面的传质阻力忽略不计；4）油茶籽周围热空气温度、相对湿

收稿日期：2024-06-19 修订日期：2024-07-26
基金项目：国家自然科学基金项目（32171906；32101637；32401725）；广州市科技计划项目 (2024A0J3960)
作者简介：黄建江，研究方向为智能干燥工艺装备设计。
Email：hjj0723@stu.scau.edu.cn
※通信作者：李成杰，博士，副教授，研究方向为智能干燥装备系统理论与技术。Email：chengjie.li@scau.edu.cn

度、风速恒定不变；5）不考虑油茶籽在干燥过程中的收缩变形。

1.1.2　物理模型

图 1a 为油茶果内茶籽分布情况，整体近似为一球体，为简化计算过程，对油茶籽整体结构作二维轴对称简化，并进行网格划分，用游标卡尺对 100 颗油茶果进行测量，其平均粒径约为 27 mm，平均蒲厚约为 2.5 mm，取油茶籽半径为 11 mm，如图 1b 所示，使用 COMSOL Multiphysics 软件自带的物理场控制网格，单元大小为超细化的自由剖分三角形网格对几何模型进行网格划分，网格顶点数为 1 487，三角形数为 2 842，网格面积为 190 mm^2。

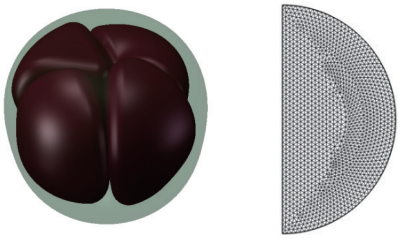

a. 油茶籽三维模型
a. 3D model of *Camellia oleifera* seed

b. 网格划分
b. Meshing situation

图 1　物理模型
Fig.1　Physical model

1.1.3　传热方程

根据热量守恒定律，热风干燥过程中油茶籽内部的传热过程可以描述为

$$\nabla(\lambda\cdot\nabla T)=\rho C_p\frac{\partial T}{\partial t}-\rho h_g\frac{\partial M}{\partial t} \tag{1}$$

初始条件和边界条件为：

$$\begin{cases} t=0;\ T=T_0 \\ -\lambda\dfrac{\partial T}{\partial t}=h_t(T-T_a) \end{cases} \tag{2}$$

式中λ为油茶籽导热系数，W/(m·K)；T_0为油茶籽的初始温度，℃；T为油茶籽的内部温度，℃；T_a为干燥空气的温度，℃；M为油茶籽的内部干基含水率，%；ρ为油茶籽的密度，kg/m^3；C_p为油茶籽的比热容，J/(kg·K)；t为时间，s；h_g为水的汽化潜热，J/kg；h_t为油茶籽对流传热系数，W/(m^2·K)。

油茶籽对流传热系数（h_t）采用努塞尔数（Nu）估算[14]：

$$\begin{cases} Nu=\dfrac{h_t d}{\lambda_a}=2+0.552Re^{(0.53)}Pr^{(\frac{1}{3})} \\ Re=\dfrac{v_a\rho_a d}{\mu_a} \\ Pr=\dfrac{\mu_a C_a}{\lambda_a} \end{cases} \tag{3}$$

式中Re为雷诺数；Pr为普朗特数；v_a为热空气的风速，m/s；ρ_a为热空气的密度，kg/m^3；d为油茶籽等效直径，m；μ_a为热空气的动力黏度，Pa·s；C_a为热空气的比热容，J/(kg·K)；λ_a为热空气的导热系数，W/(m·K)。

1.1.4　传质方程

根据质量守恒定律，热风干燥过程中油茶籽内部的传质过程可以描述为

$$\frac{\partial M}{\partial t}=\nabla(D_{eff}\cdot\nabla M) \tag{4}$$

初始条件和边界条件为

$$\begin{cases} t=0;\ M=M_0 \\ -D_{eff}\dfrac{\partial M}{\partial t}=h_m(M-M_e) \end{cases} \tag{5}$$

式中D_{eff}为油茶籽的有效水分扩散系数，m^2/s；M_0为初始时刻干基含水率，%；h_m为油茶籽的对流传质系数，m/s；M_e为油茶籽干燥到平衡态时的干基含水率，%。

油茶籽对流传质系数（h_m）采用舍伍德数（Sh）估算[14]：

$$\begin{cases} Sh=\dfrac{h_m d}{D_a}=2+0.552Re^{(\frac{1}{2})}Sc^{(\frac{1}{3})} \\ Sc=\dfrac{\mu_a}{\rho_a D_a} \end{cases} \tag{6}$$

式中D_a为热风的有效水分扩散系数，m^2/s；Sc为施密特数。

CRANK[15] 以无穷级数的形式提出了 Fick 第二定律在球体中水分传递的解析解：

$$M_R=\frac{6}{\pi^2}\sum_{n=1}^{\infty}\frac{1}{n^2}\exp\left(-\frac{n^2\pi^2 D_{eff}t}{r^2}\right) \tag{7}$$

式中n为项数，M_R为水分比；r为油茶籽的等效半径，m；随着t的增加，$n>1$的序列中的每个项都接近于 0。忽略高阶项（$n>1$），方程变换为式(8)，两边取对数变换为式(9)：

$$M_R=\frac{6}{\pi^2}\exp\left(-\frac{\pi^2 D_{eff}t}{r^2}\right) \tag{8}$$

$$\ln M_R=\ln\frac{6}{\pi^2}-\frac{\pi^2 D_{eff}t}{r^2} \tag{9}$$

由式(9)可知，干燥过程中水分比的对数$\ln M_R$与干燥时间t呈线性关系，对其进行线性回归，可得斜率$k=-\dfrac{\pi^2 D_{eff}}{r^2}$，进而可得油茶籽的有效水分扩散系数。

水分比M_R计算式为[16]

$$M_R=\frac{M_t-M_e}{M_0-M_e} \tag{10}$$

式中M_t为t时刻油茶籽的干基含水率，%。

采用逆推法，根据试验测得的有效水分扩散系数，建立有效水分扩散系数、干燥温度和活化能的 Arrhenius 关系式[17-19]：

$$D_{eff}=D_0\exp\left(-\frac{E_a}{R(T_a+273.15)}\right) \tag{11}$$

式中D_0为有效扩散系数指前因子，m^2/s；E_a为干燥活化能，kJ/mol；R为理想气体常数，取8.314×10^{-3} kJ/（mol·K）；T_a为干燥空气的温度，℃。

1.1.5　模型参数

为了求解传热传质数学模型，通过查阅文献和实际测量，所需的油茶籽和热空气特性参数如表 1 所示。

表 1 油茶籽和热空气的特性参数

Table 1 Characteristic parameters of *Camellia oleifera* seed and hot air

参数 Parameters	数值或方程 Value or equations	来源 Source
油茶籽初始温度 Initial temperature of *Camellia oleifera* seed T_0/(℃)	20	测定
干空气温度 Drying air temperature T_a/(℃)	52;62;72	测定
油茶籽密度 Density of *Camellia oleifera* seed ρ/(kg·m^{-3})	$13\ 590\times(10+3.59M_x)^{-1}$	计算
油茶籽导热系数 Thermal conductivity of *Camellia oleifera* seed λ/(W·m^{-1}·K^{-1})	$0.053\ 6+0.005\ 454M_x$	计算
油茶籽比热容 Specific heat capacity of *Camellia oleifera* seed C_p/(J·kg^{-1}·K^{-1})	2 100～2 500	[20]
干空气密度 Drying air density ρ_a/(kg·m^{-3})	$8.666\times10^{-6}T_a^2-4.318\times10^{-3}T_a+1.288$	[21]
干空气比热容 Specific heat capacity of drying air C_a/(J·kg^{-1}·K^{-1})	$4.834\times10^{-4}T_a^2-2.218\times10^{-2}T_a+1\ 007$	[21]
干空气导热系数 Thermal conductivity of drying air λ_a/(W·m^{-1}·K^{-1})	$2.401\times10^{-8}T_a^2+7.554\times10^{-5}T_a+2.364\times10^{-2}$	[22]
干空气动力黏度 Dynamic viscosity of drying air μ_a/(Pa·s)	$3.238\times10^{-11}T_a^2+4.839\times10^{-8}T_a+1.73\times10^{-5}$	[23]
干空气水分扩散系数 Diffusion coefficient of moisture in drying air D_a/(m^2·s^{-1})	$3.229\times10^{-10}T_a^2+1.577\times10^{-7}T_a+2.089\times10^{-5}$	[23]
水的汽化潜热 Latent heat of vaporization h_g/(J·kg^{-1})	2 256 267	[24]

注：M_x 为油茶籽湿基含水率，%；T_a 为干燥空气的温度，℃。

Note: M_x is the moisture content of Camellia oleifera seeds in wet base, %; T_a is the temperature of the drying air, °C.

材料的导热系数测量方法大致分为稳态法和瞬态法，本文采用热防护平板法测量油茶籽绝干物质的导热系数：将烘至绝干的油茶籽磨碎并压制成具有一定几何形状的样本，在材料两侧建立稳定的温差，并测量通过材料的热流，计算其导热系数。为了使得模型更为准确，干燥过程中油茶籽的导热系数和密度随着水分及组织结构发生的变化不可忽视，本文采用了近似计算方法，根据油茶籽当前的水分含量及其绝干物质在总质量中的占比，动态调整其导热系数与密度的数值，以确保模型能够更真实地反映干燥过程中的物理变化。

油茶籽导热系数计算式为[25]

$$\lambda=\lambda_m\frac{M_x}{100}+\frac{100-M_x}{100}\lambda_g \tag{12}$$

式中λ_m为水的导热系数，W/(m·K)；λ_g为油茶籽绝干物质的导热系数，W/(m·K)；M_x为油茶籽湿基含水率，%。

油茶籽密度计算式为[26]

$$\rho=\frac{1}{\frac{M_x}{100\rho_m}+\frac{100-M_x}{100\rho_g}} \tag{13}$$

式中ρ_m为水的密度，kg/m^3；ρ_g为油茶籽绝干物质的密度，kg/m^3。

1.1.6 模型求解

利用 Lenovo 计算机工作站（Windows 10 64 位操作系统，CPU Intel(R) Core(TM) i5-9 500，3.00 GHz，16.0 GB 运行内存）搭载的 COMSOL Multiphysics 6.1 有限元分析软件的传热传质模块进行求解，相对误差和绝对误差分别设定为 0.01 和 0.001。

1.2 试 验

1.2.1 物料制备

试验所用新鲜油茶果采购于广州市某农贸市场，试验地点为华南农业大学工程学院干燥研究室。将油茶果置于密封袋中，并存放于 4 ℃ 的恒温冷藏箱中进行保存，在每次试验开始前，将所需量的油茶果从冷藏箱中取出，筛选出外观均匀、尺寸大小相近的油茶果作为试验样本，将挑选好的油茶果放置至室温环境中，待放置至室温 20 ℃ 后进行试验，确保试验条件一致。

1.2.2 试验设备

电热恒温干燥箱（101-1A，精度±0.1 ℃），绍兴市尚诚仪器制造有限公司；电子天平（FA2204 N，精度 0.000 1 g），上海菁海仪器有限公司；导热系数仪（DRH-V，精度±2%），湘潭湘仪仪器有限公司。试验过程记录干燥箱每小时的耗电量。

1.2.3 试验方法

本研究设置两类试验，分别为油茶果热风干燥爆蒲后茶籽的干燥特性试验和干燥工艺优化试验，前者旨在探究油茶籽的热风干燥特性，后者则着眼于干燥工艺的优化，包括进行单因素试验和 Box-Behnken 试验。

热风干燥特性试验：开启热风干燥烘箱，预热 30 min 以上，当内部温度传感器所读取数值稳定在 52、62、72 ℃ 时，将样品油茶果以单层形式摆放，迅速放入烘箱进行试验，在试验过程中，待大部分油茶果开裂时起，每间隔 1 h 随机取出一定量样品进行人工蒲籽分离，称量茶籽、测温并做好标记后迅速放入 105 ℃ 烘箱，通过油茶籽的质量和干物质质量计算含水率。根据 GB/T 14489. 1-2008《油料 水分及挥发物含量测定》测定油茶籽初始干基含水率[27]，干基含水率 M_t 的计算式为

$$M_t=\frac{W_t-W_d}{W_d}\times100\% \tag{14}$$

式中W_t为t时刻油茶籽的质量，g；W_d为油茶籽的干物质质量，g。

单因素试验：根据热风干燥特性试验的结果，参考段续等[28]的研究，共设置前期风温、水分转换点（转换干燥风温时油茶籽的含水率）、后期风温 3 个因素，每一因素均设 5 组试验，风速均为 1.2 m/s。前期风温设置：设为 52、57、62、67、72 ℃，待油茶籽含水率降至 35% 时，将风温切换至后期风温 62 ℃ 进行后续干燥。后期风温设定：前期风温维持在 52 ℃，待含水率降至 35% 时，调整后期风温为 57、62、67、72、77 ℃，观察不同后期风温对干燥效果的影响。水分转换点设定：设置前期风温维持在 52 ℃，待含水率降至 20%、25%、30%、35%、40% 时，将风温切换至后期风温 62 ℃ 进行后续干燥。干燥的终点含水率设置为 10%，该烘箱油茶籽薄层干燥满载容量约为 3 400～3 800 g，取 3 600 g 计算。

Box-Behnken 试验：根据 Box-Behnken 试验设计原理，结合单因素试验数据分析结果，以前期风温、水分转换点、后期风温 3 个因素为自变量，研究其与单位能耗、干燥速率的关系，试验因素水平见表 2。

表 2　试验因素水平表

Table 2　Factors and levels of the test

水平 Levels	干燥前期风温 Drying air temperature in previous stage A/ ℃	水分转换点 Conversion point of moisture content B/%	干燥后期风温 Drying air temperature in late stage C/℃
−1	57	30	67
0	62	35	72
1	67	40	77

1.3　评价指标

1.3.1　干燥速率

干燥速率计算式为[29]

$$D_R = \frac{M_t - M_{t+\Delta t}}{\Delta t} \tag{15}$$

式中D_R为干燥速率，g/(g·h)；Δt为时间差，h；$M_{t+\Delta t}$为$t+\Delta t$时刻的干基含水率，%。

1.3.2　单位能耗

单位能耗定义为每去除 1 g 水分所需的能耗（kJ），按式（16）进行计算[30]。

$$W = \frac{3\,600 P_0 t}{m_1} \tag{16}$$

式中 W 为单位能耗，kJ/g；m_1 为脱水量，g；P_0 为功率，kW。

1.3.3　加权综合评分法

油茶籽变温干燥试验目的是探究一种既节能又快速的干燥工艺方案，故综合考虑单位能耗和干燥速率两个指标，并分别设置权值为 6 和 4，进行工艺优化。利用式（17）计算综合评分，设各指标最大值对应 100 分，最小值对应 0 分，而单位能耗越小越好，为了保证综合加权值越大越好，应将变化趋势越小越好的指标值转化为越大越好，因此在计算综合指标时应在单位能耗指标前加负号[31]。

$$\begin{cases} y'_{ij} = \dfrac{y_{ij} - y_{ijmin}}{y_{ijmax} - y_{ijmin}} \times 100\%,\ i = 1,2;\ j = 1,2,3,\cdots,n \\ y'_i = \sum w_i y'_{ij}, \qquad i = 1,2;\ j = 1,2,3,\cdots,n \end{cases} \tag{17}$$

式中y_{ij}为实际指标值；w_i为指标的加权系数；y'_{ij}为单个指标评分值；y'_i为综合评分值。

1.4　数据处理

采用 Excel、Origin 2022、Design-Expert 13.0 软件对试验数据进行分析处理和作图，用决定系数（R^2）来评价线性拟合的有效性[32]。

2　结果与分析

2.1　油茶籽热风干燥特性

2.1.1　不同热风温度下油茶籽的干燥特性

图 2 为油茶籽在 52、62 及 72 ℃ 不同干燥温度下的干燥特性曲线，描绘其含水率与干燥速率随时间的动态变化。在干燥前期，干燥速率随温度升高而显著加快，此现象归因于油茶籽表面温度的急剧提升，促进了表层水分的迅速汽化，形成了显著的温度梯度和湿度梯度，有效驱动了水分自内向外的高效迁移。在干燥后期阶段（M < 20%），不同温度下油茶籽的干燥速率趋于稳定并收敛至相近水平，表明温度对干燥速率的调控作用减弱，转而受物质传输阻力主导。在此阶段，水分蒸发界面深入内部，延长了迁移路径，从而限制了整体干燥速率的进一步提升。整个过程以降速干燥为主要特征，凸显了内部传质速率对干燥过程的控制作用[33]，故可采用式（8）测定油茶籽的有效水分扩散系数[34]。

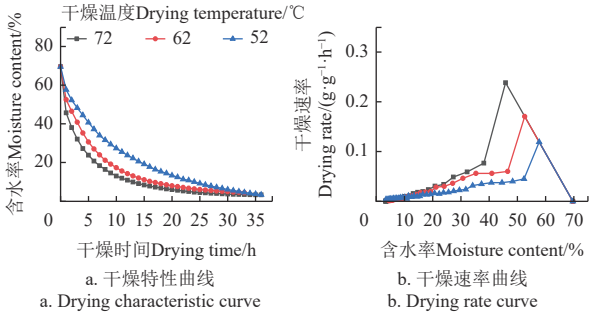

图 2　油茶籽在不同热风温度下的干燥特性曲线和干燥速率曲线

Fig.2　Drying characteristics and drying rate curves of *Camellia oleifera* seed at different hot air temperatures

2.1.2　油茶籽的有效水分扩散系数与干燥活化能

前述针对油茶籽的热风干燥试验数据，明确揭示了油茶籽干燥过程遵循典型的降速干燥动力学，由式（9）可知，干燥过程中水分比的对数$\ln M_R$与干燥时间t之间存在明确的线性相关性，如图 3 所示。

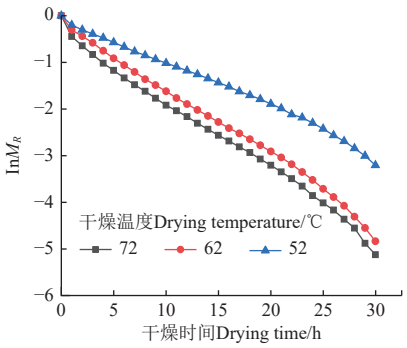

图 3　水分比对数与干燥时间的关系曲线

Fig.3　Relationship curve between the logarithm of moisture ratio (M_R) and drying time

通过将试验数据进行线性回归，可得斜率k，进而可得不同干燥温度条件下油茶籽的有效水分扩散系数。如表 3 所示，油茶籽的有效水分扩散系数展现出随干燥温度线性递增的趋势，且所有条件下的决定系数 R^2均超过 0.99，高度验证了线性回归模型与试验数据之间的紧密拟合性。温度的升高有效提升了水分子的平均热动能，加剧了分子间的碰撞频率与强度，这些微观层面的协同效应显著加速了油茶籽内部水分的扩散过程[35]；同时较高的干燥温度促使干燥介质的相对湿度下降，从而在油

茶籽与干燥介质界面间构建了更大的水蒸气分压差，这一物理驱动力进一步促进了水分的迁移与扩散速率。采用逆推法得到不同热风温度条件下油茶籽的有效水分扩散系数计算方程式。逆推法原理如下：在不同温度下进行油茶籽干燥试验，将试验数据绘制成干燥特性曲线（图 2），计算各热风温度下油茶籽的有效水分扩散系数（表 3），对式（11）两边取对数：

$$\ln D_{eff} = \ln D_0 - \frac{E_a}{R(T_a + 273.15)} \tag{18}$$

表 3 油茶籽有效水分扩散系数

Table 3 Effective moisture diffusivity of *Camellia oleifera* seed

温度 Temperature/℃	斜率 Slope k	有效水分扩散系数 Effective moisture diffusivity D_{eff}/(10^{-10} m^2·s^{-1})	决定系数 Coefficient of determination R^2
52	$-2.691\ 21\times10^{-5}$	3.299 4	0.991 94
62	$-4.075\ 36\times10^{-5}$	4.552 4	0.993 84
72	$-4.166\ 23\times10^{-5}$	5.582 6	0.995 41

基于试验测定的油茶籽有效水分扩散系数，进行线性回归可得$\ln D_{eff}$与$1/(T_a+273.15)$的线性函数为式（19），决定系数R^2为0.987 58，可得干燥活化能E_a=25.025 kJ/mol，有效扩散系数指前因子D_0=3.23×10^{-6} m^2/s。在干燥前期，油茶籽内部温度分布呈现显著的不均匀性，而试验数据表明油茶籽的有效水分扩散系数对干燥温度具有高度的敏感性，而干燥中后期，油茶籽内部温度逐渐趋近于干空气温度，为了降低干燥前期的模型误差，在模型求解时用油茶籽内部温度T替代 Arrhenius 关系式中干空气温度T_a得到式（20）。

$$\ln D_{eff} = -12.643 - \frac{3\,009.981}{(T_a + 273.15)} \tag{19}$$

$$D_{eff} = 3.23\times10^{-6}\exp\left(-\frac{25.025}{8.314\times10^{-3}(T+273.15)}\right) \tag{20}$$

2.2 油茶籽传热传质模型

2.2.1 油茶籽干燥模型验证

图 4 为油茶籽在 3 种不同热风干燥温度（55，65 和 75 ℃）条件下，油茶籽含水率的试验测定值与基于传热传质模型的预测值所构建的拟合曲线。

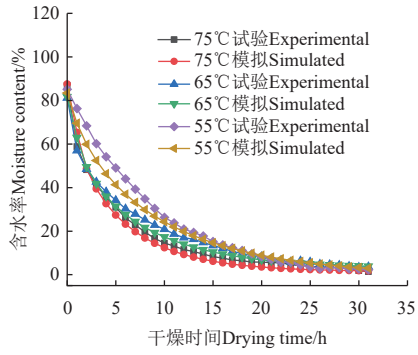

图 4 油茶籽模拟与试验的干燥曲线对比

Fig.4 Comparison of drying curves of *Camellia oleifera* seed simulation and experiment

基于油茶籽传热传质模型计算得出的含水率预测值与实测值在各个干燥阶段的变化趋势保持高度一致，且干燥后期拟合曲线与实测曲线的贴合度皆呈现出较高水平。在相同干燥时间跨度内，各温度条件下油茶籽干基含水率预测值与试验值之间的最大误差为 8.5%，这一误差水平低于数值模拟通常所要求的精度范围 15%[36]。因此，可以认为该油茶籽传热传质模型具备足够的精确度，足以满足数值模拟的需求，并能以此为基础，准确高效地预测和分析油茶籽在热风干燥过程中的水分变化规律。在此基础上，本研究将此模型应用于油茶籽干燥工艺的优化工作，旨在探索出一套既能降低干燥能耗又能提高干燥速率的干燥工艺方案。

2.2.2 干燥过程油茶籽温度梯度变化

为分析干燥过程油茶籽干燥模型中的温度和水分分布，图 5 为模型内部监测点的空间布局。图 6 为干燥温度设定为 62 ℃ 时，油茶籽干燥模型中内部各监测点的温度随时间变化的动态趋势。图 7 则通过不同干燥时刻（0、5、15、50、150、300 min）的截面图，直观地呈现了油茶籽内部温度分布的演变过程。

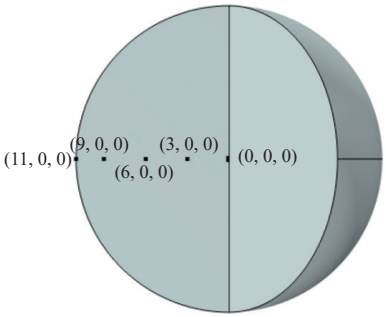

图 5 模型内部点位置分布图

Fig.5 Distribution of points inside the model

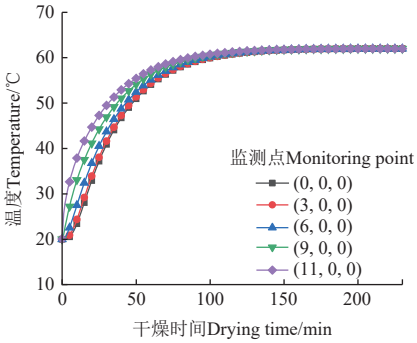

图 6 油茶籽内部不同位置点温度随干燥时间的变化

Fig.6 Changes of temperature in different positions of *Camellia oleifera* seed with drying time

综合图 6 与图 7 分析油茶籽内部温度随时间的演化规律：在干燥初期的 0～50 min 油茶籽内部温度经历了一个加速上升期，50～100 min 升温速率逐渐趋缓，当干燥时间超过 100 min后温度变化速率显著降低，进入一个近乎线性的缓慢增长阶段，直至 180 min 左右接近并稳定于预设的干燥温度 62 ℃，并在此后始终保持在这个水平附近。在干燥初期，油茶籽内部形成了显著的温度梯度，这一梯度于 6～16 min 之间达到峰值，约为 14 ℃，随后逐渐下降，直到 94 min 后降至 1 ℃ 以下，而在

156 min 之后，温度梯度进一步减小至小于 0.1 ℃，相对于油茶籽完整干燥周期（约 33 h），温度梯度持续的时间相对较短，而水分梯度的存在周期则明显更长，这表明在油茶籽的干燥过程中，水分的传递与扩散机制相较于热量的传递过程占据更为主导的地位，是控制干燥的关键因素。

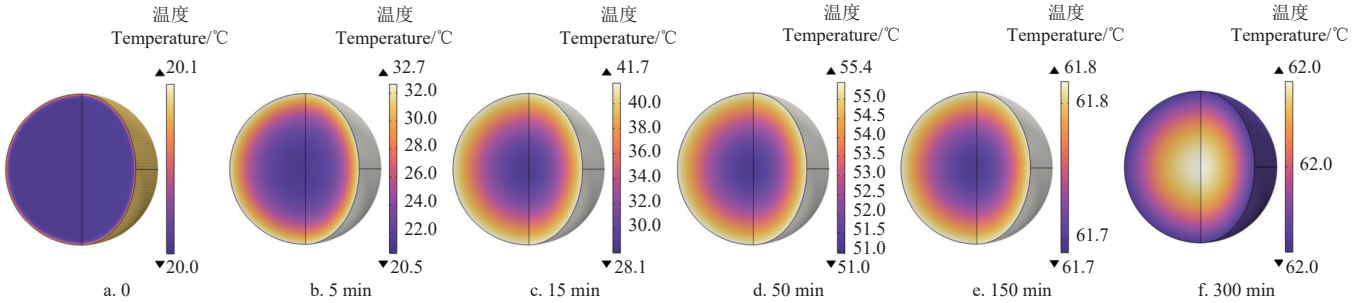

图 7　不同时刻油茶籽内部温度分布图

Fig.7　Internal temperature distribution of *Camellia oleifera* seed at different time

2.2.3　干燥过程油茶籽水分梯度变化

图 8 为干燥温度设定为 62 ℃ 时，油茶籽干燥模型中内部各监测点的水分随时间变化的动态曲线。图 9 则直观展示了在不同时间段（0、3、8、16、24、33 h）油茶籽内部水分的空间分布状态。结合两图深入分析，干燥初期油茶籽内部水分分布相对均匀，随着干燥进程深入，其内部水分展现出由核心向外围递减的规律性迁移，整体含水率持续下降，此趋势与热量自外向内的传递方向形成鲜明对比。油茶籽内部水分主要由自由态水与结合态水构成，自由水以其游离状态和高流动性为特征，易于脱除；而结合水则紧密依附于蛋白质及生物大分子，去除难度较大[23]。干燥初期，油茶籽内的自由水迅速扩散至表层并蒸发至环境，导致内部形成明显的水分梯度，含水率急剧下降。然而，随着干燥过程的持续进行，自由水占比逐渐减少，水分蒸发界面逐渐向内部推移，水分传递路径延长，进而引发干燥速率的减缓，这一过程深刻揭示了油茶籽干燥过程中水分迁移与蒸发机制的复杂性。

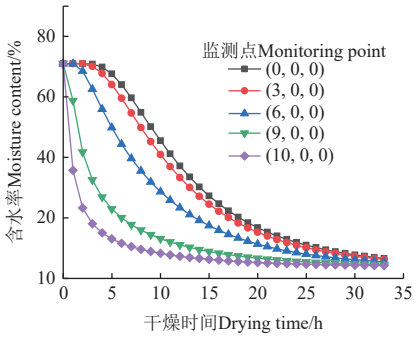

图 8　油茶籽内部不同位置点含水率随干燥时间的变化

Fig.8　Changes of moisture content in different positions of *Camellia oleifera* seed with drying time

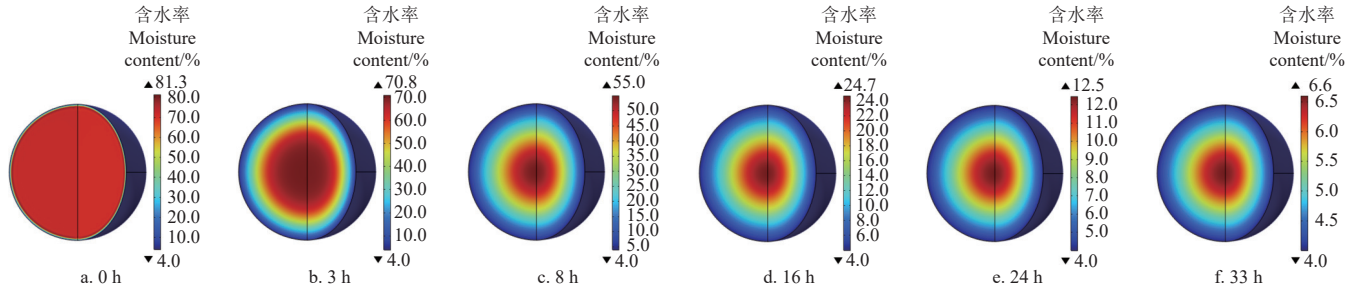

图 9　不同时刻油茶籽内部水分分布图

Fig.9　Internal moisture distribution of *Camellia oleifera* seed at different time

2.3　单因素试验

图 10a 为前期风温条件下的干燥曲线，图 10b 展示了单位能耗和干燥速率随前期风温（52～72 ℃）的变化趋势。在此范围内，随着干燥温度的升高，到达水分转换点所需的干燥时间缩短，由 238 min 缩短至 156 min，单位能耗则呈现出先减后增的趋势，在 62 ℃ 时达到最小值 1.88 kJ/g。干燥前期，油茶籽处于高含水率状态，此时水分的结合能相对较低，无需较高的干燥温度也可维持比较高的干燥速率，如图 10b 所示，相对于后期风温条件下进行干燥（图 11b），各前期风温条件下油茶籽的干燥速率均保持在较高水平。干燥过程中的前期阶段虽耗时较短，但大部分的水分是在这一阶段被去除的，故将单位能耗作为重要指标，选取 62 ℃ 作为前期风温的较优水平。

图 11a 为后期风温条件下的干燥曲线，图 11b 展示了单位能耗和干燥速率随后期风温（57～77 ℃）的变化趋势。如图 11a 所示，随着后期风温的逐步升高，由水分转换点到干燥终点含水率所需的干燥时间由 827 min 缩短至 505 min，单位能耗呈现出与前期风温相同的趋势，在 72 ℃ 时达到最小值 8.54 kJ/g，表明在干燥后期选择恰当的风温不仅能够提高干燥效率，且能有效降低能耗。鉴于强结合水在高温条件下相较于低温更易实现蒸发，故在干燥后期应适度提升热风温度，增大干燥速率，有效缩短干燥周期并降低单位能耗，综上选取 72 ℃ 作为

后期风温的较优水平。

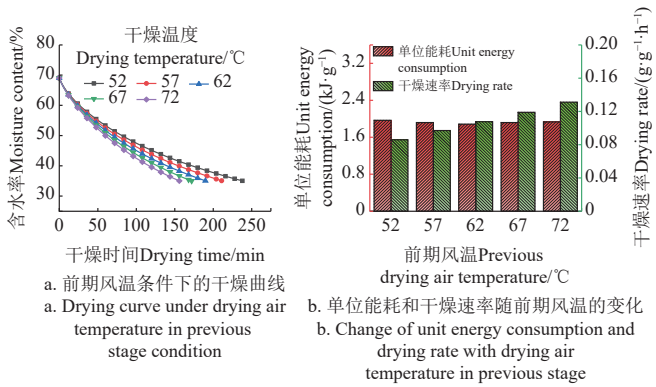

a. 前期风温条件下的干燥曲线 a. Drying curve under drying air temperature in previous stage condition

b. 单位能耗和干燥速率随前期风温的变化 b. Change of unit energy consumption and drying rate with drying air temperature in previous stage

图 10 前期风温条件下的干燥特性与能耗分析

Fig.10 Analysis of drying characteristics and energy consumption with drying air temperature in previous stage

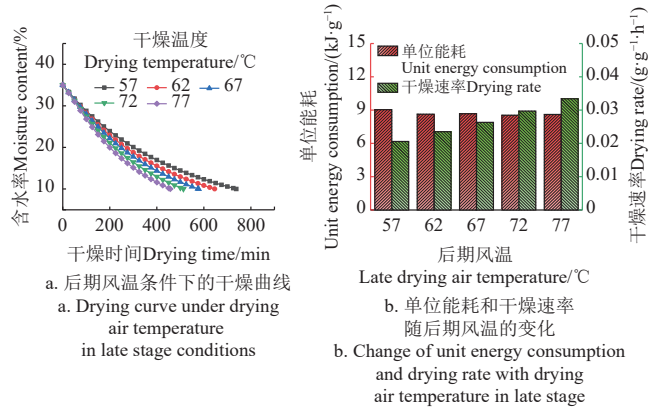

a. 后期风温条件下的干燥曲线 a. Drying curve under drying air temperature in late stage conditions

b. 单位能耗和干燥速率随后期风温的变化 b. Change of unit energy consumption and drying rate with drying air temperature in late stage

图 11 后期风温条件下的干燥特性与能耗分析

Fig.11 Analysis of drying characteristics and energy consumption with drying air temperature in late stage

图 12 展示了单位能耗与干燥速率随水分转换点变化的趋势。单位能耗随水分转换点的增大而逐渐下降，前期风温水分转换点的高低直接影响风温转换时机，而水分转换点越高，风温便越快转换为后期风温，增大干燥速率，进而压缩干燥周期。

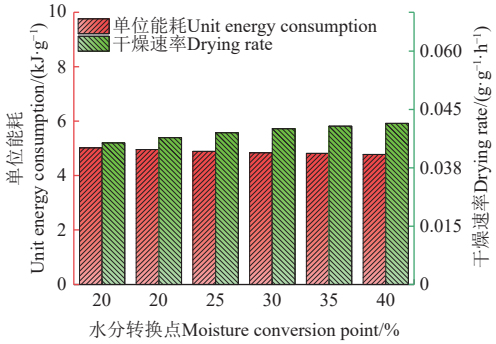

图 12 单位能耗和干燥速率随水分转换点的变化

Fig.12 Change of unit energy consumption and drying rate with moisture conversion point

水分转换点的选择并非没有限制，过低的水分转换点会导致油茶籽在相对较低的前期风温条件下干燥过久，而随着干燥进程的深入，油茶籽水分的结合能升高，低温不能提供足够的去水势能，干燥变得极为缓慢，单位能耗也随之大幅上升；而过高的水分转换点会导致油茶籽在后期风温条件下经历较长时间的干燥，固然能够提高干燥速率，但是持续高温干燥环境容易引发美拉德反应以及苯并芘含量超标[37]。综合考虑，选取 35% 作为水分转换点的较优水平。

2.4 Box-Behnken 试验

2.4.1 试验结果

结合单因素试验数据分析结果，本研究采用响应面法深入分析了前期风温（*A*）、水分转换点（*B*）和后期风温（*C*）水平对单位能耗和干燥速率的影响，并基此进行优化设计，试验结果见表 4。

表 4 响应面试验设计与结果

Table 4 Design and results of response surface test

试验号 Test No.	*A*	*B*	*C*	单位能耗 Unit energy consumption/(kJ·g^{-1})	干燥速率 Drying rate /(g·g^{-1}·h^{-1})	综合评分值 Comprehensive score
1	0	1	1	4.684 6	0.057 15	24.25
2	−1	0	−1	4.769 0	0.045 43	−60
3	0	0	0	4.661 2	0.052 11	20.17
4	1	−1	0	4.657 7	0.052 57	23.63
5	−1	−1	0	4.805 3	0.047 37	−73.1
6	0	0	0	4.681 3	0.051 50	7.37
7	1	0	−1	4.712 7	0.048 41	−19.83
8	0	0	0	4.677 7	0.050 84	7.10
9	0	1	−1	4.702 7	0.047 50	−17.44
10	1	1	0	4.659 1	0.053 37	25.48
11	0	−1	1	4.726 6	0.053 85	−9.27
12	0	0	0	4.662 0	0.051 21	16.79
13	−1	1	0	4.697 5	0.050 77	−3.81
14	1	0	1	4.707 0	0.057 52	13.40
15	−1	0	1	4.728 0	0.053 85	−10.04
16	0	0	0	4.689 9	0.052 50	6.03
17	0	−1	−1	4.717 0	0.046 56	−28.24

表 5 为单指标回归方程分析结果，单位能耗回归方程的显著性 *F* 值为 7.1，干燥速率回归方程的显著性 *F* 值为 108.31，这两项 *F* 值所对应的 *P* 值皆小于 0.01，充分证明两个模型均具备有极高的统计显著性。Y_1 模型（单位能耗模型）的决定系数 R^2=0.901 3，失拟项的 *F* 值为 5.66，对应的 *P* 值为 0.063 7；Y_2 模型（干燥速率模型）的决定系数 R^2=0.984 8，失拟项的 *F* 值为 0.394 8，对应的 *P* 值为 0.851 6，说明两个模型的拟合度良好，能够准确地预测单位能耗以及干燥速率。此外，前期风温（*A*）、水分转换点（*B*）和后期风温（*C*）对单位能耗的影响从大到小为 *A*、*B*、*C*，且平方项的影响程度大小依次为 C^2、A^2、B^2，交互作用影响的主次顺序为 *AB*、*AC* 、*BC*；对干燥速率的影响从大到小为 *C*、*A*、*B*，交互作用影响的主次顺序为 *AB*、*BC*、*AC*。

以综合评分值为响应变量，采用 Design-Expert 13.0 软件对试验结果进行回归分析，得到综合评分值的二次多项式回归方程为式（21），方差分析结果见表 6。该模型中 *F* 值为 12.02，*P* 值小于 0.01，表明模型极显著，模型的决定系数 R^2=0.939 2，失拟项的 *F* 值为 6.41，对应的 *P* 值为 0.052 3，说明回归模型与数据拟合程度较好，可以用该模型对综合评分值进行预测。由模型均值 *F* 检验可得前期风温（*A*）、水分转换点（*B*）和后期风温（*C*）对综合评分值的影响从大到小为 *A*、*C*、*B*，二次

项影响大小为 C^2、A^2、B^2，交互作用影响的主次顺序为 AB、BC、AC。

$$Y = 10.49 + 23.94A + 14.58B + 18.03C - 17.05AB + 4.24AC + 5.74BC - 14.29A^2 - 2.70B^2 - 15.03C^2 \quad (21)$$

表 5　单指标回归方程

Table 5　Single index regression equation

指标 Index	模拟方程 Simulation equation	方程 Equation		失拟项 Lack of fit		校正决定系数 Correction coefficient of determination R^2_{adj}
		F 值 F value	P 值 P value	F 值 F value	P 值 P value	
单位能耗 Unit energy consumption	$Y_1 = 4.68 - 0.032\,9A - 0.020\,4B - 0.006\,9C + 0.027\,3AB + 0.008\,8AC - 0.006\,9BC + 0.025\,1A^2 - 0.003\,5B^2 + 0.027\,8C^2$	7.1	0.008 5	5.66	0.063 7	0.901 3
干燥速率 Drying rate	$Y_2 = 0.051\,3 + 0.001\,806A + 0.001\,055B + 0.004\,31C - 0.000\,65AB + 0.000\,173AC + 0.000\,59BC$	108.31	<0.000 1	0.394 8	0.851 6	0.984 8

表 6　综合评分值方差分析结果

Table 6　ANOVA table of comprehensive score regression equation

方差来源 Source of variance	平方和 Sum of squares	自由度 Degree of freedom	均方 Mean square	F 值 F value	P 值 P value	显著性 Significance
模型 Model	12 241.87	9	1 360.21	12.02	0.001 7	**
A	4 583.55	1	4 583.55	40.49	0.000 4	**
B	1 700.03	1	1 700.03	15.02	0.006 1	**
C	2 599.57	1	2 599.57	22.97	0.002 0	**
AB	1 163.49	1	1 163.49	10.28	0.014 9	*
AC	72	1	72	0.636 0	0.451 4	
BC	131.56	1	131.56	1.16	0.316 7	
A^2	860.26	1	860.26	7.60	0.028 2	*
B^2	30.61	1	30.61	0.270 4	0.619 1	
C^2	951.64	1	951.64	8.41	0.023 0	*
残差 Residual	792.36	7	113.19			
失拟项 Lack of fit	655.87	3	218.62	6.41	0.052 3	
纯误差 Pure error	136.48	4	34.12			
总计 Total	13 034.23	16				
系数 Coefficient	R^2=0.939 2，;R^2_{adj}=0.861 1					

注：** 表示差异极显著，* 表示差异显著。

Note: ** indicates extremely significant difference, * indicates significant difference.

采用方差分析（ANOVA）统计方法，借助软件对数据进行深入剖析，通过模型适配与参数调优，得到油茶籽变温干燥工艺的最优参数组合为：前期风温 63.674 ℃、水分转换点 38.478 %、后期风温 74.787 ℃。为保证这些工艺参数能在实际生产中得以顺利实施，并兼顾操作的便利性与生产实际的可操作性，对上述优化工艺参数进行适度微调，将优化工艺参数调整为前期风温 63.7 ℃、水分转换点 38.5 %、后期风温 74.8 ℃，预测单位能耗为 4.667 kJ/g，干燥速率为 0.055 g/(g·h)，综合评分值为 28.62。在此条件下进行实际烘箱干燥验证，验证结果为单位能耗为 5.040 kJ/g，干燥速率为 0.048 g/(g·h)，相对误差分别为 7.4% 和 12.1 %，均在可接受的误差范围内，鉴于数值模拟通常基于理想化假设，而实际操作中难免受到环境条件波动、设备性能限制及样品预处理差异等多重因素的影响，此类偏差符合预期。因此，尽管实测单位能耗略高于预测值，干燥速率略低于预测，但总体上验证了该干燥工艺对于油茶籽干燥的有效性与适用性。

3　结　论

1）油茶籽热风干燥过程主要由内部传质过程控制，水分梯度存在的时间远远大于温度梯度，在不同干燥温度条件下的热风干燥速率变化趋势相似。在 52～72 ℃的温度区间内，油茶籽的有效水分扩散系数范围为 $3.299\,4\times10^{-10}$～$5.582\,6\times10^{-10}$ m^2/s，随温度的升高而增大，其活化能为 25.025 kJ/mol。

2）构建的油茶籽传热传质数学模型能够有效预测干燥过程中油茶籽内部的水分和温度分布，模型精度较高，模型预测得到的干基含水率与试验值之间的最大误差不超过 8.5%。

3）通过对干燥工艺参数进行优化，确定了最佳的前期风温为 63.7 ℃、水分转换点 38.5 %、后期风温 74.8 ℃。在此工艺条件下，实际烘箱验证结果为单位能耗为 5.040 kJ/g，干燥速率为 0.048 g/(g·h)。在保证干燥速率的同时降低能耗，在油茶籽干燥的效率与节能之间取得了良好的平衡与优化。

［参　考　文　献］

[1] 莫燕婷，曹清明. 油茶籽油中组成成分及其影响因素研究进展[J]. 粮食与油脂，2023，36（9）：10-13.
MO Yanting, CAO Qingming. Research progress on the composition of oil-teac amellia seed oil and its influencing factors[J]. Cereals & Oils, 2023, 36(9): 10-13. (in Chinese with English abstract)

[2] 王志贤，赵洲桥，孙乐，等. 不同干燥方式对油茶籽油品质的影响[J]. 粮食与食品工业，2024，31(1)：1-5.
WANG Zhixian, ZHAO Zhouqiao, SUN Le, et al. Effect of different drying methods on the quality of camellia seed oil[J]. Cereal & Food Industry, 2024, 31(1): 1-5. (in Chinese with English abstract)

[3] 赵海瑞，滕兆丽，杨浩勇，等. 油茶果干燥特性及烘干脱蒲技术[J]. 农业工程，2021，11(10)：61-67.
ZHAO Hairui, TENG Zhaoli, YANG Haoyong, et al. Drying characteristics of *Camellia oleifera* fruit and shelling technologies[J]. Agricultural Engineering, 2021, 11(10): 61-67. (in Chinese with English abstract)

[4] 粟振灿，郭志中，黎瑞荣. 广西山茶果脱蒲技术的研究现状及对策[J]. 南方农机，2023，54(7)：62-65.
SU Zhencan, GUO Zhizhong, LI Ruirong. The present research status and strategy exploration of the skinning exocarp technology for camellia fruit in Guangxi[J]. China Southern Agricultural Machinery, 2023, 54(7): 62-65. (in Chinese with English abstract)

[5] 李长友. 干燥物系解析理论研究进展[J]. 农业工程学报，2024，4(6)：1-13.
LI Changyou. Research progress in analytical theory of drying system[J]. Transactions of the Chinese Society of Agricultural

Engineering (Transactions of the CSAE), 2024, 4(6): 1-13. (in Chinese with English abstract)
[6] 李长友. 干燥物系的特征函数及其理论解[J]. 农业工程学报，2020，36(12)：286-295.
LI Changyou. Characteristic functions of drying material system and its theoretical solution[J]. Transactions of the Chinese Society of Agricultural Engineering (Transactions of the CSAE), 2020, 36(12): 286-295. (in Chinese with English abstract)
[7] 张艳珍，谢永康，王菲，等. 不同干燥方式对羊肚菌品质特性的影响[J]. 农业工程学报，2024，40(6)：111-119.
ZHANG Yanzhen, XIE Yongkang, WANG Fei, et al. Effects of different drying methods on the quality characteristics of *Morchella*[J]. Transactions of the Chinese Society of Agricultural Engineering (Transactions of the CSAE), 2024, 40(6): 111-119. (in Chinese with English abstract)
[8] 何婷，张睿，任广跃，等. 机械破壳机结构、工作原理及应用[J]. 食品与机械，2023，39(7)：215-222.
HE Ting, ZHANG Rui, REN Guangyue, et al. Structure, working principle and application of mechanical shell breaker[J]. Food & Machinery, 2023, 39(7): 215-222. (in Chinese with English abstract)
[9] 吴均毅，王毅，熊平原，等. 油茶果机械化脱壳装置研究现状及展望[J]. 食品与机械，2023，39(8)：208-217.
WU Junyi, WANG Yi, XIONG Pingyuan, et al. Research status and prospect of mechanized hulling device for *Camellia oleifera* fruit[J]. Food & Machinery, 2023, 39(8): 208-217. (in Chinese with English abstract)
[10] 杨友志，陈劲松，吴丹，等. 鲜油茶果快速制油工艺研究[J]. 中国油脂，2024，49(1)：7-10.
YANG Youzhi, CHEN Jinsong, WU Dan, et al. Rapid oil production technology of fresh *Camellia oleifera* fruit[J]. China Oils and Fats, 2024, 49(1): 7-10. (in Chinese with English abstract)
[11] 田潇潇，方学智，刘四黑，等. 脱蒲处理对油茶籽油营养品质及抗氧化能力的影响[J]. 中国粮油学报，2020，35(11)：98-103.
TIAN Xiaoxiao, FANG Xuezhi, LIU Sihei, et al. Effects of shelling treatment on nutritional qualities and antioxidant properties of oil-tea camellias seed oil[J]. Journal of the Chinese Cereals and Oils, 2020, 35(11): 98-103. (in Chinese with English abstract)
[12] 曾艳玲，颜亚丹，谭晓风，等. 采后晾晒对油茶种仁油脂产量及组分的影响[J]. 植物生理学报，2018，54(2)：316-324.
ZENG Yanling, YAN Yandan, TAN Xiaofeng, et al. Effect of air-drying on seed oil yield and component of *Camellia oleifera* after harvest[J]. Plant Physiology Journal, 2018, 54(2): 316-324. (in Chinese with English abstract)
[13] 兰峰，苏子昊，邹和东. 油茶果脱蒲清选技术进展[J]. 南方林业科学，2020，48(4)：46-51.
LAN Feng, SU Zihao, ZOU Hedong. Development on shelling and sorting technology of *Camellia oleifera* fruit[J]. South China Forestry Science, 2020, 48(4): 46-51. (in Chinese with English abstract)
[14] KURPASKA S, LATAA H, KIEBASA P, et al. Experimental and modeling approach to heat and mass transfer in a porous bed of a rock-bed heat accumulator[J]. International Journal of Heat and Mass Transfer, 2021, 179(2): 121654.
[15] CRANK J. The mathematics of diffusion[M]. Oxford: Oxford University Press, 1979.
[16] 张继凯，郑霞，肖红伟，等. 山药片红外联合热风干燥热质传递收缩模拟与品质[J]. 农业工程学报，2024，40(6)：134-145.
ZHANG Jikai, ZHENG Xia, XIAO Hongwei, et al. Simulation of heat and mass transfer shrinkage and quality of yam slices dried using infrared combined hot air[J]. Transactions of the Chinese Society of Agricultural Engineering (Transactions of the CSAE), 2024, 40(6): 134-145. (in Chinese with English abstract)
[17] NSIBI C, LAJILI M. Experimental study and mathematical modeling under various hot-air drying conditions of thin layer olive pomaces [J]. Processes. 2023; 11(9): 2513.
[18] TOPUZ F C, BAKKALBA E, ALDEMIR A, et al. Drying kinetics and quality properties of Mellaki (*Pyrus communis* L.) pear slices dried in a novel vacuum-combined infrared oven[J]. Journal of Food Processing and Preservation, 2022, 46(10): e16866.
[19] TAN S, MIAO Y W, ZHOU C B, et al. Effects of hot air drying on drying kinetics and anthocyanin degradation of blood-flesh peach [J]. Foods. 2022, 11(11): 1596.
[20] 李立君，周健. 油茶果微波爆壳的特性研究[J]. 中南林业科技大学学报，2011，31(11)：49-52.
LI Lijun, ZHOU Jian. Analysis of *Camellia oleifera* cracking properties by micro-wave[J]. Journal of Central South University of Forestry & Technology, 2011, 31(11): 49-52. (in Chinese with English abstract)
[21] ÇENGEL Y A. Heat and mass transfer: A practical approach[M]. Singapore: McGraw Hill, 2006.
[22] 魏硕，陈鹏枭，谢为俊，等. 基于三维湿热传递的玉米籽粒干燥应力裂纹预测[J]. 农业工程学报，2019，35(23)：296-304.
WEI Shuo, CHEN Pengxiao, XIE Weijun, et al. Prediction of stress cracks in corn kernels drying based on three-dimensional heat and mass transfer[J]. Transactions of the Chinese Society of Agricultural Engineering (Transactions of the CSAE), 2019, 35(23): 296-304. (in Chinese with English abstract)
[23] CHEN P X, CHEN N, ZHU W X, et al. A heat and mass transfer model of peanut convective drying based on a two-component structure[J]. Foods, 2023, 12(9): 1823.
[24] CHEN H Q, MARKS B P, MURPHY R Y. Modeling coupled heat and mass transfer for convection cooking of chicken patties[J]. Journal of Food Engineering, 1999, 42(3): 139-146.
[25] 李长友. 粮食干燥解析法[M]. 北京：科学出版社，2018：17-18.
[26] 马云海. 农业物料学[M]. 北京：化学工业出版社，2022：14-15.
[27] 郭劲廷，张立伟，罗质，等. 焙炒工艺对葵花籽仁油风味及微观结构的影响[J]. 粮食与油脂，2024，37(2)：74-80.
GUO Jinting, ZHANG Liwei, LUO Zhi, et al. Effect ofroasting technology on flavor and microstructure of sunflowerseed kernel oil[J]. Cereals &Oils, 2024, 37(2): 74-80. (inChinese with English abstract)
[28] 段续，徐一铭，任广跃，等. 香菇分段变温红外喷动床干燥工艺参数优化[J]. 农业工程学报，2021，37(19)：293-302.
DUAN Xu, XU Yiming, REN Guangyue, et al. Optimization of the drying process parameters for lentinus edodes in segment variable temperature infrared assisted spouted bed[J]. Transactions of the Chinese Society of Agricultural Engineering (Transactions of the CSAE), 2021, 37(19): 293-302. (in Chinese with English abstract)
[29] 代建武，周厚彬，黄杰，等. 不同干燥方式对红托竹荪干燥特性和品质的影响[J]. 农业工程学报，2024，40(6)：90-100.
DAI Jianwu, ZHOU Houbin, HUANG Jie, et al. Effects of different drying technologies on the drying characteristics and quality of *Dictyophora rubrovolvata*[J]. Transactions of the Chinese Society of Agricultural Engineering (Transactions of the CSAE), 2024, 40(6): 90-100. (in Chinese with English

abstract)
[30] 段续，李格格，李琳琳，等. 基于转换点调控的怀山药多相态微波干燥及品质特性[J]. 农业工程学报，2024，40(2)：134-143.
DUAN Xu, LI Gege, LI Linlin, et al. Multiphase microwave drying and quality characteristics of Chinese yam based on conversion point regulation[J]. Transactions of the Chinese Society of Agricultural Engineering (Transactions of the CSAE), 2024, 40(2): 134-143. (in Chinese with English abstract)
[31] 张迎敏，任广跃，段续，等. 红薯叶复合面条热泵-热风联合干燥特性及干燥模型建立[J]. 中国粮油学报，2022，37(4)：15-24.
ZHANG Yingmin, REN Guangyue, DUAN Xu, et al. Analysis of heat pump-hot air combined drying characteristics and water migration of sweet potato leaf compound noodles[J]. Journal of the Chinese Cereals and Oils Association, 2022, 37(4): 15-24. (in Chinese with English abstract)
[32] QIU F, SHEN X J, ZHOU C, et al. Rice ears detection method based on multi-Scale image recognition and attention mechanism[J]. IEEE Access, 2024, 12: 68637-68647.
[33] 满晓兰，李龙，张宏，等. 基于结构异质性的核桃热风干燥特性及数学模型[J]. 江苏农业学报，2021，37(3)：731-738.
MAN Xiaolan, LI Long, ZHANG Hong, et al. Hot-air drying characteristics and mathematical model of walnut based on structural heterogeneity[J]. Jiangsu Journal of Agricultural Sciences, 2021, 37(3): 731-738. (in Chinese with English abstract)
[34] CHEN C, VENKITASAMY C, ZHANG W P, et al. Effective moisture diffusivity and drying simulation of walnuts under hot air[J]. International Journal of Heat and Mass Transfer, 2020, 150: 1-10.
[35] 耿智化，李孟卿，朱丽春，等. 基于控温控湿的沙棘红外联合热风干燥均匀性与工艺[J]. 农业工程学报，2024，40(6)：120-133.
GENG Zhihua, LI Mengqing, ZHU Lichun, et al. Drying uniformity and technology of sea buckthorn with infrared combined hot air vir temperature and humidity control[J]. Transactions of the Chinese Society of Agricultural Engineering(Transactions of the CSAE), 2024, 40(6): 120-133. (in Chinese with English abstract)
[36] LI C J, CHEN Y F , FANG Z D, et al. Exergy analysis and optimisation of an industrial-scale circulation counter-flow paddy drying process[J]. Energy, 2022, 251: 123901.
[37] 周兴旺，杨代明，冯敏，等. 降低压榨油茶籽油中苯并芘含量关键加工技术的研究[J]. 粮食科技与经济，2013，38(5)：47-49,60.
ZHOU Xingwang, YANG Daiming, FENG Min, et al. Study of key processing technology for reducing benzo pyrene content in traditional pressed *Camellia oleifera* seed oil[J]. Grain Science and Technology and Economy, 2013, 38(5): 47- 49,60. (in Chinese with English abstract)

Heat and mass transfer characteristics and drying process optimization of *Camellia oleifera* seeds after hot air drying and shelling of the fruits

HUANG Jianjiang[1] , GUO Ziyang[1] , LI Shengtao[1] , ZHANG Ye[1] , LI Changyou[1] , LI Tao[2] , LI Chengjie[1※]

(1. *College of Engineering*, *South China Agricultural University*, *Guangzhou* 510642, *China*;　2. *College of Engineering*, *Jiangxi Agricultural University*, *Nanchang* 330000, *China*)

Abstract: This study aims to elucidate the dynamics of moisture and temperature alterations in *Camellia oleifera* seeds during hot air drying and subsequent bursting. A systematic investigation was carried out to optimize the parameters for superior drying. The exceptional energy efficiency was characterized by minimizing energy consumption. The physical attributes of *Camellia oleifera* seeds were measured to determine their inherent properties, including thermal conductivity and density. The thermodynamic behavior of *Camellia oleifera* seeds was explored during drying at distinct temperature intervals of 52, 62, and 72 °C. According to Fick's Second Law, the effective moisture diffusion was then obtained corresponding to each temperature regime. An Arrhenius equation model was constructed in the empirically derived data on effective moisture diffusivity using reverse engineering. There was a significant correlation between effective moisture diffusivity, drying temperature, and activation energy. At the same time, a mathematical framework was designed to combine the heat and mass transfer, in order to simulate the drying of *Camellia oleifera* seeds. The predictions exhibited striking consistency with the experiments, with a maximum error of 8.5%, indicating the remarkable precision and reliability of the model. The results show that the hot-air drying dynamics of *Camellia oleifera* seeds were fundamentally dominated by internal mass transfer. The higher moisture gradients were observed than those of temperature ones. The fluctuation of drying rates shared a uniform pattern over the varying drying temperatures. The effective moisture diffusivity of *Camellia oleifera* seeds increased significantly over the temperature spectrum from 52 °C to 72 °C, ranging from 3.299 4×10-10−5.582 6×10-10 m^2/s. The energetic transformations were computed as the activation energy of 25.025 kJ/mol during drying. Therefore, the variable temperature drying was performed better for *Camellia oleifera* seeds. There was the governing impact of three parameters— the initial wind temperature, the moisture conversion threshold, and the concluding wind temperature on specific energy consumption and drying velocity. Response surface optimization was applied to determine the optimal combination of drying parameters: an initial wind temperature of 63.7 °C, a moisture conversion point of 38.5%, and a terminal wind temperature of 74.8 °C. The better performance was achieved under these optimal conditions. Specific energy consumption was reduced to 5.040 kJ/g and a drying rate peaking at 0.048 g/(g·h). Compared with the model, relative errors for specific energy consumption and drying rate were 7.4% and 12.1%, respectively, indicating the pragmatic applicability and accuracy of the optimized parameters. In summary, a robust theoretical groundwork was offered to refine the practical drying parameters for *Camellia oleifera* fruit hot air drying and bursting, paving the way for industrial implementation and dissemination of *Camellia oleifera* fruit drying. Thus, considerable academic significance was provided for the promising practical application.

Keywords: process optimization; models; *Camellia oil*; shelling; heat and mass transfer; hot air drying

全国中文核心期刊 | 主管单位：中国兵器装备集团有限公司 | 主办单位：中国兵器装备集团西南技术工程研究所

包装工程

Packaging Engineering

2024年11月 第45卷 第21期

/ 封 面 文 章 /

放射性物品运输容器栓系系统安全分析方法探究

作者：张煜航，庄大杰,*，孙谦，王长武，李国强
单位：中国辐射防护研究院

ISSN 1001-3563
CN 50-1094/TB

包装工程
BAOZHUANG GONGCHENG
第45卷 第21期 2024年11月10日

目次

放射性物品运输包装容器专题

先进材料

期刊基本参数：CN 50-1094/TB*1980*s*A4*273*zh*P*￥45.00*3000*36*2024-11

包装工程

Packaging Engineering

全国中文核心期刊

主管单位:中国兵器装备集团有限公司
主办单位:中国兵器装备集团西南技术工程研究所

ISSN 1001-3563
CN 50-1094/TB
定价：45.00元

邮发代号：78-30
国外发行号：BM1799

ISSN 1001-3563
21>
9 771001 356243

基于响应面的白萝卜热风干燥品质及工艺研究

张烨，莫豪裕，江伟檀，李圣陶，黄建江，王晗，李成杰*
（华南农业大学 工程学院，广州 510642）

摘要：目的 探究不同工艺条件下白萝卜热风干燥品质和效率的变化。**方法** 采用单因素试验方法，研究了干燥温度、相对湿度、物料厚度对白萝卜的品质、干燥特性的影响规律；以复水比、色泽、干燥时间为评价指标，对数据进行归一化处理，然后构建综合评分模型；采用 Box-Behnken 响应面法进行优化试验，将综合评分作为响应值建立回归模型，得到干燥品质最佳、干燥用时最短的工艺参数组合。**结果** 在干燥温度 55 ℃、相对湿度 23%、物料厚度 10 mm 的条件下，白萝卜的干燥时间为 490 min，复水比为 3.851，色差为 25.724，综合评分为 0.953，干燥效果最佳，说明采用该干燥工艺参数能够有效提高干燥品质，缩短干燥时间；拟合模型的 R^2 为 0.957 1，实际值与模型理论值之间的误差仅为 1.4%，表明模型稳定可靠，适用于白萝卜热风干燥。**结论** 基于响应面优化获得的最优工艺参数及回归模型，能更好地预测白萝卜在不同工艺条件下的干燥特性变化，有效提升了干燥效果，为白萝卜热风干燥工业化应用和高品质储存提供了理论基础。

关键词：白萝卜；响应面法；工艺参数优化；干燥特性；品质
中图分类号：TS255.3 **文献标志码：**A **文章编号：**1001-3563(2024)21-0147-11
DOI：10.19554/j.cnki.1001-3563.2024.21.021

Hot-air Drying Quality and Process of White Radish Based on Response Surface

ZHANG Ye, *MO Haoyu*, *JIANG Weitan*, *LI Shengtao*, *HUANG Jianjiang*, *WANG Han*, *LI Chengjie**
(College of Engineering, South China Agricultural University, Guangzhou 510642, China)

ABSTRACT: The work aims to investigate the changes in quality and efficiency of white radish dried by hot air under various processes. The effect law of three variables including drying temperature, relative humidity, and material thickness on the quality and drying characteristics of white radish was analyzed with the single-factor experimental method. Quality and efficiency indicators such as rehydration ratio, color difference, and drying time were normalized to construct a comprehensive evaluation model. Subsequently, the Box-Behnken response surface methodology was adopted to facilitate the optimization experiments, and a regression model was developed with the comprehensive score as the response variable. This model helped identify the optimal combination of process parameters that yielded the best drying quality and shortest drying time. The optimal conditions were found to be drying temperature of 55 °C, relative humidity of 23%, and material thickness of 10 mm. Under these conditions, the drying time was 490 min, the rehydration ratio was 3.851, the color difference was 25.724, and the comprehensive score was 0.953, indicating an optimal drying effect. These drying process parameters could effectively improve the drying quality and shorten the drying time. The R^2 value of the fitting model was 0.954 1 and the error between the actual value and the theoretical value of the model was only 1.4%, confirming the stability and reliability of the model for application in hot-air drying processes of white radish. The optimal process parameters and the regression model optimized based on response surface can effectively predict changes

收稿日期：2024-07-01
基金项目：国家自然科学基金（32171906）；广州市科技计划（2024A0J3960）
*通信作者

in drying characteristics under various conditions, thereby improving the drying effect of white radish and providing a theoretical basis for the industrial application and high-quality storage of hot-air drying of white radish.

KEY WORDS: white radish; response surface method; process parameter optimization; drying characteristics; quality

白萝卜（*Raphanus sativus*）为十字花科萝卜属植物[1]，富含膳食纤维、胡萝卜素等营养物质，具有一定的食用价值和药用价值[2]。在广东潮汕地区，将白萝卜干燥去水后再腌制而成的特色美食——菜脯具有独特风味和营养价值，从而广受消费者的好评。在菜脯的生产过程中，干燥脱水有助于促进食盐在其组织内的渗透和扩散，以此保证腌制品质[3]。传统的自然晾晒去水方式严重依赖生产经验，且易受到环境因素的影响，导致其干燥品质不稳定，生产效率低下。随着消费市场对产品质量和卫生要求的不断提高，农产品脱水方式也正逐步由自然晾晒向机械化干燥发展[4]。探索先进的干燥工艺代替传统晾晒，解决菜脯干燥去水耗时长、品质低等问题，对于菜脯等腌制品的生产具有重要意义。

常见的机械干燥方法包括热风干燥[5]、热泵干燥[6]、饱和蒸汽联合热泵干燥[7]、红外联合热风干燥[8]、真空干燥[9]、微波干燥[10]等。对于拥有一定食用及药用价值但价格廉价的白萝卜，通常采用热风干燥方式[11]，这种干燥效果受到温度、相对湿度、物料厚度等多种因素的影响。目前，国内外学者研究了黄姜[12]、香菇[13]、火龙果[14]、枣果[15]、香蕉[16]等物料的干燥特性，针对白萝卜的热风干燥品质和工艺优化的相关研究相对较少。刘盼盼[17]研究了不同干燥组合方式对白萝卜干燥特性及品质的影响，发现饱和蒸汽联合热泵的干燥方法能促进水分的扩散，有效提高干燥速率和品质，降低干燥能耗。韦强等[4]在研究仅考虑热风干燥温度对脱水白萝卜干燥品质的影响时发现，在干燥温度为 70 ℃时，干燥速率较快，白萝卜品质较好，营养成分的保留率较高。车刚等[18]基于远红外真空干燥方式对白萝卜的干燥展开了研究，得到了真空度为 3 000 Pa、加热温度为 70 ℃、物料厚度为 7 mm 条件下的干燥效果最优的结论。Nayi 等[19]采用太阳辐射和全光谱人工太阳光的干燥方法对白萝卜进行试验，发现该方法能够显著缩短干燥时间，并提高干燥效率，能够有效替代传统日晒干燥方法。然而上述学者并未深入探究热风干燥下白萝卜品质的变化与干燥温度、相对湿度、物料厚度等关键工艺参数之间的关系，尚未确定最佳的干燥工艺参数组合。

由此，本文以潮汕菜脯制作中的干燥去水环节为背景，以白萝卜为对象，通过单因素试验研究热风干燥工艺下干燥温度、相对湿度和物料厚度对复水比、干燥时间、色泽的影响，并在此基础上使用 Box-Behnken 响应面法进行优化设计。最终确定了在保证白萝卜干燥品质及干燥效率的前提下的最优干燥工艺参数，拟为白萝卜干燥脱水工艺优化提供理论基础。

1 试验

1.1 物料制备

选用的新鲜白萝卜（品种为白沙玉春）产自广东省汕头市郊区，大小基本一致，外表光亮且无破损。在试验前，将白萝卜置于热风烘箱（105 ℃）中干燥 24 h，确定初始含水率[20]，上述试验重复 7 次，最终得到初始湿基含水率为 86.31%~95.92%。在正式试验时，将白萝卜切成条状，长度和宽度分别为 80、20 mm，厚度依次为 5、10、15、20 mm。

1.2 仪器与方法

主要试验仪器：KX-系列干燥机，瑞安市口喜口喜机械有限公司；DLPXL-70 高精度称重测力传感器，蚌埠启晟传感器有限公司；RS-WS-N01-2 温湿度变送器，山东仁科测控技术有限公司；DF-101S 集热式恒温加热磁力搅拌器，上海力辰西仪器科技有限公司；GH-200A 卤素快速水分检测仪，上海格宏仪器有限公司；CJS-10C 德东超声波加湿器，绍兴市上虞德东电机有限公司；DS-40C 立式高精度分光色差仪，广东三恩时科技有限公司。农产品干燥试验平台如图 1 所示。

试验采用单因素试验法和 Box-Behnken 响应面法。单因素试验法：以干燥温度（30、40、50、60 ℃）、相对湿度（20%、30%、40%、50%）、物料厚度（5、10、15、20 mm）为变量，设计单因素试验。通过单因素试验，确定 3 个试验因素的最佳范围。Box-Behnken 响应面法：在单因素试验的基础上，根据 Box-Behnken 响应面法的设计原理，以干燥温度、相对湿度、物料厚度这 3 个因素为自变量，研究它们与复水比、干燥时间、色泽的关系，因素水平见表 1。

在试验开始前，按设定干燥温度和相对湿度预热机器，随后将规格一致的白萝卜物料有序放置于干燥室中。如图 1 所示，农产品干燥试验平台通过农产品干燥监控系统实时监测并调整干燥参数；由温湿度传感器检测干燥室的温湿度状态；由湿度控制比例阀调节干燥室的相对湿度；由高精度称重传感器检测白萝卜样品的质量变化。

当物料水分蒸发，使得相对湿度升高时，打开干燥设备排湿口和新风口，将湿分外排，以调节干燥室的相对湿度。在试验开始后，干燥监控系统每隔 30 min 采集一次白萝卜的质量数据，当相邻两次质量变化小于 0.2 g/h 时停止干燥[21]。每组试验重复 3 次，取其平均值。

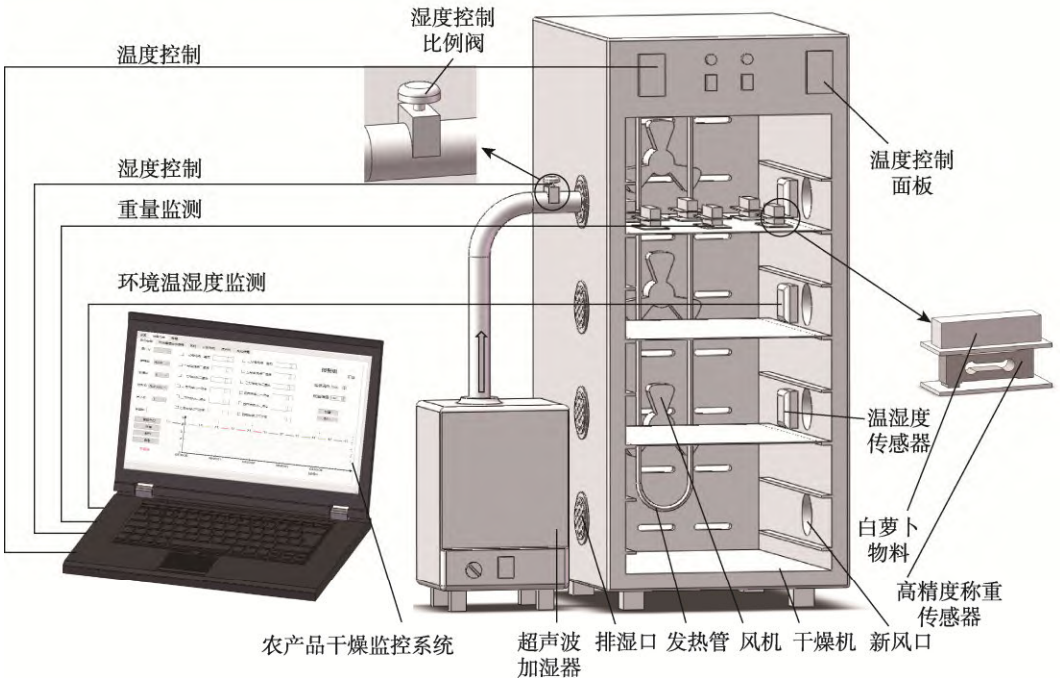

图 1　农产品干燥试验平台
Fig.1 Drying test platform for agricultural products

表 1　Box-Behnken 试验因素水平
Tab.1 Box-Behnken test factor level

水平	因素		
	干燥温度/℃	相对湿度/%	物料厚度/mm
–1	40	20	10
0	50	30	15
1	60	40	20

1.3　试验指标

1.3.1　干基含水率

干基含水率[22]（M_t）的计算见式（1）。

$$M_t = \frac{m_t - m_g}{m_g} \tag{1}$$

式中：m_t 为 t 时刻白萝卜样品的质量，g；m_g 为绝干时白萝卜样品的质量，g。

1.3.2　干燥速率

干燥速率[23]（D）的计算见式（2）。

$$D = \frac{M_{t+dt} - M_t}{d_t} \tag{2}$$

式中：M_{t+dt} 为白萝卜样品在 t+dt 时刻的干基含水率，kg/kg；M_t 为白萝卜样品在 t 时刻的干基含水率，kg/kg；d_t 为时间变化量，h。

1.3.3　复水比

复水是脱水蔬菜重新利用的重要步骤[24]，复水性指干制蔬菜重新吸收水分的程度[25]，常用复水比（R）表示，它是衡量脱水蔬菜品质的重要指标[26-27]。白萝卜在干燥时细胞结构会发生不可逆的破坏，复水比越高，表明其细胞结构受破坏的程度越小、风味越佳、品质越好[28]。复水比的测定参考 Shi 等[29]的方法，将完全干燥后得到的白萝卜物料取出测其质量，然后置于温度为 60 ℃的水浴锅中浸泡 1 h，待浸泡结束后取出沥干表面水分后再次测量。复水比的计算见式（3）。

$$R = \frac{m_1}{m_2} \tag{3}$$

式中：m_1 为白萝卜样品复水后的质量，g；m_2 为白萝卜样品复水前的质量，g。

1.3.4　色泽

白萝卜在干燥前后的色泽变化能直观反映其干燥品质。在试验中，选取不同干燥工艺下的白萝卜样品，使用分光色差仪重复进行测量，取其平均值，计算总色差（ΔE），见式（4）[30]。ΔE 越小，表明白萝卜的色泽、品质越好。

$$\Delta E = \sqrt{(L - L_0)^2 + (a - a_0)^2 + (b - b_0)^2} \tag{4}$$

式中：L_0、a_0、b_0 分别为干燥前白萝卜样品的明度值、红绿值、蓝黄值；L、a、b 分别为干燥后白萝卜样品的明度值、红绿值、蓝黄值；ΔE 为总色差。

1.3.5　综合评分法

为了消除变量量纲差异及变异范围的影响，需要对各指标进行归一化处理。参考代建武等[31]的方法，设定各项指标的最优值为 1，最差值为 0。综合评分由上述指标值经加权计算后得到。将干燥时间、复水比、色泽作为干燥品质和干燥效率的评价指标，参考

段续等[13]的线性加权综合评分法，将这 3 个指标的加权系数分别设置为 0.8、0.1、0.1[32]。通过式（5）、（6）、（7）计算出不同干燥工艺条件下单个指标的评分，由式（8）采用线性加权法求得综合评分。干燥时间指标评分计算见式（5）。

$$F_1=\frac{t_{max}-t_i}{t_{max}-t_{min}} \tag{5}$$

式中：t_i 为第 i 个白萝卜样品的干燥时间；t_{min} 为样品干燥时间的最小值；t_{max} 为样品干燥时间的最大值。

复水比指标评分的计算见式（6）。

$$F_2=\frac{R_i-R_{min}}{R_{max}-R_{min}} \tag{6}$$

式中：R_i 为第 i 个白萝卜样品的复水比；R_{min} 为样品复水比的最小值；R_{max} 为样品复水比的最大值。

色泽指标评分的计算见式（7）。

$$F_3=\frac{\Delta E_{max}-\Delta E_i}{\Delta E_{max}-\Delta E_{min}} \tag{7}$$

式中：ΔE_i 为第 i 个白萝卜样品的色差；ΔE_{min} 为样品色差的最小值；ΔE_{max} 为样品色差的最大值。

综合评分的计算见式（6）。

$$L=0.8F_1+0.1F_2+0.1F_3 \tag{8}$$

1.4　数据处理

针对干基含水率、干燥速率、干燥时间、复水比等指标，使用 Excel 软件对试验数据进行处理，使用 Origin 2022 软件进行绘图，使用 Design-Expert 13 软件对不同干燥参数组合进行回归处理和响应面分析。

2　结果与分析

2.1　单因素试验

2.1.1　干燥温度对白萝卜干燥特性及品质的影响

在相对湿度（20%）、物料厚度（10 mm）相同的情况下，不同干燥温度对白萝卜干燥特性的影响如图 2 所示。从图 2a 可以看出，白萝卜的干基含水率随着时间的增加而下降，温度越高，则曲线越陡，水分含量下降得越快。与干燥温度 30 ℃相比，在干燥环境温度为 60 ℃下干燥所需时间约为 510 min，干燥时间缩短了近 70.69%。干燥温度提高了白萝卜对热能的吸收量[28]，改变了水分子热运动的剧烈程度，进而缩短了干燥时间。

白萝卜干燥速率的变化趋势如图 2b 所示，白萝卜在干燥过程中呈现降速干燥的趋势，前期干燥速率快，后期干燥速率变慢并趋于 0。在干燥前期，白萝卜因表面含有丰富的自由水，提高干燥温度能够加快其表面水分的蒸发速度及内部水分向外扩散的速度；在干燥后期，随着表面水分的蒸发，白萝卜内部的结合水难以干燥，导致干燥速率下降[33]。

在不同干燥温度下白萝卜复水比的变化如图 3a 所示。可见复水比呈现随干燥温度的增加而上升的趋势。干燥温度过低，则水分的迁移速度较慢，导致白萝卜尚未充分干燥，其内部含水率较高、复水比较低，这与曹东等[34]的结论相似。相应地提高干燥温度能够改变细胞膜的通透性，破坏细胞结构，提高复水比。白萝卜的色差变化如图 3b 所示，在有氧热风干燥下，白萝卜自身会发生美拉德反应和酶促反应，导致其发生褐变[35]。温度越高，则褐变程度越明显，因此干燥温度对白萝卜干燥特性和品质具有显著影响。

2.1.2　相对湿度对白萝卜干燥特性及品质的影响

在干燥温度（60 ℃）、物料厚度（20 mm）相同的情况下，不同相对湿度对白萝卜干燥特性的影响如图 4 所示。白萝卜干基含水率变化曲线如图 4a 所示，4 条曲线均呈现逐渐下降的趋势，干燥前期含水率的下降速度比后期快，干燥时间随着相对湿度的降低而减少。

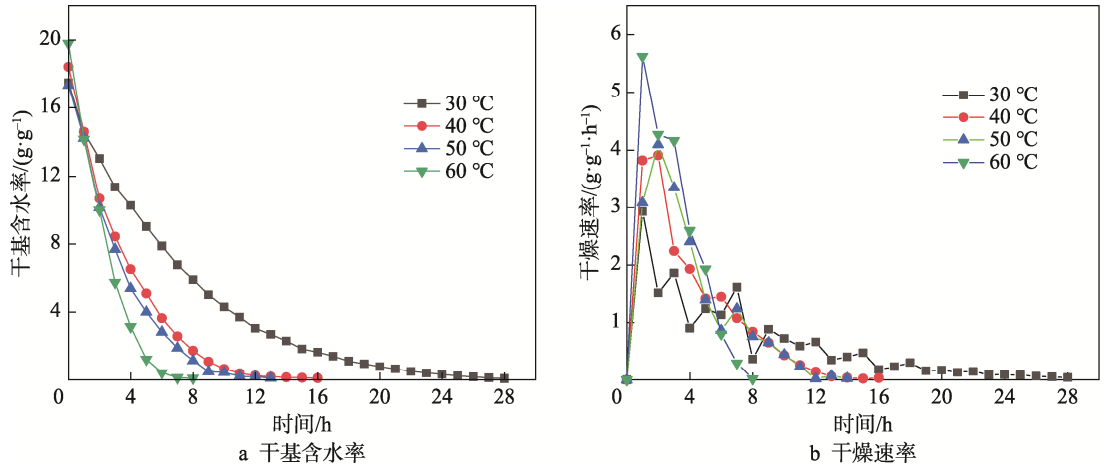

图 2　干燥温度对干燥特性的影响

Fig.2 Effect of drying temperature on drying characteristics

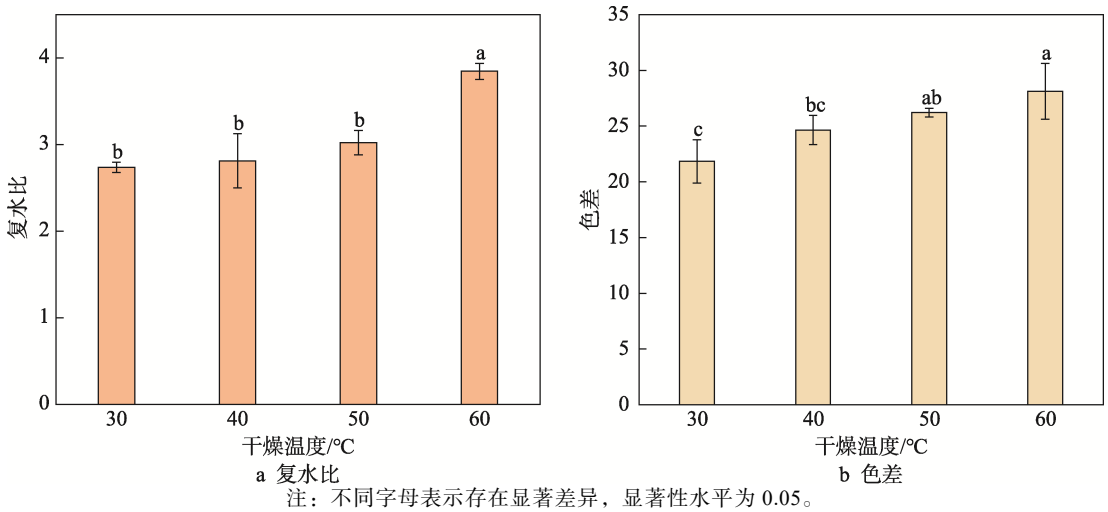

a 复水比　　b 色差

注：不同字母表示存在显著差异，显著性水平为 0.05。

图 3　干燥温度对品质的影响

Fig.3 Effect of drying temperature on quality

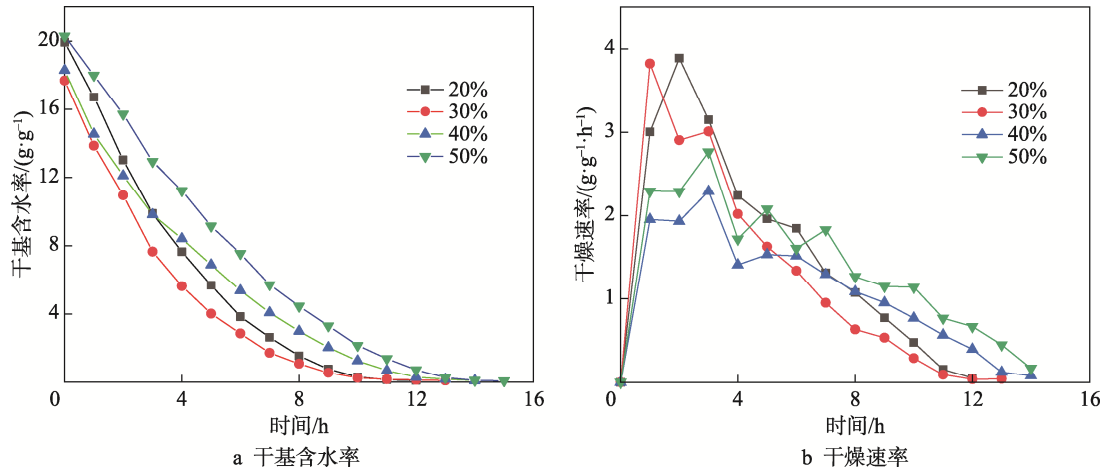

a 干基含水率　　b 干燥速率

图 4　相对湿度对干燥特性的影响

Fig.4 Effect of relative humidity on drying characteristics

相对湿度对干燥品质的影响主要体现在物料的表面结壳：相对湿度越大，则内部水分迁移量越大，出现结壳的时机就越晚，从而延缓了物料表面的结壳[36]。干燥速率变化曲线如图 4b 所示，在相对湿度较高的干燥环境下，白萝卜在干燥后期仍能保持较高的干燥速率，说明其结壳程度较弱，这也印证了上述结论。

由于不同农产品物料的属性不同，其变化趋势不同，因此针对复水比与相对湿度的关系目前尚无统一结论。Balbay 等[37]研究发现，开心果干制品的复水比随着相对湿度的升高而增大。刘明宝等[38]在山楂片微波干燥试验中发现，山楂片的复水比随着恒定相对湿度的升高而降低。本次试验关于白萝卜复水比的变化情况如图 5a 所示，该值随着相对湿度的增加呈先下降后上升的趋势。高相对湿度主要影响传热过程，延缓表面结壳，提高复水性；低相对湿度主要影响传质过程，易使物料表面结壳[36],本次的试验结果也与该结论相符。相对湿度对色差的影响如图 5b 所示，色差随着相对湿度的升高呈现出先增加后降低的趋势。这是因为高湿环境延缓了细胞结构破坏后的化学反应，起到了保护色泽的作用[39]。此外，Wang 等[40]在针对辣椒进行高湿热风冲击试验中也观察到类似结果。

2.1.3　物料厚度对白萝卜干燥特性及品质的影响

在干燥环境（60 ℃）、相对湿度（30%）相同的情况下，不同物料厚度对白萝卜干燥特性的影响如图 6 所示。由图 6a 可知，随着物料厚度的减小，干燥曲线变陡，干燥过程达到平衡所需的时间变短。原因是随着物料厚度的增大，白萝卜内部水分向外扩散的运动路径延长。另外从图 6b 可以得知，白萝卜的厚度对干燥速率也有着显著影响，白萝卜的总体干燥速率处于下降趋势。物料相对表面积会随着物料厚度的增大而减小[24]，厚度的增大使得传热传质速度减慢，干燥时间相应延长。

物料厚度对干燥品质的影响如图 7 所示，随着厚度的增加，白萝卜干燥趋于困难，其内部水分尚未充分蒸发，复水比不断下降；色泽呈现出先下降后升高的趋势。上述结果在胡萝卜[41]、香菇[42]干燥试验中也得到印证，因此相应降低物料厚度能有效缩短干燥时间，提高复水比，降低色差。

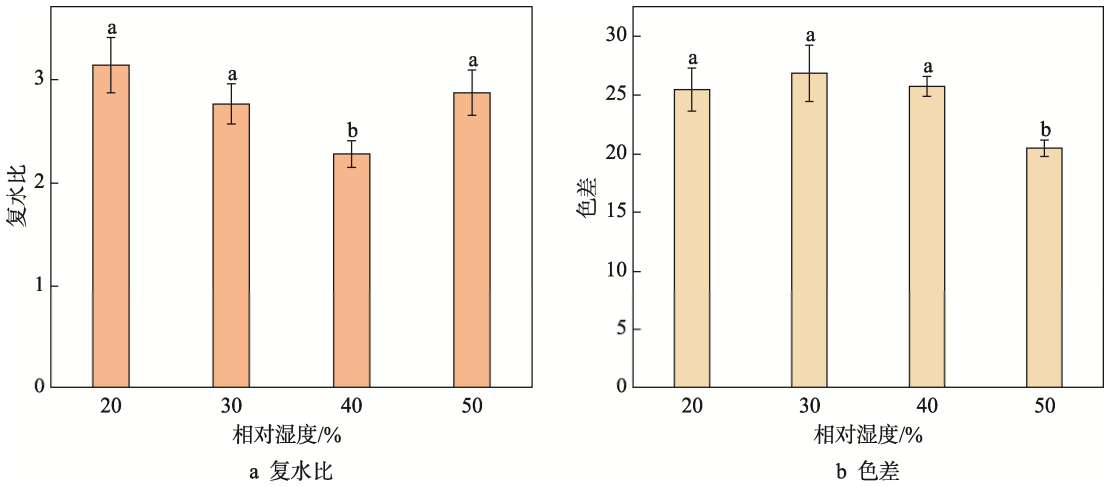

注：不同字母表示存在显著差异，显著性水平为 0.05。

图 5　相对湿度对品质的影响

Fig.5 Effect of relative humidity on quality

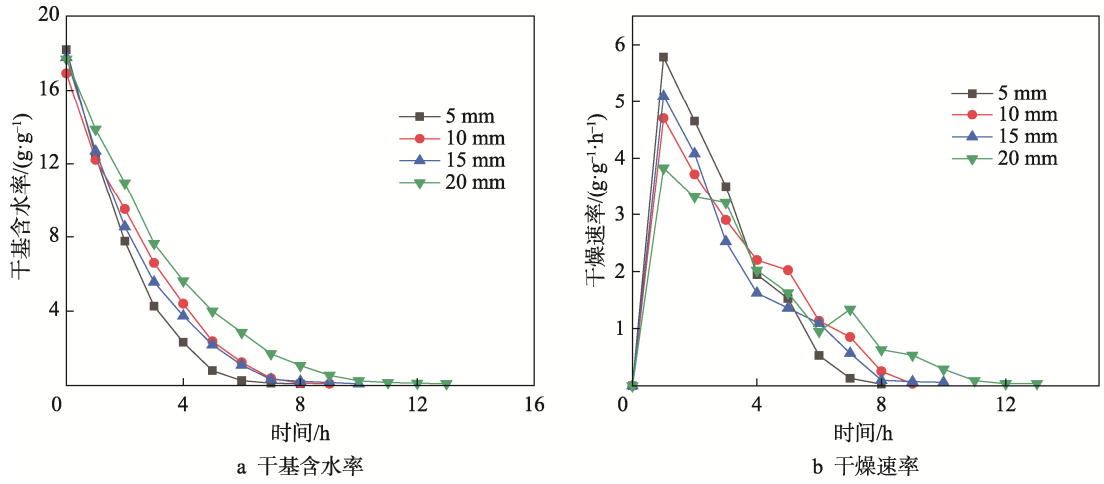

图 6　物料厚度对干燥特性的影响

Fig.6 Effect of material thickness on drying characteristics

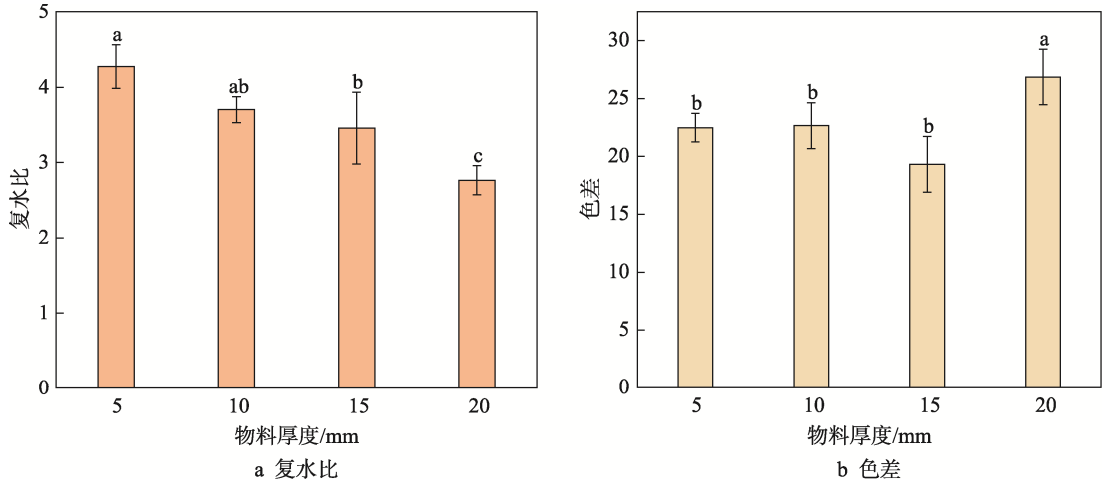

注：不同字母表示存在显著差异，显著性水平为 0.05。

图 7　物料厚度对品质的影响

Fig.7 Effect of material thickness on quality

2.2　Box-Behnken 试验

2.2.1　响应面试验结果及方差分析

在上述单因素试验的基础上得到干燥温度、相对湿度、物料厚度的最佳范围依次为 40~60 ℃、20%~40%、10~20 mm。根据 Box-Behnken 试验方案，以干燥温度、相对湿度、物料厚度为变量，以综合评分为响应值进行优化设计。由 Design-Expert 13 软件生成了 17 组试验，组别及试验结果如表 2 所示。综合评分的回归模型及方差分析如表 3 所示。

表 2　响应面试验设计与结果

Tab.2 Response surface test design and results

组号	干燥温度/℃	干燥环境的相对湿度/%	物料厚度/mm	综合评分
1	40	20	15	0.416
2	60	20	15	0.823
3	40	40	15	0.121
4	60	40	15	0.658
5	40	30	10	0.644
6	60	30	10	0.966
7	40	30	20	0.174
8	60	30	20	0.640
9	50	20	10	0.837
10	50	40	10	0.698
11	50	20	20	0.627
12	50	40	20	0.499
13	50	30	15	0.695
14	50	30	15	0.759
15	50	30	15	0.668
16	50	30	15	0.739
17	50	30	15	0.676

以综合评分为响应值，拟合得到白萝卜关于干燥温度（A）、相对湿度（B）、物料厚度（C）、综合评分（L）的回归方程，见式（9）。

$$L=-2.254\ 58+0.132\ 175A+0.016\ 932B-0.103\ 385C+0.000\ 325AB+0.000\ 720AC+0.000\ 055BC-0.001\ 311A^2-0.000\ 718B^2+0.001\ 187C^2 \quad (9)$$

由表 3 可知，回归模型的 P 为 0.000 5，符合 $P<0.01$ 的要求，模型显著；失拟项的 P 为 0.065 7，大于 0.05，失拟项不显著。此外模型的相关系数 R^2 为 0.957 1，修正系数 Adjusted R^2 为 0.902 0，二者均接近于 1，表明模型与实际数据之间具有较优的拟合效果，对实际生产具有指导意义。3 个试验因素对综合评分的影响程度由大到小的顺序为干燥温度（A）、物料厚度（C）、相对湿度（B），且各个交互作用影响的主次为 $AC>AB>BC$。

2.2.2　响应面分析

综合评分受到干燥温度、相对湿度、物料厚度三者共同的影响。3 个因素交互作用的响应曲面如图 8 所示，响应曲面坡度越大，表明对结果的影响越大[43]。从图 8a 可知，当物料厚度一定，干燥温度的曲面变化较大，说明与相对湿度相比，干燥温度对综合评分的影响更为显著。从图 8b 可知，当相对湿度一定时，物料厚度的曲面变化较干燥温度更为陡峭，说明相较于干燥温度，物料厚度对综合评分的影响更大。从图 8c 可知，当干燥温度一定时，物料厚度的曲面变化更为陡峭，可见在该条件下物料厚度对综合评分的影响更显著。

表 3　综合评分的回归模型及方差分析

Tab.3 Regression model and variance analysis of comprehensive score

方差来源	平方和	自由度	均方	F	P	显著性
回归模型	0.731 9	9	0.081 3	17.37	0.000 5	显著
A	0.375 0	1	0.375 0	80.09	<0.000 1	
B	0.066 1	1	0.066 1	14.11	0.007 1	
C	0.181 5	1	0.181 5	38.77	0.000 4	
AB	0.004 2	1	0.004 2	0.902 4	0.373 8	
AC	0.005 2	1	0.005 2	1.11	0.327 6	
BC	0.000 0	1	0.000 0	0.006 5	0.938 2	
A^2	0.072 3	1	0.072 3	15.45	0.005 7	
B^2	0.021 7	1	0.021 7	4.64	0.068 2	
C^2	0.003 7	1	0.003 7	0.792 0	0.403 1	
残差	0.032 8	7	0.004 7			
失拟项	0.026 4	3	0.008 8	5.54	0.065 7	不显著
纯误差	0.006 4	4	0.001 6			
合计	0.764 7	16				

注：R^2=0.957 1，Adjusted R^2=0.902 0。

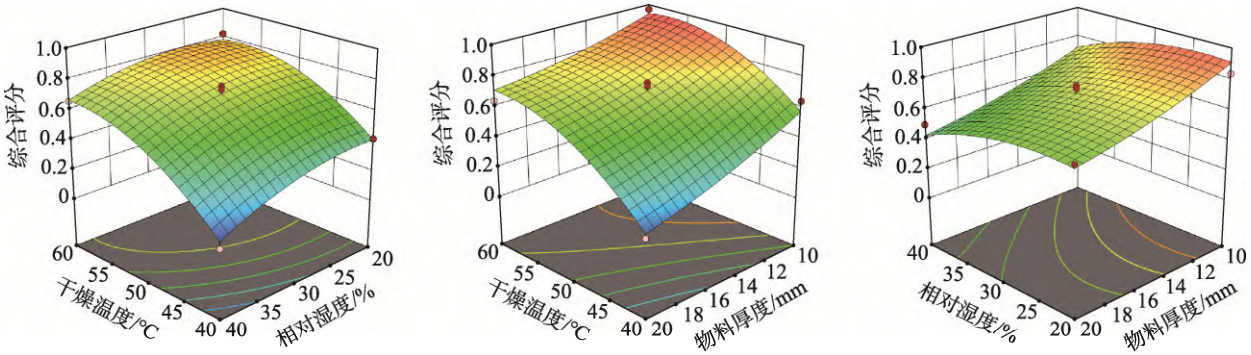

a 干燥温度与相对湿度交互作用　　b 干燥温度与物料厚度交互作用　　c 相对湿度与物料厚度交互作用

图 8　试验因素交互作用的响应曲面

Fig.8 Response surface of the interaction of test factors

2.2.3　最佳干燥工艺参数的确定及验证

对试验数据进行处理，最终经响应面优化得到白萝卜的最佳干燥工艺参数：干燥温度为 56.050 ℃，相对湿度为 23.639%，物料厚度为 10.008 mm。在该干燥条件下，白萝卜的干燥综合评分为 0.967。考虑到实际试验及生产的可操作性，需要对干燥参数进行修正，修正后的干燥参数：干燥温度为 55 ℃，相对湿度为 23%，物料厚度为 10 mm。另外将修正值代入二次回归方程后，得到综合评分为 0.964。使用修正后的干燥参数开展验证试验，其实际干燥时间为 490 min，复水比为 3.851，色差为 25.724，综合评分达到 0.953，实际值与模型理论值的误差仅为 1.4%。上述结果表明由该回归模型得到的干燥工艺参数的可靠程度较高，适用于白萝卜热风干燥。验证试验的结果见表 4。

表 4　验证试验的结果

Tab.4 Results of verification test

序号	干燥温度/℃	相对湿度/%	物料厚度/mm	综合评分
1	55	23	10	0.947
2	55	23	10	0.960
3	55	23	10	0.953

3　结语

基于单因素试验研究了干燥温度、相对湿度、物料厚度对白萝卜热风干燥特性及品质的影响，并在此基础上采用 Box-Behnken 响应面法得到了最佳的干燥工艺参数和回归模型。

1）白萝卜干燥过程为降速干燥，前期的干燥速率较快，后期的干燥速率不断下降；干燥时间随着干燥温度的升高而减少，随着相对湿度的升高而增加，随着物料厚度的增加而减少。

2）复水比随着干燥温度的升高而升高，随着相对湿度的升高呈先下降后升高的趋势，随着物料厚度的增加而降低。

3）白萝卜的色差随着干燥温度的升高而增大，随着相对湿度的升高呈先上升后下降的趋势，随着物料厚度的增加呈先下降后升高的趋势。

4）以复水比、色泽、干燥时间为品质、效率指标，基于响应面试验获得了回归模型，模型的 R^2 为 0.957 1，实际值与模型理论值的误差仅为 1.4%，证明该模型有效、可靠。

5）得到最佳干燥工艺参数：干燥温度为 55 ℃，相对湿度为 23%，物料厚度为 10 mm。经试验验证，在该工艺下白萝卜的干燥效率最高、品质最好，干燥时间为 490 min，复水比为 3.851，色差为 25.724，综合评分为 0.953。该结果可为白萝卜热风干燥工业化应用和高品质贮藏提供理论基础。

参考文献：

[1] 曹琳, 邢亚阁, 曹东, 等. 新型萝卜泡菜正反压生产工艺优化及货架期预测[J]. 食品工业科技, 2018, 39(5): 175-179.
CAO L, XING Y G, CAO D, et al. Optimization of Positive and Negative Pressure Production Process and Shelf-Life Prediction for New Radish Pickle[J]. Science and Technology of Food Industry, 2018, 39(5): 175-179.

[2] 刘盼盼, 任广跃, 段续, 等. 基于变异系数法对不同干燥方式白萝卜品质及风味的评价[J]. 食品与发酵工业, 2022, 48(13): 218-226.
LIU P P, REN G Y, DUAN X, et al. The Evaluation of the Quality and Flavor of Dried White Radish by Different Drying Methods Based on Coefficient of Variation[J]. Food and Fermentation Industries, 2022, 48(13): 218-226.

[3] 金龙. 萝卜干的加工工艺及保藏研究[D]. 杭州: 浙江工商大学, 2015: 3-4.
JIN L. Study on the Processing Technology and Preser-

vation of the Pickled Radish[D]. Hangzhou: Zhejiang Gongshang University, 2015: 3-4.

[4] 韦强, 郑丽静, 武冬雪. 热风干燥温度对脱水白萝卜品质的影响[J]. 保鲜与加工, 2020, 20(1): 165-169.
WEI Q, ZHENG L J, WU D X. Effect of Hot-Air Drying Temperature on Physicochemical Properties of Dehydrated White Radish[J]. Storage and Process, 2020, 20(1): 165-169.

[5] 黄珊, 王修俊, 沈畅萱. 白萝卜薄层热风干燥特性及其数学模型[J]. 食品与机械, 2017, 33(8): 137-143.
HUANG S, WANG X J, SHEN C X. Drying Characteristics and Mathematical Model on Hot-Air Drying of Chinese Radish Slices[J]. Food & Machinery, 2017, 33(8): 137-143.

[6] HOU H N, CHEN Q Q, BI J F, et al. Understanding Appearance Quality Improvement of Jujube Slices during Heat Pump Drying *via* Water State and Glass Transition[J]. Journal of Food Engineering, 2020, 272: 109874.

[7] 刘盼盼, 任广跃, 段续, 等. 饱和蒸汽-热泵组合干燥处理对白萝卜干燥特性及品质的影响[J]. 中国食品学报, 2022, 22(5): 157-168.
LIU P P, REN G Y, DUAN X, et al. Effects of Saturated Steam and Heat Pump Combined Drying on Drying Characteristics and Quality of White Radish[J]. Journal of Chinese Institute of Food Science and Technology, 2022, 22(5): 157-168.

[8] 姜大龙, 王文杰, 王善钰, 等. 红外联合热风干燥白萝卜片的耦合建模与热质传递分析[J]. 农业工程学报, 2022, 38(1): 314-323.
JIANG D L, WANG W J, WANG S Y, et al. Coupled Modeling and Heat and Mass Transfer Analysis of White Radish Slices Dried by Infrared Radiation Combined Hot Air Drying[J]. Transactions of the Chinese Society of Agricultural Engineering, 2022, 38(1): 314-323.

[9] KUMAKURA K, KATO R, KOBAYASHI T, et al. Nutritional Content and Health Benefits of Sun-Dried and Salt-Aged Radish (Takuan-Zuke)[J]. Food Chemistry, 2017, 231: 33-41.

[10] ISHIBASHI R, NUMATA T, TANIGAWA H, et al. In-Situ Measurements of Drying and Shrinkage Characteristics during Microwave Vacuum Drying of Radish and Potato[J]. Journal of Food Engineering, 2022, 323: 110988.

[11] 吕朝燕, 高智席, 马秀情, 等. 不同热风干燥温度对方竹笋品质的影响[J]. 食品工业科技, 2021, 42(11): 23-29.
LYU C Y, GAO Z X, MA X Q, et al. Effect of Different Hot Air Drying Temperatures on Quality of Chimonobambusa Quadrangularis Shoots[J]. Science and Technology of Food Industry, 2021, 42(11): 23-29.

[12] 康宏彬, 陈锶钦, 肖波, 等. 基于 Modified Page 函数和 Box-Behnken 响应面法的黄姜干燥参数优化[J]. 中国农机化学报, 2024, 45(2): 135-142.
KANG H B, CHEN S Q, XIAO B, et al. Optimization of Yellow Ginger Slices Drying Parameters Based on Modified Page Function and Box-Behnken Response Surface Method[J]. Journal of Chinese Agricultural Mechanization, 2024, 45(2): 135-142.

[13] 段续, 徐一铭, 任广跃, 等. 香菇分段变温红外喷动床干燥工艺参数优化[J]. 农业工程学报, 2021, 37(19): 293-302.
DUAN X, XU Y M, REN G Y, et al. Optimization of the Drying Process Parameters for Lentinus Edodes in Segment Variable Temperature Infrared Assisted Spouted Bed[J]. Transactions of the Chinese Society of Agricultural Engineering, 2021, 37(19): 293-302.

[14] 靳学远, 黄丽萍, 张培旗. 火龙果粉冷冻-真空微波干燥工艺优化及贮藏品质[J]. 食品研究与开发, 2024, 45(6): 136-141.
JIN X Y, HUANG L P, ZHANG P Q. Freeze Drying Combined with Vacuum Microwave Drying Process and Storage Quality of Dragon Fruit Powder[J]. Food Research and Development, 2024, 45(6): 136-141.

[15] HADIBI T, MENNOUCHE D, BOUBEKRI A, et al. Experimental Investigation, Performance Analysis, and Optimization of Hot Air Convective Drying of Date Fruits *via* Response Surface Methodology[J]. Renewable Energy, 2024, 226: 120404.

[16] KREETACHAT T, IMMAN S, SUWANNAHONG K, et al. Dataset on the Optimization by Response Surface Methodology for Dried Banana Products Using Greenhouse Solar Drying in Thailand[J]. Data in Brief, 2023, 49: 109370.

[17] 刘盼盼. 饱和蒸汽-热泵干燥组合处理对白萝卜干燥特性的影响[D]. 洛阳: 河南科技大学, 2022: 67-68.
LIU P P. Effects of Combined Drying Treatments of Saturated Steam and Heat Pump on Drying Characteristics of White Radish[D]. Luoyang: Henan University of Science and Technology, 2022: 67-68.

[18] 车刚, 王鑫, 万霖, 等. 远红外真空干燥白萝卜的实验研究[J]. 食品科技, 2015, 40(10): 34-38.
CHE G, WANG X, WAN L, et al. Experimental Study of the Far-Infrared and Vacuum Dry of Turnip[J]. Food Science and Technology, 2015, 40(10): 34-38.

[19] NAYI P, MA F Y, HUANG T C, et al. Effect of Solar Radiation and Full Spectrum Artificial Sun Light Drying

on the Drying Characteristics, Ultra-Structural and Textural Properties of White Radish (Raphanus Sativus L.)[J]. Solar Energy, 2024, 272: 112465.

[20] GENG Z H, TORKI M, KAVEH M, et al. Characteristics and Multi-Objective Optimization of Carrot Dehydration in a Hybrid Infrared/Hot Air Dryer[J]. LWT, 2022, 172: 114229.

[21] 巨浩羽, 肖红伟, 白竣文, 等. 苹果片的中短波红外干燥特性和色泽变化研究[J]. 农业机械学报, 2013, 44(增刊 2): 186-191.
JU H Y, XIAO H W, BAI J W, et al. Medium and Short Wave Infrared Drying Characteristics and Color Changing of Apple Slices[J]. Transactions of the Chinese Society for Agricultural Machinery, 2013, 44(Sup.2): 186-191.

[22] 沈琪, 李顺峰, 王安建, 等. 双孢菇废弃物菇柄热风干燥特性及动力学模型[J]. 中国食品学报, 2015, 15(1): 129-135.
SHEN Q, LI S F, WANG A J, et al. Hot-Air Drying Properties and Kinetics Model of Agaricus Bisporus Waste Stipe[J]. Journal of Chinese Institute of Food Science and Technology, 2015, 15(1): 129-135.

[23] FALADE K O, ABBO E S. Air-Drying and Rehydration Characteristics of Date Palm (Phoenix Dactylifera L) Fruits[J]. Journal of Food Engineering, 2007, 79(2): 724-730.

[24] MARABI A, THIEME U, JACOBSON M, et al. Influence of Drying Method and Rehydration Time on Sensory Evaluation of Rehydrated Carrot Particulates[J]. Journal of Food Engineering, 2006, 72(3): 211-217.

[25] 阚明琪, 王庆惠, 郭俊先, 等. 基于响应面法的哈密瓜片热风干燥工艺优化研究[J]. 中国农机化学报, 2023, 44(3): 94-100.
KAN M Q, WANG Q H, GUO J X, et al. Optimization of Hot Air Drying Process for Hami Melon Slice Based on Response Surface Methodology[J]. Journal of Chinese Agricultural Mechanization, 2023, 44(3): 94-100.

[26] PRAKASH S, JHA S K, DATTA N. Performance Evaluation of Blanched Carrots Dried by Three Different Driers[J]. Journal of Food Engineering, 2004, 62(3): 305-313.

[27] WANG J, XI Y S. Drying Characteristics and Drying Quality of Carrot Using a Two-Stage Microwave Process[J]. Journal of Food Engineering, 2005, 68(4): 505-511.

[28] 余洋洋, 唐道邦, 温靖, 等. 热泵温度对白萝卜干燥速率及品质的影响[J]. 食品与机械, 2020, 36(2): 211-214.
YU Y Y, TANG D B, WEN J, et al. Effect of Different Heat Pump Temperatures on Drying Rate and Quality of White Radish[J]. Food & Machinery, 2020, 36(2): 211-214.

[29] SHI Q Q, HAN G, LIU Y, et al. Nutrient Composition and Quality Traits of Dried Jujube Fruits in Seven Producing Areas Based on Metabolomics Analysis[J]. Food Chemistry, 2022, 385: 132627.

[30] 刘德成, 郑霞, 肖红伟, 等. 红枣片冷冻-红外分段组合干燥工艺优化[J]. 农业工程学报, 2021, 37(17): 293-302.
LIU D C, ZHENG X, XIAO H W, et al. Optimization of Sequential Freeze-Infrared Drying Process of Jujube Slices[J]. Transactions of the Chinese Society of Agricultural Engineering, 2021, 37(17): 293-302.

[31] 代建武, 付琪其, 黄欢, 等. 青花椒真空脉动干燥特性及干燥品质工艺优化[J]. 农业工程学报, 2021, 37(8): 279-287.
DAI J W, FU Q Q, HUANG H, et al. Drying Characteristics and Quality Optimization of Green Prickly Ashes during Vacuum Pulsed Drying[J]. Transactions of the Chinese Society of Agricultural Engineering, 2021, 37(8): 279-287.

[32] 袁迪, 李洋, 陈丰, 等. 蓝莓微波冷冻干燥特性及品质分析[J]. 中国食品学报, 2024, 24(6): 248-263.
YUAN D, LI Y, CHEN F, et al. Analysis of Microwave Freeze-Drying Characteristics and Quality of Blueberry[J]. Journal of Chinese Institute of Food Science and Technology, 2024, 24(6): 248-263.

[33] 吕俊龙, 杨薇, 郭徽, 等. 白萝卜热风干燥特性试验[J]. 农产品加工, 2015(16): 4-7.
LYU J L, YANG W, GUO H, et al. Experiments of Hot-Air Drying Characteristics on White Radish[J]. Farm Products Processing, 2015(16): 4-7.

[34] 曹东, 邢亚阁, 杨华, 等. 干燥温度对萝卜品质的影响及动力学模型建立[J]. 包装工程, 2020, 41(11): 40-45.
CAO D, XING Y G, YANG H, et al. Effect of Drying Temperature on the Quality of Radish and Establishment of Kinetic Model[J]. Packaging Engineering, 2020, 41(11): 40-45.

[35] 吕莹, 陈芹芹, 李旋, 等. 干燥对果蔬加工色泽影响的研究进展[J]. 食品科学, 2023, 44(13): 368-377.
LYU Y, CHEN Q Q, LI X, et al. Recent Progress in Research on the Effect of Drying on the Color of Processed Fruits and Vegetables[J]. Food Science, 2023, 44(13): 368-377.

[36] 巨浩羽, 张卫鹏, 于贤龙, 等. 恒温下相对湿度对果蔬热风干燥特性和品质的影响及调控[J]. 农业工程学报, 2024, 40(2): 29-40.
JU H Y, ZHANG W P, YU X L, et al. Influence of Relative Humidity on the Drying Characteristics and Quality of Fruits and Vegetables during Constant Temperature

Hot Air Drying as Well as Controlling Strategy[J]. Transactions of the Chinese Society of Agricultural Engineering, 2024, 40(2): 29-40.

[37] BALBAY A. Effects of Environmental Temperature and Relative Humidity on the Rehydration of Dried Pistachios[J]. Drying Technology, 2019, 37(10): 1239-1250.

[38] 刘明宝，李静，何方健，等. 山楂微波干燥过程中环境相对湿度的影响[J]. 江苏农业学报，2020，36(2): 487-493.
LIU M B, LI J, HE F J, et al. Effect of Environmental Relative Humidity on Microwave Drying Process of Hawthorn[J]. Jiangsu Journal of Agricultural Sciences, 2020, 36(2): 487-493.

[39] 代建武，周厚彬，黄杰，等. 不同干燥方式对红托竹荪干燥特性和品质的影响[J]. 农业工程学报，2024, 40(6): 90-100.
DAI J W, ZHOU H B, HUANG J, et al. Effects of Different Drying Technologies on the Drying Characteristics and Quality of Dictyophora Rubrovolvata[J]. Transactions of the Chinese Society of Agricultural Engineering, 2024, 40(6): 90-100.

[40] WANG H, ZHANG Q, MUJUMDAR A S, et al. High-Humidity Hot Air Impingement Blanching (HHAIB) Efficiently Inactivates Enzymes, Enhances Extraction of Phytochemicals and Mitigates Brown Actions of Chili Pepper[J]. Food Control, 2020, 111: 107050.

[41] 彭钰航，王广红，孙飞雪，等. 胡萝卜热泵干燥工艺优化[J]. 食品与机械, 2022, 38(1): 211-216.
PENG Y H, WANG G H, SUN F X, et al. Optimization of Carrot Heat Pump Drying Process by Response Surface Methodology[J]. Food & Machinery, 2022, 38(1): 211-216.

[42] 高婵，贾凤娟，王文亮，等. 响应面法优化切片香菇热泵干燥工艺研究[J]. 中国果菜, 2021, 41(12): 7-16.
GAO C, JIA F J, WANG W L, et al. Optimization of Sliced Lentinus Edodes by Heat Pump Drying Using Response Surface Methodology[J]. China Fruit & Vegetable, 2021, 41(12): 7-16.

[43] 惠靖茹，程洋洋，黄占旺. 响应面优化茶树菇发酵调味料的制曲工艺[J]. 中国调味品, 2022, 47(4): 97-101.
HUI J R, CHENG Y Y, HUANG Z W. Optimization of Koji-Making Technology of Agrocybe Aegerita Fermented Seasoning by Response Surface Methodology[J]. China Condiment, 2022, 47(4): 97-101.

華南農業大學
South China Agricultural University

技术成果申请专利（软件著作权）审批

拟申请软件著作权名　　称	稻谷多段逆流连续式干燥出机粮含水率预测系统V1.0		
申请人	华南农业大学	申请类型	软件著作权
联 系 人	黄建江	手机号码	[redacted]
E-Mail	[redacted]		

发明人

第一发明人	李成杰	性　别	男
所在单位	工程学院	职　称	副教授

姓　　名	性　别	所在单位	职　　称
李成杰	男	工程学院	副教授
黄建江	男	工程学院	学生
李韵怡	女	工程学院	学生
李悦	女	工程学院	学生
柳嘉桐	男	工程学院	学生
苏健彬	男	工程学院	学生
陈衍成	男	工程学院	学生

支持课题情况

课题名称	基于迁移学习融合长短期记忆网络的粮食深床干燥瞬态信息感知系统设计
课题来源及编号	大学生创新创业大赛
申请类别	☐发明专利　☐实用新型专利　☐外观设计专利
代理机构名称	广州市卓佳知识产权代理事务所（普通合伙） 代理机构资质查询：http://www.acpaa.cn/view/agencySearch.jhtml
拟申请软件著作权简　　介	本系统是一款基于智能算法与多段逆流干燥工艺深度融合的稻谷含水率预测软件，专为粮食干燥加工领域设计。系统通过实时采集干燥塔内温度、湿度、风速等多维参数，结合稻谷初始含水率与干燥阶段特性，利用机器学习模型（LSTM等）动态预测出机粮的最终含水率。V1.0版本创新性地引入逆流干燥工艺仿真模块，支持不同稻谷品种、干燥时长及环境条件的自适应校准，有效解决传统经验法误差大、滞后性强的问题。系统界面友好，支持数据可视化与历史回溯，为粮食仓储与加工企业提供科学决策依据，显著提升干燥效率并降低能耗。
发明人承诺	本人将按照学校有关规定，积极配合学校知识产权办的工作，做好专利（软件著作权）申请过程中的答复等相关事宜，并及时将收到的有关通知、材料交学校知识产权办处理。

是否为第一发明人	○是　◉否	日　　期	2025-04-13

所在单位审核	本人代表学院对该专利（软件著作权）申请进行了审查。 学院将积极配合学校督促发明人按照学校的有关规定和工作需要做好该专利（软件著作权）的申请、宣传、转化等工作。			
		审核人	胡炼	审核时间	2025-04-14

科研院业务科室科员审核	科研院已备存，无需提交纸质版专利（软件著作权）审批表；如有材料需加盖公章，请在办事服务大厅--知识产权类材料用章申请办理。				
		审核人	张晓佳	审核时间	2025-04-14

科研院业务科室科长审核	已核。				
		审核人	韩雨辰	审核时间	2025-04-14

科研院分管副处长审核	同意				
		审核人	倪慧群	审核时间	2025-04-14

中华人民共和国国家版权局
计算机软件著作权登记证书

证书号： 软著登字第15631493号

软 件 名 称： 稻谷多段逆流连续式干燥出机粮含水率预测系统V1.0

著 作 权 人： 华南农业大学

权利取得方式： 原始取得

权 利 范 围： 全部权利

登 记 号： 2025SR0975295

根据《计算机软件保护条例》和《计算机软件著作权登记办法》的规定，经中国版权保护中心审核，对以上事项予以登记。

中华人民共和国国家版权局 计算机软件著作权登记专用章

2025年06月11日

華南農業大學
South China Agricultural University

技术成果申请专利（软件著作权）审批

拟申请软件著作权名　　称	稻谷逆流循环干燥粮食流速预测控制系统V1.0		
申请人	华南农业大学	申请类型	软件著作权
联 系 人	黄建江	手机号码	[redacted]
E-Mail	[redacted]		

发明人

第一发明人	李成杰	性　别	男
所在单位	工程学院	职　称	副教授

姓　　名	性　别	所在单位	职　　称
李成杰	男	工程学院	副教授
黄建江	男	工程学院	学生
苏祥康	男	工程学院	学生
叶锦桦	男	工程学院	学生
陈嘉奋	男	工程学院	学生
陶文俊	男	工程学院	学生
纪思涵	男	工程学院	学生

支持课题情况

课题名称	基于机器学习的粮食空气源热泵干燥系统能耗预测及其节能控制
课题来源及编号	大学生创新创业大赛
申请类别	☐发明专利　☐实用新型专利　☐外观设计专利
代理机构名称	广州市卓佳知识产权代理事务所（普通合伙） 代理机构资质查询：http://www.acpaa.cn/view/agencySearch.jhtml
拟申请软件著作权简　　介	一款基于智能算法与逆流循环干燥工艺深度融合的粮食流速预测控制软件，专为粮食干燥加工领域优化设计。系统通过实时监测干燥塔内粮食流速、温度、湿度等关键参数，结合稻谷品种特性和干燥阶段需求，利用机器学习模型动态预测并调控粮食流速，确保干燥均匀性，控制精度。V1.0版本创新性地引入逆流循环干燥工艺仿真模块，支持不同粮食种类、干燥时长及环境条件的自适应调节，有效解决传统人工调控效率低、稳定性差的问题。系统具备友好的人机交互界面，支持数据可视化与历史回溯，为粮食加工企业提供智能化决策支持，显著提升干燥效率并降低能耗，保障粮食品质。
发明人承诺	本人将按照学校有关规定，积极配合学校知识产权办的工作，做好专利（软件著作权）申请过程中的答复等相关事宜，并及时将收到的有关通知、材料交学校知识产权办处理。

是否为第一发明人	○是　◉否	日　　期	2025-04-13

所在单位审核	本人代表学院对该专利（软件著作权）申请进行了审查。 学院将积极配合学校督促发明人按照学校的有关规定和工作需要做好该专利（软件著作权）的申请、宣传、转化等工作。			
		审核人	胡炼	审核时间	2025-04-14

科研院业务科室科员审核	科研院已备存，无需提交纸质版专利（软件著作权）审批表；如有材料需加盖公章，请在办事服务大厅--知识产权类材料用章申请办理。				
		审核人	张晓佳	审核时间	2025-04-14

科研院业务科室科长审核	已核。				
		审核人	韩雨辰	审核时间	2025-04-14

科研院分管副处长审核	同意				
		审核人	倪慧群	审核时间	2025-04-14

中华人民共和国国家版权局
计算机软件著作权登记证书

证书号： 软著登字第15631508号

软 件 名 称： 稻谷逆流循环干燥粮食流速预测控制系统 V1.0

著 作 权 人： 华南农业大学

权利取得方式： 原始取得

权 利 范 围： 全部权利

登 记 号： 2025SR0975310

根据《计算机软件保护条例》和《计算机软件著作权登记办法》的规定，经中国版权保护中心审核，对以上事项予以登记。

中华人民共和国国家版权局 计算机软件著作权登记专用章

2025年06月11日

Q/ZKH

广东肇庆市科华食品机械实业有限公司企业标准

Q/ZKH-5HP-1-2023

粮食热泵干燥机

2023-07-15 发布　　2023-07-31 实施

广东肇庆市科华食品机械实业有限公司　发布

目　　次

前　言

本标准按照 GB/T 1.1—2020《标准化工作导则》的规定起草。

本标准等效引用DG/T 017—2021《谷物烘干机》标准。

本标准由肇庆市农业机械安全监督管理所提出。

本标准起草单位：华南农业大学、广东肇庆市科华食品机械实业有限公司

本标准主要起草人：李长友、张烨、张永博、李成杰、王晗、麦智炜、夏学仪、严涌、容添年。

粮食热泵干燥机

1 范围

本标准规定了粮食热泵干燥机的术语和定义，分类和编码，技术要求，试验方法，检验规则，标志和随行文件，包装、运输和贮存等。

本标准适用于以空气源热泵为热能发生和利用装置，配套粮食烘干机，用于烘干稻谷、小麦、玉米、高粱、小杂粮和油菜籽的烘干机。

2 规范性引用文件

下列文件对于本文件的应用是必不可少的。凡是注日期的引用文件，仅注日期的版本适用于本文件。凡是不注日期的引用文件，其最新版本(包括所有的修改单)适用于本文件。

DG/T 017—2021 谷物烘干机

GB/T 21162 顺流粮食干燥机单位耗热量与处理量折算规则

GB/T 30467 横流粮食干燥机单位耗热量与处理量折算规则

GBT 6970-2007 粮食干燥机试验方法

GBT 14095-2007 农产品干燥技术 术语

GBT 16714-2007 连续式粮食干燥机

GBT30466-2013 粮食干燥系统 安全操作规范

GBT 30466-2013 粮食干燥系统 安全操作规范

GBT 26550-2011 粮食干燥机同比热效率的测试与评价

GBT 21399-2008 粮食干燥机自动控制系统评定规则

GBT 21015-2007 稻谷干燥技术规范

GBT 21016-2007 小麦干燥技术规范

GBT13306-2011标牌

JBT10268-2011 批式循环谷物干燥机

JBT 10200-2000 种子加工与粮食处理设备 产品型号编制规则

JBT 10200-2013 加工机械与粮食处理设备产品型号编制规则

NB/T 10156 空气源热泵干燥机组通用技术规范

3 术语和定义

GB/T 14095 界定的以及下列术语和定义适用于本文件。

3.1 粮食热泵干燥机

以空气为热源，通过热泵为干燥机提供粮食水分蒸发所需的汽化热，使粮食达到安全贮藏水分的烘干机，称为粮食热泵干燥机。

3.2 连续式粮食干燥工艺装备

在烘干机调试到正常作业状态后，连续进湿粮，源源不断地排出达到目标水分的干粮的干燥工艺装备；烘干机包括压粮段、干燥段、缓苏段、冷却段，排粮段等，处理能力按每小时处理量计算，单位为吨/小时，用符号t/h表示。

3.3 批次式粮食循环干燥工艺装备

粮食在赶在机内经历的是周而复始的干燥-缓苏过程，直至机内粮食水分达到安全贮藏值的干燥设备。批次式粮食循环干燥机包括缓苏、干燥段、冷却排粮段等；每批次的处理量按干燥机有效容积一次装满的湿粮质量计算，单位为吨，用符号t表示。

3.4 含水率

粮食的含水率，采用湿基含水率或干基含水率表示。湿基含水率是指粮食内含的水分量与其总质量之比的百分数，用符号%w.b表示。干基含水率是指粮食内含的水分量与粮食中除水分以外的绝干物质量之比的百分数，用符号%d.b表示。

设湿物料质量为 G，kg，其中所含的水量为 W，kg，干燥物质量为 D，kg。

湿基含水率：$$M=\frac{W}{G}=\frac{W}{D+W}\times 100\ \%w.b. \quad (1)$$

干基含水率：$$M_d=\frac{W}{D}=\frac{W}{G-D}\times 100\ \%d.b. \quad (2)$$

M 与 M_d，两者之间的关系为：$M=\frac{M_d}{100+M_d}$（%w.b.）；$M_d=\frac{M}{100-M}$（%d.b.）

3.5 干燥速率

干燥速率是指单位时间内粮食的降水量，即单位时间内粮食含水率的变化。用符号%/h 表示；物料的总降水量与总干燥时间之比称为平均干燥速率。

3.6 单位耗电量

干燥过程中，从粮食中每蒸发1kg水，烘干机、空气源热泵和辅助电加热所消耗的总电量，用符号kW/kg表示。

4 分类和编码

4.1 分类

按烘干机类型分为：单塔循环式、单塔连续式、双塔循环式、双塔连续式。

按空气源热泵利用空气热量的结构型式分为：闭式、开式、半开式、能量内循环式。

4.2 编码

烘干机的产品编码结构应符合JB/T 8574的规定，每个码位所代表的含义如图1所示：

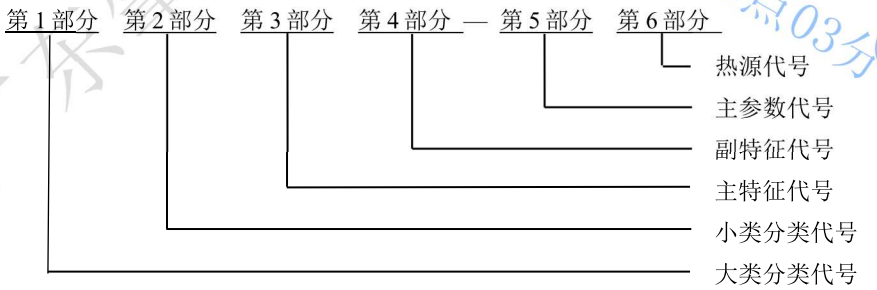

图1 编码结构图

第 4 部分和第 5 部分之间用“—”隔开，从左到右每个码位上所使用的代码字符见表 1。

表 1　代码字符

第 1 部分	第 2 部分	第 3 部分	第 4 部分	第 5 部分	第 6 部分
5：脱粒、清选、干燥和储存机械	H：粮食烘干机	P：循环式 L：连续式	ST：双塔 单塔缺省	用阿拉伯数字表示烘干机处理量或批处理量，取整数	R：空气源热泵 RN:能量内循环热泵 RB：半开式热泵

示例：5HPST-50R 表示批处理量（单批次机内容量）为 50t 的双塔循环式粮食热泵干燥机。

4.3 主参数

烘干机的主参数和主参数系列见表 2。

表2　主参数和主参数系列

烘干机类型	主参数	主参数系列
循环式干燥机	批处理量，t	2、3、5、8、10、12、15、20、25、30、50、60、100、120、150
连续式烘干机	处理量，t/d / t/h	100/4.17、150/6.25、200/8.33、300/12.50、500/20.83、600/25.00、800/33.33、1000/41.67、1200/50.00

5　技术要求

5.1　一般要求

5.1.1　烘干机的热风管道应设置有热空气温度监测装置。

5.1.2　烘干机热风温度和粮食受热允许温度应符合表 3 的要求。

表3　热风温度和粮食受热允许温度　　单位为℃

粮食种类	热风温度		粮食受热允许温度
	连续式	循环式	
玉米	90~120	80~105	≤68
稻谷	70~90	50~70	≤33
小麦	80~105	70~80	≤50
高粱	80~90	70~80	≤50

5.2　性能指标

烘干机性能指标应符合表4的要求。

表4　性能指标

序号	项目	指标
1	处理量（连续式）	≥明示值
2	批处理量（循环式）	≥明示值
3	干燥速率（循环式）	≥明示值
4	单位耗电量（kJ/kg）	≤明示值

5	破碎率增值		小麦、稻谷≤0.3%，玉米≤0.5%
6	稻谷爆腰增率	连续式	≤3.0%
		循环式	≤1.0%
	玉米裂纹增率		≤1%（降水幅度≤5%） ≤2%（5%＜降水幅度≤10%） ≤2.5%（降水幅度＞10%）
	小麦湿面筋率		不低于干燥前
7	热风温度波动范围		≤±4℃
8	干燥不均匀度	循环式	≤1.0%
		连续式	≤1.0%（降水幅度≤5%） ≤1.5%（5%＜降水幅度≤10%） ≤2.0%（降水幅度＞10%）
9	出机粮食温度		≤8℃（环境温度＜0℃）
			≤环境温度+8℃（环境温度≥0℃）
10	色泽、气味		无变化、正常

5.3 装配质量

5.3.1 整机装配后，烘干机外形应无擦伤、错位；内表面应平滑，无凸台、凹槽；底座应稳固、平整、无歪斜；预埋件应连接良好，无松动。

5.3.2 轴、齿轮、带轮及其他旋转件装配后不应有窜动、跳动、偏摆或振动现象。

5.3.3 烘干机的排粮机构应转动灵活，无卡滞和刮擦，同时还应保证足够的强度，运转时不应出现变形。

5.3.4 整机的热风管管道应敷设保温层，外表应平整无凹陷，管道气密性良好。

5.4 外观质量

5.4.1 烘干机的外表面不应有锈蚀和毛刺。

5.4.2 电镀件表面应光滑，色泽均匀，不应有剥落和划伤等。

5.5 涂层质量

5.5.1 涂漆表面不应有明显的气泡、流痕、漏涂、底漆外漏及损伤等。

5.5.2 表面涂漆涂层厚度应符合 JB/T 9832.2 的要求。

5.6 电气控制

5.6.1 一般要求

5.6.1.1 电气控制应包括烘干机主机、进出粮输送和清理设备等的控制。

5.6.1.2 辅助热源可单独控制，也可与烘干机主机集成控制。

5.6.1.3 所有电气控制应具有过载、欠压、短路、断路和漏电保护等功能。

5.6.2 绝缘

设备应有良好的绝缘，机组带电部位有可能接地的非带电部位之间的绝缘电阻应不小于2MΩ。

5.7 有效度

烘干机按6.7的方法进行试验，烘干机不应发生导致机具功能完全丧失、危及作业、人身安全或引起重要总成报废的致命故障，以及导致功能严重下降，主要零部件损坏的严重故障，使用有效度应不小于98%。

5.8 安全

5.8.1 安全防护

5.8.1.1 对操作人员有危险的外露传动和回转部件应有可靠的防护罩。

5.8.1.2 平台、通廊、爬梯和塔架等应设置扶手或围栏防护设施，围（护）栏高度应≥1100 mm，爬梯距离地面 3000 mm 以上应安装护圈。

5.8.1.3 连续式烘干机所有正压风机进风口应安装安全防护装置。

5.8.1.4 除移动式烘干机外，循环式烘干机单体顶部应有上盖，并设置防止操作人员坠落的防护栅栏。

5.8.2 安全信息

5.8.2.1 对操作者存在或有潜在危险的电机传动装置、风机进风口、高温热源装置和排粮链传动机构等部位，应在其附近明显位置上固定永久性安全警示标志，安全标志应符合 GB 10396 的要求。

5.8.2.2 使用说明书中应有安全注意事项，产品上设置的安全警示标志应在使用说明书中复现。

5.8.3 安全装备

5.8.3.1 循环式烘干机应设置粮位观察孔或料位显示装置、满粮报警装置、热风温度超温报警装置和开机前警示装置；连续式烘干机应有热风温度超温报警装置、开机前警示装置、料位器或料位显示监控装置。

5.8.3.2 连续式和静态式烘干机下部应设置具有快开门机构的紧急排粮口，紧急排粮口应对称分布。

5.8.3.3 室外作业的烘干机组应设置有接闪器、引下线和接地体的避雷装置。

5.8.3.4 电控系统应设置过载和漏电保护装置，所有电气及设备的安全均应符合 GB/T 5226.1 的要求。

5.9 环境保护

5.9.1 噪声

操作人员经常活动的地方，循环式烘干机工作现场噪声值应≤85 dB(A)，连续式烘干机工作现场噪声值应≤92 dB(A)的要求，静态式烘干机工作现场噪声值应≤80 dB(A)。

5.9.2 粉尘浓度

在烘干机周围操作人员活动区域的粉尘浓度应≤8 mg/m^3 。

6 试验方法

6.1 试验要求

6.1.1 一般要求

6.1.1.1 所有试验应在铭牌上的额定电压、额定电流和额定频率下进行。

6.1.1.2　进入烘干机的湿粮应符合下列要求：

a)　水分不均匀度≤3 %；

b)　湿粮含杂率≤2 %，其中秸秆（≤50 mm）含量不超过 0.2 %，且不应有秸秆（>50 mm）、果穗、石子、绳头、包装物和金属物等大型异物。

6.1.2　测试仪器

测试仪器应符合表5的要求。

表5　测试仪器要求

序号	参数		测量范围	准确度等级/最大允许误差
1	噪声		（34～130）dB（A）	2 级
2	长度		（0～50）m	1 mm
3	质量	粉尘采样称重	（0～200）g	0.0001 g
		样品处理称重	（0～600）g	0.1 g
		样品水分称重	（0～200）g	0.001 g
		试验物料称重	（10～1000）kg	3 级
4	时间		（0～24）h	0.5 s/d
5	环境温度		（-30～70）℃	1℃
6	热风温度		（-50～300）℃	1℃
7	环境相对湿度		0～100%	5 %

6.1.3　样机状态

6.1.3.1　烘干机在经过空载和负载调试后，达到稳定运行状态。

6.1.3.2　空气源热泵机组应处于正常提供热空气运行状态，且提供热空气的温度和流量能满足干燥需求。

6.1.4　安全检查

6.1.4.1　在试验前应进行作业前、作业中和作业后的检查，安全检查通过后方可进行试验和结束试验。

6.1.4.2　试验前应检查烘干机的风管和连接管、辅助元件、管路、电路和接口等是否正确安装，风机和电机等所有转动件的运转方向是否正确。

6.2　性能指标

6.2.1　取样

6.2.1.1　样品

每个取样样品的质量应不小于0.5 kg。

6.2.1.2　进机粮

连续式烘干机应在上粮装置入口处每 10 min～15 min 等间隔接取一个样品，样品数量 9 个；循环式烘干机在物料进机稳定时，等间隔接取样品，样品数量 7 个。静态式烘干机在装量后的平面中取样，样品数量 9 个。

6.2.1.3 出机粮

连续式烘干机应在排粮装置出口处每 10 min～15 min 等间隔接取一个样品，样品数量 9 个；循环式烘干机在物料出机时每 5 min 等间隔接取一个样品，样品数量 7 个。静态式烘干机的出机物料与进机物料取样位置和数量相同。

6.2.1.4 干燥不均匀度

连续式烘干机在冷却段两侧同一平面角盒口等间隔取样，水平伸入机内 200 mm～300 mm 抓取，根据烘干机机体尺寸的大小，每侧各取 4 个～6 个样品；在冷却段无角盒口的烘干机，应在排粮斗内排粮装置底部的烘干机四角和中心位置，接取 5 个点的样品。循环式烘干机干燥不均匀度取样按 6.2.1.3 执行，不单独取样。静态式烘干机干燥不均匀度取样按粮食铺平后的平面内均等取 9 个取样点。

6.2.1.5 小麦湿面筋率

接取进、出机样品各一个。

6.2.2 测试步骤

6.2.2.1 记录

测试过程中，作好下列记录：

a) 记录测试时间和测试人，以及烘干机的结构参数、配套电机功率、风机额定风量和风压等相关参数。

b) 记录进风管和排风管管道截面积，分别测量进风管和排风管的热风温度、风速和风压，每30min记录一次，并计算其平均值。

6.2.2.2 含杂率

样品用分样器分样，大样样品质量应控制在450 g～550 g，对大样分2次进行筛分，用1.5 mm（小麦）、3.0 mm（玉米）、2.0 mm（稻谷）、1.0 mm（油菜籽）圆孔筛筛出筛下物，2次筛分样品均匀混合后用分样器分小样，小样样品质量：玉米90 g～110 g、小麦、稻谷和油菜籽均为45 g～55 g，筛下物为杂质。

6.2.2.3 含水率

对接取的进、出机样品，含水率按照GB/T 5262 中的籽粒含水率要求进行测试，籽粒含水率大于18%w.b.时，采用二次烘干法，测定时，每个样品取2个小样进行籽粒含水率测定取其平均值为该样品含水率。分别记录干燥前、后样品的水分，并分别计算出其平均值和极差。

6.2.2.4 降水幅度

含水率及降水幅度按式(3)计算。

$$\Delta M = M_1 - M_2 \qquad (3)$$

式中： ΔM——降水幅度，%w.b；M_1——进机粮含水率，%w.b；M_2——出机粮含水率，%w.b。

6.2.2.5 处理量

连续式和静态式烘干机应在干粮出口用容器、麻袋或车接收干粮，记录和称量单位时间内干粮质量，计算出湿粮处理量。用连续式和静态式烘干机的处理量按公式（4）计算，连续式烘干机处理量折算分别按 GB/T 21162 和 GB/T 30467 进行。

$$G_1 = \frac{G_2(100 - M_2)}{100 - M_1} \quad (4)$$

式中：G_1——处理量，单位为吨每小时（t/h）；G_2——干粮产量，单位为吨每小时（t/h）。

6.2.2.6 干燥产品量

进入干燥室的湿物料，根据干燥任务要求除去水分而获得产品，由物料衡算可写出：

$$G_2 = G_1 - W \quad 或 \quad G_2 = G_1 \frac{100 - M_1}{100 - M_2}$$

式中：G_1——进入干燥器的湿物料量，kg 湿物料/h；

G_2——干燥产品量，kg/h；

W——水分蒸发量，kg/h；

M_1——湿物料的湿基含水率，kg 水/kg 湿物料；

M_2——干燥产品的湿基含水率，kg 水/kg（产品）。

6.2.2.7 批处理量

方法 1：装入湿粮前，测量并记录循环式烘干机的有效容积，循环式烘干机的批处理量按公式（5）计算。

$$P = R \cdot V_c \quad (5)$$

式中：P——批处理量，单位为吨（t）；R——粮食标准容重，单位为吨每立方米（t/m³），稻谷取 0.56 t/m³，玉米 0.76t/m³；小麦：0.8 t/m³; V_c——有效容积，单位为立方米（m³）。

方法2：当循环式烘干机有效容积不易测量时，可在装入湿粮时称量并记录装满循环式烘干机的湿粮总质量和稻谷实测容重，循环式烘干机的批处理量按公式（6）计算。

$$P = R\frac{G}{r} \quad (6)$$

式中：G——循环式烘干机装满含湿粮食总质量，单位为吨（t）；r——实测机内湿粮的饱和容重，单位为吨每立方米（t/m³）。

6.2.2.8 平均干燥速率

记录循环式烘干机的干燥开始时间和排出干粮结束时间，平均干燥速率按公式（7）计算。

$$-\frac{\overline{dM}}{d\theta} = \frac{M_2 - M_1}{\theta_{12}} \quad (7)$$

式中：$-\frac{\overline{dM}}{d\theta}$——平均干燥速率，单位为（%/h）；$\theta_{12}$——干燥总时间（含热风干燥、缓苏干燥、冷却干燥以及额定进排粮时间）单位为小时（h）

6.2.2.9 单位耗电量

开始干燥前，在烘干机主机及其风机、空气源热泵及辅助电加热的总电源上接入功率表，测定并记录干燥过程中的小时耗电量，小时耗电量的测试时间应不小于48h。连续式烘干机的单位失水量按公式（8）计算，循环式烘干机的单位失水量按公式（9）计算，单位耗电量按公式（10）计算。

$$w=\frac{1000\cdot G_1(M_1-M_2)}{1-M_2} \tag{8}$$

$$w=\frac{1000\cdot P(M_1-M_2)}{\theta_{12}(1-M_2)} \tag{9}$$

式中：w——单位失水量，单位为千克每小时（kg/h）。

$$Q_{DP}=\frac{3600\cdot D}{w} \tag{10}$$

式中：Q_{DP}——单位耗电量，单位为千焦每千克（kJ/kg）；D——小时耗电量，单位为千瓦每小时（kW /h）

6.2.2.10 破碎率增值

从干燥前、后粮食中各取出至少 3 个样品进行测定。脱壳的整粒和破碎粒、未脱壳破损的稻谷均为破碎；玉米籽粒有破损及残缺程度达到颗粒体积 1/5 以上的均为破碎。破碎率增值按公式（11）计算。

$$\Delta p = p_2 - p_1 \tag{11}$$

式中：Δp——破碎率增值，（%）；p_2——干燥后样品破碎率平均值，（%）；p_1——干燥前样品破碎率平均值，（%）。

6.2.2.11 稻谷爆腰率增值

从干燥前、后粮食中各取出至少 3 个样品，每个样品取 100 粒完整籽粒，封存放置 24 h 后在正常温度下，手工剥去外壳，用爆腰检测箱或检测仪检查。如稻谷胚乳出现裂缝，或一条横裂纹清晰贯穿全粒，或有 2 条及以上横裂纹，或有纵向裂纹长度超过全粒 2/3 均属爆腰粒，爆腰粒所占的百分比即为稻谷爆腰率。稻谷爆腰率增值按公式（12）计算。

$$\Delta b = b_2 - b_1 \tag{12}$$

式中：Δb——爆腰率增值，（%）；b_2——干燥后样品爆腰率平均值，（%）；b_1——干燥前样品爆腰率平均值，（%）。

6.2.2.12 玉米裂纹率增值

从干燥前、后粮食中各取出至少 3 个样品，每个样品取出 100 个完整籽粒，发现玉米粒的胚乳有裂痕或粒上裂纹长度达粒长的 1/2 以上，或一条裂痕贯穿全粒，或裂痕两条以上的均属裂纹，裂纹粒所占的百分比即为玉米裂纹率。玉米裂纹率增值按公式（13）计算。

$$\Delta \tau = \tau_2 - \tau_1 \tag{13}$$

式中：$\Delta\tau$——玉米裂纹率增值，（%）；τ_2——干燥后样品裂纹率平均值，（%）；τ_1——干燥前样品裂纹率平均值，（%）。

6.2.2.13 小麦湿面筋率

接取的进机、出机小麦样品，小麦湿面筋率试验方法按 GB/T 5506.1 或 GB/T 5506.2 的要求进行。

6.2.2.14　热风温度波动范围

测试期间，每 10 min～20 min 记录 1 次热风管道的热风温度，记录最大值和最小值，并计算出热风温度的平均值。最大值减平均值为正值，最小值减平均值为负值。

6.2.2.15　干燥不均匀度

干燥不均匀度为出机粮含水率极差，按公式（14）计算。

$$M_{bj} = M_{\max} - M_{\min} \tag{14}$$

式中：M_{bj}——干燥不均匀度，（%）；$M_{\max}$——出机粮最大含水率，（%w.b.）；$M_{\min}$——出机粮最大含水率。

6.2.2.16　出机粮食温度

每个出机样品装入保温杯内，在 3 min 内完成粮食温度测试，计算其平均值，用该平均值减去测试期间的大气环境温度平均值为出机粮食温度。

6.2.2.17　色泽、气味

目测和嗅觉感官识别烘干后粮食的综合颜色、光泽和气味，记录检查结果。

6.3　装配质量

视检烘干机的装配情况，记录检查结果。

6.4　外观质量

视检烘干机的外观，记录检查结果。

6.5　涂层质量

检测烘干机的涂漆表面及涂层厚度，记录检查结果。

6.6　电气控制

逐项检查并验证电气控制的各项功能，检查防触电保护是否符合保护要求，检查元器件和电机外壳等部位的温升是否异常，检查电气强度及部分零部件的耐高温性等。用1000V兆欧表测定绝缘电阻，记录检查结果。

6.7　有效度

连续式工艺模式，干燥机连续运行72小时无故障，循环式烘干机连续运行两个干燥批次无故障，记录烘干机故障情况、无故障运行时间和故障排除时间，使用有效度按公式（15）计算。

$$K = \frac{\sum T_Z}{\sum T_Z + \sum T_g} \times 100\% \tag{15}$$

式中：K——使用有效度，（%）；T_z——连续无故障运行时长，单位为小时（h）；T_g——运行期间的故障及排除时间，单位为小时（h）。

6.8　安全

视检烘干机的安全防护、安全信息和安全装备，记录检查结果。

6.9 环境保护

6.9.1 噪声

噪声的试验方法按 GB/T 3768 的要求执行，在烘干机工作区域操作人员经常活动地点，包括烘干机两侧和人员操作位置等正前方各测试 1 点（操作人员不去的地方不测），每点距离机械外表面 1.0 m，离地面 1.5 m，用声级计的计权网络 A 档测量噪声值，测点为 5 个，取测试结果的算数平均值。

6.9.2 粉尘浓度

在烘干机排粮口靠近输送机的位置测试 1 点，测点位于距离机械外表面 1.0 m，离地面 1.5 m 处，用粉尘测试仪采样时，采用短时间采样方式，以 20 L/min 流量采集 15 min 空气样品。

7 检验规则

7.1 检验项目

干燥机装配后逐台进行检验。检验项目按其对产品质量的影响程度分为A类、B类和C类，见表6。

表6 检验项目

项目分类	序号	项目	技术要求	试验方法
A	1	处理量（连续式、静态式） 批处理量（循环式）	5.2	6.2.2
	2	有效度	5.7	6.7
	3	安全	5.8	6.8
	4	噪声	5.9.1	6.9.1
	5	粉尘浓度	5.9.2	6.9.2
B	1	干燥速率（循环式）	5.2	6.2.2
	2	单位耗电量	5.2	6.2.2
	3	破碎率增值	5.2	6.2.2
	4	稻谷爆腰率增值 玉米裂纹率增值 小麦湿面筋率	5.2	6.2.2
	5	热风温度波动范围	5.2	6.2.2
	6	干燥不均匀度	5.2	6.2.2
	7	色泽、气味	5.2	6.2.2
	8	电气控制	5.6	6.6
C	1	出机粮食温度	5.2	6.2.2
	2	装配质量	5.3	6.3
	3	外观质量	5.4	6.4
	4	涂层质量	5.5	6.5
	5	标志	8.1	8.1
	6	产品使用说明书	8.2.2	8.2.2

7.2 判定规则

检验项目中，A 类项目应全部合格，B类项目不合格项目不超过1项，C 类项目不合格项目不超过2项，则为合格产品，否则判为不合格产品。

8 标志和随行文件

8.1 标志

每台烘干机应在明显位置固定符合GB/T 13306规定的铭牌，应包括以下内容：

a) 产品名称、型号；
b) 额定功率；
c) 热源型式、型号和制热量；
d) 主参数；
e) 质量；
f) 出厂编号或出厂日期；
g) 制造商名称。

8.2 随行文件

8.2.1 随行文件应包括以下内容：

a) 装箱单；
b) 产品合格证；
c) 产品使用说明书。

8.2.2 烘干机的使用说明书应符合 GB/T 9969 的规定。

9 包装、运输和储存

9.1 包装

9.1.1 宜采用木箱或按用户要求包装，部件和配件、附件及随行文件在包装箱内应固定牢靠。

9.1.2 包装箱内应有防水层，随行文件应放置在塑料袋内。

9.2 运输

烘干机的运输应符合公路、铁路和水路运输的规定。吊卸和装载时，应注意包装箱上的包装储运标志，不应颠倒、重压、碰撞和剧烈振动，应有防雨措施。

9.3 储存

烘干机露天存放时底部应垫支撑物，应有防雨淋、日晒和积水的设施；室内存放时应有良好的通风与防潮措施。

参 考 文 献

[1] GB/T 1.1—2020《标准化工作导则》。
[2] GB/T 6970-2007 粮食干燥机 试验方法
[3] DG/T 017-2021 谷物干燥机
[4] 李长友. 粮食干燥解析法[M]. 北京：科学出版社，2018.
[5] 李长友. 工程热力学与传热学[M]. 北京：中国农业大学出版社，2012.

荣誉证书

CERTIFICATE OF ACHIEVEMENT

INTELLIGENT ROBOT FIGHTING AND GAMING COMPETITION

2024 中国智能机器人格斗及竞技大赛

二等奖

智能机器人创新设计

参赛学校：华南农业大学

指导老师：李成杰 张亚莉

参赛队员：黄展鸿 程美娟 陈嘉奋 李万权

领队：黄展鸿

队伍名称：跟他爆了战队

中国人工智能学会

2024 年 11 月 24 日

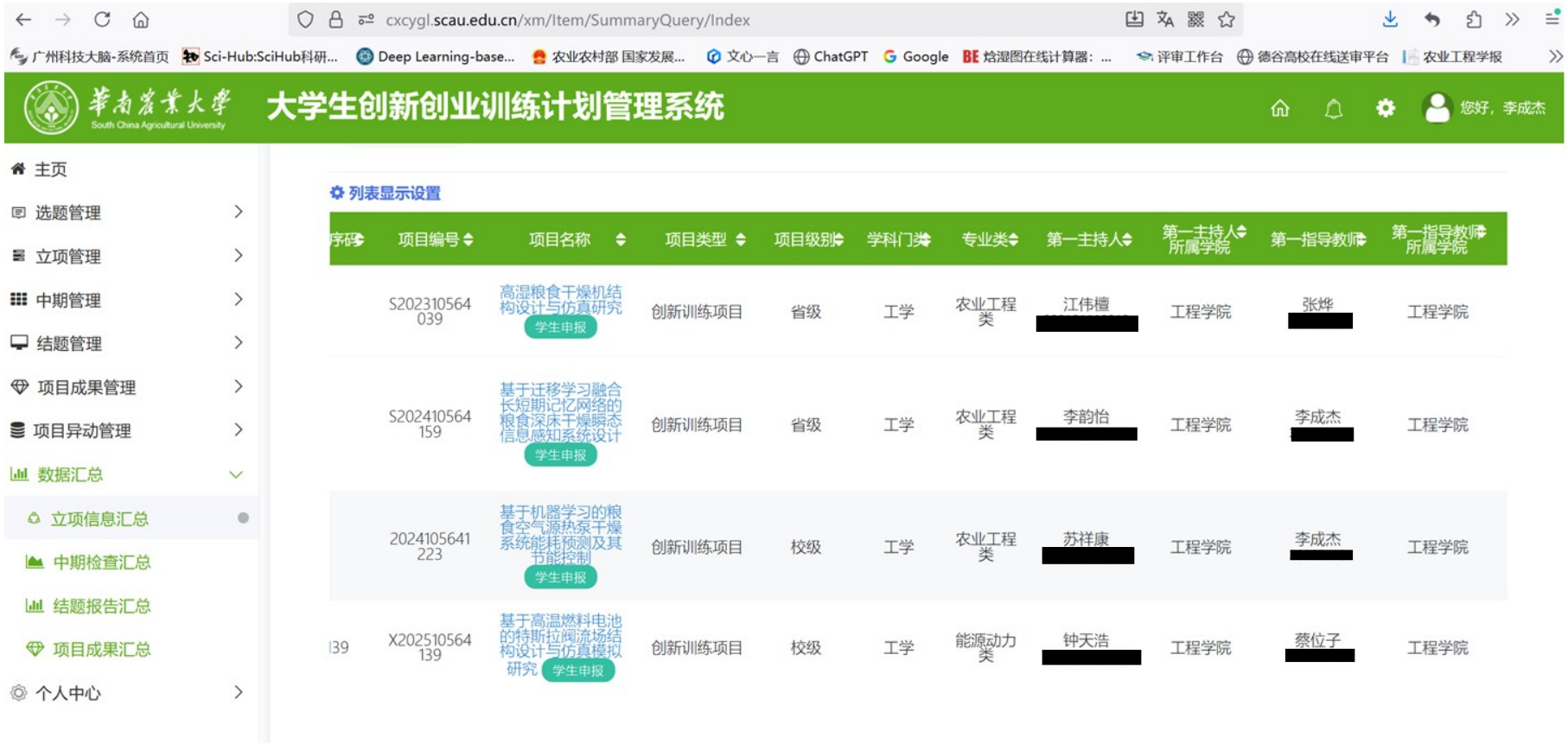
cxcygl.scau.edu.cn/xm/Item/SummaryQuery/Index
广州科技大脑-系统首页
Sci-Hub:SciHub科研...
Deep Learning-base...
农业农村部 国家发展...
文心一言
ChatGPT
Google
焓湿图在线计算器：...
评审工作台
德谷高校在线送审平台
农业工程学报
華南農業大學
South China Agricultural University
大学生创新创业训练计划管理系统
您好，李成杰
主页
选题管理
立项管理
中期管理
结题管理
项目成果管理
项目异动管理
数据汇总
立项信息汇总
中期检查汇总
结题报告汇总
项目成果汇总
个人中心
列表显示设置
序码
项目编号
项目名称
项目类型
项目级别
学科门类
专业类
第一主持人
第一主持人所属学院
第一指导教师
第一指导教师所属学院
S202310564039
高湿粮食干燥机结构设计与仿真研究
学生申报
创新训练项目
省级
工学
农业工程类
江伟檀
工程学院
张烨
工程学院
S202410564159
基于迁移学习融合长短期记忆网络的粮食深床干燥瞬态信息感知系统设计
学生申报
创新训练项目
省级
工学
农业工程类
李韵怡
工程学院
李成杰
工程学院
2024105641223
基于机器学习的粮食空气源热泵干燥系统能耗预测及其节能控制
学生申报
创新训练项目
校级
工学
农业工程类
苏祥康
工程学院
李成杰
工程学院
139
X202510564139
基于高温燃料电池的特斯拉阀流场结构设计与仿真模拟研究
学生申报
创新训练项目
校级
工学
能源动力类
钟天浩
工程学院
蔡位子
工程学院